IEEES-2026

17th International Exergy, Energy and Environment Symposium, Nicosia, N. Cyprus, June 1 - 3, 2026

Conference PROCEEDINGS

Eastern Mediterranean University Energy Research Center erc

Ontario Tech University

National Hydrogen Association H2 Türkiye

aee® Association of Energy Engineers Cyprus Chapter

17th International Exergy, Energy and Environment Symposium (IEEES-2026)

BOOK OF PROCEEDINGS
of the 17th International Exergy, Energy and Enviroment Symposium (IEEES-2026)

Published online on June 1, 2026.

https://ieees2026.emu.edu.tr

TABLE OF CONTENTS

PREFACE

It is with great pleasure that we present the Book of Abstracts for the 17th International Exergy, Energy and Environment Symposium (IEEES-2026), a multidisciplinary and interdisciplinary conference that brings together scientists, engineers, industrialists, and researchers from around the world. This symposium provides a dynamic platform for sharing ideas, research findings, and practical expertise on issues related to sustainable energy and the environment.

Since its inception in 2003, the IEEES conference series has evolved into a well-established and recurring scientific meeting, covering a wide spectrum of topics including renewable energy, energy efficiency, smart grids, green transportation, and climate change technologies. Founded by Prof. Ibrahim Dincer, the symposium reflects a strong vision of advancing knowledge and fostering innovation in the fields of energy and environment. Through keynote lectures, technical sessions, and workshops, IEEES continues to promote the exchange of ideas and the development of forward-looking, cleaner technologies.

The 17th edition of the symposium is hosted in Nicosia and is organized by the Energy Research Center (ERC) of Eastern Mediterranean University in collaboration with the Association of Energy Engineers (AEE) Cyprus Chapter. The abstracts compiled in this volume represent the breadth and depth of current research, highlighting both emerging challenges and innovative solutions in the global transition toward sustainability.

The successful realization of IEEES-2026 would not have been possible without the dedication and hard work of many individuals and institutions. We would like to express our sincere appreciation to the organizing committee for their commitment and professionalism in bringing this event together. We also gratefully acknowledge the valuable support of our sponsors, whose contributions have been instrumental in making this conference possible.

Finally, we extend our heartfelt thanks to all contributors and participants for their valuable input and for making IEEES-2026 a meaningful and impactful gathering. We hope that this Book of Abstracts will serve as a source of inspiration and a catalyst for further collaboration and innovation.

Prof. Dr. Uğur Atikol
Conference Chair

ORGANIZING COMMITTEE

Founding Chair

Prof. Dr. Ibrahim Dincer *University of Ontario, Canada*

Conference Chair

Prof. Dr. Uğur Atikol, *Eastern Mediterranean University, Energy Research Center*

Organizing Committee Members

Prof. Dr. Mustafa Dağbaşı, *Cyprus International University, Department of Mechanical Engineering, N. Cyprus*

Assoc. Prof. Dr. Keyvan Bahlouli, *Cyprus International University, Department of Mechanical Engineering, N. Cyprus*

Assoc. Prof. Dr. Soad Mousavi, *Arkin University of Arts and Design, Department of Architecture, N. Cyprus*

Assoc. Prof. Dr. Mohammad Karimzadeh Kolamroudi, *Near East University, Department of Mechatronics, N. Cyprus*

Assist. Prof. Dr. Meliz Hastunç, *Bahçeşehir Cyprus University, Department of Electrical and Electronics Engineering, N. Cyprus*

Ali Korakan, *Association of Energy Engineers (AEE) Cyprus Chapter*

Tamer Zaim *Green Efficiency Energy Services Ltd N. Cyprus*

SCIENTIFIC COMMITTEE

Title and Name	University	Country
Prof. Dr. Arif Hepbaşlı	*Yaşar University*	*Türkiye*
Prof. Dr. Tien-Chien Jen	*University of Johannesburg*	*South Africa*
Prof. Dr. Adnan Midilli	*İstanbul Technical University*	*Türkiye*
Prof. Dr. Reinhard Haas	*Vienna University of Technology*	*Austria*
Prof. Dr. Fuat Egelioğlu	*Eastern Mediterranean University*	*N. Cyprus*
Prof. Dr. Hasim Altan	*United Arab Emirates University*	*UAE*
Prof. Dr. Danijel Topić	*J. J. Strossmayer University of Osijek*	*Croatia*
Prof. Dr. Ali Muhtaroğlu	*Oslo Metropolitan University*	*Norway*
Prof. Dr. Mohammad Jafar Kermani	*Amirkabir University of Technology*	*Iran*
Prof. Dr. İbrahim Sezai	*Eastern Mediterranean University*	*N. Cyprus*
Prof. Dr. Hikmet Aybar	*Cyprus Aydin University*	*N. Cyprus*
Prof. Dr. Reinhard Haas	*Vienna University of Technology*	*Austria*
Prof. Dr. Qasim Zeeshan	*Eastern Mediterranean University*	*N. Cyprus*
Prof. Dr. Tanay Sıdkı Uyar	*Istanbul Gedik University*	*Turkey*
Prof. Dr. Mustafa Dağbaşı	*Cyprus International University*	*N. Cyprus*
Prof. Dr. Serkan Abbasoğlu	*Cyprus International University*	*N. Cyprus*
Prof. Dr. Murat Fahrioğlu	*Middle Eastern Technical University*	*N. Cyprus*
Assoc. Prof. Dr. Zhaoye Qin	*Tsinghua University*	*China*
Assoc. Prof. Dr. Amela Ajanovic	*Vienna University of Technology*	*Austria*
Assoc. Prof. Dr. Nader Javani	*Yildiz Technical University*	*Türkiye*
Assoc. Prof. Dr. Babak Safaei	*Eastern Mediterranean University*	*N. Cyprus*
Assoc. Prof. Dr. Keyvan Bahlouli	*Cyprus International University*	*N. Cyprus*
Assoc. Prof. Dr. Mina Farmanbar	*Universitetet i Stavanger*	*Norway*
Dr. Petra Bele	*Technical University of Munich*	*Germany*

PROCEEDINGS

(Listed by ID numbers)

TWO DECADES OF RESEARCH ON ENERGY EFFICIENCY IN BUILDINGS: A BIBLIOMETRIC AND KEYWORD CO-OCCURRENCE ANALYSIS (2005-2025)

Manta Marcelinus Dakyen[1], Murat Özdenefe* [2,3], Mustafa Dağbaşı[4]*
[1]Girne American University, Faculty of Engineering, Energy Systems Engineering Department, Kyrenia, Turkey
[2] Eastern Mediterranean University, Faculty of Engineering, Mechanical Engineering Department, Gazimağusa, Turkey
[3] Eastern Mediterranean University, Energy Research Centre, Gazimağusa, Turkey
[4] Cyprus International University, Faculty of Engineering, Energy Systems Engineering Department, Nicosia, Turkey
*Corresponding author e-mail: mantadakyen@gau.edu.tr
Ref # BES-01

ABSTRACT

This study conducts a bibliometric and keyword co-occurrence analysis of research on energy efficiency in buildings published between 2005 and 2025. Data retrieved from the Web of Science Core Collection were analyzed using VOSviewer to examine publication trends, collaboration networks, citation patterns, and research themes. The results indicate a steady increase in publications over the past two decades, reflecting growing global interest in improving building energy performance in response to climate change and sustainability goals. Co-authorship analysis identifies China, the United States, and Italy as leading contributors. Keyword co-occurrence analysis highlights major research themes such as energy efficiency, sustainability, thermal comfort, performance, and optimization. Overall, the findings provide a concise overview of the intellectual structure and evolving research trends in energy efficiency in buildings, offering a foundation for future research and collaboration toward sustainable building development.

Keywords: Building design, Energy efficiency, Research collaboration, Sustainability, VOSviewer

INTRODUCTION

The building sector has served as one of the most fundamental needs in our daily lives, contributing to facilitating social and economic development. However, it is also one of the largest consumers of energy and contributors to greenhouse gas (GHG) emissions worldwide. In the European Union (EU), buildings account for approximately 40% of total energy consumption and 36% of GHG emissions [1]. Globally, there is a growing tendency of energy use in the building sector, with estimates suggesting an 88% rise between 2003 and 2050 if no substantial efficiency measures are implemented [2]. This trend has intensified environmental concerns and underscores the need for improved energy performance in buildings. Consequently, increasing public awareness and policy initiatives have propelled research on energy efficiency in buildings – particularly strategies such as adaptive thermal comfort and sustainable building design – to the forefront of efforts at achieving sustainable development. This intensified focus is clearly reflected in the existing body of literature, and the evolving intellectual landscape can be systematically mapped out by utilizing bibliometric and keyword co-occurrence analyses, which help reveal publication trends, thematic evolution and collaborative networks, thereby elucidating key research interests and emergent topics.

This study conducts a comprehensive bibliometric and keyword co-occurrence analysis of research on energy efficiency in buildings published between 2005 and 2025. Specifically, the study aims to examine publication trends, citation patterns, and collaborative networks in order to map the intellectual landscape of the field and identify emerging research directions. To achieve this objective, the study addresses the following research questions: (1) What are the dominant research themes and evolving trends in energy efficiency in buildings from 2005 to 2025? (2) How have international collaborations evolved over the past two decades? (3) Which authors, institutions, and countries have been the most prolific and influential in this field? (4) What key keywords and emerging topics are shaping the future trajectory of energy efficiency research in buildings?

METHODOLOGY

Bibliometrics applies statistical techniques to evaluate the structure, techniques and development of scientific research within a given field [3]. Its main objective is to provide a systematic and visual overview of existing publications, enabling the identification of research trends, influential studies, and knowledge structures. By integrating computational and visual analytical techniques, bibliometric analysis enhances the accessibility, transparency, and reproducibility of literature-based research [4].
In this study, the visualization tool, VOSviewer, is used to construct and analyze bibliometric networks. VOSviewer enables the visualization of relationships such as citations, bibliographic coupling, co-citation, or co-author relationships [5]. Using this tool, three bibliometric approaches – general publication analysis, collaboration network analysis and keyword analysis – are applied to examine the research status and development trends of energy efficiency in buildings. The bibliometric analysis began with the identification of an appropriate database for retrieving publications in the research field. Commonly used databases for bibliometric studies include Scopus, Web of Science and ScienceDirect [6]. In this study, the Web of Science Core Collection (WoSCC) was selected due to its rigorous indexing standards, extensive historical coverage, and high-quality bibliographic data [7,8]. WoSCC includes the Science Citation Index Expanded, which ensures the inclusion of high-impact, peer-reviewed research relevant to energy efficiency in buildings published between 2005 and 2025. In addition, its standardized indexing system facilitates reliable citation analysis and compatibility with bibliometric visualization tools [9]. The retrieval strategies was defined as follows: Topic search = *building design* energy efficiency**; Timespan = *2005 – 2025*; Document type = *articles or reviews*; Language = *English*.

RESULTS

Trend in annual publication

The analysis of annual publication volume illustrates the evolution and intensity of research on energy efficiency in buildings over the past two decades. Publications increased steadily from 118 in 2005 to 3991 in 2025, reflecting an intensification of scholarly activity and research productivity. This sustained growth underscores the rising global focus on energy efficiency in buildings, driven by climate change mitigation, decarbonization policies and sustainable development goals. Overall, the continuous expansion of research output confirms that energy efficiency in buildings remains a dynamic and highly active area of scientific exploration (See Fig 1).

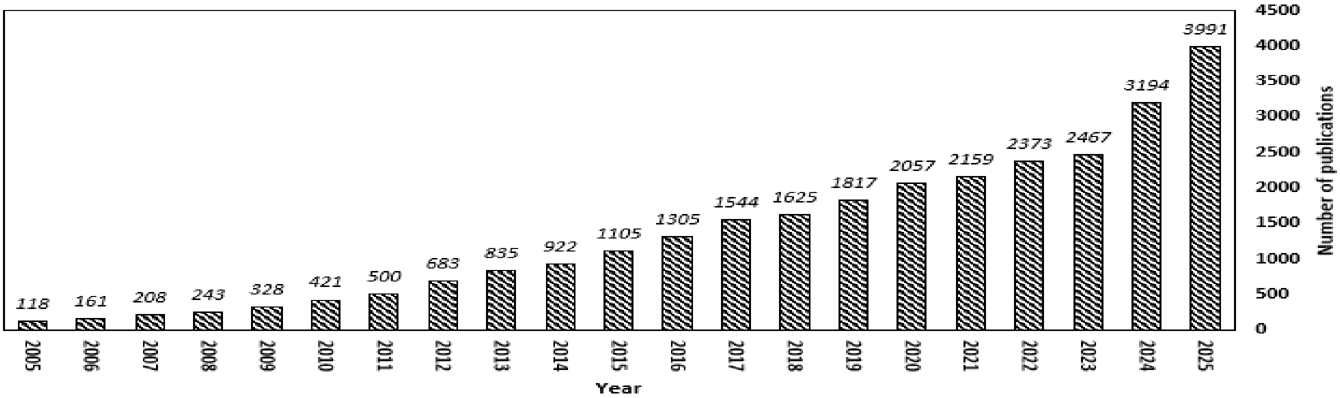

Fig. 1. Annual publication Count (2005 – 2005)

Co-authorship analysis

A co-authorship analysis was conducted to examine international research collaborations, focusing on countries with at least 398 published documents. This criterion reduced the dataset from 151 to 21 collaborating countries. The results indicated that the People's Republic of China is the most productive and influential contributor, with 8699 publications, the highest total citations (220964), and the strongest collaboration link strength. Other major contributors include the United States (4134 documents, 132368 citations) and Italy (1942 documents, 50714 citations). These findings suggest that while Chile plays a central role in driving research output, substantial high-impact collaborations exist among leading research nations. The country collaboration network generated using VOSviewer is illustrated in Fig. 2.

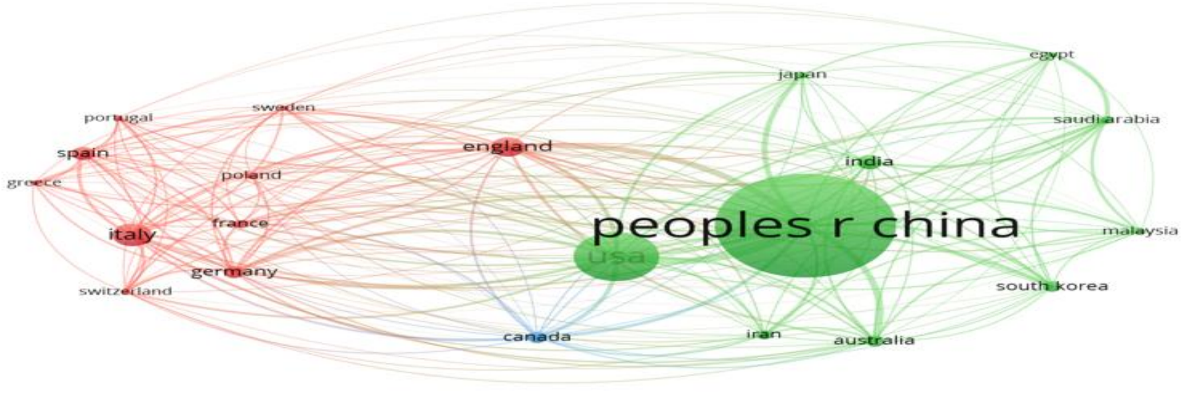

Fig. 2. Country collaboration network

Co-occurrence analysis

Keyword co-occurrence network visualization was used to examine the relationships among frequently used terms and reveal the conceptual structure of the research field.

A co-occurrence analysis of all keywords was conducted to capture the thematic development of energy efficiency in building research. Applying a minimum occurrence threshold of 438 reduced the dataset from 71163 keywords to 30 significant terms, forming a network of three clusters with 48279 total links. The term design recorded the highest occurrence (5407) and link strength (10914); its prominence is largely attributed to its use as a broad search term during literature retrieval. Followed by performance, energy efficiency, efficiency, and optimization. The network visualization generated from VOSviewer is presented in Fig. 3.

A co-occurrence analysis of authors' keywords was also performed to identify key research themes. With a minimum occurrence threshold of 222, 20 keywords were retained. The most frequent terms were energy efficiency (3721 occurrences), sustainability (704), and thermal comfort (681), which evidently validate the search strategy, which was set as the premise of this research.

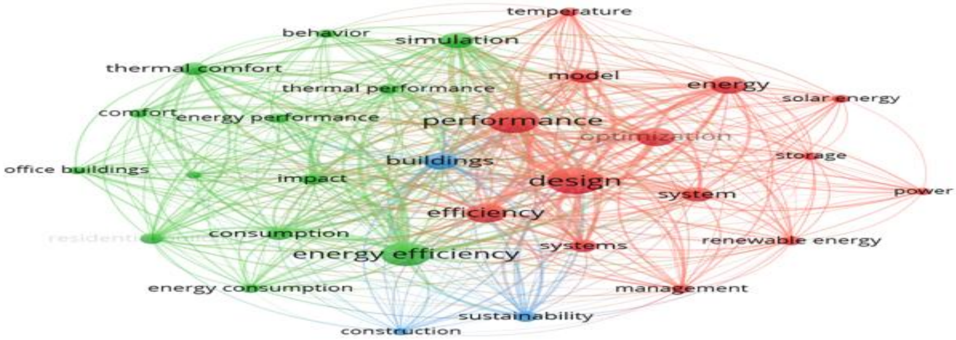

Fig. 3. All keywords co-occurrence map

Citation-analysis

Citation analysis was conducted using the author and citation fields. A minimum publication threshold of 30 documents per author was applied, resulting in 25 authors meeting the criterion. The network analysis produced 4 clusters with 23 links. The most cited authors include Tianzhen Hong (3844 citations), Hongxing Yang (2567 citations), Xin Wang (2505 citations), and Fabrizio Ascione (2181 citations). Several other authors also recorded substantial citation counts. The visualization map of the most cited authors generated from VOSviewer is presented in Fig. 4.

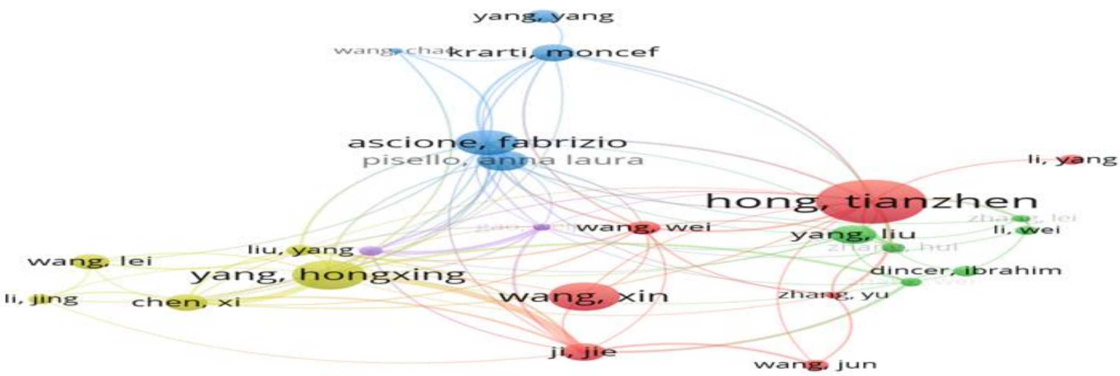

Fig. 4. Network visualization of the Top 25 most cited authors (Citation analysis)

Most cited institution

To identify the most cited organizations, the citation and organization fields were selected. A minimum citation threshold of 184 documents was applied, resulting in 15 organizations meeting the criterion and forming 3 clusters. The results indicate that Chinese Academy of Sciences (24058 citations), Tsinghua University (14596 citations), and Hong Kong Polytechnic University (13530 citations) are the most cited institutions in this research field. Other institutions with notable citation impact include Tianjin University of China and City University of Hong Kong. The citation network of the most cited organizations is presented in Fig. 5.

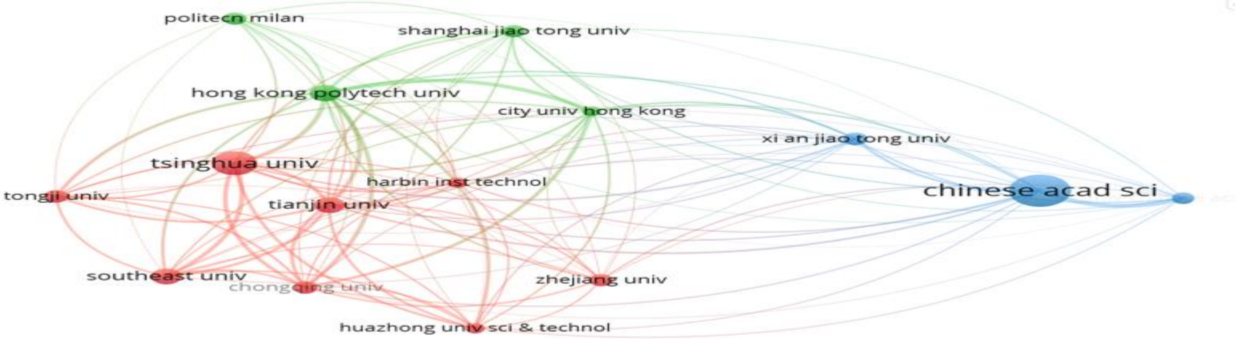

Fig. 5. Network visualization of the Top 15 most cited institutions (Citation analysis)

DISSCUSSION

The bibliometric analysis reveals a substantial and sustained growth in research on energy efficiency in buildings between 2005 and 2025. The increasing publication trend indicates heightened global attention to reducing energy consumption in the building sector, largely driven by climate change mitigation policies, decarbonization targets, and sustainable development initiatives. The co-authorship analysis highlights strong international collaboration patterns, with China emerging as the most productive and influential contributor, followed by the United States and Italy. This suggests that while certain countries dominate research output, the field is increasingly characterized by global collaboration networks that facilitate knowledge exchange and innovation. Keyword co-occurrence analysis further reveals that core research themes revolve around energy efficiency, sustainability, thermal comfort, performance, and optimization. These themes indicate a growing interdisciplinary focus on integrating energy-efficient design strategies with occupant comfort and sustainable building performance. Additionally, citation analysis identifies influential authors and institutions that play central roles in shaping the knowledge structure and research direction of the field.

CONCLUSION AND IMPLICATIONS

This study provides a bibliometric and keyword co-occurrence analysis of research on energy efficiency in buildings published between 2005 and 2025, using data from the Web of Science Core Collection and visualization through VOSviewer. The findings reveal a steady growth in research output over the past two decades, reflecting increasing global interest in improving building energy performance in response to climate change and sustainability objectives. The analysis also identifies China, the United States, and Italy as key contributors to the field, while major research themes include energy efficiency, sustainability, thermal comfort, performance, and optimization.

Building on these findings, future research may focus on expanding bibliometric analyses by integrating multiple databases, such as Scopus, to enhance dataset coverage and improve the robustness of results. Further studies could also employ advanced scientometric and data-driven approaches, including machine learning and topic evolution analysis, to identify emerging research fronts and technological innovations in building energy efficiency. Additionally, greater emphasis on interdisciplinary collaboration, smart building technologies, and climate-responsive design strategies may help advance sustainable building development and support global decarbonization goals.

REFERENCES

1. https://energy.ec.europa.eu/topics/energy-efficiency/energy-performance-buildings/energy-performance-buildings-directive_en. Accessed on Feb 15, 2026
2. Transition to Sustainable Buildings – Analysis - IEA. Accessed on Feb 15, 2026
3. Alan Pritchard. (1969). Statistical bibliography or bibliometrics? Journal of Documentation, 25(4), 348–349.
4. Chaomei Chen. (2017). Science Mapping: A Systematic Review of the Literature. Journal of Data and Information Science, 2(2), 1–40.
5. Nees Jan van Eck and Ludo Waltman. (2010). Software survey: VOSviewer, a computer program for bibliometric mapping. Scientometrics, 84(2), 523–538.
6. Ullah, S., Ahmad, S., and Irfan, M. (2023). Trends in bibliometric studies: A review of major databases and analytical tools. Library Philosophy and Practice.
7. Caputo, A., & Kargina, M. (2022). A bibliometric analysis of research trends in management studies using the Web of Science database. Scientometrics.
8. Farooq, R., Mihardjo, L., & Darmasetiawan, N. (2021). A bibliometric analysis of global research on sustainable development. Sustainability, 13, 123.
9. Huang, Y., Zhao, Y., & Wang, J. (2022). Mapping research trends using Web of Science bibliometric data. Journal of Informetrics.

THE IMPACT OF MATERIAL USE ON THERMAL COMFORT: A CASE STUDY OF HOUSING RENOVATION IN GHARDAÏA, ALGERIA

Younes Boukhari[1], Harun Sevinç[2]*

[1] Eastern Mediterranean University, Faculty of Architecture, Department of Interior Architecture, Mimar Sinan Street, 99628 Gazimağusa, North Cyprus via Mersin 10, Türkiye

[2] Eastern Mediterranean University, Faculty of Architecture, Department of Architecture, Mimar Sinan Street, 99628 Gazimağusa, North Cyprus via Mersin 10, Türkiye

*Corresponding author e-mail: harun.sevinc@emu.edu.tr

Ref # BES-02

ABSTRACT

Indoor thermal comfort represents a critical challenge in hot–arid climates such as Algerian desert, notably within heritage protected dwellings where external modifications are restricted. This study investigates thermal comfort improvement strategies for a vernacular Ksar house located in Ghardaïa, part of the M'zab Valley World Heritage site. A mixed-method was used, combining real-time indoor temperature and relative humidity measurements, field observations, direct questionnaires covering 73 participants, and dynamic thermal simulations using DesignBuilder software. Hence, results reveal that summer overheating, with indoor temperatures reaching 39°C in July with low relative humidity (HR) registered (≈11%). Furthermore, passive cooling strategies, including evaporative cooling, natural ventilation enhancement, and the application of insulation materials, were evaluated according to ASHRAE Standard 55 (2023) adaptive and PMV models. Evaporative cooling combined with increased air velocity reduced operative temperature by up to 1.6°C, achieving thermal comfort compliance in June, while July and August remain out of comfort zone. Although external insulation materials prove effective, they conflict with heritage conservation regulations. Findings demonstrate that passive measures alone are insufficient under extreme heat conditions. A hybrid cooling system combining evaporative cooling and assisted mechanical air movement such as fans can help perceive comfort, while air-conditioning is still effective to cope with summer overheat. The study proposes a renovation framework balancing thermal comfort, cultural continuity, and energy efficiency using solar panel in Saharan heritage dwellings.

***Keywords*:** Thermal comfort, passive cooling strategies, heritage conservation, hybrid cooling system, renovation framework.

INTRODUCTION

Algeria embraces different climatic regions, ranging from Mediterranean in the north to hot-arid desert climate in the south. The Sahara Desert covers nearly 80% of the national territory area, making Saharan settlements critical areas for architectural and environmental research. However, in recent decades, global warming has profoundly affected thermal comfort, occupant well-being and increasing reliance on air-conditioning systems in Algerian desert [1]. This environmental phenomenon is evident in the M'zab Valley and Ghardaïa region, where traditional Ksour (vernacular settlements) is established. The heritage houses within Ksar, designed with adaptive passive systems, are now struggling to cope with climate changes [2]. The growing installation of air-conditioning units on building façades has disrupted the visual coherence of the Ksar fabric and altered its microclimatic balance. While several studies have compared the thermal performance of traditional and contemporary buildings materials [3][4]. Few studies have explored how the application of insulation materials with passive renovation strategies can improve indoor thermal comfort while preserving architectural identity. Addressing this gap, the present study investigates whether thermal comfort in M'zab Ksar houses can be achieved through sustainable material used during renovation. The research aims to develop a responsive interior intervention framework that improves spatial quality and occupants' well-being through passive strategies and locally appropriate materials. By aligning environmental performance with heritage conservation principles. Hence, the study suggests a holistic renovation approach capable of reducing dependence on mechanical cooling while respecting the socio-cultural values of the M'zab community.

METHODS

This study adopted a mixed-methods combining quantitative measurements, dynamic simulation, and qualitative assessment to evaluate indoor thermal comfort in M'zab Ksar houses.

Quantitative Method

Field Measurements

Indoor air temperature and relative humidity were recorded using a calibrated thermohygrometer during the summer months (June–August). Measurements were taken at representative locations within selected dwellings in two Ksour; Ksar Ghardaïa and Ksar Beni Isguen in order to understand daily thermal variations under extreme climatic conditions.

Simulation and Experimental Design

A dynamic thermal simulation was conducted using DesignBuilder software to model existing building conditions and proposed renovation scenarios for one building. The simulation was calibrated based on local climatic data, building geometry, interior space layout, material characteristics, ventilation patterns and occupancy schedules. An experimental scenario examined the installation of mycelium bio-based material for insulation during renovation process. Comparative analysis between existing mechanical cooling practices and proposed passive techniques was conducted to evaluate their impact on indoor thermal comfort. Thermal comfort assessment was conducted according to the adaptive comfort model defined by ASHRAE Standard 55. The Occupancy Residential profile occupancy and activity schedules has been chosen in DesignBuilder for 25 m²/per person (Table 1). A fraction of 1.00 corresponds to the maximum occupancy density of 25 m²/person. Total surface wall area was 44.2 m2, total window surface area 1.25 m2 and windows to wall ratio ws 2.83%. The thermal conductivity, specific heat and density of bio-based Thermal Insulation Material Mycelium (Thickness: 5 cm) from DesignBuilder Simulation (ASHRAE 90.1 Standards) are given as 0.0500 W/mK, 900 J/kgK and 1000 kg/m3 respectively.

Table 1. Occupancy Schedule from DesignBuilder Simulation (ASHRAE 90.1 Standards)

Time Period	**Weekdays (Fraction)**	**Saturdays / Sundays / Holidays (Fraction)**
00:00 – 05:00	1.00	1.00
05:00 – 06:00	0.80	1.00
06:00 – 07:00	0.75	1.00
07:00 – 08:00	0.75	0.80
08:00 – 09:00	0.50	0.75
09:00 – 10:00	0.43	0.50
10:00 – 15:00	0.43	0.43
15:00 – 18:00	0.50	0.50
18:00 – 21:00	0.75	0.75
21:00 – 24:00	0.80	0.80

Table 2. Thermophysical Properties of Building Elements from DesignBuilder Simulation (ASHRAE 90.1 Standards)

	External Wall Configuration		**Roof / Floor**	**Windows**
Material Properties	Existing external Stone wall (Uninsulated)	Insulated external wall (Internal layer: Mycelium 5 cm + Stone)	Trink palm 30 cm+ lime stone 10 cm+ ceramic tile 10 cm	Windows (50 cm x 50 cm), single-pane 5 mm clear glass and wooden frame
Total Thickness (cm)	55	60	50	/
U-Value (W/m²-k)	1.80	0.64	0.35	4.9

Qualitative Method

The qualitative component aimed to assess occupants' perceptions of indoor thermal comfort and spatial organization during summer. Data were collected through structured questionnaires and semi-structured interviews administered face-to-face and electronically to residents of the Ksar. The survey examined:

• Perceived indoor thermal comfort during summer
• Satisfaction with spatial functionality and well-being
• Experience with traditional passive cooling systems
• Attitudes toward renovation materials and mechanical cooling use

Given the architectural homogeneity of Ksar houses, randomized questionnaires and systematic observations were considered appropriate to ensure reliable and valid findings.

Data Analysis

Quantitative data were statistically analyzed to identify temperature trends, averages, and thermal performance patterns. Questionnaire responses were processed using Excel to generate visual descriptive statistics. Secondary climatic data were obtained from publicly available meteorological records (meteostat.com) to contextualize measured results. The findings were interpreted through the adaptive thermal comfort framework as the most adequate model to evaluate the effectiveness of passive buildings.

RESULTS AND DISCUSSIONS

The key survey results of the questionnaires and semi-structured interviews with 73 participants from different gender and age-groups are presented In Table 3. Between June and August 2025, average outdoor temperatures ranged from 32.4°C to 36.6°C, peaking in July. The lowest indoor temperatures were recorded in the early morning at approximately 32°C. The registered relative humidity remained below 30%, reflecting a notably dry climate.
Field measurements confirmed persistent summer overheating, particularly on upper floors, where indoor air temperatures reached 39°C in July and August under very low relative humidity (11–12%). Although, such dry conditions theoretically favor evaporative cooling, simulation results indicate that its standalone performance remains limited.
Under the Adaptive Model of ASHRAE 55–2023 [5], the combined scenario integrating evaporative cooling, full

window opening, and air velocity between 0.9–1.2 m/s achieved comfort compliance only in June. However, July and August remained outside the comfort zone. Using the PMV model, increasing air velocity to 2 m/s (mechanically assisted) with operative temperature set at 32.5°C and Relative Humidity (RH) at 26% showed partial compliance in June but complete non-compliance during peak summer months (July and August). These findings confirm that airflow enhancement may improve thermal perception but still away from fully offset extreme outdoor summer heat. Similarly, simulation results indicate that internal insulation layers can mitigate the beneficial time-lag effect coming for the existing heavy-thick stone walls by isolating the thermal mass from indoor space. This confirms the critical role of thermal inertia in hot–arid climates such as that of Ghardaïa. These findings align with the existing literature [6] [7].

Table 3. Key survey results

	Survey Question	Age	Female	Yes	No	Male	Yes	No	Yes (F/M)	No (F/M)
1	**Indoor temperature increase over the last 10 years**	20-50	14 (18%)	100%	0%	19 (27%)	100%	0%	100%	0%
		50-60	10 (14%)	100%	0%	13 (18%)	100%	0%	100%	0%
		60-85	7 (10%)	80%	20%	10 (13%)	78%	22%	79%	21%
2	**Use of air conditioning in summer**	20-50	14 (18%)	28%	72%	19 (27%)	10%	90%	19%	71%
		50-60	10 (14%)	30%	70%	13 (18%)	30%	70%	30%	70%
		60-85	7 (10%)	30%	70%	10 (13%)	55%	45%	42%	58%
3	**Grilled door for natural ventilation during summer**	20-50	14 (18%)	92%	8%	19 (27%)	92%	8%	92%	8%
		50-60	10 (14%)	91%	9%	13 (18%)	91%	9%	91%	9%
		60-85	7 (10%)	90%	10%	10 (13%)	90%	10%	90%	10%
4	**Thermal Comfort in basement floor in summer**	20-50	14 (18%)	100%	0%	19 (27%)	100%	0%	100%	0%
		50-60	10 (14%)	100%	0%	13 (18%)	100%	0%	100%	0%
		60-85	7 (%)	100%	0%	10 (13%)	100%	0%	100%	0%
5	**Thermal comfort in ground and first floor in summer**	20-50	14 (18%)	28%	72%	19 (27%)	10%	90%	19%	81%
		50-60	10 (14%)	20%	80%	13 (18%)	30%	70%	25%	75%
		60-85	7 (10%)	30%	70%	10 (13%)	55%	45%	42%	58%
6	**Use of fans during summer for ventilation**	20-50	14 (10%)	28%	72%	19 (27%)	26%	74%	27%	73%
		50-60	10 (10%)	70%	30%	13 (18%)	70%	30%	70%	30%
		60-85	7 (10%)	70%	30%	10 (13%)	66%	34%	68%	32%

Hence, renovation interventions should be conceived as multidimensional processes adopting thermal mass preservation, locally available sustainable materials and perceptual adaptivity of finishing material selection. Nevertheless, simulation findings reveal that passive measures alone remain insufficient during peak summer periods, highlighting the requirement for complementary hybrid cooling solutions.

Table 6. Comparison of outdoor and indoor climatic conditions (June – August 2025) in Ghardaïa (Case Study of Ksar Beni-Isguen) (Compiled by the authors based on Meteostat (2025), Wanderlog (2025), and on-site measurements

Month	Exterior Average Temperature (°C)	Exterior Average Relative Humidity (%)	Time	Ground floor Indoor Temperature (°C)	Ground floor Indoor Relative Humidity (%)	First floor Indoor Temperature (°C)	First floor Indoor Relative Humidity (%)
June	32.4°C	24	8:00	33.9	13.2	36.5	11.0
			17:00	34.3	12.0	37.6	10.2
			23:00	34.4	12.0	37.1	10.0
July	36.6°C	18	8:00	34.5	11.4	36.7	10.5
			17:00	35.1	10.8	39.1	10.3
			23:00	35.2	11.2	38.6	10.3
August	33.1°C	23	8:00	33.8	10.6	37.3	10.0
			17:00	35.5	10.3	38.8	10.7
			23:00	35.3	10.1	38.6	10.6

Fig. 1. Entrance and interior view of the courtyard and upper-floor arcade of the case study (Photos taken by authors)

Table 7. Passive Strategies applied to the Case Study (DesignBuilder Simulation)

Month	**Floor**	**Initial state**		**Windows fully opened**		**Mycelium insulation 50mm (Internal)**		**Evaporative cooling**		**Combined scenarios**	
		Temp (°C)	RH (%)	Temp(°C)	RH (%)	Temp (°C)	RH (%)	Temp (°C)	RH (%)	Temp (°C)	RH (%)
June	G.F	34.0	21.0	33.0	24.0	34.1	23.4	32.5	26.0	32.93	25.35
	F.F	35.0	18.5	34.2	21.0	36.0	20.0	33.4	25.0	33.94	24.27
July	G.F	36.1	19.0	35.0	22.0	36.3	21.5	35.0	24.0	35.02	23.22
	F.F	37.0	17.3	36.4	19.0	37.0	18.5	35.7	23.0	36.16	22.1
August	G.F	35.9	20.1	35.0	24.0	36.2	23.5	34.8	26.0	34.83	25.5
	F.F	36.8	18.0	36.0	18.0	37.0	19.0	35.7	25.0	36.15	24.2

CONCLUSIONS

This research illustrates that vernacular M’zab Ksar houses are experiencing significant indoor thermal discomfort during extreme summer months due to climatic severity, dense urban fabric, and heritage preservation restrictions. While passive strategies such as passive evaporative cooling and enhanced air velocity offer measurable improvements leading to achieve comfort compliance only in June month. The findings confirm the essential role of thermal mass in such hot–arid climates and caution against internal insulation solution that may alter wall inertia. On the other hand, renovation approaches should prioritize locally available, breathable, and thermally responsive materials finishes yielding perceive comfort enhancement.

A holistic intervention package is therefore recommended, balancing aesthetic coherence, thermal performance, sustainability principles and cultural authenticity. Ultimately, hybrid cooling systems integrating passive evaporative cooling, mechanical air movement, while air-conditioning associated with solar panels represent the most realistic thermal comfort compliance scenario during the peak heat period, it also helps control energy consumption.

REFERENCES

1. International Energy Agency. 2025. National climate resilience assessment for Algeria. Available: https://www.iea.org/reports/national-climate-resilience-assessment-for-algeria
2. Boudalia S, Gueroui Y, Zebsa R, Arbia T, Elhassen Chiheb A, Benada M, Hadri Z, Youcefi A and Bousbia A. 2023. Camel livestock in the Algerian Sahara under the context of climate change: Milk properties and livestock production practices. AGRIS, Food and Agriculture Organization of the United Nations.
3. Bajracharya SB. 2014. The thermal performance of traditional residential buildings in Kathmandu Valley. Journal of the Institute of Engineering 10(1):172-183.
4. Lotfabadi P and Hançer P. 2019. A comparative study of traditional and contemporary building envelope construction techniques in terms of thermal comfort and energy efficiency in hot and humid climates. Sustainability 11(13):3582.
5. ASHRAE. 2017. ASHRAE handbook: Fundamentals. Atlanta, GA: ASHRAE.
6. Bekkouche SMA, Ali Smadi A, et al. 2015. Energy savings approaches of buildings in hot-arid region, Saudi Arabia: Case study. Journal of Engineering Research 3:7-XX.
7. Kaddour A, Attia MEH, Arıcı M, Benbelgacem K and Driss Z. 2022. A numerical evaluation on the utilization of earth to air heat exchangers in arid regions (Ghardaïa, Algeria). Journal of Thermal Engineering 8(4):505-514. doi:10.18186/thermal.1150003.
8. Wanderlog. (2025). *Ghardaïa humidity and climate guide*. https://wanderlog.com
9. Meteostat. (2025). *Historical weather data for Ghardaïa, Algeria (Station 60566).* https://meteostat.net/en/station/60566

FROM "BLUEPRINT" TO "GREEN PRINT" NEW URBAN AGENDA: FOR SUSTAINABLE SOCIAL HOUSING DEVELOPMENT IN YAOUNDÉ BASED ON THE UN SUSTAINABLE DEVELOPMENT GOALS.

Erna Audrey Mangaleu Toukam[1], Harun Sevinç[1]*
[1] Eastern Mediterranean University, Department of Architecture, Faculty of Architecture, Famagusta, North Cyprus
*Corresponding author e-mail: audrey.mangaleu@emu.edu.tr

Ref # BES-03

ABSTRACT

Rapid urbanization in Yaoundé, Cameroon, has worsened the housing crisis. Conventional "blueprint" social housing relies on imported, standardized concrete designs that ignore the hot-humid tropical climate. This leads to thermal discomfort, heavy dependence on mechanical cooling, higher utility costs, and severe energy poverty among low-income households. This study proposes a shift from inefficient blueprint models to climate-protection settlements through the Green-Print model. The model integrates affordable housing with climate adaptation by combining renewable energy (mainly solar), energy-efficient technologies, passive cooling strategies (natural ventilation, shading), and culturally responsive spatial layouts adapted to Yaoundé's local conditions, cultural practices, and economic realities. The core research question is: How can social housing in Yaoundé be reconfigured into energy-efficient, affordable climate-protection settlements aligned with local tropical, cultural, and economic parameters? Using a User-Centered Design methodology, the research analyzes existing housing through field observations, stakeholder interviews, and energy performance simulations. It develops a replicable decision-making framework with context-specific guidelines for architects, planners, and policymakers. Evaluation of the Green-Print prototype shows significant reductions in energy consumption, improved indoor thermal comfort, lower operational costs, and better alignment with Cameroon's social housing goals and SDGs 7, 11, and 13. The study offers a transferable approach for sustainable, comfortable, and cost-effective social housing in tropical urban environments.

Keywords: Sustainable Social Housing, Green-Print Model, Climate-Responsive Architecture, Renewable Energy Integration, Energy Poverty, User-Centered Design, Affordable Housing, Tropical Urbanism.

1. INTRODUCTION

Architecture in Cameroon carries the imprint of successive colonial planning regimes under German, French, and British administration. Urban housing introduced during these periods relied on standardized "blueprint" models that prioritized administrative efficiency over climatic adaptation or socio-cultural fit [1], [2]. These typologies privileged non-porous materials, repetitive layouts, and centralized planning logic, marginalizing local bioclimatic knowledge shading, cross-ventilation, thermal-mass construction — proven effective in hot-humid tropical conditions [3]. Sub-Saharan Africa remains the fastest-urbanizing region globally, with Cameroon facing a persistent annual deficit of 150,000 housing units [4]. As of 2026, over 53% of the Cameroonian population lives in urban centres, driven by annual growth rates of 3.6–5% [5], [6]. The national housing shortfall stands at approximately 2.5 million units, most acutely felt in Yaoundé and Douala [7], [8]. State institutions such as the Société Immobilière du Cameroun (SIC) have perpetuated the same imported typologies, delivering estates primarily for civil servants while leaving low-income majorities underserved [9]. Climate vulnerability intensifies the crisis. Yaoundé's hot-humid conditions (Aw/Am classification) expose residents to persistent heat stress and flooding [10]. Thin concrete walls and corrugated metal roofing act as heat traps, raising indoor temperatures and forcing reliance on mechanical cooling that low-income households cannot afford [11]. The result is a compound crisis of structural deficit, energy poverty, climatic vulnerability, and socio-spatial inequality. This paper argues that a transition from the "Blueprint" to a "Green-Print" framework — integrating passive design, decentralized renewable energy, and participatory planning — is a structural imperative, not a luxury [12], [13].

1.1 Research Questions and Objectives

The core question is: How can social housing in Yaoundé be reconfigured into energy-efficient, affordable climate-protection settlements adapted to local tropical, cultural, and economic conditions? Sub-questions address (i) thermal performance of existing typologies; (ii) socio-economic barriers to energy access; (iii) the potential of passive design and solar systems to reduce energy poverty; and (iv) the policy framework required to institutionalize such a shift. Objectives are to analyse existing typologies, develop a Green-Print prototype, evaluate its performance through simulation, and produce replicable design and policy guidelines.

1.2 Conceptual Shift: Blueprint to Green-Print

Three structural barriers perpetuate Blueprint dependence: (i) architectural education in Cameroon remains dominated by Eurocentric curricula offering minimal bioclimatic design training **[24]**; (ii) national building codes do not mandate thermal comfort or ventilation performance benchmarks for social housing **[12]**; and (iii) the market default driven by SIC procurement rewards lowest upfront cost, not lifecycle performance.
The shift can be carried out as follows:

- Institutionally: through Regulatory reform Implementing building codes that mandate minimum shading coefficients and natural ventilation ratios for social housing.

- Community-Led Construction: Utilizing User-Centered Design (UCD) to educate residents on maintaining decentralized energy.

The Green-Print is not an incremental improvement of the Blueprint; it is a holistic systemic redesign across five dimensions (see Table 1 below)

Table 1. Comparative dimensions of the Blueprint and Green-Print housing models.

Dimension	Blueprint Model	Green-Print Model
Design Logic	Standardized, imported typologies	Contextual, climate-responsive design
Energy Role	Passive consumer	Active producer (solar, biogas)
Community Role	End-user recipient	Co-designer and stakeholder
Construction Material	Concrete-dominant (zinc roofing)	Earth blocks, timber, hybrid thermal mass
Lifecycle Thinking	Build and hand over	Maintain, adapt, and evolve
Design Knowledge	Imported expertise	Local bioclimatic + professional training

2. LITERATURE REVIEW AND CONTEXTUAL ANALYSIS

In hot-humid tropical climates like Yaoundé's, architecture must function as a passive climate machine rejecting heat and managing moisture without mechanical assistance [14]. Key strategies include high thermal mass materials such as compressed earth blocks (CEB) to dampen temperature swings, extended roof overhangs and *brise-soleil* to block direct solar gain, and cross-ventilation exploiting the stack effect to address relative humidity levels that frequently exceed 80% [15], [16]. Energy decentralization through Solar Home Systems (SHS) complements passive design by enabling household-level independence from an unreliable national grid, though tropical dust and humidity require dedicated maintenance protocols to prevent PV efficiency losses of up to 15% [17], [18]. Energy poverty is another issue which in this context is not simply a lack of access it is the high cost-to-income ratio of maintaining basic domestic functions. Thermally inefficient Blueprint dwellings trap heat, forcing residents to choose between discomfort and unaffordable mechanical cooling. Passive design therefore functions simultaneously as an environmental and economic intervention, freeing household income for education and healthcare [11]. Finally, international frameworks such as LEED and BREEAM are poorly suited to this reality: they reward imported high-tech systems unavailable or unmaintainable locally. This research instead proposes a localized sustainability matrix valuing low-carbon local materials, informal construction labour, and indigenous bioclimatic knowledge over high-cost international benchmarks [21].

3. METHODOLOGY

The study adopts a User-Centered Design (UCD) methodology emphasizing participatory and iterative processes. Rather than imposing standardized technical solutions, community knowledge is integrated into the design process. This approach aligns with contemporary sustainable urban frameworks emphasizing resilience, inclusivity, and environmental performance [11] see figure 2 .

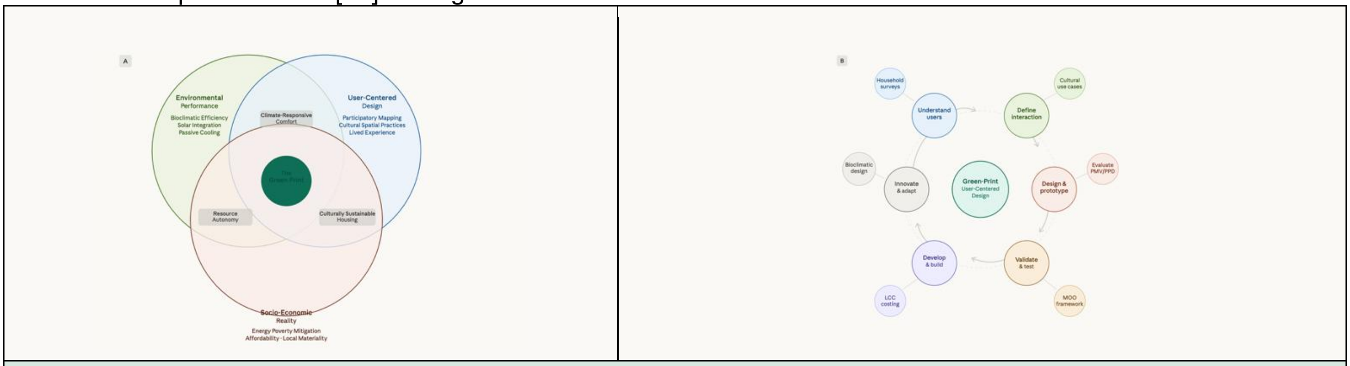

Figure 4.1 — The Green-Print UCD Framework (A) and Methodology Cycle (B)

User-Centered Design (UCD) is essential for aligning sustainable housing with the social realities of Yaoundé's residents. Housing failures in African contexts often stem from cultural misalignment rather than technical shortcomings [15]. Key considerations include semi-open spaces to accommodate outdoor cooking and biomass fuel use, and spatial layouts that reflect collective living and informal economic activity. The "Green-Print" framework embeds UCD to promote long-term user acceptance rather than imposing rigid technical solutions [5].A mixed-methods approach bridges technical performance and human experience. Quantitative: EnergyPlus simulations to model indoor temperatures and PV yields. Qualitative: Resident interviews to identify "cultural mismatches" in current housing. Optimization: Prototype validation via Multi-Objective Optimization (MOO) targeting a 4°C–8°C reduction in peak indoor temperatures.

4. LIMITATIONS

While the study develops a replicable model, its immediate application is confined to the climatic, cultural, and socio-economic context of Yaoundé. Broader applicability to other tropical cities may require contextual adaptation. The limitation considered as follows: Geographical Scope: Focused on Yaoundé, Cameroon, with analysis of urban housing typologies, climatic conditions, and socio-economic realities. Thematic Scope: Sustainable social housing, renewable energy integration, climate-responsive architecture, and energy-efficient design strategies. Methodological Scope: Utilizes User-Centered Design, field observations, stakeholder interviews, and energy performance simulations to develop and evaluate the Green-Print prototype.

5. YAOUNDÉ'S CONTEXTUAL PROFILE

Yaoundé's Aw/Am transitional climate persistent humidity above 80% and low diurnal temperature range produces Urban Heat Islands in dense neighbourhoods **[10]**. Over 60% of residents occupy informal settlements with no basic services. High unemployment makes upfront cost the decisive barrier to improved housing. Spatial needs consistently identified in field surveys include flexible outdoor cooking areas, transitional veranda spaces, and adaptable multi-generational layouts **[7]**.

6. THE GREEN-PRINT MODEL AND THE KIGALI PRECEDENT

Kigali's affordable housing programme, developed with the Rwanda Housing Authority and international partners, offers a compelling proof of concept for the Green-Print approach in Sub-Saharan Africa.Key features mirroring Green-Print principles include compressed earth block construction reducing peak indoor temperatures by 4–6°C; calibrated roof overhangs (600–900 mm) eliminating wall solar gain without compromising PV output; cross-ventilation corridors aligned with prevailing easterly winds; rooftop PV arrays (1.5–2 kWp/unit) with shared storage achieving 70–80% energy autonomy; and semi-covered communal courtyards supporting cooking, socializing, and small-scale commerce.The programme cut household energy expenditure by ~40% versus conventional estates and kept construction costs within 15% of standard concrete-block equivalents through local sourcing and skills transfer. This precedent confirms the Green-Print thesis: climate-responsive, affordable, and culturally appropriate social housing is not aspirational — it is already achievable within realistic budgetary and institutional constraints.

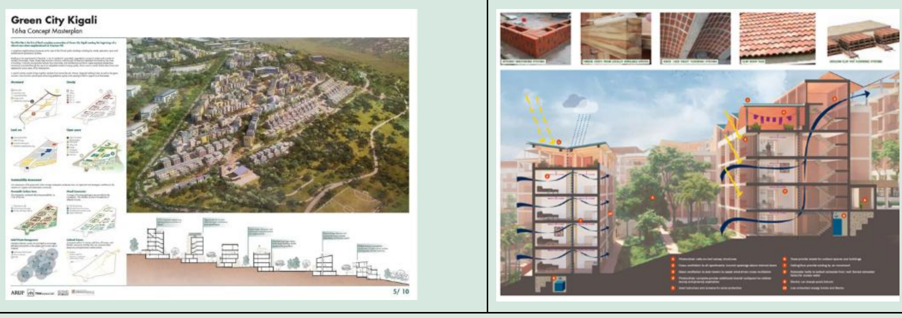

Kigali climate-responsive affordable housing: (a) aerial view showing courtyard typology; (b) section illustrating cross-ventilation, roof overhang, and PV integration (source: Rwanda Housing Authority [22]).

6.2 GREEN-PRINT DESIGN TYPOLOGY PRINCIPLES FOR YAOUNDÉ

A layered system of design strategies operating simultaneously across three interdependent dimensions: environmental performance, energy autonomy, and social fit. Each dimension is necessary but insufficient alone their integration is what distinguishes the Green Print from incremental improvement of the Blueprint model. Passive Cooling and Shading; Buildings are oriented with primary facades on the north-south axis to minimize east and west solar exposure, Renewable Energy Integration ; Each housing cluster incorporates a modular rooftop PV array (1.5–2.5 kWp), solar thermal water heaters, and provision for a community mini-grid with battery storage, Culturally Adaptive Spatial Layout; Multi-generational unit configurations include a semi-covered external cooking terrace, flexible internal room partitions, and shared courtyard spaces with shade trees and permeable paving. Water Efficiency and Low-Carbon Materials Integration of water efficiency as an inseparable component of overall resource management: Rainwater harvesting Greywater recycling.Low-flow fixtures and water-efficient sanitation Permeable surface design These features emerges directly from resident participatory workshops and align with the UCD evidence base [20].

7 CONCLUSION

The housing crisis in Yaoundé is not merely quantitative; it reflects a qualitative failure of imported construction models to ensure thermal comfort, energy equity, and cultural relevance **[7], [11]**. This research advocates a transition from the “Blueprint” to a new “Green Print” prototype, representing a systemic recalibration of social housing in Cameroon. The "Green-Print" model offers a modular, scalable framework for Sub-Saharan urban centers to address the dual challenges of heat stress and energy poverty. By prioritizing locally sourced bio-based materials and passive cooling, this research advocates for a systemic shift from imported "blueprint" models toward climateprotective settlements that ensure thermal comfort and energy equity. While conventional housing in Yaoundé has historically overlooked climatic responsiveness, this study identifies a clear path forward through three strategic pillars: Building Code Reform: Integrating mandatory thermal comfort and natural ventilation standards into national housing policies. Financial Incentives: Implementing micro-subsidies and tax exemptions to encourage the adoption of decentralized solar PV systems. Capacity Building: Training local contractors in bioclimatic construction to reduce reliance on foreign expertise and foster local resilience. By aligning architectural design with the lived realities of residents, the Green-Print model directly supports SDG 7, 11, and 13. In rapidly urbanizing Africa, environmentally responsive housing is no longer an optional path to modernization; it is a structural imperative for achieving equitable and climate-resilient urban futures. Final implementation will require coordinated efforts across housing policy, renewable energy planning, and regulatory frameworks to ensure social housing simultaneously addresses the housing shortage and climate protection.

REFERENCES

[1] Njoh, A.J. (2004). The experience and legacy of French colonial urban planning in sub-Saharan Africa. Planning Perspectives, 19, 435–454.

[2] Njoh, A.J. and Bigon, L. (2015). Germany and the deployment of urban planning to create, reinforce and maintain power in colonial Cameroon. Habitat International, 49, 71–81.

[3] Britannica (n.d.). African architecture – Forest dwellings. [Online] Available at: https://www.britannica.com/art/African-architecture/Forest-dwellings

[4] Djatcheu Kamgain, H. and Mounvera, A. (2022). Urbanization and the housing challenge in Cameroon: A review of the Olembé social housing project. Journal of African Urban Studies, 4(2), 88–104.

[5] UN-Habitat (2024). World Cities Report 2024: Urbanization and Climate Resilience. Nairobi: United Nations Human Settlements Programme.

[6] World Bank (2025). Cameroon Economic Update: Navigating Urban Expansion. Washington, DC: World Bank Group.

[7] Ahmadou, S. and Okpwe Mbarga, R. (2022). Social housing in Cameroon: State of the affairs. International Journal of Emerging Technologies and Innovative Research, 9(11), f157–f167.

[8] Ministry of Housing and Urban Development [MINHDU] (2024). National Program for Social Housing: 2024 Progress Report. Yaoundé: Government Press.

[9] Société Immobilière du Cameroun (SIC) (n.d.). About us. [Online] Available at: https://sic.cm/en/about-us

[10] Bang, H. et al. (2023). Climate change and urban vulnerability in the Congo Basin: The case of Yaoundé. African Geographical Review, 42(3), 312–329.

[11] Mouchili, I. and Mougoué, B. (2023). Thermal performance and energy poverty in social housing: The case of Central Africa. Sustainable Cities and Society, 91, 104–118.

[12] MINHDU (2024). All starts at home: Local actions for sustainable cities and communities. [Online] Available at: https://www.minhdu.gov.cm/

[13] United Nations (2017). New Urban Agenda. [Online] Available at: http://habitat3.org/the-new-urban-agenda/

[14] Nkuina, C. (2024). Bioclimatic architecture as a potential for developing countries. HAL Open Science. [Online] Available at: https://hal.science/

[15] Kameni Nematchoua, M. et al. (2025). Reducing the environmental footprint of urban housing in Sub-Saharan Africa: A case study of Cameroon. Buildings, 15(12), 2141.

[16] Bah, I. (2025). Normative pluralism and socio-environmental vulnerability in Cameroon. Urban Science, 9(6), 219.

[17] International Energy Agency (2022). Africa Energy Outlook 2022. Paris: IEA. [Online] Available at: https://www.iea.org/

[18] World Bank (2021). Climate Risk Profile: Cameroon. Washington, DC: World Bank Group.

[19] Njoh, A.J. (1999). The state, urban development policy and society in Cameroon. Cities, 16(4), 275–286.

[20] UN-Habitat (2023). Cameroon Country Profile: Building inclusive and sustainable cities. Nairobi: United Nations Human Settlements Programme.

[21] Kameni Nematchoua, M. et al. (2025). [See ref. 15 above — green certification critique.] Buildings, 15(12), 2141.

[22] Rwanda Housing Authority (2023). Affordable and Climate-Responsive Housing Programme — Kigali Pilot Report. Kigali: Government of Rwanda.

[23] UN-Habitat (2022). World Cities Report 2022. Nairobi: United Nations Human Settlements Programme. [Online] Available at: https://unhabitat.org/

[24] Djatcheu Kamgain, H. and Mounvera, A. (2022). [See ref. 4 — curriculum and capacity discussion.] Journal of African Urban Studies, 4(2), 88–104

DYNAMIC SIMULATION OF A SOLAR ASSISTED COOLING SYSTEM FOR RESIDENTIAL PURPOSE IN THREE CITIES IN TURKEY

Oluwaponmile David Alao[1], Muhammad Abid [2], Mustafa Dagbasi[1]*
[1] Department of Energy Systems Engineering, Cyprus International University, Lefkosa, Turkey
[2] Department of Energy Systems Engineering, Universiti Darussalam, Brunei
*Corresponding author e-mail: davepommyalao@gmail.com

Ref # BES-04

ABSTRACT

This paper designs and describes the modeling and dynamic simulation of an absorption solar cooling system. This is performed in the transient TRNSYS environment for a typical single-story residential building and simulated for the climatic conditions of three cities in Turkey: Antalya, Adana and Ankara. Adana and Antalya's hot Mediterranean subtropical climate, and Ankara's solar energy potential make the three cities suitable locations for the operation of solar absorption cooling systems. A 17.6 kW capacity absorption chiller is used in the cooling system with a 120m^2 evacuated tube collector. The findings showed that the energy efficiency of 63.54%, 48.87% and 43.75% were obtained for the proposed cooling system for the cities of Antalya, Adana and Ankara respectively, utilizing an indoor air set point temperature of 24◦C for the considered building.

Keywords: Solar cooling, Dynamic simulation, Absorption chiller, Turkey, TRNSYS

INTRODUCTION

Global energy demand is rising at an unprecedented rate, and with the depletion of fossil fuel reserves alongside the harmful increase in greenhouse gas (GHG) emissions, there is an urgent need to adopt sustainable, eco-friendly energy sources. This transition is crucial not only to mitigate environmental damage but also to ensure the optimal performance of mechanical and electrical systems. As a result, the utilization of renewable energy technologies has become a significant development in powering systems efficiently while minimizing environmental impact. Due to its geographical location, Turkey has a high energy potential with an annual average daily solar radiation of 3.6 kWh/m^2 [1]. Antalya, which is located on the Mediterranean coast and the Southwestern part of Turkey, is one of the few Turkish metropolitan cities with a very sunny climate. The summer periods are hot and dry while the winter is generally mild. Antalya experiences nearly 3000 hours of sunlight annually, making it very sunny with the presence of abundant solar energy. It is a vital requirement to reduce the indoor temperature of buildings for the comfort of the residents and the numerous tourists flooding the popular tourist city. Adana, also located in the Mediterranean region, has hot and dry summers with the maximum daily average temperature around 28 ^{o}C. It has mild and rainy winters [2]. Ankara, located in the Central Anatolia Region of Turkey, also has a high solar energy potential, with the maximum daily temperature reaching its peak at above 35^{o}C during the summer season. The sunny climatic condition, therefore, provides a ready tool for the application of solar cooling in buildings in these three cities in Turkey.

Turkey's unique geographical location characterized by its diverse climate and topography offers an immense potential for harvesting renewable energy, especially solar energy. Solar-driven cooling systems are promising both in terms of energy savings and lower environmental impact. Although several previous works on the dynamic simulation and performance of solar-powered cooling system for small scale applications can be found in literature [3], [4], very few studies have investigated the technical feasibility of using the vast solar resources in Turkey for combined cooling and hot water production purposes. Also, unlike some of these related works, which typically focus on a single climatic condition within Turkey, the present study fully performs dynamic simulation and analysis of the cooling system, evaluating the performance across three distinct climatic regions within the country. This approach provides profound insight into how operational behavior, as well as the system configuration vary with climatic conditions. By modeling the geometry of the real building using sketchup and the Trnsys3d extension, before importing into the TRNSYS studio environment, the study is able to provide a realistic and more effective assessment of the building cooling energy requirements across diverse climates. The study goes ahead to assess the optimal factors for improving the efficiency of the proposed solar driven cooling system. Therefore, in this present paper, the development and transient simulation of a solar-powered absorption cooling system was carried out using TRNSYS software for a typical meteorological year file containing the weather data of three cities in Turkey: Antalya, Adana and Ankara. The simulation and system optimization was carried out, with the system behavior observed for enhanced performance.

BUILDING DESCRIPTION AND COOLING LOAD CHARACTERIZATION

In order to adequately illustrate the real-life system, an initial modeling of a single-story residential building was carried out for the determination of the residential condition and occupied space. This is done using SketchUp and TRNBuild which is a section of the TRNSYS simulation program. The modelled building has a total area of 96 m2 with a volume of 336 m3. For the determination of the average u-values of the construction materials used for the building layers, the Turkish Standard TS 825 which specifies the thermal insulation requirements for buildings served as the guiding principle. In TS 82, specifications that are lesser than those in the standard values are also recommended for efficiency measures (Turkish Standard Institute, 2008). The external walls consist of four layers viz: Finish, Plater, Airspace and Brick. The total thickness of the external wall is 0.400m while its thermal resistance coefficient is 0.485 W/m2K. The windows thermal insulation coefficient is 1.1 W/m2K while the g-value is 0.62. For the building conditioning design, the energy gain due to lights, people, and electrical equipment are 13.5 KJ/hr, 560 KJ/hr, and 1000 KJ/hr, respectively. The maximum set temperature for the building indoor air is 24°C.

SYSTEM DESCRIPTION

The modeling and simulation of the proposed system was performed with TRNSYS software (Fig. 1). The weather conditions of a typical meteorological year (TMY) file for Antalya, Adana and Ankara obtained from Meteonorm software were employed for the simulation [5]. The cooling system consists of an evacuated tube solar collector represented by

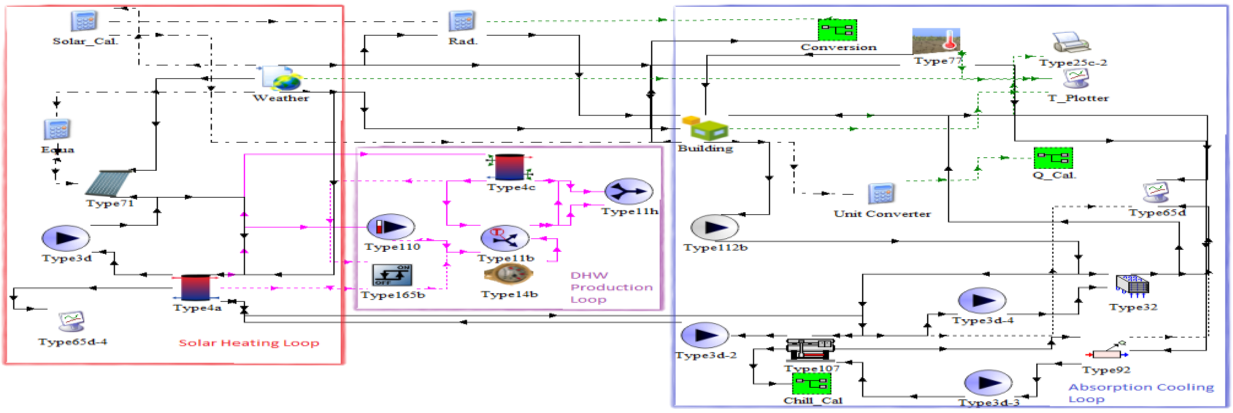

Fig. 1. TRNSYS Model of the Solar Absorption Cooling System

Type 71 in TRNSYS. The solar collector supplies the energy it receives from the sunlight to the load through a thermal storage tank at 85 °C. The thermal storage tank is therefore able to supply heat energy to the load which consists of the absorption chiller unit and the domestic hot water (DHW) unit. The hot water transferred to the generator of the absorption chiller from the thermal storage tank is employed to evaporate the refrigerant and subsequently the absorption chiller supplied chilled water to the air-cooling coil represented by Type 32. A single speed fan represented by Type 112 circulates the room air through the cooling coil. The cooling load is supplied to the system by coupling the building model with the cooling system using Type 56. The total annual cooling loads generated are 16218.12 KJ/hr, 14582.97 KJ/hr, and 14405.12 KJ/hr in a 336 m^3 residential building located in Antalya, Adana and Ankara, respectively. The occupancy schedule in a working day with a maximum of four people considered to live in the building is from 4:00 pm to 8:00 am. A variable air changing rate was set up for the building and added to the zone similar to [6], [7]. The absorption chiller represented by Type 107 is a hot water-fired single-effect absorption chiller modeled after Yazaki WFC-SC5 which is a Lithium bromide – water absorption chiller with rated capacity of 17.6 kW. Hot water stream serves as the input energy into the chiller's generator. The solar collector total area is 120 m^2 and the thermal storage tank capacity is 5 m^3. The solar energy stored in the thermal storage tank is also used to produce DHW for the building's occupants through the DHW tank which has a capacity of 1.5 m^3. For the typical application such as laundry, dish washing and showering, the hot water delivery set point temperature is 60 °C. This is achieved through the use of a tempering valve and tee-piece (Fig. 1). The tempering valve adjusts the hot water output temperature from the DHW tank to the set point temperature. It is coupled with the tee-piece flow mixer to mix the higher temperature stream from DHW tank and low temperature stream from the city water mains to achieve a steady temperature delivery of 60°C for domestic usage. The variable pump located between helps to recirculate the heated water back into the tank. It is controlled by differential controller.

RESULTS AND DISCUSSION

The dynamic simulation with TRNSYS was run on the cooling system under the metrological data of Antalya, Adana and Ankara in Turkey with a simulation time step of 0.125 hr. and the results were obtained. The cooling load profile was instrumental in the sizing of system's operational parameters, with the maximum value of cooling demand for Antalya, Adana and Ankara obtained as 16218.12 KJ/hr, 13832.4 KJ/hr, and 12798.06 KJ/hr, respectively. These occur during the Summer in July, and they represent the maximum cooling rate at any day of the year for the three cities respectively. The solar resource in the three cities is high, resulting into higher amount of solar energy for the collector array. However, the overall system energy efficiency and the thermal COP of the system for the city of Ankara is noticeably lower as compared to Antalya and Adana. The overall thermal energy efficiency achieved by the designed solar absorption cooling system was 63.54%, 48.87% and 43.75% for the cities of Antalya, Adana and Ankara respectively (Table 1).

Table 1. System performance in Antalya, Adana and Ankara

Parameter	City		
	Antalya	Adana	Ankara
Maximum collector outlet temp. (°C)	110.4	109.5	108.6
Thermal COP	0.72	0.66	0.62
System Energy Efficiency (%)	63.54	48.87	43.75

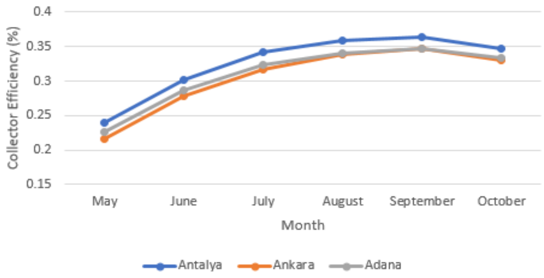

Fig. 2. Monthly variation of collector array efficiency

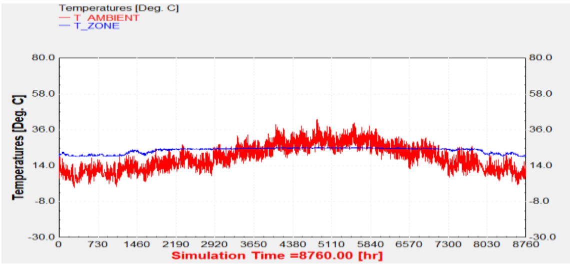

Fig. 3. Simulated building room temperature and ambient temperature variation for a year

The monthly variation of the collector array efficiency in the three cities for the sunny months of May to October is shown in Fig. 2. Antalya with higher monthly average sunshine hours has higher collector efficiencies compared to Adana and Ankara. The cooling system was able to maintain the room temperature of the building around the set point temperature, that is 24 °C throughout the year which includes the summer period and in July when the ambient temperature was above 40 °C at certain days (Fig. 3). Fig. 4 and Fig. 5 show the performance of the absorber cooling system's solar collector for the three Turkish cities on a typical hot day over a 24-hour period. The simulation was run for the 6th of July. After 7:00am, the temperature of the solar collector water starts to rise due to the Sun radiation. Between the hours of 12:00 noon and 14:00 when the sun radiation was high, the output temperature of the collector for the three cities reaches its peak which 110.4, 108.6 and 108.0 for Antalya, Ankara and Adana respectively (Fig. 4). Fig. 5 shows the solar collector energy gain for the three cities and it can be seen that at similar time intervals, the collector has maximum energy gain to the collector, which peaked at around 13:00.

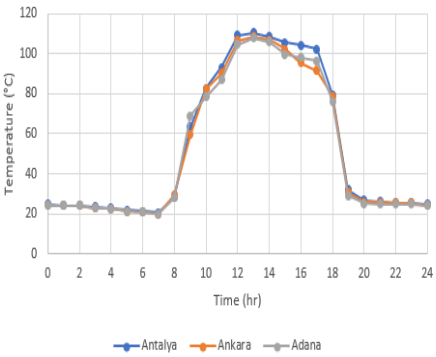

Fig. 4. Hourly variation of collector outlet temp.(July 6th)

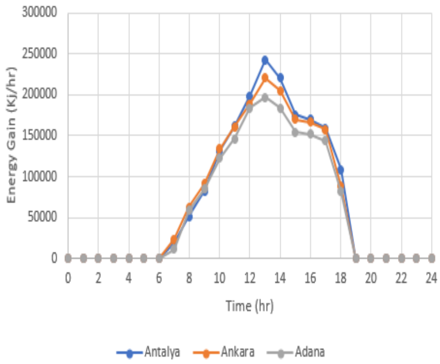

Fig. 5. Hourly variation of solar collector energy gain (July 6th)

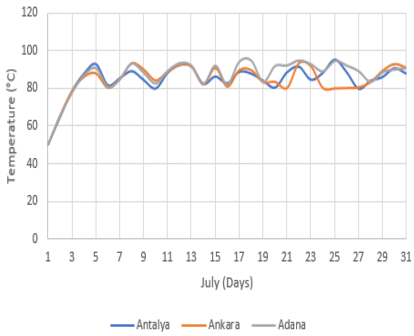

Fig. 6. Main storage tank outlet temperatures for the month of July

Fig. 6 depicts the variation of the main storage tank temperature for the three cities run for the month of July which has the highest solar irradiance. The temperature of the main storage tank for the three cities rarely drops below 70 °C and the peak values are 95 °C, 93.65 °C and 94.49 °C for Antalya, Ankara and Adana respectively. The optimization of the system parameters was performed by carrying out a number of runs in TRNSYS simulation studio in order to determine some variable values at which the system is able to achieve the highest efficiency without oversizing issue. The solar collector surface area, the solar collector mass flow rate and the main storage tank volume are all considered for optimization. The results show that increase in the solar collector area has significant increase on the collector efficiency (Fig. 7). Consequently, 120 m^2 is regarded as the optimal value of the collector area for this system as efficiencies of 0.5,0.48 and 0.49 could be achieved for the cities of Antalya, Ankara, and Adana respectively.

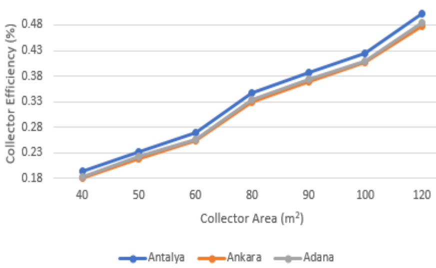

Fig. 7. Variation of collector efficiency with collector area for collector slope of 20 °C

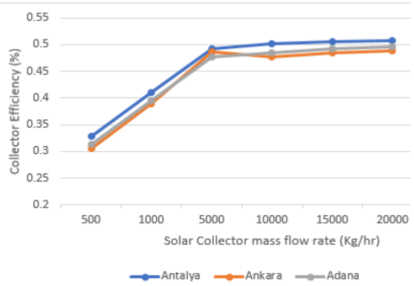

Fig. 8. Variation of collector efficiency with the collector mass flow rate

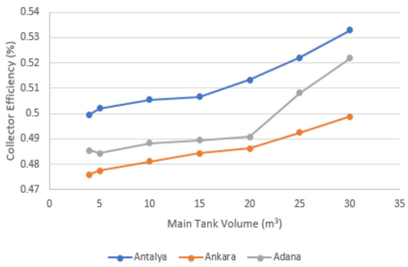

Fig. 9. Variation of collector efficiency with main storage tank volume

It can be observed from Fig. 8 that hot water flow rate in the solar collector of 10,000 kg/hr significantly raises the collector efficiency above 0.5 for the city of Antalya (i.e. 0.51) and 0.5 and 0.49 for the cities of Adana and Ankara respectively. The variation in the collector mass flow rate from 10,000 kg/hr to 20,000 kg/hr represents no substantial variation with respect to the collector efficiency. Usually, as the flow rate through the collector increases, there is less time for the collector to transmit its heat to the incoming stream. It is thus vital to obtain an optimal flow rate to ensure adequate collector's performance. Fig. 9 shows the variation of the main storage tank volume with collector efficiency. The system simulation reveals that the minimum volume at which the needed hot water volume could flow to the absorption chiller is 4 m^3. The initial 5 m^3 chosen is therefore used as the optimum value. It is also observed that storage tanks with smaller size results in less energy consumption by the boiler of an absorption refrigerating system [8].

CONCLUSIONS

This study has carried out numerical simulation-based performance analysis of a solar powered absorption cooling system making use of TRNSYS simulation program with the cooling load generated from a modeled single-story residential building using both SketchUp and TRNBuild. The results show that an evacuated tube solar collector with an area of 120 m^2 feeding a 5m^3 thermal storage tank with hot water to drive an absorption chiller with rated capacity of 17.6 kW at an average generator driving temperature of 80 °C and also supply DHW to the occupants is sufficient to adequately operate the cooling system for long-term performance. The study investigates the dynamic behavior of the cooling system for combined performance of air-conditioning of a typical residential building and hot water production in the cities of Antalya, Ankara, and Adana. The utilization of solar energy for cooling of buildings in regions with high solar radiation and cooling demand as in Antalya, Ankara, and Adana regions is very advantageous in terms of environmental consideration and simplicity. The proposed solar-cooling system's performance for three Turkish climatic conditions has shown promising results, with its attendant benefits on climate change mitigation and the move towards more sustainable buildings. It can be further validated in future work through the performance comparison with a real system.

REFERENCES

[1] A. N. Çelik and A. N. Çelik, "Analysis of Ankara's Exposure to Solar Radiation: Evaluation of Distributional Parameters Using Long-Term Hourly Measured Global Solar Radiation Data," *TURKISH J. ENG. ENV. SCI*, pp. 115--126, 2006.

[2] R. Tuğrul Oğulata and S. Noyan Oğulata, "Solar radiation on Adana, Turkey," *Appl. Energy*, vol. 71, no. 4, pp. 351–358, Apr. 2002.

[3] D. Redpath, A. Paneri, H. Singh, A. Ghitas, and M. Sabry, "Design of a Building-Scale Space Solar Cooling System Using TRNSYS," *Sustainability 2022, Vol. 14,* vol. 14, no. 18, Sep. 2022, doi: 10.3390/SU141811549.

[4] M. S. A. Khan, A. W. Badar, T. Talha, M. W. Khan, and F. S. Butt, "Configuration based modeling and performance analysis of single effect solar absorption cooling system in TRNSYS," *Energy Convers. Manag.*, vol. 157, pp. 351–363, Feb. 2018, doi: 10.1016/j.enconman.2017.12.024.

[5] "Meteonorm 8." Accessed: Sep. 12, 2021. [Online]. Available: https://meteonorm.com/

[6] R. Alayi, A. Kasaeian, and F. Atabi, "Thermal analysis of parabolic trough concentration photovoltaic/thermal system for using in buildings," *Environ. Prog. Sustain. Energy*, vol. 38, no. 6, p. 13220, Nov. 2019.

[7] E. Marrasso, C. Roselli, M. Sasso, F. Tariello, and F. Calise, "Analysis of a Hybrid Solar-Assisted Trigeneration System".

[8] G. A. Florides, S. A. Kalogirou, S. A. Tassou, and L. C. Wrobel, "Modelling and simulation of an absorption solar cooling system for Cyprus," *Solar Energy*, vol. 72, no. 1, pp. 43–51, Jan. 2002.

POTENTIAL OF BIOGAS PRODUCTION USING ANIMAL WASTE IN POWER SECTOR: AN ENERGY AND EXERGY ANALYSIS

Ibrahim Modibbo Ahmed[1], Ertan Akun[1], Rena Kidak[3]*
[1]Cyprus International University, Department of Energy Systems Engineering, Lefkosa, Mersin 10, Turkey
[2]Cyprsu International University, Department of Petroleum and Natural Gas Engineering, Lefkosa, Mersin 10, Turkey
[3]Cyprus International University, Department of Environmental Engineering, Lefkosa, Mersin 10, Turkey
[*]Corresponding author: modibbo.edu@gmail.com

REF # BIO-01

ABSTRACT

This study investigates the biogas production potential of animal wastes in through laboratory experiments and energy modeling. Cow dung (CD), egg-laying chicken manure (EC), and meat chicken manure (MC) were evaluated in co-digestion setups under mesophilic conditions (35 °C) using 720 mL batch digesters with a 20-day retention time. Experimental results showed the ternary mixture of (CD+MC+EC) achieved 17.38mL/g TS**.** The produced biogas was modeled as a fuel input in a Brayton cycle-based power generation system. Energy and exergy analyses were conducted to evaluate system performance, efficiency, and irreversibility distribution. The simulation results indicate a net-work output of 105.3 kJ/kg and a thermal efficiency of 37%, demonstrating the feasibility of utilizing biogas derived from animal waste as a renewable fuel for gas turbine power generation. Because of combustion irreversibilities, the analysis also showed that the combustion chamber accounts for the majority of exergy destruction. Overall, the combination of thermodynamic power cycle analysis and anaerobic digestion offers insightful information on the potential of waste-derived biogas for sustainable energy production.
Keywords: Anaerobic digestion, Animal waste, Biogas, Energy analysis, Exergy analysis

INTRODUCTION

As an alternative to fossil fuels or non-renewable energies, biogas generated from waste-derived biomass is a feasible renewable energy source [1]. Anaerobic digestion (AD) is a biological process that breaks down complex organic materials into simpler chemical components in the absence of oxygen [2,3]. AD produces biogas, which is composed of 35% CO_2, 65% CH_4, and trace gases such as H_2S, N_2, and H_2. The main substrates for the AD process that produces biogas are organic waste, such as crop residues and animal manure or wastes [1]. Animal waste includes cow dung, poultry waste, fish waste, etc. Cow dung, sometimes referred to as cow manure, is primarily composed of broken-down grass plus grains, fruits, or vegetables, depending on what the animals were fed. It contains traces of hay, straw, bedding, grains, and other organic materials that were used to feed the cows [4]. On the other hand, meat chicken manure refers to the waste produced by chickens that are specifically bred for their meat. Meanwhile, egg chicken manure is waste produced by chickens specifically bred for their eggs [4].

Studies demonstrated in the context of industrial companies, renewable energy sources, and energy efficiency research play a significant role in addressing these issues in terms of resource efficiency and pollution reduction [5]. Waste-to-energy conversion is a popular renewable energy source and an effective waste management technique [5,6]. Through the conversion of organic matter into biogas AD is a sustainable approach to waste management that reduces pollution from industrial and agricultural processes, recovers resources and energy, and balances the operational use of fossil fuels and protects the environment [7].

The biogas production potential using corn straw has been evaluated by Zhong et al. [9] the result of biogas yield for 5, 10, 15, and 20 days is 286, 306, 342, and 365 mL/gram of volatile solids. This study also demonstrated that the longer the retention time, the higher the biogas yield. The potential for producing biogas from municipal sewage sludge was assessed by Zhou et al. [8] The AD was conducted at 37 degrees Celsius, and the pH was 8.2. The biogas yield per volatile solid was found to be between 260.5 and 342.1 milliliters per gram of volatile solid.

Although a number of earlier studies have looked at the biogas potential of animal and agricultural wastes in different regions, such as Turkey, Iran, and Southeast Asia, many of these studies rely heavily on theoretical or numerical estimations based on outdated statistical data and lack substrate-specific experimental validation.

Therefore, there is an urgent need for new, experimentally based research that includes biodegradability assessment, energy potential modeling. The key objectives of this research are:

[1] To experimentally evaluate the biogas production efficiency of Co-digested CD+EC+MC substrates under mesophilic condition.
[2] To Simulate the energy conversion performance of the produced biogas in a Brayton Cycle-based power generation system.
[3] To Perform energy and exergy analyses pf the proposed power generation system, identify efficiency, exergy destruction and irreversibility distribution.

MATERIALS AND METHODS

Fresh substrate of cow dung, egg-laying chicken manure, and meat-chicken manure were collected from the Cyprus International University farm located in Lefkosa, Mersin 10, Turkey, and immediately transferred into large airtight plastic containers. Using the three different fresh samples which have been collected, seven experimental samples were prepared on equivalent mass ratios for every set of experiment.

The pH, which measures the acidity or alkalinity of a substance, was measured for each sample using a pH meter according to APHA 4500-H^+ B [10]. Chemical Oxygen Demand (COD) which measures the amount of organic matter (expressed in oxygen equivalents) present in the substrate that can be oxidized biologically or chemically is measured using APHA 5220 D. The moisture and total solid (TS) content are measured using APHA 2540 B and the Volatile Solid (VS) is measured using APHA 2540 standard [10]. Each test is performed three times and the average readings is presented in the Table 1. In this study, initial values in the tables refer to the measurements taken on the feedstock samples before undergoing AD, whereas final values correspond to the measurements taken on the digestate after completion of the AD process.

Table 1 Initial and Final Test from Each Substrate for the Second Sets

Parameter	CD		EC		MC	
	Initial	Final	Initial	Final	Initial	Final
pH	6.09	6.98	7.55	7.56	7.65	5.76
COD (mg/L)	84,763.75	23,448.1	70,970	90,660.25	76,487	123,073
Moisture (%)	82	87	71	96	7	81
TS (%)	18	13	29	4	93	19
VS (%)	14.57	11.93	20.53	10.6	8.38	8.2

A 20g of each sample is weighed and co-digested with 350 mL of wastewater collected from a water treatment plant in Cyprus International University. The samples were properly mixed using a paddle mixer. The samples were then fed to a digester of 720 mL volume and are further placed in an electric bath containing water supplying heat at 35℃. This means that the digester operated in a mesophilic condition [6], and this condition is selected because mesophilic systems exhibit better process stability and higher richness in bacteria [2]. Each digester has a tube that is connected to a water container filled with water. The water container has an outlet tube placed in a measuring cylinder to measure the quantity of water displaced due to the biogas production effect as shown in Fig. 1. Therefore, the measured quantity of the displaced water is assumed to be the quantity of biogas produced, according to Kalloum et al. [25]. The biogas yield per unit mass of total solids from each sample is obtained using Eq. 1.

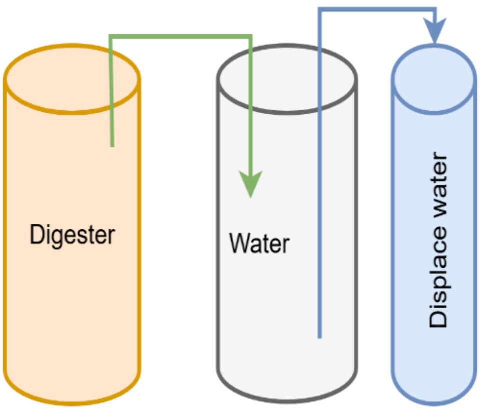

Fig. 1. Experimental Set-up

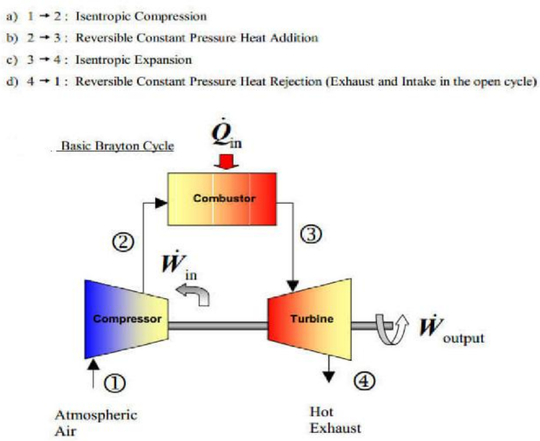

Fig. 2. Proposed Brayton cycle

$$\mathrm{BYts} = \frac{\mathrm{TBP}}{\mathrm{M}} \tag{1}$$

Where BYts is the biogas yield per kilogram of total solid (mL/kg), TBP is the total biogas produced over the retention time (mL), and M is the total solid mass of the substrate (g).

The produced biogas was modeled as fuel input to a simple open Brayton cycle shown in Fig. 2 consisting of a compressor, combustion chamber, and gas turbine. The governing equations for both energy (First Law) and exergy (Second Law) analyses are summarized in Table 2 and the input specification are listed in Table 3.

Table 2 List of Thermodynamics equations Used in the Model

Component	Energy Balance (First Law)	Exergy Balance (Second Law)	Efficiency Definition
Biogas Fuel Input	$\dot{Q}\_in = \dot{m}\_bg \times LHV\_bg$	$\dot{E}\_fuel = \dot{m}\_bg \times ex\_ch,bg$	-
Compressor	$W\_c = \dot{m}\_air (h_2 - h_1)$	$\dot{E}\_D,c = \dot{m}\_air (ex_1 - ex_2) + W\_c$	$\eta\_c = (h_2s - h_1) / (h_2 - h_1)$
Combustion Chamber	$\dot{m}\_air\ h_2 + \dot{m}\_bg\ LHV\_bg = \dot{m}\_gas\ h_3$	$\dot{E}\_D,cc = \dot{E}\_fuel + \dot{m}\_air\ ex_2 - \dot{m}\_gas\ ex_3$	$\eta\_ex,cc = (\dot{m}\_gas\ ex_3) / (\dot{E}\_fuel + \dot{m}\_air\ ex_2)$
Turbine	$W\_t = \dot{m}\_gas (h_3 - h_4)$	$\dot{E}\_D,t = \dot{m}\_gas (ex_3 - ex_4) - W\_t$	$\eta\_t = (h_3 - h_4) / (h_3 - h_4s)$
Net System	$W\_net = W\_t - W\_c$	$\dot{E}\_D,total = \Sigma\ \dot{E}\_D,i$	-
Thermal Efficiency	$\eta\_th = W\_net / \dot{Q}\_in$	-	-
Exergy Efficiency	-	$\eta\_ex = W\_net / \dot{E}\_fuel$	-

Table 3 In-put Specification of the Model

Item	Symbol	Value	Unit
Methane mole fraction	x_CH4	0.60	-
CO2 mole fraction	x_CO2	0.40	-
Compressor inlet pressure	P1	1	atm
Compressor inlet temperature	T1	298	K
Compressor discharge pressure	P2	10	atm
Turbine inlet temperature	T3	1300	K
Compressor efficiency	ηc	0.85	-
Turbine efficiency	ηt	0.90	-
Combustion efficiency	ηcomb	0.95	-
Dead-state temperature	T0	298	K
Dead-state pressure	P0	1	atm
Methane LHV	LHV_CH4	50.03	MJ/kg

RESULTS AND DISCUSSION

The Experimental result shows that the co-digested substrate has potential to produce an average value of 17.38mL/g of Total Solid. Table 4 shows the experimental results of this study.

Table 4 Total Recorded Biogas Produced and Biogas Yield Per unit mass of Total Solid

Trial	TBP (mL)	BYts (mL/g TS)
1st	1027.30	17.12
2nd	902.70	15.05
3rd	1198.30	19.97
Mean	1042.77	17.38
Min	902.70	15.05
Max	1198.30	19.97

Despite these differences, the overall mean value of 17.38 mL/g TS indicates that the co-digestion process improves the substrates' biodegradation efficiency because mixing various organic wastes can enhance microbial synergy, nutrient balance, and the carbon-to-nitrogen ratio during anaerobic digestion. The experimental procedure's adequate repeatability is further demonstrated by the comparatively little discrepancy between the minimum and maximum values, which validates the experimental setup's dependability.

Energy and exergy evaluations were used to assess the thermodynamic performance of the suggested biogas-fueled Brayton cycle. While exergy analysis assesses the quality of energy and finds irreversibilities within system components, energy analysis calculates the quantity of useful work obtained from the system. Table 5 provides a summary of the simulation's outcomes. The overall performance of the cycle is represented by the net-work output of 105.3 kJ/kg, which is obtained as the difference between the turbine work output and the compressor work input. This net-work represents the actual useful power that can be converted into electricity through a generator. Based on the simulation results, the system achieves a thermal efficiency of 37%, indicating that 37% of the chemical energy supplied by the biogas fuel is converted into useful mechanical energy. This efficiency is within the typical range reported for simple Brayton cycle systems operating with gaseous fuels. Overall, the analysis shows that while the combustion chamber provides the largest energy contribution to the cycle, it also introduces the highest thermodynamic losses, suggesting that improvements in combustion efficiency and heat management could significantly enhance the overall system performance.

Table 5 Result of the out-put Model

Components	Energy (KJ/kg)	Exergy (KJ/kg)
Compressor	613	25.24
Combustion Chamber	28517	97.08
Turbine	718.3	25.59
Work net	105.3	
Thermal efficiency	37%	

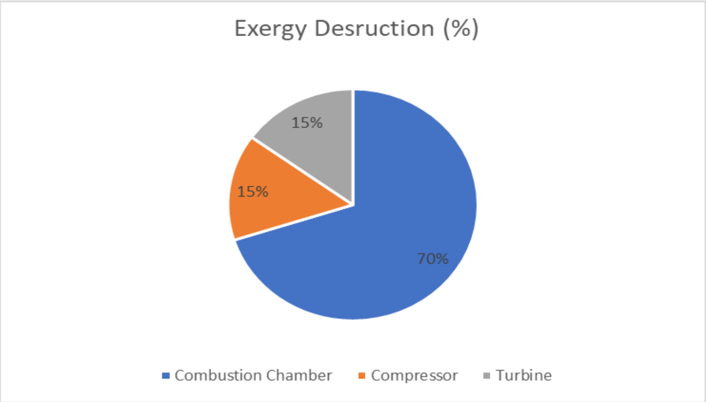

Fig. 3. Percentage of Exergy Destruction from each component

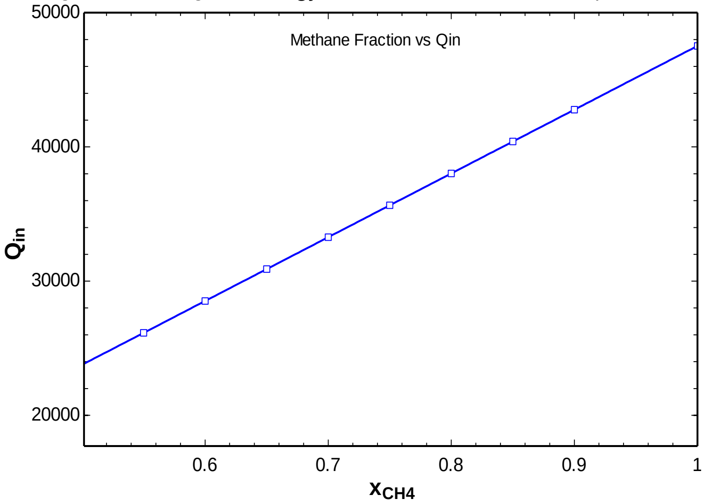

Fig. 4. Effect of Methane Composition on Fuel heat

CONCLUSION

The energy potential of the co-digested substrate can be thoroughly inspected by combining the results of experimental anaerobic digestion with thermodynamic cycle modeling. The thermodynamic study shows that this biogas may be efficiently used as a fuel in a Brayton cycle-based power production system, and the experimental results reveal that the substrate mixture can create a consistent and measurable quantity of biogas. These findings demonstrate the viability of using biogas made from organic waste as a sustainable fuel source for gas turbine systems, helping to manage waste and produce renewable energy at the same time.

The results of the thermodynamic modeling also show that the generated biogas can be used as a fuel for gas turbine-based power production systems. The Brayton cycle simulation yielded a thermal efficiency of roughly 37% and a net-work output of 105.3 kJ/kg, which is within the usual efficiency range of basic gas turbine cycles. The combustion chamber is the primary source of irreversibility in the system, according to energy analysis, underscoring the significance of enhancing heat management and combustion performance to improve total system efficiency.

NOMENCLATOR

$\dot{m}$	Mass flow rate (kg s^{-1})
h	Specific enthalpy (kJ kg^{-1})
s	Specific entropy (kJ kg^{-1} K^{-1})
ex	Specific exergy (kJ kg^{-1})
$\dot{W}$	Power or work rate (kW)
Wc	Compressor work (kJ kg^{-1})

W_t	Turbine work (kJ kg^{-1})
W_{net}	Net-work output (kJ kg^{-1})
$\dot{Q}_{in}$	Heat input rate (kW)
LHV	Lower heating value of fuel (kJ kg^{-1})
η_{th}	Thermal efficiency (-)
η_{ex}	Exergy efficiency (-)
η_c	Compressor isentropic efficiency (-)
η_t	Turbine isentropic efficiency (-)
η_{comb}	Combustion efficiency (-)
T	Temperature (K)
P	Pressure (kPa or atm)
T_0	Dead-state temperature (K)
P_0	Dead-state pressure (kPa)
x_{CH4}	Methane mole fraction in biogas (-)
x_{CO2}	Carbon dioxide mole fraction in biogas (-)
TBP	Total biogas produced (mL)
BY_{ts}	Biogas yield per unit mass of total solids (mL g^{-1} TS)
M	Mass of substrate sample (g)
TS	Total solids (%)
VS	Volatile solids (%)
COD	Chemical oxygen demand (mg L^{-1})

ACKNOWLEDGEMENT

The authors have acknowledged the support from Cyprus International University for providing the materials used in the study.

REFERENCES

[1] S. M. Safieddin Ardebili, “Green electricity generation potential from biogas produced by anaerobic digestion of farm animal waste and agriculture residues in Iran,” *Renew. Energy*, vol. 154, pp. 29–37, Jul. 2020, doi: 10.1016/j.renene.2020.02.102.

[2] D. Roy Barman, S. Bhattacharjee, and S. Rajak, “Analysis of an anaerobically digested animal waste-based microturbine driven-biogas energy system,” *Renew. Energy*, vol. 234, p. 121205, Nov. 2024, doi: 10.1016/j.renene.2024.121205.

[3] T. Kunatsa and X. Xia, “A review on anaerobic digestion with focus on the role of biomass co-digestion, modelling and optimisation on biogas production and enhancement,” *Bioresour. Technol.*, vol. 344, p. 126311, Jan. 2022, doi: 10.1016/j.biortech.2021.126311.

[4] M. M. Uddin and M. M. Wright, “Anaerobic digestion fundamentals, challenges, and technological advances,” *Phys. Sci. Rev.*, vol. 8, no. 9, pp. 2819–2837, Sep. 2023, doi: 10.1515/psr-2021-0068.

[5] Nazari, M. Soltani, M. Hosseinpour, W. Alharbi, and K. Raahemifar, “Integrated anaerobic co-digestion of municipal organic waste to biogas using geothermal and CHP plants: A comprehensive analysis,” *Renew. Sustain. Energy Rev.*, vol. 152, p. 111709, Dec. 2021, doi: 10.1016/j.rser.2021.111709.

[6] L. Lower, Y. Qiu, R. C. Sartor, W. J. Sagues, and J. J. Cheng, “Kinetic Modeling of Thermophilic Anaerobic Digestion of Lemnaceae for Biogas Production,” *BioEnergy Res.*, vol. 18, no. 1, p. 23, Feb. 2025, doi: 10.1007/s12155-025-10824-0.

[7] J. Pan *et al.*, “Factors Influencing Biochar-Strengthened Anaerobic Digestion of Cow Manure,” *BioEnergy Res.*, vol. 17, no. 2, pp. 1145–1154, Feb. 2022, doi: 10.1007/s12155-022-10396-3.

[8] H. Zhou, R. C. Brown, and Z. Wen, “Biochar as an Additive in Anaerobic Digestion of Municipal Sludge: Biochar Properties and Their Effects on the Digestion Performance,” *ACS Sustain. Chem. Eng.*, vol. 8, no. 16, pp. 6391–6401, Apr. 2020, doi: 10.1021/acssuschemeng.0c00571.

[9] W. Zhong, Z. Zhang, Y. Luo, S. Sun, W. Qiao, and M. Xiao, “Effect of biological pretreatments in enhancing corn straw biogas production,” *Bioresour. Technol.*, vol. 102, no. 24, pp. 11177–11182, Dec. 2011, doi: 10.1016/j.biortech.2011.09.077.

[10] L. L. Bridgewater *et al.*, Eds., *Standard methods for the examination of water and wastewater*, 23rd edition. Washington, DC: American Public Health Association, 2017.

Effect of Biomass Type on Electrochemical Behavior of $FeSO_4.7H_2O$ Activated Biochars

Ayca Capoglu[1*], *Ibrahim Dincer*[1]
[1] Clean Clean Energy Research Laboratory (CERL), Faculty of Engineering and Applied Science, Ontario Tech. University, 2000 Simcoe Street North, Oshawa, Ontario L1G 0C5, Canada
*Corresponding author e-mail: Ayca.Capoglu@ontariotechu.net

Ref # BIO-02

ABSTRACT
This study investigates the electrochemical performance of biomass-derived biochars magnetically activated using $FeSO_4.7H_2O$. Biochar samples are produced from tea waste, coffee waste, maple leaf, and pinecone, and their electrochemical behaviors are evaluated using cyclic voltammetry (CV) and galvanostatic charge-discharge (GCD) analyses. A comparative assessment is conducted to determine the effect of biomass type on electrochemical performance. The results show that the biochar derived from coffee waste exhibits superior electrochemical behavior compared to the other samples. The CV curves indicate higher current response, with a maximum value of approximately 0.0026 A, suggesting enhanced conductivity and surface activity. In contrast, the pinecone-derived sample shows lower current values, around 0.0012 A, indicating weaker electrochemical performance. The findings demonstrate that the type of biomass plays a critical role in determining the electrochemical properties of magnetically activated biochar. The improved performance of coffee-derived biochar is attributed to its favorable porous structure and enhanced distribution of iron-based active sites. This study highlights the potential of magnetically activated biomass-derived carbons for energy storage applications.

Keywords: Hydrogen storage; Solid state storage; Activated charcoal; Renewable energy; Energy

INTRODUCTION

Rising energy demand and the environmental impact of fossil fuels have increased the need for sustainable and clean energy systems. In this context, hydrogen stands out as a promising energy carrier due to its high energy density and zero carbon emissions during use. However, efficient and safe hydrogen storage is one of the most significant challenges to the widespread adoption of a hydrogen economy [1].

Solid-state hydrogen storage systems, particularly adsorption-based approaches using carbon-based materials, are attracting attention because they provide safe storage under low pressure and temperature conditions. The porosity, surface area, and electrical conductivity of the materials used in these systems directly affect hydrogen storage performance. Therefore, the development of adsorbents with improved structural and electrochemical properties is of great importance [2].

Biomass-derived biochar stands out as promising materials for hydrogen storage applications due to their low cost, sustainable sourcing, and porous structure. Modifications, especially with transition metals, can significantly alter the surface properties and electrical behavior of these materials. In this context, the magnetic activation method using $FeSO_4.7H_2O$ has the potential to improve both adsorption behavior and electrochemical performance by imparting metal-based active sites to the biochar surface. Although there are many studies in the literature on different biomass sources and activation methods, studies that comparatively examine the electrochemical behavior of different biomass-derived biochar obtained using only magnetic activation are limited. Systematic evaluation of the conductivity, current density, and charge-discharge behavior of materials activated with $FeSO_4.7H_2O$ is important for understanding the potential of these materials in energy storage applications [3].

In this study, biochar obtained from tea waste, coffee waste, maple leaves, and pinecones were magnetically activated using $FeSO_4.7H_2O$, and their electrochemical performances were comparatively investigated. Results obtained using linear scanning voltammetry, cyclic voltammetry, and charge-discharge tests reveal the effect of biomass type on electrochemical behavior. This study aims to evaluate the effect of magnetic activation methods on different biomass sources, thereby making significant contributions to the selection of suitable materials for hydrogen storage and energy storage applications.

MATERIALS AND METHODS

In this study, biochar derived from tea waste, coffee waste, maple leaves, and pinecones were prepared using magnetic activation with $FeSO_4.7H_2O$. As a pretreatment, the biomass was washed, dried, and reduced to a fine particle size, then subjected to pyrolysis at approximately 320 °C in a limited oxygen environment. The resulting biochar samples were impregnated with $FeSO_4.7H_2O$, magnetic activation was applied and then washed with pure water to bring to a neutral pH and dried.

The electrochemical analyses were performed using a Gamry Reference 3000 potentiostat/galvanostat. The prepared biochar samples were coated onto a stainless-steel surface and used as working electrodes. Platinum wire was chosen as the counter electrode, and measurements were performed in a 1M KOH electrolyte solution. A schematic representation of the electrochemical test setup and the experimental setup are given in Figure 1. The electrochemical behavior of the samples was evaluated using LSV, CV, and GCD tests. CV measurements determined the capacitive behavior and redox properties of the electrodes. GCD tests were used to evaluate the charge-discharge performance and energy storage capacity of the samples. All obtained electrochemical data were transferred to analysis software, and the performance of magnetically activated biochar obtained from different biomass sources was evaluated comparatively.

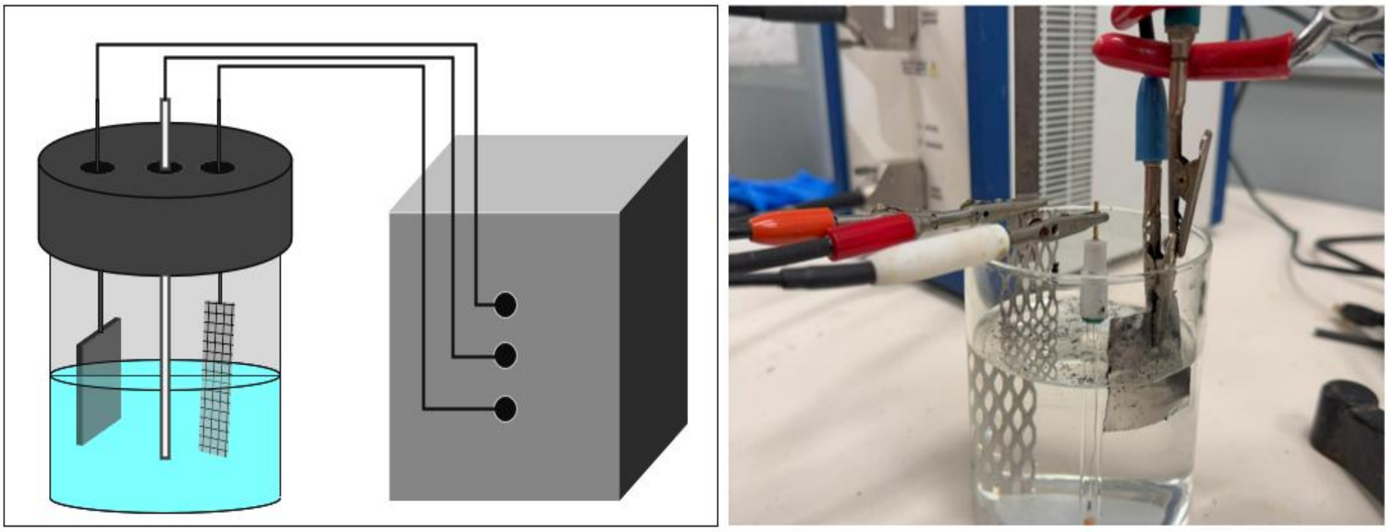

Fig.1. Schematic representation and experimental setup of the electrochemical system in 1 M KOH electrolyte.

RESULTS AND DISCUSSION

When the CV curves are examined, it is observed that the magnetically activated biochar obtained from coffee waste has a wider curve area. This indicates higher electrochemical activity and more effective surface interaction. In contrast, the pinecone-derived sample exhibited a narrower CV curve and showed lower capacitive behavior.

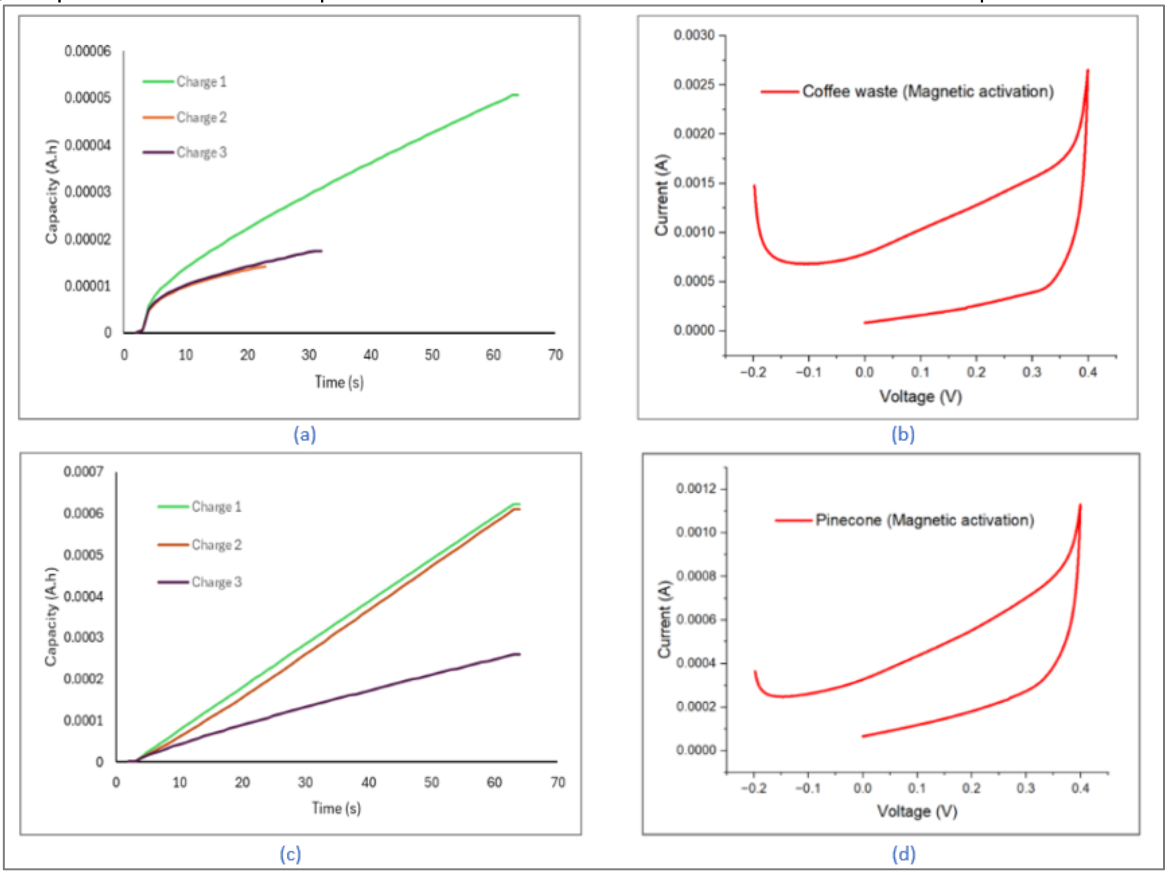

Fig.2. The CV and GCD results of magnetically activated coffee and pinecone biochar.

When current values measured in the potential range of approximately -0.2 V to 0.4 V are analyzed, it is observed that the coffee-derived sample reaches a maximum level of approximately 0.0026 A. In contrast, the maximum current value of the pinecone-derived sample remains at approximately 0.001-0.0012 A. This indicates that the coffee-derived biochar exhibits higher electrochemical activity and conductivity.

The GCD results also support this trend. The maximum capacity obtained in the third cycle for coffee-derived biochar reaches approximately 1.7×10^{-4} Ah, while in the first cycle this value is around 5.0×10^{-4} Ah. In the pinecone sample, the maximum capacitance was approximately 6.0×10^{-4} Ah, and it was observed that this value decreased to approximately 2.5×10^{-4} Ah in the third cycle. This indicates that coffee-derived biochar exhibits a more stable and improving performance over time, while the pinecone sample shows a more limited capacitance behavior.

The generally linear and symmetrical charge-discharge curves in both samples indicate good electrochemical stability. When the obtained numerical data are evaluated together, it is determined that coffee waste-derived biochar offers superior electrochemical performance by exhibiting both higher current density and more stable capacitance behavior.

CONCLUSIONS

This study presents a comparative electrochemical evaluation of biomass-derived biochar magnetically activated using $FeSO_4.7H_2O$. The results clearly show that the type of biomass significantly influences the electrochemical behavior of the produced materials. Among the tested samples, coffee waste-derived biochar exhibits the highest electrochemical performance, demonstrating higher current response in CV analysis and more stable and enhanced capacity behavior in GCD measurements. In contrast, pinecone-derived biochar shows lower current values and shorter discharge times, indicating relatively weaker electrochemical activity. The improved performance of the coffee-based sample is attributed to its more favorable porous structure and more effective distribution of iron-based active sites introduced during magnetic activation. Overall, the findings highlight that magnetic activation using $FeSO_4.7H_2O$ is an effective method for enhancing the electrochemical properties of biomass-derived carbons. This study emphasizes the importance of biomass selection in the design of high-performance carbon materials and demonstrates the potential of these materials for future energy storage applications.

REFERENCES

1) Karayel, G. K., Javani, N., & Dincer, I. (2023). A comprehensive assessment of energy storage options for green hydrogen. Energy Conversion and Management, 291, 117311. https://doi.org/10.1016/j.enconman.2023.117311
2) Dincer, I., & Erdemir, D. (2023). *Introduction to energy systems*. John Wiley & Sons Inc.
3) Chen, Z., Kirlikovali, K. O., Idrees, K. B., Wasson, M. C., & Farha, O. K. (2022). Porous materials for hydrogen storage. *Chem*, *8*(3), 693-716.

FIELD-BASED SCREENING CRITERIA FOR CO_2 STORAGE IN ONSHORE SALINE AQUIFERS: A COMPARATIVE REVIEW OF SIX PROJECTS

[1*] *Haris Nusrat*, [2] *Gamze Ipek,*
[1]Middle East Technical University, Northern Cyprus Campus, Kalkanlı, Güzelyurt, Turkish Republic of Northern Cyprus
[2]Middle East Technical University, Northern Cyprus Campus, Kalkanlı, Güzelyurt, Turkish Republic of Northern Cyprus
*Corresponding author e-mail: haris.nusrat@metu.edu.tr

Ref # CRB-01

ABSTRACT

Carbon capture and storage (CCS) have been identified as a key technology for reducing atmospheric carbon emissions and addressing climate change. Saline aquifers are common and have some of the largest potential capacities for CO_2 storage. Therefore, they are considered a promising option for achieving net zero emissions targets. These are underground reservoirs filled with brine solutions and are usually covered by a caprock consisting of low permeability sealing formations. The capacity of a saline aquifer is not a guarantee of its suitability for CO_2 storage. The success of a CO_2 storage project is usually determined by geology and reservoir properties such as porosity, permeability, thickness, depth, pressure conditions and caprock quality. This review paper represents a comparative synthesis of six large-scale CCS onshore saline aquifers worldwide including Quest (Canada), Aquistore (Canada), Illinois Basin-Decatur Project (USA), SECARB Citronelle (USA), Ketzin (Germany), and Gorgon (Australia). Each of these projects was studied in terms of their geological background, characteristics, and injection and storage performances. These projects are important to provide knowledge that is necessary to achieve a future deployment scenario of CCS on a gigaton scale to meet net-zero emission targets.

Keywords: CO_2 storage, CO_2 Saline Aquifers, Carbon storage, Onshore Saline Aquifers CO_2 storage

INTRODUCTION

Carbon capture and storage (CCS), from a novel concept to a proven technology, has been developed through the past three decades, facilitated by increasing levels of evidence from operational experience. This paper consolidates operational performance, monitoring results, and subsurface lessons from six CO_2 storage onshore saline aquifers across varied tectonic settings, reservoir architectures, and regulatory contexts: Ketzin (Germany), Gorgon (Australia), Quest (Canada), Aquistore (Canada), the SECARB Anthropogenic Test at Citronelle (USA), and the Illinois Basin-Decatur Project (IBDP) (USA). Collectively, these sites range from shallow to deep saline aquifers and structurally complex reservoirs hosted in diverse lithologies, including fluvial-tidal and eolian sandstones and volcaniclastic intervals. They also represent the full CCS workflow: capture, conditioning and transport, injection and storage, and measurement monitoring verification (MMV) implemented under real operating constraints and risk controls.
Several projects have become reference points for how storage performance and containment can be demonstrated. Ketzin, Europe's first onshore pilot, advanced integrated MMV seismic monitoring while documenting operational handling near critical conditions [1] [2]. In North America (Canada), Quest and Aquistore demonstrated large-scale saline storage under thick regional seals (Lotsberg Salts; Prairie Evaporite), pairing industrial capture with multi-well monitoring and strong injectivity in deep Cambrian clastic [3] [4]. Citronelle (USA) delivered an end-to-end CCS chain and helped establish above-zone pressure monitoring as a practical tool for confining-unit assurance[5], while IBDP (USA) provided a high-quality MMV dataset (microseismic, logging, pressure/temperature, and fluid sampling) to history-match models and confirm stratigraphic containment [6]. Finally, Gorgon (Australia) highlights the scale and complexity of mega-project CCS, combining active pressure management through formation-water extraction and reinjection with engineering upgrades to support reliable CO_2 compression and dehydration [7]. Across the six cases, common conclusions emerge: containment is best demonstrated through risk-proportionate, periodic 3D/4D seismic, injectivity depends strongly on heterogeneity and operational history, not just average porosity or permeability, redundant seals and well integrity verification are critical barriers, pressure management can expand practical capacity and protect caprock performance, and clear regulatory pathways and stakeholder engagement materially reduce delivery risk.

MATERIALS AND METHODS

This study utilizes a comparative literature study methodology to compile parameters that can be compared across six field-scale CCS projects in onshore saline aquifers. The parameters are compared based on recurring cross-project patterns that can be used to control storage performance and key risks. Table 1 provides a brief description of the key parameters of six onshore CO2 storage saline aquifers case studies used for comparison. The parameters are based on key reservoir depth and thickness, porosity, permeability, pressure conditions, and key injection features. The study is based on publicly available project documents, including technical reports and research articles. [1], [2], [3], [4], [5], [6], [7]
In order to compare parameters and data collected from various projects on a consistent basis, a common framework

is utilized to collect information on each project based on a set of standardized categories. The categories are based on key geological settings, reservoir parameters, and performance outcomes. This structured extraction enabled direct cross-case comparison and supported synthesis of shared lessons across diverse storage settings.

Table 1 Cross-project comparison of six onshore CO_2 storage saline aquifers case studies.

	Completed			**Ongoing**		
Project	**Ketzin**	**SECARB Citronelle**	**Decatur (IBDP)**	**Aquistore**	**Quest**	**Gorgon**
Location	Brandenburg	Alabama	Illinois	Saskatchewan	Alberta	Western Australia
Reservoir	Stuttgart formation	Paluxy Formation	MT. Simon Sandstone	Deadwood/Winnipeg Sandstone	Basal Sandstone	Dupuy Formation
Operation Period	2008 – 2013	2012 – 2014	2011 – 2014	2015 – present	2015 – present	2019 – present
Capacity (CO_2)	67,000 t	30 Mt (est.)	1 Mt	2.5 Mt	27 Mt	100+ Mt
Injected (CO_2)	67,000 t	~74,000 t	999,215 t	~500,000 t (by 2025)	7.78 Mt	~7 Mt
Reservoir (Depth)	(~650 m)	(~2,900 m)	(~2,150 m)	(~3,200 m)	(~2,000 m)	2250m
Thickness	~80 m	145 m net	500 m gross	>150 m	~45 m	200–500 m
Porosity	0.2	0.195	0.21	0.125	0.15	0.22
Permeability mD	50-100md=75mD	12–3,950 mD (avg ~284mD)	33-1000mD (avg 174mD)	4.89=5 mD	1000 mD	30–100=avg 65 mD
Initial Reservoir Pressure (kPa)	6200	39000	23000	34000	19600	21000

RESULTS AND DISCUSSION

Across Ketzin, Gorgon, Quest, Aquistore, Citronelle, and IBDP, the evidence consistently shows that: CCS can be implemented safely and reliably when the storage concept is tailored to local geology, built with redundant barriers, and operated with an adaptive, data-driven approach. Four shared takeaways stand out. First, plume conformance and containment can be demonstrated in practice: repeated 3D/4D seismic combined with continuous pressure-temperature monitoring and targeted logging/sampling can map plume geometry, identify high-saturation intervals, and confirm that sealing units perform as intended. Where models have been challenged with real monitoring data, long-term behavior is consistent with increasing trapping (e.g. dissolution and stratigraphic baffling) and a stabilizing free-phase footprint over long timescales.
Second, injectivity is manageable, but it requires discipline: heterogeneity, compartmentalization, and internal baffles can reduce early performance, yet operational measures optimized completions, near wellbore remediation, thermal control, and (when needed) pressure relief through brine handling can restore or sustain injectivity; multi-interval injection can also help distribute pressure and limit areal plume growth when actively managed. Third, well and seal integrity remain the main risk focus, but they are controllable with standard practices such as cement evaluation, mechanical integrity testing, above-zone pressure monitoring, and reliance on thick, laterally continuous sealing sequences (shales and/or evaporites). Finally, execution and governance matter as much as subsurface quality: high uptime, maintenance discipline, clear permitting pathways, transparent engagement, open data-sharing accelerate learning and strengthen public and regulatory confidence.

CRITICAL ANALYSIS AND LIMITATIONS

Although the six projects collectively support the technical credibility of CCS, a critical reading shows that performance and perceived success are strongly shaped by data availability, monitoring intensity, and how constraints are reported, not only by subsurface quality. Some sites provide rich, long-term datasets that enable tight history matching and clear containment narratives, while others publish fewer operational details (e.g. pressure management decisions, downtime causes, injectivity interventions), which makes cross-project comparison less uniform. In addition, most of the information on reservoir properties cited in the cases actually reflects a range of values from various scales (core, well tests, log analysis, model calibration), and such a comparison of porosity and permeability can obscure the real controlling factors of connectivity, heterogeneity, architecture, and near-well conditions.

In terms of deployment, the cases also point to a number of trade-offs that should be carefully balanced in the design of future hubs. For example, monitoring can provide evidence of conformance and build confidence, but it must be balanced against costs and site accessibility. Hence, it is suggested that MMV should be risk-proportionate and responsive to what is to be proven in each phase of a project (baseline, operational, post-injection). Likewise, storage capacity is not only a volumetric estimate pressure margin and boundary conditions can become the binding constraint, especially when multiple wells or emitters interact within a hub. These observations suggest that transferring "best practice" requires caution: what generalizes well are the principles (robust seals, verified well integrity, continuous pressure surveillance, adaptive operations), while the specific operating envelopes and monitoring intensity must be tuned to each site's geology, regulatory setting, and hub-scale pressure management strategy.

CONCLUSION

Among the six case studies, Quest stands out as the most relevant onshore analogue for future CCS hub development, where multiple emitters will rely on shared transport and a single storage complex operating continuously for decades. Unlike pilot-scale demonstrations that mainly prove injectivity and monitoring feasibility, Quest reflects the realities that hubs must manage every day: sustained industrial operations, high system availability, predictable injection performance, and routine integration of monitoring and risk controls into normal field workflows. It therefore provides a practical benchmark for how to translate site characterization into an operable storage design, how to maintain stable injection under real operating constraints, and how to structure monitoring so it supports long-term conformance and containment assurance without becoming operationally burdensome. While Aquistore and IBDP contribute important complementary lessons i.e. deep saline storage under strong evaporite sealing in Aquistore and a best-in-class regulatory dataset in IBDP, Quest most closely captures the integrated, reliability-driven performance that will be required as storage moves from single projects to regional hub networks.

Looking ahead, scaling from individual projects to hub-style networks will depend on three priorities: (i) hub-scale pressure management, including coordinated well patterns and (where appropriate) brine handling strategies to expand effective capacity; (ii) fit-for-purpose MMV built around risk-based combinations of seismic, pressure, and geochemical methods that retain diagnostic value while controlling cost; and (iii) operational playbooks that anticipate thermal mechanical effects, rate-dependent injectivity, and near-wellbore processes such as salt-related impairment. Together, these priorities translate the lessons from the reviewed projects into practical requirements for predictable, industrial-scale storage performance.

REFERENCES

[1] A. Förster *et al.*, "Baseline characterization of the CO2SINK geological storage site at Ketzin, Germany," *Environmental Geosciences*, vol. 13, no. 3, pp. 145–161, Sep. 2006, doi: 10.1306/EG.02080605016.

[2] A. Förster, R. Giese, C. Juhlin, B. Norden, and N. Springer, "The Geology of the CO2SINK Site: From Regional Scale to Laboratory Scale," *Energy Procedia*, vol. 1, no. 1, pp. 2911–2918, Feb. 2009, doi: 10.1016/J.EGYPRO.2009.02.066.

[3] "THE SHELL QUEST CARBON CAPTURE AND STORAGE PROJECT".

[4] D. J. White, C. D. Hawkes, and B. J. Rostron, "Geological characterization of the Aquistore CO2 storage site from 3D seismic data," *International Journal of Greenhouse Gas Control*, vol. 54, pp. 330–344, Nov. 2016, doi: 10.1016/J.IJGGC.2016.10.001.

[5] G. J. Koperna, S. M. Carpenter, R. Petrusak, R. Trautz, S. D. Rhudy, and R. Esposito, "Project Assessment and Evaluation of the Area of Review (AoR) at the Citronelle SECARB Phase III Site, Alabama USA," *Energy Procedia*, vol. 63, pp. 5971–5985, Jan. 2014, doi: 10.1016/J.EGYPRO.2014.11.632.

[6] S. M. Frailey, J. Damico, and H. E. Leetaru, "Reservoir characterization of the Mt. Simon Sandstone, Illinois Basin, USA," *Energy Procedia*, vol. 4, pp. 5487–5494, Jan. 2011, doi: 10.1016/J.EGYPRO.2011.02.534.

[7] M. Trupp, S. Ryan, I. Barranco, D. Leon, and L. Scoby-Smith, "Developing the world's largest CO2 Injection System – a history of the Gorgon Carbon Dioxide Injection System," *15th Greenhouse Gas Control Technologies Conference 2021, GHGT 2021*, Mar. 2021, doi: 10.2139/SSRN.3815492.

THE RELATIONSHIP BETWEEN DECARBONIZATION AND EXERGY IN THE TRANSPORTATION SECTOR IN TURKEY

[1*] *Büşra Selenay Önal*, [2] *Zafer Utlu*
[1] Istanbul Gelisim University, Aircraft Maintenance and Repair, Faculty of Applied Sciences, Istanbul, Turkey, bsonal@gelisim.edu.tr, ORCID: 0000-0002-4856-9816
[2] Istanbul Atlas University, Faculty of Engineering and Natural Sciences, Istanbul, Turkey zafer.utlu@atlas.edu.tr, ORCID: 0000-0003-1981-9107
*Corresponding author e-mail: bsonal@gelisim.edu.tr

REF # ENV-01

ABSTRACT

The transportation sector accounts for a significant share of Turkey's total energy consumption and greenhouse gas emissions. The sector's heavy reliance on fossil fuels constitutes a critical problem area for achieving decarbonization goals. Classical energy analyses are insufficient for evaluating energy efficiency; exergy analysis, which considers energy quality and irreversibilities, offers a more comprehensive approach. This study examines the main energy sources used in the Turkish transportation sector from an exergy perspective and evaluates the relationship between exergy destruction and carbon emissions. Furthermore, the decarbonization potential of electric and alternative fuel transportation systems in terms of exergy efficiency is discussed. This study demonstrates that exergy analysis is a critical decision-support tool in determining decarbonization strategies in the Turkish transportation sector and emphasizes the necessity of a holistic approach based on energy quality for transitioning to a sustainable and low-carbon transportation system.

Keywords: Transportation sector, Exergy analysis, Decarbonization, Energy efficiency

INTRODUCTION

Decarbonizing energy systems is one of the key objectives in combating global climate change. In Turkey, the transportation sector accounts for approximately a quarter of final energy consumption and is responsible for a significant portion of CO_2 emissions. The dominance of road transport, the widespread use of inefficient internal combustion engines, and the increasing number of vehicles further highlight the need for decarbonization in this sector.

Traditional energy analyses focus solely on the quantity of energy, neglecting its availability and irreversibilities within the system. Exergy analysis, however, reveals the actual losses in an energy conversion process, allowing for a more accurate assessment of system performance. In this context, the exergy approach is a powerful tool for identifying processes in the transportation sector that exhibit high carbon intensity and low thermodynamic performance.

The concept of exergy refers to the maximum theoretical work a system can produce until it reaches equilibrium with its environmental conditions; thus, it quantitatively reveals the actual losses in energy conversion processes. When examining transportation technologies such as internal combustion engines, gas turbines, and electric propulsion systems, it is known that the high entropy production and irreversibilities occurring in combustion processes lead to low exergy efficiencies. This explains the direct relationship between energy consumption and carbon emissions on a thermodynamic basis. While numerous studies exist in the literature on energy efficiency and carbon emissions in the transportation sector, studies that comprehensively analyze decarbonization performance using sub-sector-based exergy analysis at the Turkish level are limited. Existing research mostly evaluates systems based on energy intensity or emission factors, without thoroughly examining irreversibility sources and exergy destruction mechanisms. This deficiency creates uncertainty in policy-making processes regarding which technological transformations are truly sustainable. Some of the studies in the literature on decarbonization, energy, and exergy efficiency are summarized.

The study conducted by Utlu and Hepbasli [1] examined the energy and exergy efficiency of the Turkish transportation sector during the period 2000–2020. It was observed that total energy efficiency increased from 23.71% to 28.75%, and exergy efficiency increased from 23.65% to 28.85%. For 2020, an exergetic improvement potential of approximately 700 PJ was identified, with road transportation having the highest share within the sector. The findings revealed that improvements, particularly in internal combustion engine technologies, will play a critical role in increasing sectoral efficiency. In the study conducted by Kanberoğlu et al. [2], the energy efficiency of the Turkish-owned ship fleet was quantitatively evaluated based on the International Maritime Organization's (IMO) Energy Efficiency Existing Ship Index (EEXI) regulation in the context of decarbonization. Calculations for the 1,077 Turkish ships analyzed showed that the percentage of ships initially compliant with the IMO's Phase 2 reference line was only 15.6%; however, by applying main engine power limitation (EPL), this rate increased to 53.1%, meaning that more than one-third could meet stricter efficiency targets. According to component types, a compliance rate of 51.3% was found in general cargo ships, and with 20% EPL, this rate exceeded 70%; in tanker fleets, compliance increased

from 35.3% to 69.3%. The study by Jovet [3] evaluates different technologies for decarbonizing industrial heating processes using a 4E (energy, exergy, economic, and environmental) optimization approach. According to the results, CO_2 emissions are reduced by 20–40% with high-efficiency heat pumps and waste heat recovery applications, while improving the energy and exergy performance of the systems; however, an increase in total investment and operating costs is observed in advanced decarbonization scenarios. The findings indicate that the most sustainable solution in industrial heating systems can be achieved by finding the optimum balance between emission reduction, exergy efficiency, and economic feasibility. The study by Maghrabi et al. [4], quantitatively investigated how the decarbonization of industrial heating processes can be accelerated through energy efficiency improvements. The analyses found that implementing energy efficiency improvements could lead to a 15–30% reduction in industrial heating energy consumption, corresponding to a 12–28% decrease in CO_2 emissions. In particular, the use of high-efficiency heat pumps increased thermal efficiency from approximately 60–80% to approximately 90–95% compared to conventional fossil fuel heating systems, thus significantly reducing primary energy consumption. Exergy analyses in isolated processes showed that heat recovery networks could reduce total exergy losses by approximately 10–18%. In the study conducted by Guo et al.,[5], the effect of partial oxidation on the microscopic morphology of soot particles was experimentally investigated. The magnitude of the crystalline curvature directly reflected the proportion of odd-numbered carbon rings in polycyclic aromatic hydrocarbons. The decrease in degradation indicated a decrease in the number of odd-numbered carbon rings, while the increase in internal dehydrocarbonization of soot particles resulted in a more regular microstructure and a higher degree of graphitization.
The study by Xu et al. [6] investigated the structural evolution of polyaluminocarbosilane during the polymer-ceramic transformation process. Similar to PCS, weight loss resulted from the thermal decomposition of precursor molecules. At this stage, decomposition of side chains and dehydrogenation and dehydrocarbonation condensation reactions occurred, and some gases such as H2,CH4 etc. were released. Finally, a three-dimensional network-structured inorganic structure was formed [7-10].

MATERIALS AND METHODS

This study examines energy consumption data for the Turkish transportation sector, broken down by sub-sectors of road, rail, air, and sea transport. The primary energy carriers used in the analysis were identified as gasoline, diesel, LPG, jet fuel, and electricity.

For each mode of transport, the following were calculated as part of the thermodynamic evaluation:

- Chemical exergy values of the fuels,
- Average exergy efficiencies of the transport systems,
- Exergy destruction and exergy loss rates.

Exergy efficiency was defined as the ratio of useful mechanical work exergy to the total exergy entering the system. Carbon emissions were calculated using fuel-based emission factors and correlated with CO_2 emissions per passenger-km or ton-km transported. Furthermore, as part of the scenario analysis, the changes in exergy efficiency and emissions were comparatively evaluated when internal combustion engine vehicles were partially replaced by electric vehicles and alternative fuel systems. Table 1 shows the lower calorific value (LHV) and chemical exergy coefficients of fuels. Table 2 shows typical emission factors of fuels.

Table 1. The lower calorific value (LHV) and chemical exergy coefficients of fuels

Fuel	LHV (MJ/kg)	β	Chemical Exergy (MJ/kg)
Gasoline	43	1.07	46.0
Diesel	42.5	1.06	45.1
LPG	46	1.05	48.3
Jet Fuel	43	1.06	45.6
Electric	-	1.00	1 kWh = 3.6 MJ exergy

Energy and Exergy Analysis

The energy efficiency of a system is expressed as follows:

$$\eta_{en} = \frac{\dot{W}_{useful}}{\dot{E}_{input}} \tag{1}$$

The exergy efficiency for processes is expressed as follows:

$$\eta_{II} = \frac{\dot{E}x_{useful}}{\dot{E}x_{input}} \tag{2}$$

The general exergy balance for a steady-state control volume is expressed as:

$$\sum \dot{E}x_{in} = \sum \dot{E}x_{out} + \dot{E}x_{dest} \tag{3}$$

where $\dot{E}x_{dest}$ represents the total exergy destruction rate due to irreversibilities.

The steady-state exergy balance is given by:

$$\sum \dot{E}x_{in} - \sum \dot{E}x_{out} = \dot{E}x_{dest} \tag{4}$$

where $\dot{E}x_{dest}$ represents exergy destruction due to irreversibilities and is directly related to entropy generation:

$$\dot{E}x_{dest} = T_0 \dot{S}_{gen} \tag{5}$$

Below is the total carbon emissions for an energy system:

$$CO_2 = E.EF \tag{6}$$

where,
CO_2: $Total\ carbon\ emissions\ (kg\ CO_2)$
E: Energy consumption (kWh, MJ)
EF: Emission factor (kg CO_2/kWh or kg CO_2/MJ)

Table 2.Typical emission factors of fuels

fuel	kg CO_2 / GJ
gasoline	69
diesel	74
Jet Fuel	73
Electricity (Türkiye mixed)	450 kg/MWh

RESULTS AND DISCUSSION

Annual energy consumption, energy efficiency, exergy efficiency, exergy destruction and annual CO_2 emission amount calculated for road, air, sea and electric railway transportation are given in Table 3.

Table 3. Annual energy consumption, energy efficiency, exergy efficiency, exergy destruction and annual CO_2 emission amount calculated for road, air, sea and electric railway transportation

Sector	Energy (PJ)	Energy Efficiency (%)	Exergy Efficiency (%)	Exergy Destruction (PJ)	CO_2 (Mt)	kg CO_2/GJ
Road	1050	25	22	868	77	73
Air	420	30	28	321	31	73
Maritime	210	40	38	138	16	70
Railway	120	85	80	24	6	50

When sub-sectors are compared in terms of exergy efficiency, significant differences emerge. The average exergy efficiency in road transportation is calculated as 22%, and this value represents the lowest performance among the analyzed systems. On the other hand, a very high exergy efficiency of 28% in air transportation, 38% in maritime transportation and 80% in railway transportation was achieved. Particularly the high efficiency of electric railway systems can be explained by the direct conversion of electrical energy into mechanical work and the elimination of combustion-based irreversibility. Exergy destruction results clearly reveal the magnitude of real thermodynamic losses in systems. 868 PJ of exergy destruction occurs annually in road transportation, and this value corresponds to approximately 64% of the total transportation sector exergy destruction. An exergy destruction of 321 PJ was calculated for air transportation, 138 PJ for maritime transport, and only 24 PJ for railway transportation. The low amount of destruction in the railway is consistent with both low energy consumption and high exergy efficiency. When the relationship between carbon emissions and exergy destruction is examined, it is seen that there is a strong correlation. Road transport has the highest emission value with 77 million tons of CO_2 per year. Airline produces 31 Mt, maritime transport 16 Mt and railway 6 Mt CO_2 emissions. The parallel between exergy destruction and CO_2 emissions is striking: the sector with the highest exergy destruction also has the highest carbon emissions. This shows that reducing irreversibilities will directly contribute to emission reduction. In the final analysis, it was calculated that if road transport was replaced by electric vehicles at a rate of 30%, the exergy efficiency increased from 22% to approximately 40%. As a result of this transformation, highway exergy destruction decreases from 868 PJ to 620 PJ, that is, a decrease of approximately 29%. In the same scenario, CO_2 emissions decrease from 77 Mt to 54 Mt, a reduction of approximately 30%. This parallel decrease between exergy destruction and carbon reduction shows that thermodynamic improvements are directly reflected in environmental performance.

CONCLUSIONS

In this study, energy consumption, exergy efficiency, exergy destruction and carbon emissions in the Turkish transportation sector were analyzed comparatively on a sub-sector basis. The findings show that there is a strong and linear relationship between thermodynamic performance and environmental impact in transportation systems. Road transportation stands out as the sector with both the highest energy consumption and the lowest exergy efficiency. The exergy efficiency of 22% and the annual exergy destruction of 868 PJ clearly reveal the high irreversibility and inefficient combustion processes in the system. In parallel, with 77 million tons of CO_2 emissions, the sector constitutes the largest part of total transportation-related emissions. This situation shows that road transportation should be the priority target area in decarbonization policies. Railway transportation, on the other hand, exhibits the highest thermodynamic performance with 80% exergy efficiency and only 24 PJ exergy destruction. Low carbon intensity and limited emissions confirm the structural advantage of electric systems. Airline and maritime transportation are in an intermediate position in terms of performance; Combustion-based irreversibilities appear to be important, especially in the airline industry. As a result, the key to transition to a sustainable and low-carbon structure in the Turkish transportation sector is not only reducing energy consumption; At the same time, improving energy quality and minimizing intra-system irreversibilities. Integrating exergy-based indicators into national transportation policies will allow determining on a scientific and quantitative basis which subsectors and which technologies require priority transformation. In this context, accelerating road electrification, increasing the share of railway transportation and shifting the energy production mix to low-carbon sources are considered the most effective strategies in terms of both thermodynamic efficiency and emission reduction.

REFERENCES

1. Utlu, Z., & Hepbasli, A. (2006). Assessment of the energy utilization efficiency in the Turkish transportation sector between 2000 and 2020 using energy and exergy analysis method. *Energy Policy*, *34*(13), 1611-1618.

2. Kanberoğlu, B., Turan, E., & Kökkülünk, G. (2023). Decarbonization of maritime transportation: A case study for Turkish ship fleet. *Journal of Marine Science and Application*, *22*(4), 716-727.

3. Jovet, Y. (2023). Sustainability of industrial heat decarbonisation strategies through 4E (energy, exergy, economic and environmental) optimisation (Doctoral dissertation, INSA de Lyon).

4. Maghrabi, A. M., Song, J., & Markides, C. N. (2023). How can industrial heat decarbonisation be accelerated through energy efficiency? Applied Thermal Engineering, 233, 121092.

5. Guo, G., Dai, R., Wang, J., & Wu, S. (2022). Experimental Study on the Effect of Partial Oxidation on the Microscopic Morphology of Soot Particles. Energies, 15(12), 4295.

6. Xu, C., Gao, Y., Xu, G., Li, X., Zhao, S., & Yang, Y. (2019). A thermodynamic analysis and economic evaluation of an integrated cold-end energy utilization system in a de-carbonization coal-fired power plant. Energy Conversion and Management, 180, 218-230.An, L., Wang, Y., Bharadwaj, L., Zhang, L., Fan, Y., Jiang, D., ... & Chow, L. C. (2004). Silicoaluminum carbonitride with anomalously high resistance to oxidation and hot corrosion. Advanced Engineering Materials, 6(5), 337-340.

7. An, L., Wang, Y., Bharadwaj, L., Zhang, L., Fan, Y., Jiang, D., ... & Chow, L. C. (2004). Silicoaluminum carbonitride with anomalously high resistance to oxidation and hot corrosion. Advanced Engineering Materials, 6(5), 337-340.

8. Duan, Y., Mo, G., Huangfu, Z., Liang, Y., Cui, Z., He, L., ... & Huang, Q. (2019). Effects of aluminium content on the molecular structure and properties of polyaluminocarbosilane for SiC fibre fabrication. Ceramics International, 45(13), 16380-16386.

9. Wang, Y., An, L., Fan, Y., Zhang, L., Burton, S., & Gan, Z. (2005). Oxidation of polymer-derived SiAlCN ceramics. Journal of the American Ceramic Society, 88(11), 3075-3080.

10. Zheng, C. M., Li, X. D., Wang, H., Zhao, D. F., & Hu, T. J. (2008). Evolution of crystallization and its effects on properties during pyrolysis of Si–Al–C–(O) precursor fibers. Journal of materials science, 43(9), 3314-3319.

THERMAL ANALYSIS OF A VANADIUM REDOX FLOW BATTERY WITH A GRADED POROSITY ELECTRODE

Phil-Jacques Alphonse[1,2], Mert Taş[1,3,4], Gülşah Elden[3,4]*
[1] Energy Systems Engineering Program, Graduate School of Natural and Applied Sciences, Erciyes University, Kayseri 38039, Turkey
[2] Norwegian University of Science and Technology, Faculty of Natural Sciences, Department of Materials Science and Engineering, 7034, Trondheim, Norway
[3] Erciyes University, Faculty of Engineering, Energy Systems Engineering, Kayseri, 38039, Turkey
[4] Hydrogen Energy and Technologies Laboratory, Department of Energy SystemsEngineering, Erciyes University, Kayseri, 38039, Turkey
*Corresponding author: phil.j.alphonse@ntnu.no

Ref # EST-02

ABSTRACT

Vanadium redox flow batteries (VRFBs) are a promising energy storage system for large-scale, efficient energy storage. In VRFBs, thermal analysis is essential for maintaining proper electrolyte temperatures, reducing vanadium precipitation, and ensuring high efficiency. The current study numerically investigates the thermal effects of porosity variation in the porous electrode on VRFB performance. To do this, a two-dimensional, single-phase model is developed using COMSOL Multiphysics 5.5 and validated with experimental data. The porosity distribution in the porous electrode is examined in four different cases. Case 1 fixes the porosity of both the positive and negative electrodes at 94%. In Case 2, the positive electrode's porosity remains fixed at 94%, while the negative electrode's porosity gradually increases from 64% to 94% in 10% steps along the electrode thickness toward the membrane. In Case 3, the negative electrode's porosity is held constant, while the positive electrode's porosity increases gradually from 64% to 94% in 10% steps. Finally, in Case 4, both electrodes' porosities gradually increase from 64% to 94% in 10% steps toward the membrane. The results show that Case 4 demonstrates good performance and produces less heat during charging and discharging.

Keywords: Thermal Analysis, Electrode Porosity, Vanadium Redox Flow Battery

INTRODUCTION

The shift to renewable energy is vital for reducing the energy sector's negative environmental effects. However, because of their intermittency, developing energy storage technologies such as vanadium flow redox batteries is essential for maintaining the stability and efficiency of renewable energy systems. The thermal management remains a considerable challenge in a VRFB performance. To enhance VRFB performance, various studies have focused on electrode porosity and thermal management. Ali et al. [1] examined how electrode porosity affects cell performance during discharge, finding that increased porosity reduced concentration polarization and improved performance. Another study assessed the performance and velocity distribution of electrodes with different porosities at various locations [2], revealing a more uniform velocity distribution in areas with high porosity near the membrane. In VRFBs, thermal modeling of the battery setup and self-discharge reactions was also performed [3], showing that the battery generates minimal heat during self-discharge, keeping the chemical reaction almost constant. Andrea et al. [4] and Zhanga [5] created a 2D thermal model of VRFB, demonstrating that the reversible entropic heat source was positive during discharge and negative during charging.

As indicated in the literature, the thermal behavior of graded porosity electrodes has not been investigated. Therefore ,the current study examines the effects of the graded porosity electrode on heat sources generation, temperature distribution, and efficiency in a VRFB system.

PROCEDURE

This work thoroughly investigates the thermal analysis of various porosity distributions in a porous electrode. Four porosity distribution cases are explored using a numerical model. In the first case, the porosity of both electrodes is fixed at 94%. In the second case, the porosity of the negative electrode increases from 64% to 94% in 10% steps toward the membrane, while that of the positive electrode remains steady at 94%. In the third case, the positive electrode's porosity gradually increases from 64% to 94% in 10% increments across its thickness, while the negative electrode's porosity remains constant. In the fourth case, the porosity of both electrodes increases progressively from 64% to 94% as they approach the membrane, in 10% increments.

THE NUMERICAL MODEL

The schematic of the computational domain includes two porous electrodes, and the membrane is shown in Figure

1. The model incorporates numerous assumptions and simplifications:

1. The model is steady state
2. The electrolyte flow is laminar and incompressible.
3. Species transport is described using the dilute-solution approximation.
4. The bubble formation and the side reaction (hydrogen evolution and oxygen evolution) are not considered.
5. Physical properties of porous electrodes and membrane are homogeneous and isotropic.

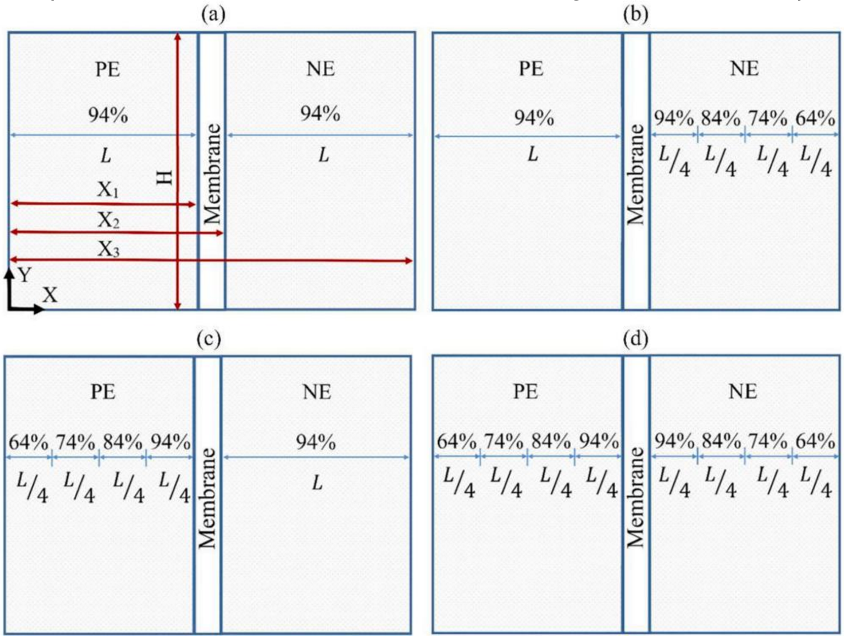

Fig. 1. 2D Schematic of model domains of VRFB.

Based on the model developed by previous work [6], the main conservation equations applied to the model are:

Continuity: $\nabla.(\vec{v}) = 0$ (1)

Momentum conservation: $\frac{\mu}{K}\vec{v} = -\nabla P$ (2)

Species conservation: $\vec{v}\nabla c_i - D_i^{eff}\nabla^2 c_i = S_i$ (3)

Charge conservation : $\nabla\vec{\iota_s} = -\nabla\vec{\iota_l} = \sigma_s^{eff}\nabla^2\phi_s = k_l^{eff}\nabla^2\phi_l = S_\emptyset$ (4)

Energy conservation : $\nabla(\vec{v}\rho_l C_p) - \bar{\lambda}\nabla^2 T = \sum_j q_j$ (5)

RESULTS AND DISCUSSION

In this work, a two-dimensional numerical model of a VRFB is presented to investigate the thermal effects of porosity variation in the porous electrode.

Fig. 2 shows how cell voltage varies with SOC during charging and discharging for each case. As shown in the figure, the maximum battery cell voltage at the end of charging is 1.62 V, 1.57 V, 1.59 V, and 1.55 V for Cases 1, 2, 3, and 4, respectively. During discharge, the battery cell voltage increases from 1.42 V to 1.47 V when all cases are considered. It is known that battery performance, is best when the battery is charged at low voltage and discharged at high voltage. Based on this information, Case 4 has the best electrode design among the cases considered.

The variation of the Joule heat source with SOC, which is generated due to resistance during the transfer of charged ions at the positive and negative electrodes during charging and discharging processes, is illustrated in Fig. 3. It was found that as the SOC increases from 0.05 to 0.95 during charging and discharging, the Joule heat source decreases. Furthermore, it is observed that Case 1 and Case 3 have higher Joule heat values at the negative electrode compared to Case 2 and Case 4. At the positive electrode, the Joule heat in Cases 1 and 2 is higher than in Cases 3 and 4 during both charging and discharging. From these results, it is concluded that Joule heat is reduced by lowering the ohmic resistances at the electrodes in the Case 4 design. Also, while the maximum Joule heat at the positive electrode is nearly 680 W/m³ for Cases 1 and 2, it is about 790 W/m³ at the negative electrode for Cases 1 and 3.

Fig. 4 shows the variation in reversible and irreversible heat sources due to entropy and activation overpotential within the cell at both the positive and negative electrodes during charge and discharge processes across four Cases. It is observed that Cases 1 and 2 have higher reversible and irreversible heat values at the positive electrode compared to Cases 3 and 4. Additionally, at the negative electrode, during both charge and discharge processes, the reversible and irreversible heat values are higher for Cases 1 and 3 than for Cases 2 and 4. These results indicate that when a design like Case 4 is used, the activation overpotential is reduced at both electrodes, leading to a decrease in heat source values.

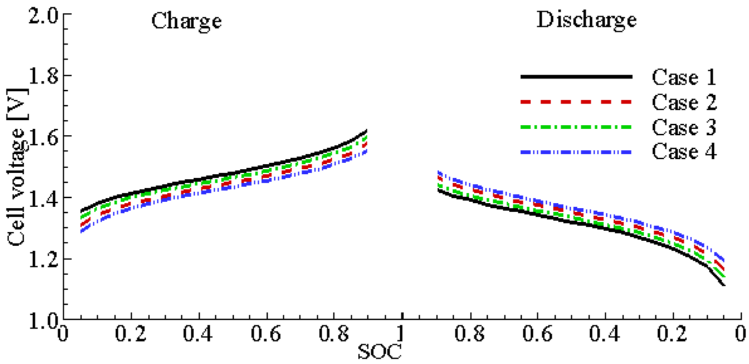

Fig.2. Variation of cell voltage with SOC during charging and discharging for each case [7].

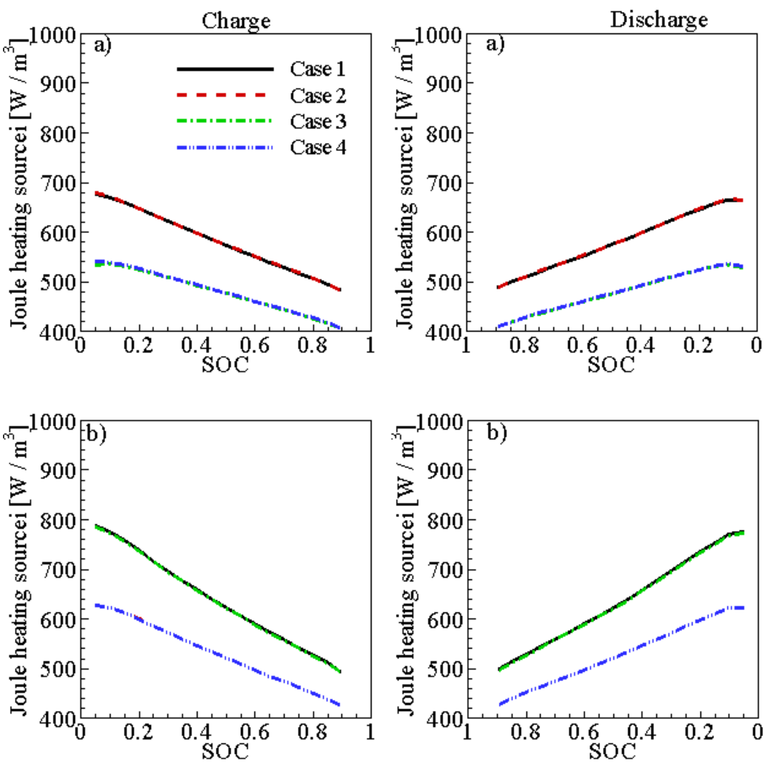

Fig.3. Variation of Joule heat source with SOC during charging and discharging for four different cases (a): positive electrode and (b): negative electrode [7].

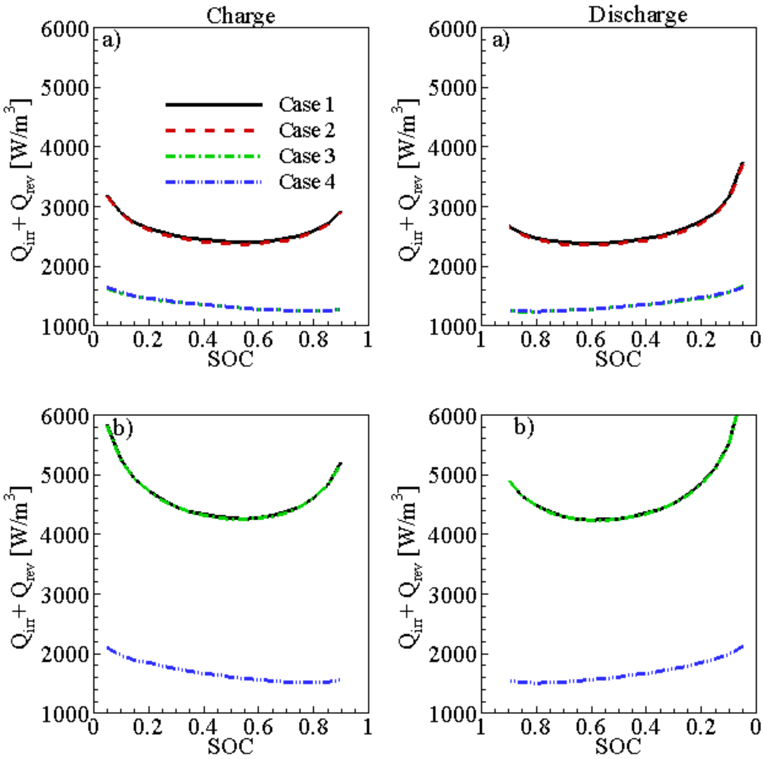

Fig.4. Variation of reversible and irreversible heat sources with SOC during charging and discharging for four different cases. (a): positive electrode and (b): negative electrode [7].

CONCLUSIONS

The effects of graded porosity in the electrodes on heat transfer phenomena have been analyzed thoroughly. Four different cases are considered to illustrate these effects. Case 4, where the electrode porosity is increased from 64% to 94% toward the membrane in both the negative and positive electrodes, shows a higher potential for performance compared to the other cases. This improved performance is likely due to porosity enhancing the ohmic activation in the electrodes. The heat generated within the battery decreases with the design in Case 4, leading to the conclusion that the battery with the Case 4 design has better thermal stability.

ACKNOWLEDGEMENT

The authors would like to thank the Scientific Research Projects Unit of Erciyes University for funding supported by project coded FDK-2019- 9340.

REFERENCES

1. E. Ali, H. Kwon, J. Choi, J. Lee, J. Kim, H. Park, A numerical study of electrode thickness and porosity effects in all vanadium redox flow batteries, J. Energy Storage. 28 (2020) 101208.
2. W. Chen, J. Kang, Optimization of electrolyte flow and vanadium ions conversion by utilizing variable porosity electrodes in vanadium redox flow batteries, Chem. Phys. 529 (2020) 110577.
3. A. Tang, J. Bao, M. Skyllas-Kazacos, Thermal modelling of battery configuration and self-discharge reactions in vanadium redox flow battery, J. Power Sources. 216 (2012) 489–501.
4. A. Trov`o, A. Saccardo, M. Giomo, M. Guarnieri, Thermal modeling of industrial-scale vanadium redox flow batteries in high-current operations, J. Power Sources. 424 (2019) 204–214.
5. B.W. Zhang, Y. Lei, B.F. Bai, A. Xu, T.S. Zhao, A two-dimensional mathematical model for vanadium redox flow battery stacks incorporating nonuniform electrolyte distribution in the flow frame, Appl. Therm. Eng. 151 (2019) 495–505.
6. P.J. Alphonse, G. Elden, The investigation of thermal behavior in a vanadium redox flow battery during charge and discharge processes, J. Energy Storage. 40 (2021).
7. P.J. Alphonse, THERMAL AND STRUCTURAL ANALYSIS OF VANADIUM REDOX FLOW BATTERIES, PhD thesis, Erciyes University, Kayseri, Turkey, 2023.

A LEARNING-FREE EXPLAINABLE INTELLIGENT AGENT FOR REAL-TIME HOME ENERGY MANAGEMENT WITH PHOTOVOLTAIC AND BATTERY STORAGE

Ozan Gül[1*]
[1]Bingöl University, Engineering Faculty, Department of Electrical and Electronics Engineering, Bingöl, Türkiye
*Corresponding author e-mail: ogul@bingol.edu.tr

Ref # EST-03

ABSTARCT

Home energy management systems (HEMS) integrating photovoltaic (PV) generation and battery energy storage systems (BESS) are essential for maximizing self-consumption, reducing grid dependency, and minimizing costs under time-of-use (ToU) tariffs. This paper proposes a lightweight, learning-free intelligent agent based on transparent utility-score maximization for real-time decision-making in residential HEMS. The agent evaluates three discrete actions—grid interaction, battery discharge, and charging—using a weighted utility function that balances electricity cost savings, grid relief, and state-of-charge (SOC) preservation. Inherent explainability is achieved through per-timestamp utility score visualizations, enabling clear traceability of decisions.
A 24-hour simulation with synthetic yet realistic PV, load, and ToU pricing profiles demonstrates effective arbitrage: charging during low-price midday periods, exporting excess PV, and discharging during evening peaks. Results include a self-consumption rate of 78%, self-sufficiency of 65%, near-zero grid import during high-price hours and estimated 25–35% daily cost savings compared to no-EMS baselines. The approach provides a computationally efficient, interpretable alternative to black-box reinforcement learning methods, suitable for edge devices in smart homes.
Keywords: Home energy management system, explainable artificial intelligence, battery energy storage, photovoltaic integration, real-time optimization.

INTRODUCTION

The rapid growth of rooftop photovoltaic (PV) systems and residential battery energy storage systems (BESS) has empowered prosumers to increase self-consumption, reduce grid reliance, and engage in dynamic energy markets [1], [2]. However, PV intermittency, variable time-of-use (ToU) pricing, and unpredictable loads create challenges for optimal energy management. Without intelligent control, excess midday PV is exported at low value, while expensive evening grid imports occur, leading to suboptimal outcomes [3].
Home Energy Management Systems (HEMS) coordinate PV, BESS, and loads to minimize costs and maximize self-sufficiency. Rule-based controllers are simple but often suboptimal under dynamic conditions [4]. Advanced methods like model predictive control (MPC) and reinforcement learning (RL) achieve better performance, with RL showing 10–30% cost reductions in PV+BESS scenarios [5], [6]. Yet these approaches suffer from high complexity, training demands, and poor interpretability—hindering user trust and regulatory acceptance in demand response [7].
Explainable Artificial Intelligence (XAI) addresses these gaps by making decisions transparent [7], [2]. Recent frameworks integrate XAI techniques (e.g., SHAP, LIME) for interpretable building energy management, including PV forecasting and automated control [2]. In residential HEMS, explainability fosters adoption by clarifying price-responsive actions without black-box opacity [5].
Learning-free, inherently interpretable methods remain underexplored for real-time PV+BESS dispatch. This work proposes a learning-free explainable intelligent agent using weighted utility maximization to select among grid interaction, battery discharge, or charging. Utility scores provide inherent explainability via visualizations, revealing decision drivers (price, net load, SOC) from deployment onward.
Contributions:

- Transparent utility framework for three-action HEMS control.
- Inherent explainability through utility trajectories.
- Simulation showing 78% self-consumption, 65% self-sufficiency, near-zero peak imports, and 25–35% cost savings.

The paper is organized as follows: Section II details the model and agent. Section III presents and discusses results, followed by conclusions.

MATERIALS AND METHODS

This section describes the residential home energy management system (HEMS) model, the synthetic data generation process, and the proposed learning-free explainable intelligent agent in detail. All simulations were implemented in MATLAB R2024b with a 15-minute time resolution (dt = 0.25 h) over a full 24-hour horizon (N = 96 timesteps), enabling real-time decision evaluation suitable for edge-device deployment.

System Model and Parameters

The modeled prosumer household integrates the following components:

- A rooftop photovoltaic (PV) array with a peak power of 5 kW, typical for residential installations.
- Household load demand with an average of 3 kW and noticeable evening peaks.
- A lithium-ion battery energy storage system (BESS) with a usable capacity of 10 kWh and state-of-charge (SOC) limits set between 20% and 90% to preserve battery lifetime.
- Initial SOC set at 50% for a neutral starting condition.
- A fixed charging/discharging rate of 2 kW, compatible with common residential inverters.

The net load at each timestep i is calculated as Eq. (1):

$$\text{Net\_Load}(i) = \text{Load}(i) - \text{PV}(i) \text{ (in kW)} \quad (1)$$

Positive values represent net demand (import required), while negative values indicate surplus generation (export possible).

Synthetic Data Generation

Synthetic yet realistic profiles were generated to ensure reproducibility and focus on algorithmic behavior under representative conditions:
PV generation follows a smooth sinusoidal shape Eq. (2):

$$\text{PV}(i) = 5 \times \max(0, \sin(t(i) - 6) \times \pi / 12)) \quad (2)$$

This yields a midday peak of approximately 5.5 kW, simulating clear-sky conditions for a south-facing 5 kWp system.
Household load is modeled as Eq. (3):

$$\text{Load}(i) = 3 + 1.5 \times \sin((t(i) - 16) \times \pi / 8) + 0.5 \times \text{rand}(1) \quad (3)$$

A base load of 3 kW is augmented with an evening hump (peaking ~4.5–5 kW between 17:00–20:00) and small Gaussian noise for realism.
Electricity price (ToU tariff) is defined as Eq. (4):

$$\text{Price}(i) = 0.15 + 0.10 \times (\text{PV}(i) == 0) + 0.05 \times \sin((i) \times \pi / 12) \quad (4)$$

This creates low prices (~0.12 $/kWh) during high-PV midday hours and higher prices (~0.25–0.28 $/kWh) in the evening and night, reflecting common residential dynamic tariffs.
These profiles effectively capture the core arbitrage opportunity: storing excess midday PV at low cost and discharging during expensive evening peaks. Use SI units only.

Utility-Based Decision Agent

At timestep i, net load is:
Net_Load(i) = Load(i) − PV(i)
Three actions are evaluated:

1. **Grid-only (a1)**: U_1 = w_cost × (Net_Load × Price(i)) + w_grid × Net_Load
2. **Battery discharge (a2)** (if SOC(i) > SOC_min): U_2 = w_cost × 0 + w_soc × |Net_Load|
3. **Battery charge (a3)** at 2 kW (if SOC(i) < SOC_max): U_3 = w_cost × (Net_Load + 2) × Price(i) + w_soc × (−2)

Weights: w_cost = −0.6, w_grid = −0.3, w_soc = −0.1.
Highest-utility action executes; SOC updates as:

- Discharge: ΔSOC = − (Net_Load × dt) / Batt_Cap
- Charge: ΔSOC = +(2 × dt) / Batt_Cap

Briefly and descriptively entitle each table and caption each figure. Place the table title above the table and the figure caption below the figure. Each table and figure should be cited in the text (e.g., Fig. 1, Table 1); and placed as close as possible to the text to which they refer. Allow single spacing between the table or figure and the adjacent text, and there should be no space between the table title and table (or between figure caption and figure). Tables and figures should be numbered consecutively with Arabic numerals. Do not reduce figures or tables to a size that is difficult to read. Please make sure there is no copyright issue with the photos/figures.

Explainability and Framework

Explainability is built-in and does not rely on post-hoc tools. All three utility scores (U_1, U_2, U_3) are recorded at every timestep and presented as a stacked area plot. This visualization immediately reveals decision rationales — for example, dominant Charge utility (yellow) during low-price periods or strongly negative Grid utility (blue) during high-price peaks — correlating directly with price signals, SOC constraints, and net load dynamics. Unlike black-box reinforcement learning methods that require external interpretability layers, this framework provides full transparency from the first operation.

RESULTS AND DISCUSSION

This section presents the key simulation outcomes of the proposed learning-free explainable intelligent agent and discusses their significance, strengths, limitations, and comparison with related work in residential PV + BESS energy management.
The 24-hour simulation used realistic synthetic profiles: 5 kW peak PV (~5.5 kW midday maximum), household load averaging 3 kW with evening peaks (~4.5–5 kW, 17:00–20:00), and ToU pricing (~0.12 $/kWh midday, 0.25–0.28 $/kWh evening/night).

Power Flow, Battery Response, and Key Metrics

Fig 1. shows the overall system behaviour.

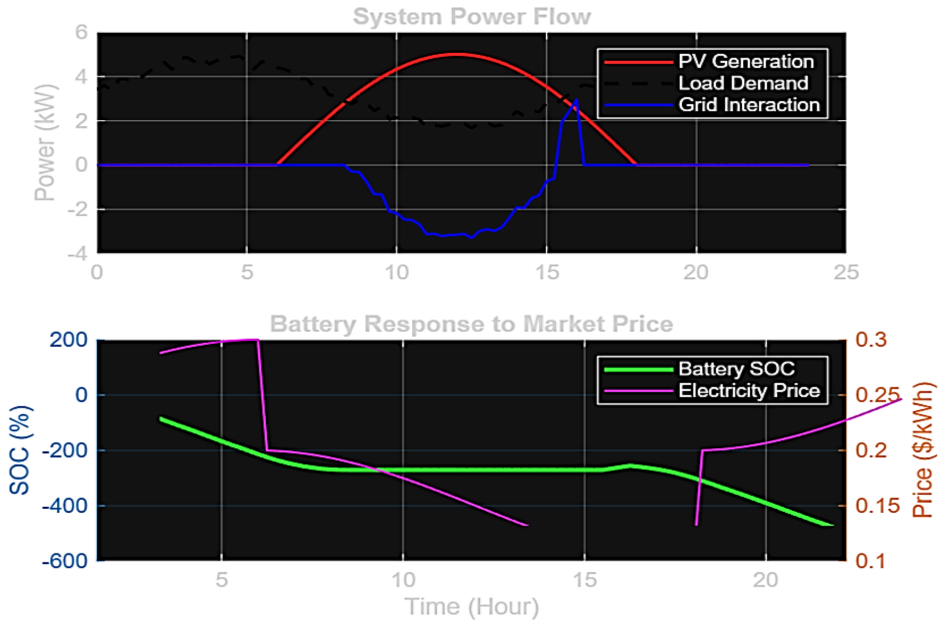

Fig. 1. (Top) Power flow: PV (red), load (black dashed), grid interaction (blue; + import, − export). (Bottom) Battery SOC (%) (green) and price ($/kWh) (magenta).

Midday PV surplus drives battery charging (SOC → ~90%) and grid export. Evening peaks trigger discharge, keeping grid import near zero despite high prices. Overnight remains passive.
Quantitative results:

- **Self-Consumption Rate (SCR)**: 78% (baseline without storage: 25–40%; typical with basic storage: 60–80%).
- **Self-Sufficiency Rate (SSR)**: 65%.
- **Peak-hour grid import (17–20 h)**: <0.5 kWh (>90% reduction vs. no-EMS baseline).
- **Estimated daily cost savings**: 25–35% vs. grid-only baseline (consistent with 20–40% reported in ToU + battery studies).
- **Battery cycling**: ~0.8–1.0 equivalent full cycles/day (moderate, battery-friendly).

These outcomes show effective arbitrage: low-cost midday charging + high-price evening discharge, with strong PV utilization.

Explainable Decision-Making

Fig 2. visualizes utility scores for inherent transparency.

Charge utility peaks midday (low price + PV surplus); Grid and Charge turn strongly negative in evening peaks → discharge prioritized. The stacked area plot clearly links decisions to price, SOC, and net load, providing intuitive explanations without external tools—unlike black-box RL methods.

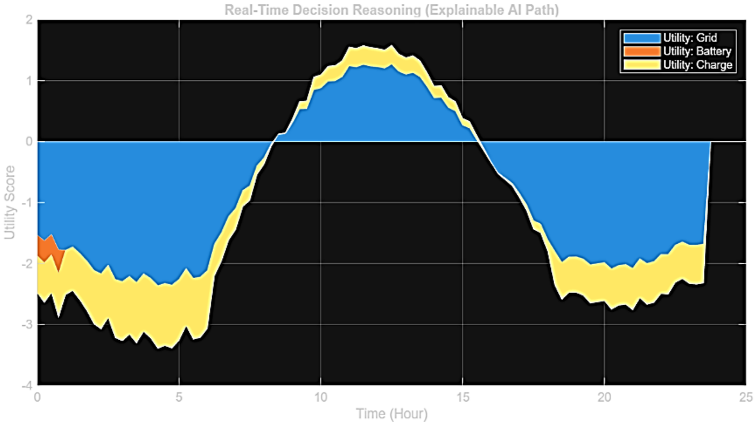

Fig. 2. Utility scores: Grid (blue), Battery (orange), Charge (yellow) over 24 hours.

Discussion

The proposed agent achieves competitive performance with high SCR and SSR, along with meaningful cost savings, while providing extreme simplicity (no training, O (1) per timestep) and built-in explainability—directly addressing barriers to user trust and deployment. Key strengths include tuneable weights for balancing cost vs. battery life, immediate edge-device deploy ability, and far superior transparency over complex MPC or RL methods. Limitations are the fixed 2 kW rate (limited flexibility), synthetic data (real-world variability untested), and single-objective utility (no degradation or multi-criteria modelling).
Results align with recent residential ToU arbitrage literature (20–40% savings, 60–80% SCR with storage). Its inherent XAI sets it apart from opaque AI-HEMS approaches. Future work will cover variable rates, real-data validation, RL/MPC benchmarking, SHAP integration, degradation modelling, and multi-home extensions. In summary, the agent offers an efficient, transparent, and cost-effective solution for residential energy management under dynamic pricing—a practical, interpretable choice for smart homes.

CONCLUSIONS

A transparent, learning-free agent for residential HEMS with PV and BESS was presented. Utility maximization yields 78% self-consumption, 65% self-sufficiency, near-zero peak imports, and 25–35% savings. Utility visualizations ensure interpretability, addressing black-box limitations in AI-EMS.
The method's simplicity and transparency suit edge devices and user-centric applications. Extensions to real data, advanced XAI, and multi-objective control will enhance its role in sustainable energy systems.

REFERENCES

1. Saleem MI et al. 2024. A stochastic MPC-based energy management system for integrating solar PV, battery storage, and EV charging in residential complexes. Energy and Buildings 318:114456.

2. Teixeira B et al. 2025. Explainable AI framework for reliable and transparent automated energy management in buildings. Energy and Buildings 347:16246.

3. Rokonuzzaman M et al. 2026. Artificial intelligence, IoT, and solar PV-integrated home energy management systems: A review. Results in Engineering 25:103996.

4. Gokhale G et al. 2024. Explainable Reinforcement Learning-based Home Energy Management Systems using Differentiable Decision Trees. ACM e-Energy '24 Companion.

5. Hassan M et al. 2025. Artificial intelligence powered intelligent energy management framework for hydrogen storage and dispatch in smart microgrids. Scientific Reports 15:24408.

6. Rizk-Allah RM et al. 2024. Explainable AI and optimized solar power generation forecasting model based on environmental conditions. PLOS ONE 19:e0308002.

7. Alsaigh R et al. 2023. AI explainability and governance in smart energy systems: A review. Frontiers in Energy Research 11:1071291.

COMPARATIVE PERFORMANCE ASSESSMENT OF EAF SLAG AND SINTERED ORE AS PACKED-BED THERMAL ENERGY STORAGE FILLERS FOR ORGANIC RANKINE CYCLE WASTE HEAT-TO-POWER CONVERSION

David Ogbemudia[1], Keyvan Bahlouli[1], Berke Eyyamoglu[1]*
[1] Energy System Engineering Program, Mechanical Engineering Department, Faculty of Engineering, Cyprus International University, Nicosia, N. Cyprus via Mersin 10, Türkiye
*Corresponding author e-mail: dogbemudia@ciu.edu.tr

Ref # EST-04

ABSTRACT
This study presents a performance assessment of a packed-bed sensible thermal energy storage (PBSTES) system which was integrated with an Organic Rankine Cycle (ORC) for waste heat-to-power conversion from Electric Arc Furnace (EAF). EAF slag and Sintered ore were chosen as the filler materials and investigated under identical bed geometry, transient boundary conditions, and ORC configuration. Using a one-dimensional, two-phase packed-bed model with Wakao–Funazkri and Ergun correlations, sintered ore delivered 37% greater thermal storage capacity and a longer discharge window of 2.13hr, which directly *translated to 39% greater cumulative ORC electrical output per cycle* when compared with EAF slag. However, both systems exhibited comparable discharge efficiencies of 80.23% and 78.17% respectively, ORC thermal efficiency of 21.07% and pressure drop of 878.1 Pa. This shows that the discharge quality is primarily governed by the thermocline propagation dynamics rather than by the absolute storage capacity. This similarity is further compounded by the similar particle diameter and thermal conductivity of both fillers. Although sintered ore is the more superior filler thermodynamically, EAF slag emerges as a technically equivalent and zero-procurement-cost sustainable alternative, thereby strongly supporting circular economy as well as industrial decarbonization objectives within steelmaking industries.
Keywords: *Electric Arc Furnace, Energy efficiency, Sustainable Energy, EAF Slag, Sintered Ore.*

INTRODUCTION
The iron and steel industry are one of the most energy-intensive sectors in the global economy, which accounts for about 4 to 5% of the world's energy consumption [1]. Interestingly, a significant proportion of this energy is rejected as waste heat across a wide range of temperatures i.e. from low-grade hot water streams at 90°C, to high-grade converter gases which exceeds 1,500°C [2]. In modern Electric Arc Furnaces (EAFs), a significant amount of energy is released as waste heat via an off-gas stream or coolant. And so, depending on the operating condition, 12–56 % of the total energy can leave as waste heat, where the sensible heat content of the off-gas alone can approach 150–250 kWh per tonne of steel [3]. Despite the immerse potential of EAF off-gas waste heat recovery, deployment remains limited due to severe dust loading, corrosive/erosive conditions, as well as strong batch-cycle fluctuations which raise the equipment complexity and maintenance needs, leading to long payback periods and high retrofit investment costs [4].
The Organic Rankine Cycle (ORC) has emerged as the most commercially viable technology for converting low-to-high temperature industrial waste heat into electricity, with operating installations at EAF plants ranging from 0.7 MW at NatSteel Singapore to 7 MW at Arvedi Cremona, Italy [1,5]. Nonetheless, there are challenges with direct ORC coupling to the EAF off-gas source due to the intermittency of the streams. EAF-driven ORCs without thermal buffering must regularly restart between heats, and operate well below their rated load, with each start-stop cycle accelerating component degradation and extending payback periods of the plant [1]. Studies conducted by Couvreur et al. [6] demonstrated that integrating hot-water tanks upstream of the ORC evaporator can effectively smoothen out the heat-source variability as well as enhance the system's stability and electricity production. Amongst the TES configurations, packed-bed sensible thermal energy storage (PBSTES) is uniquely positioned for EAF waste heat recovery. Unlike the conventional two tank molten salt systems used in high temperature power cycles, a single-tank thermocline packed-bed requires no liquid storage media, can operate with air as the direct heat transfer fluid (HTF) and still achieves effective thermal stratification needed for high quality heat delivery to an ORC power cycle [7]. Therefore, the selection of filler material used in the PBSTES is a central engineering decision that needs to be made carefully. Conventional sustainable filler materials such as natural rock, ceramics, and sand, carry procurement and transport costs and embody no circular economy benefit in the context of EAF steel production plant. EAF slag, a waste by-product of EAF Steel making, produced at 100–200 kg per tonne of crude steel, presents a compelling alternative to the others [8]. Although EAF slag is a natural candidate for PBSTES, only limited studies have evaluated its end-to-end integration with an ORC power block under realistic EAF transient off-gas conditions [9]. Moreover, the authors found no studies on comparative assessments between industrial waste-derived fillers and commercially processed alternatives such as sintered ore under identical transient EAF operating conditions for waste-heat-to-power integration. Therefore, this study addresses these gaps by conducting a baseline performance comparison of EAF slag and sintered ore as PBSTES fillers integrated with an ORC for EAF waste heat-to-power conversion. Sintered ore particles serve as an ideal commercial benchmark for comparison with EAF steel slag because it has been experimentally validated in multiple studies as a high-performance, high-temperature sensible heat storage filler in air-based packed-bed TES systems [10].

SYSTEM DESCRIPTION

The integrated system consists of a cylindrical PBSTES unit, with a diameter of 3m, height of 5.2 m and150 axial nodes charged by EAF off-gas air and discharged to an ORC power cycle as shown in Fig. 1. During the charging mode, hot EAF off-gas passes downward through the bed from the top end. Charging terminates when the cold outlet temperature reaches 500 °C, establishing a sharp thermocline. During discharge, a recirculation blower draws air upward through the bed and delivers it to the ORC heat exchanger. A maximum ORC inlet temperature of 500 °C was imposed with the use of a mixing/bypass control assumption in order to avoid excessive peak temperatures at the evaporator as well as maintain a consistent stability with the working-fluid [1]. The EAF source profile was gotten from Brandt et al. [11], which spans approximately 0.88 h with mass flow rates of 15–21 kg/s and temperatures of 108–754°C, which exhibits pronounced intermittency characteristic of EAF heat cycles. The ORC power cycle operates under steady-state conditions during discharge, with Benzene selected based on its thermal stability at EAF temperature levels as well as favorable dry-fluid expansion characteristics.

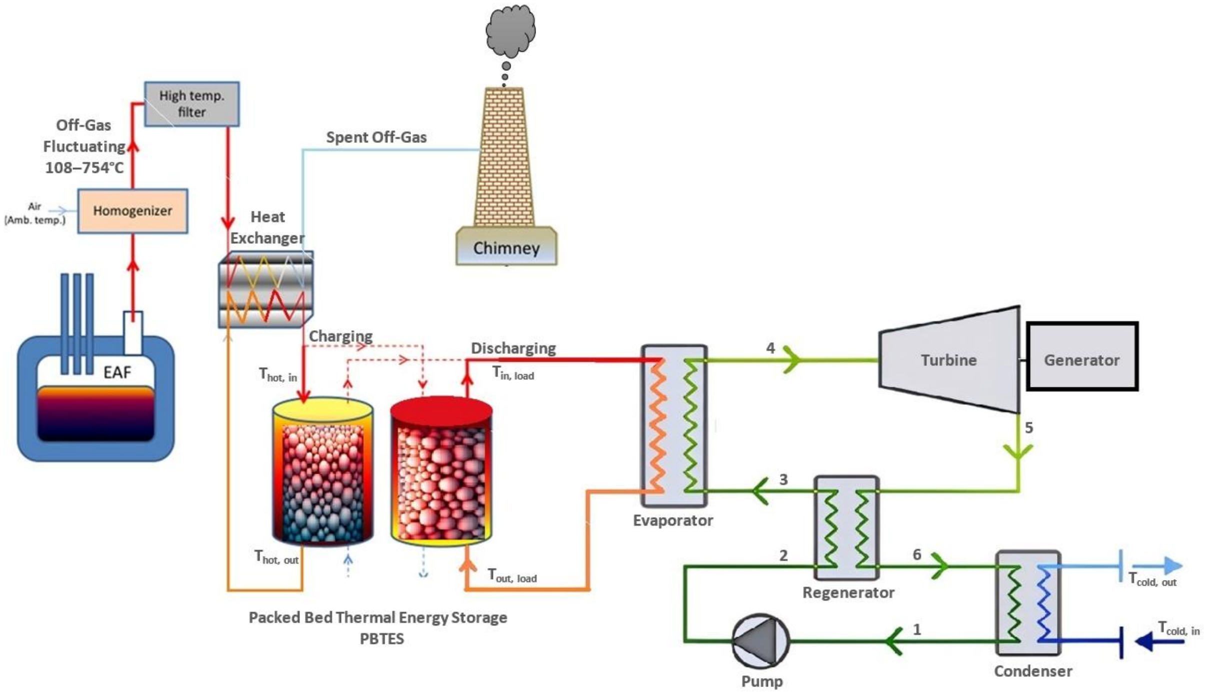

Fig. 1 Schematic diagram of the integrated EAF off-gas waste heat recovery system with thermocline packed-bed thermal energy storage and ORC power block.

METHODOLOGY

The TES unit is modelled as a one-dimensional transient two-temperature (LTNE) packed bed. The Key assumptions for the PBSTES are: (1) The model assumes transient operation under local thermal non-equilibrium within a homogeneous, rigid porous medium, while neglecting radiative heat transfer and wall heat losses [7]; (2) Incompressible fully-developed flow and uniform intra-particle temperature [9]; (3) Temperature-dependent air properties and radiation and wall losses neglected [12].

The fluid and solid energy equations are:

$$\varepsilon\rho_f c_{p,f}\frac{\partial T_f}{\partial t}=\frac{\partial}{\partial z}\left(\lambda_{eff,f}\frac{\partial T_f}{\partial z}\right)-\varepsilon\rho_f c_{p,f}u\frac{\partial T_f}{\partial z}+h_{eff}a_r\left(T_r-T_f\right) \quad (1)$$

$$(1-\varepsilon)\rho_r c_{p,r}(T)\frac{\partial T_r}{\partial t}=\frac{\partial}{\partial z}\left(\lambda_{eff,r}\frac{\partial T_r}{\partial z}\right)-h_{eff}a_r\left(T_r-T_f\right) \quad (2)$$

where $a_r = 6(1-\varepsilon)/d_p$ and h_{eff} follows the Wakao–Funazkri correlation: $Nu = 2 + 1.1\mathrm{Re}_p^{0.6}\mathrm{Pr}^{1/3}$. Pressure drop uses the Ergun equation gotten from Ref.[13]. The system is solved over MATLAB Simulation platform. Table 1 summarized the filler material properties and ORC Cycle Parameters.

Table 1. Filler material properties and ORC Cycle Parameters

Filler Properties	EAF Slag [14]	Sintered Ore[15]	ORC Parameters [16]	Value
Apparent density (kg/m³)	3,327	4,547	Working fluid	Benzene
Bed Void Fraction (ε)	0.617	0.617	ORC inlet temperature cap [°C]	500
c_p at 500°C (J/kg·K)	900	920	Pump / turbine efficiency [%]	75 / 85
λ_s (W/m·K)	1.50	1.50	Condensation temperature [°C]	95
Origin	EAF waste (zero-cost)	Commercial (BF–BOF)	Pinch point (°C)	20
Particle Diameter (mm)	35	35	Blower / Mechanical efficiency [%]	0.70/ 0.98

Table 2. Performance Metrics and Governing Equations for the ORC-Coupled Thermocline Packed-Bed TES System

Metric	Symbol	Key Equation	Reference
Thermal storage capacity	Q_{stored}	$\rho_{\text{bed}} V_{\text{bed}} c_{p,\text{ bed}} (T_{\text{hot}} - T_{\text{in}})$	[10], [14]
Discharge heat delivered	Q_{dis}	$\int_0^{t_{\text{dis}}} \dot{m}_f c_{p,f} (T_{\text{out}}(t) - T_{\text{in}}(t)) dt$	[10], [12], [14]
Discharge efficiency	η_{dis}	$Q_{\text{dis}} / Q_{\text{stored}}$	[12]
ORC thermal efficiency	η_{ORC}	$w_{\text{net}} / (h_4 - h_3)$	[2]
ORC Electrical Energy	E_{elec}	$\int_0^{t_{\text{dis}}} \dot{m}_{\text{ORC}}(t) \cdot w_{\text{net}} \cdot \eta_{\text{mech}}\, dt$	[2]
Total pumping energy	E_{pump}	$\int_0^{t_{\text{chg}}} P_{\text{pump}}\, dt + \int_0^{t_{\text{dis}}} P_{\text{pump}}\, dt$	[10], [14]

RESULTS AND DISCUSSION

It is clear from the results that the PBSTES simulations reveal distinct but complementary performance characteristics for both filler materials under the EAF waste-heat operating conditions**.** As depicted in Fig.2 and Fig.3, both EAF slag and sintered ore develop a sharp, well-stratified thermal front which advances steadily from the hot inlet towards the cold end during charging mode and retreats progressively during discharge mode. This behavior is consistent with ideal thermocline TES operation and indicative of low axial dispersion in both of the packed beds under study. During discharge, the ORC mixing valve effectively maintains the delivered fluid temperature at the 500 °C design cap until the bed outlet declines to the 460 °C cutoff threshold. This cutoff threshold corresponds to a threshold factor of 0.20 applied to the 300–500 °C operating range of the ORC, as recommended by Fasquelle et al. [12]. And so, below this threshold, thermocline front degradation reduces the delivered fluid quality to the ORC evaporator. Following this, the quantitative performance metrics is highlighted in Table 2. The results highlight the energetic superiority of sintered ore. Its greater apparent density and specific heat capacity translates into 37% higher thermal storage capacity and a considerably longer usable discharge window for power delivery at 2.13hr when compared to 1.53hr for the EAF slag.

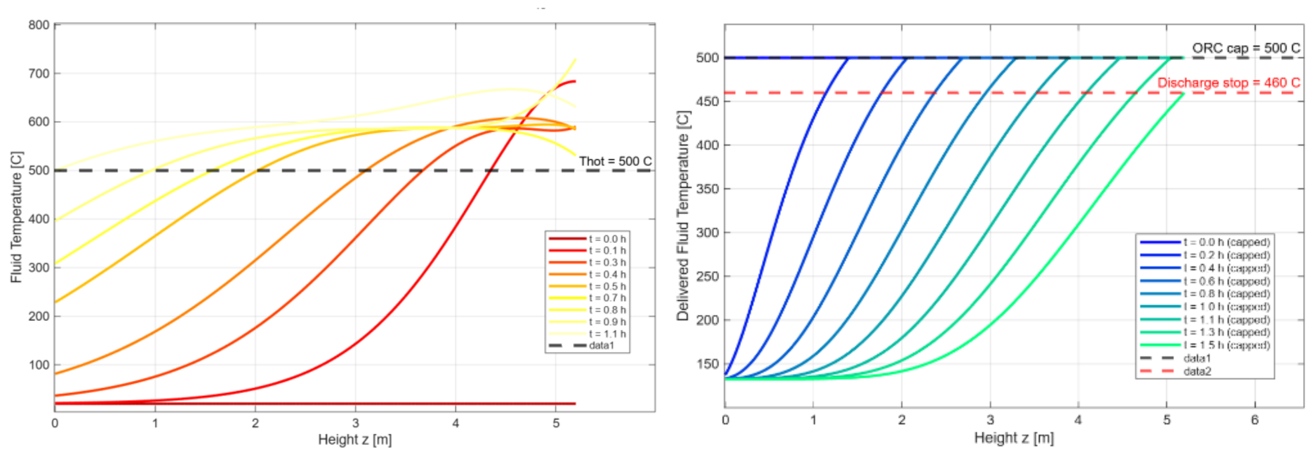

(a) Charging Phase of EAF slag PBTES

(b) Discharge Phase of EAF slag PBTES

Fig. 2. Temperature evolution along bed height during charging and discharge of thermocline packed-bed TES for EAF slag under steel-industry operating conditions (T_{hot} = 500 °C, T_{stop} = 460 °C)

Crucially, however, it can be seen from Table 2 that both fillers exhibit comparable discharge efficiencies (η_{dis}) of 80.23% (EAF slag) and 78.17% (sintered ore), a difference of 2%. This near-equivalence arises because discharge efficiency reflects the fraction of theoretical bed capacity recovered, which is primarily driven by the thermocline propagation rather than by the absolute storage capacity of the filler. And so, several factors are responsible for thermocline propagation and one of the crucial factors is the diameter of the particle and the void fraction, of which both fillers share identical values of 35mm and 0.617, respectively. And so, the resulting interstitial heat transfer coefficient, thermocline thickness, and advancement rate are effectively equivalent for both beds. This finding is consistent with Xu et al. [17], were the authors demonstrated that particle diameter is the dominant factor controlling discharge efficiency, with different filler materials yielding only marginal efficiency differences at particle size lower than 10cm. Furthermore, the cumulative energy output of the ORC for the given discharge timeframe was 730.86kWh and 1016.31kWh for the EAF Slag and Sintered Ore, respectively. This shows the superiority of sintered ore in delivering 39% more cumulative electrical energy per cycle which is a direct consequence of its larger thermal storage capacity.

(a) Charging Phase of Sintered Ore PBTES (b) Discharge Phase of Sintered Ore PBTES

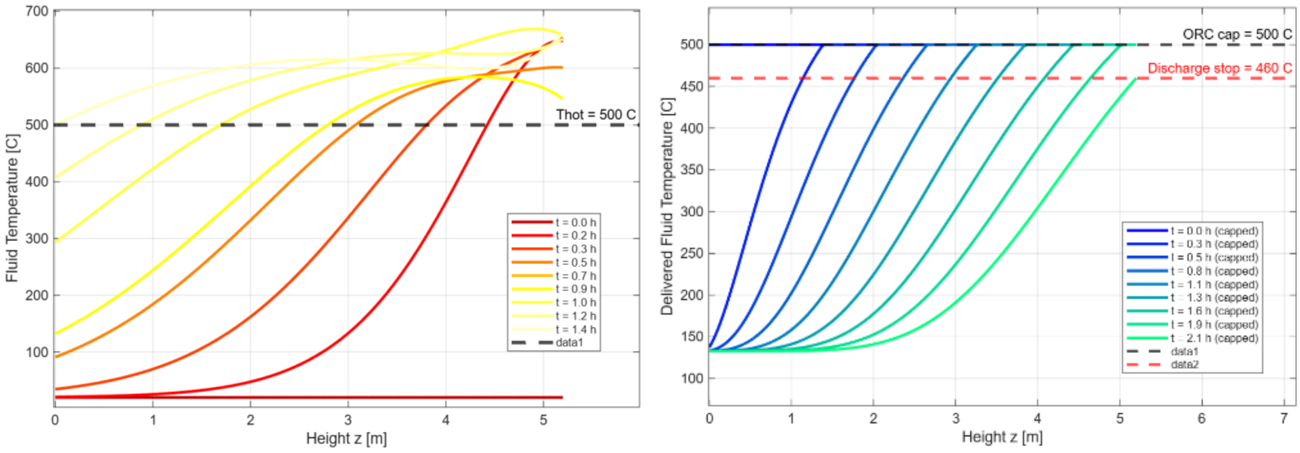

Fig. 3. Temperature evolution along bed height during charging and discharge of thermocline packed-bed TES for Sintered ore fillers under steel-industry operating conditions (T_{hot} = 500 °C, T_{stop} = 460 °C)

Table 2. Summary of ORC-Coupled Thermocline TES Filler Performance

Filler Material	t_{charge} (h)	t_{dis} (h)	Q_{stored} (kWh)	Q_{dis} (kWh)	η_{dis} (%)	ΔP_{drop} (Pa)	$\eta_{th\ (ORC)}$ (%)	E_{pump} (kWh)	$E_{net\ (ORC)}$ (kWh)
EAF slag	1.06	1.53	5730.31	4597.56	80.23	878.1	21.07	420.33	730.86
Sintered Ore	1.39	2.13	7853.39	6138.86	78.17	878.1	21.07	616.37	1016.31

Although, the longer sintered ore cycle accumulates 47% higher total pumping energy at 616.37kWh, this increase is driven by its longer discharge duration rather than any difference in flow resistance, since both beds produce the same pressure drop of 878.1 Pa. Nonetheless, the evidence is clear that sintered ore is a more energetic superior filler thermodynamically. However, EAF slag which is an industrial by-product available at near-zero material cost emerges as a more compelling and practically viable alternative where economics and feedstock constraints are the governing design considerations for the PBSTES.

CONCLUSION

This study presents a baseline performance comparison of EAF slag and sintered ore as packed-bed TES fillers integrated with an ORC for EAF waste heat-to-power conversion. The Sintered Ore exhibited 37% higher thermal energy storage capability and a longer discharge duration of 2.13 hours which directly translates to 39% greater cumulative ORC electrical output per cycle, yielding 1016.31 kWh compared with 730.86 kWh for EAF slag. Despite this energetic advantage of sintered ore, both fillers delivered comparable discharge efficiencies of 80.23% and 78.17%, a difference of 2%. This is because discharge efficiency is primarily driven by the thermocline propagation rather than by the absolute storage capacity of the filler, where the most prominent factors influencing the propagation were the particle diameter and void fractions, of which sintered ore and EAF slag were the same. Therefore, EAF Slag is established as a technologically equivalent but material wise superior environmentally friendly substitute, which removes the entire cost of purchasing the raw material from outside the Steel Mill. Future work will extend this framework to comparative cross-industry assessments encompassing cement and food processing waste heat profiles. Likewise, a cascaded PCM-sensible hybrid TES configurations will be integrated to improve thermocline sharpness and round-trip efficiency. More so, a parametric study as well as a full exergy and techno-economic analyses will be conducted to identify the most cost-effective filler-cycle pairings across industrial sectors.

NOMENCLATURE

ε	Bed void fraction
ρ_f	Fluid density(kg/m³)
T_f	Fluid Temperature (K)
a_r	Specific surface area (m²)
T_r	Solid Temperature (K)
d_p	Particle diameter
ρ_r	Solid density(kg/m³)

$c_{p,f}$ Fluid specific heat (j/kg/k)
λ_{eff} Thermal conductivity (W/m/K)
ΔP Pressure Drop (Pa)
h_{eff} Effective Heat transfer coefficient (W/m^2/K)
Nu Nusselt number
Re_p Reynolds number
Pr Prandtl Number
η_{dis} Discharge efficiency
u Superficial velocity (m/s)
$\dot{m}$ mass flow rate (kg/s)
w_{net} Specific Work (kj/kg)
E_{net} Net Electrical Energy (kWh)
h Enthalpy (kj/kg)
Q_{stored} Stored thermal energy (kWh)
Q_{dis} Discharged heat (kWh)
E_{Pump} Total Pump Energy (kWh)

REFERENCES

[1] M. Ja'fari, M. I. Khan, S. G. Al-Ghamdi, A. J. Jaworski, and F. Asfand, "Waste heat recovery in iron and steel industry using organic Rankine cycles," *Chemical Engineering Journal*, vol. 477, no. 2, p. 146925, Dec. 2023, doi: 10.1016/j.cej.2023.146925.
[2] S. Lecompte *et al.*, "Case Study of an Organic Rankine Cycle (ORC) for Waste Heat Recovery from an Electric Arc Furnace (EAF)," *Energies 2017, Vol. 10,* vol. 10, no. 5, May 2017, doi: 10.3390/en10050649.
[3] Ü. Çamdali and M. Tunç, "Modelling of electric energy consumption in the AC electric arc furnace," *Int. J. Energy Res.*, vol. 26, no. 10, pp. 935–947, Aug. 2002, doi: 10.1002/er.829.
[4] G. Hartfuß, M. Schmid, and G. Scheffknecht, "Off-Gas Waste Heat Recovery for Electric Arc Furnace Steelmaking Using Calcium Hydroxide (Ca(OH)2) Dehydration," *Steel Res. Int.*, vol. 91, no. 11, Nov. 2020, doi: 10.1002/srin.202000048.
[5] A. Foresti, S. Santarossa, N. Monti, G. Di Zanni, and C. Milo, "La Metallurgia Italiana-n," vol. 5, p. 18, 2019.
[6] K. Couvreur, W. Beyne, M. De Paepe, and S. Lecompte, "Hot water storage for increased electricity production with organic Rankine cycle from intermittent residual heat sources in the steel industry," *Energy*, vol. 200, Jun. 2020, doi: 10.1016/j.energy.2020.117501.
[7] G. Zanganeh, M. Commerford, A. Haselbacher, A. Pedretti, and A. Steinfeld, "Stabilization of the outflow temperature of a packed-bed thermal energy storage by combining rocks with phase change materials," *Appl. Therm. Eng.*, vol. 70, no. 1, pp. 316–320, Sep. 2014, doi: 10.1016/j.applthermaleng.2014.05.020.
[8] M. Enemuo, N. Enemuo, A. D. Taleghani, and O. Ogunmodimu, "Slags as Thermal Energy Storage Media for Concentrated Solar Power and Renewable Energy Integration," *Energy Storage*, vol. 7, no. 8, p. e70274, Dec. 2025, doi: 10.1002/est2.70274.
[9] I. Ortega-Fernández and J. Rodríguez-Aseguinolaza, "Thermal energy storage for waste heat recovery in the steelworks: The case study of the REslag project," *Appl. Energy*, vol. 237, pp. 708–719, Mar. 2019, doi: 10.1016/j.apenergy.2019.01.007.
[10] Z. Lai, H. Zhou, M. Zhou, L. Lv, H. Meng, and K. Cen, "Experimental study on storage performance of packed bed solar thermal energy storage system using sintered ore particles," *Solar Energy Materials and Solar Cells*, vol. 238, May 2022, doi: 10.1016/j.solmat.2022.111654.
[11] C. Brandt, N. Schüler, M. Gaderer, and J. M. Kuckelkorn, "Development of a thermal oil operated waste heat exchanger within the off-gas of an electric arc furnace at steel mills," *Appl. Therm. Eng.*, vol. 66, no. 1–2, pp. 335–345, 2014, doi: 10.1016/j.applthermaleng.2014.02.003.
[12] T. Fasquelle, Q. Falcoz, P. Neveu, and J. F. Hoffmann, "A temperature threshold evaluation for thermocline energy storage in concentrated solar power plants," *Appl. Energy*, vol. 212, pp. 1153–1164, Feb. 2018, doi: 10.1016/j.apenergy.2017.12.105.
[13] N. Wakao and T. Funazkri, "Effect of fluid dispersion coefficients on particle-to-fluid mass transfer coefficients in packed beds," *Chem. Eng. Sci.*, vol. 33, no. 10, pp. 1375–1384, 1978, doi: 10.1016/0009-2509(78)85120-3.
[14] Y. Rong, S. Y. Huang, and H. Zhou, "Experimental study on storage performance of packed bed solar thermal energy storage system using steel slag," *J. Energy Storage*, vol. 78, Feb. 2024, doi: 10.1016/j.est.2023.110042.
[15] Z. Lai, H. Zhou, M. Zhou, L. Lv, H. Meng, and K. Cen, "Experimental study on storage performance of packed bed solar thermal energy storage system using sintered ore particles," *Solar Energy Materials and Solar Cells*, vol. 238, May 2022, doi: 10.1016/j.solmat.2022.111654.
[16] B. Eyyamoglu and K. Bahlouli, "Performance and economic analysis of a nanofluid-based solar-driven trigeneration system for a residential building in Cyprus," *Appl. Therm. Eng.*, vol. 277, p. 127001, Oct. 2025, doi: 10.1016/J.APPLTHERMALENG.2025.127001.
[17] C. Xu, X. Li, Z. Wang, Y. He, and F. Bai, "Effects of solid particle properties on the thermal performance of a packed-bed molten-salt thermocline thermal storage system," *Appl. Therm. Eng.*, vol. 57, no. 1–2, pp. 69–80, Aug. 2013, doi: 10.1016/j.applthermaleng.2013.03.052.

COMPUTATIONAL THERMODYNAMIC AND DFT ANALYSIS OF A LANTHANUM MANGANITE–BASED REDOX CYCLE FOR THERMOCHEMICAL ENERGY STORAGE

Rahul R. Bhosale[1]
[1] Department of Civil and Chemical Engineering, University of Tennessee at Chattanooga, 615 McCallie Ave, Chattanooga, TN 37403, USA
*Corresponding author e-mail: rahul-bhosale@utc.edu

Ref # EST-05

ABSTRACT

Density functional theory-based quantum chemical calculations and computational non-stoichiometric thermodynamic analysis were used to systematically analyze the redox characteristics of lanthanum manganite ($LaMnO_3$) in order to evaluate its potential for use in high-temperature solar thermochemical energy storage (TCES). Equilibrium calculations spanning a range of oxygen partial pressures (0.05–0.0001 atm) and reduction temperatures (1073–1473 K) were used to calculate oxygen evolution and the related oxygen non-stoichiometry (δ). According to the analysis, oxygen release gradually rises with temperature, especially in severely reducing environments. The material had δ values close to 0.1045 at 1473 K and an oxygen partial pressure of 0.0001 atm. These results show that under different thermodynamic settings, lanthanum manganite exhibits variable redox behavior, indicating that it may be a suitable redox material for high-temperature TCES systems.

Keywords: Lanthanum Manganite, Thermochemical, Energy Storage, DFT, Thermodynamic Analysis

INTRODUCTION

The search for sustainable energy technologies that can provide dependable and low-carbon power generation[1,2] has escalated due to the ongoing rise in global energy consumption [3,4], growing worries about climate change [5,6], and rising greenhouse gas emissions [7,8]. As a result, renewable energy systems have garnered a lot of interest as potential substitutes for the generation of power from fossil fuels [9,10]. Concentrated solar power (CSP) has become one of these technologies' most appealing methods for turning solar radiation into useful thermal energy [11,12]. In CSP systems, large arrays of mirrors concentrate sunlight onto a receiver, generating high temperatures that can be used to produce steam and drive turbines for electricity generation. Despite these advantages, CSP plants face operational challenges due to the inherent variability of solar irradiation, particularly during nighttime or cloudy conditions. Consequently, the integration of efficient energy storage systems has become essential to maintain continuous and stable power generation from CSP facilities [13].

Thermochemical energy storage (TCES) has been widely proposed as a promising solution for addressing the intermittency of solar energy in CSP systems. In TCES processes, excess thermal energy collected during periods of strong solar irradiation can be stored through reversible chemical reactions and later released when solar input decreases [14]. This capability enables dispatchable power generation, enhances the operational flexibility of CSP plants, and improves their overall economic performance. Moreover, TCES technologies contribute to the broader goal of sustainable energy systems by enabling long-duration energy storage with relatively high energy density compared with conventional sensible heat storage approaches.

Because metal oxides (MOs) can reversibly store and release thermal energy at high temperatures, redox processes involving MOs have garnered a lot of attention among different TCES techniques [15]. During the charging stage, solar heat drives the endothermic reduction of the oxide, resulting in the release of oxygen gas and the formation of a reduced material. In the discharging step, the reduced oxide is reoxidized in the presence of oxygen, producing an exothermic reaction that releases the stored energy. This cyclic oxidation–reduction process forms the basis for high-temperature thermochemical storage systems.

Similar to solar thermochemical cycles for splitting CO_2 and H_2O, perovskite-type oxides (ABO_3) are becoming appealing redox materials for high-temperature TCES systems [16–19]. These materials exhibit excellent structural flexibility and fast oxygen transport properties, enabling reversible oxygen exchange under a wide range of thermodynamic conditions. The oxygen exchange process in perovskite oxides can be represented by

$$ABO_{3-\delta_i} \leftrightarrows ABO_{3-\delta_f} + \frac{\delta_f - \delta_i}{2} O_2 \tag{1}$$

where δ_i represents the initial oxygen non-stoichiometry and δ_f corresponds to the oxygen deficiency generated during the endothermic reduction step. During the oxidation stage, the material reincorporates oxygen, restoring the original non-stoichiometry and completing the reversible redox cycle.

Among the wide range of perovskite materials, lanthanum manganite ($LaMnO_3$) has attracted attention because of its favorable structural stability and redox characteristics at elevated temperatures. The oxygen exchange behavior of perovskite systems is strongly influenced by thermodynamic parameters such as the reduction temperature (T_{red}) and the oxygen partial pressure (P_{O_2}). While several experimental studies have investigated perovskite oxides for TCES applications, detailed thermodynamic assessments and predictive computational investigations remain comparatively limited. In this regard, density functional theory (DFT) has become an effective computational method for examining defect formation energies, electronic structure, and redox thermodynamics in metal oxides. By providing insight into oxygen vacancy formation and the associated thermodynamic driving forces, DFT calculations can assist in identifying promising materials for TCES applications. Therefore, the present study evaluates the thermochemical behavior of lanthanum manganite ($LaMnO_3$) as a candidate redox material for high-temperature TCES systems through combined DFT and computational thermodynamic analyses, focusing on the influence of P_{O_2} and T_{red} on the material's oxygen non-stoichiometry and redox performance.

LANTHANUM MANGANITE: NON-STOICHIOMETRIC ANALYSIS

The following equation illustrates the reversible redox reaction connected to the TCES powered by lanthanum manganite:

$$LaMnO_3 + \Delta H \leftrightarrow LaMnO_{3-\delta} + \frac{\delta}{2} O_2 \tag{2}$$

The TCES potential of lanthanum manganite was assessed by measuring the amount of oxygen released as a function of P_{O_2} and T_{red}. As seen in Fig. 1, oxygen release increased monotonically with increasing T_{red} at all investigated P_{O_2} levels. At P_{O_2} = 0.001 atm, the amount of oxygen released during the reduction (energy-storage) stage rose from 0.0014 mol at 1073 K to 0.02134 mol at 1473 K. The released oxygen followed a similar pattern, rising from 0.00192 mol at 1073 K to 0.02798 mol at 1473 K with P_{O_2} = 0.0005 atm. Under all tested conditions, the maximum reduction temperature of 1473 K consistently resulted in the greatest release of oxygen.

Table 1. Effect of P_{O_2} and T_{red} on oxygen release capacity of lanthanum manganite.

T_{red} (K)	P_{O2} = 0.01 atm	P_{O2} = 0.005 atm	P_{O2} = 0.001 atm	P_{O2} = 0.0005 atm	P_{O2} = 0.0001 atm
1073	0.00061	0.00074	0.00140	0.00192	0.00407
1173	0.00149	0.00181	0.00338	0.00459	0.00946
1273	0.00315	0.00381	0.00699	0.00938	0.01875
1373	0.00593	0.00714	0.01281	0.01700	0.03289
1473	0.01016	0.01216	0.02134	0.02798	0.05224

The measured oxygen release from lanthanum manganite was used to compute the proper oxygen non-stoichiometry (δ) associated with the heat reduction phase. δ demonstrated a progressive increase with rising T_{red} at all investigated P_{O_2} levels, which is consistent with the reported increase in oxygen release. For example, with P_{O_2} = 0.001 atm, δ increased from 0.0028 at 1073 K to 0.0427 at 1473 K. Similarly, with P_{O_2} = 0.0005 atm, δ rose from 0.0038 at 1073 K to 0.0559 at 1473 K. Across all oxygen partial pressures, the highest δ values were consistently obtained at the maximum reduction temperature of 1473 K.

Using the estimated δ values, the equilibrium oxygen content of lanthanum manganite was computed as a function of T_{red}. The findings displayed in Fig. 1 confirm that the equilibrium oxygen content of lanthanum manganite decreases when T_{red} increases at all P_{O_2} levels. For instance, the equilibrium oxygen content of lanthanum manganite dropped from 2.997 to 2.957 at P_{O_2} of 0.001 atm when T_{red} raised from 1073 K to 1473 K. Similarly, the equilibrium oxygen content of lanthanum manganite dropped from 2.996 to 2.944 at P_{O_2} = 0.0005 atm as T_{red} climbed from 1073 K to 1473 K. At P_{O_2} = 0.0001 atm and T_{red} = 1473 K, the equilibrium oxygen content of lanthanum manganite dropped from 2.992 to 2.896.

LANTHANUM MANGANITE: DFT ANALYSIS

To assess the suitability of lanthanum manganite as a redox material for TCES, DFT calculations were conducted to examine the thermodynamic factors associated with oxygen vacancy generation and redox activity. Important thermodynamic indicators such as the oxygen vacancy formation energy (OVFE), reaction enthalpy (ΔH), and Gibbs free energy change (ΔG) were determined to evaluate the likelihood of oxygen release and reintegration during the TCES cycle. The OVFE was obtained from the energy difference between the oxidized and reduced configurations of the material together with the calculated energy of the oxygen molecule. The simulations were performed using spin-polarized first-principles calculations implemented in the Quantum ESPRESSO computational package. Electron–ion interactions were represented using pseudopotentials, while the electronic states were expanded in plane-wave basis sets. Exchange–correlation effects were described using the generalized gradient approximation (GGA) within the Perdew–Wang functional, and the DFT+U approach was incorporated to properly account for strong electron correlation effects.

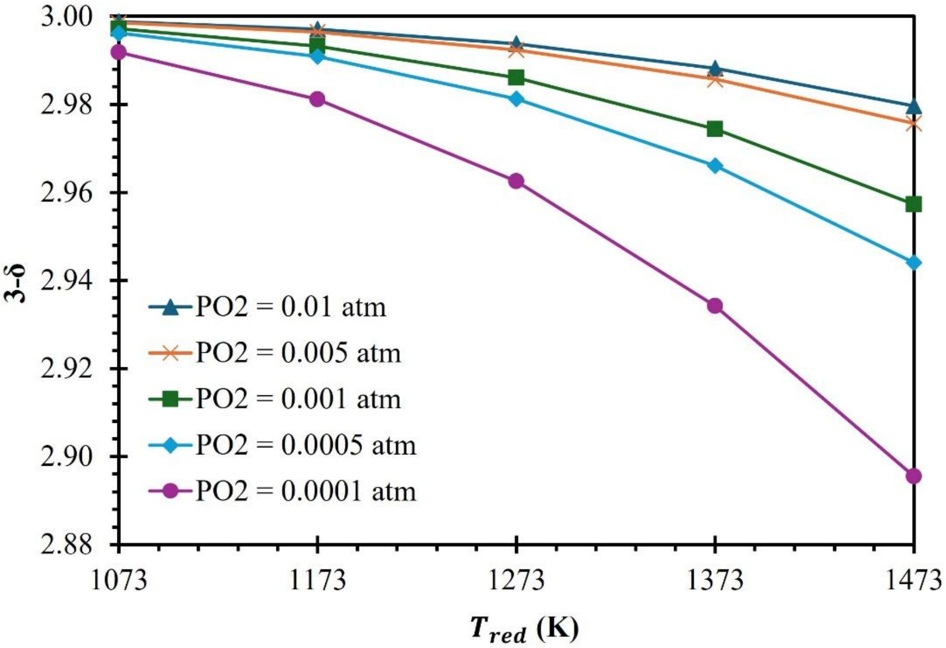

Fig. 1. Effect of P_{O_2} and T_{red} on equilibrium oxygen content of lanthanum manganite.

CONCLUSIONS

This study used both non-stochiometric and DFT analysis to explore the thermodynamic redox properties of lanthanum manganite in order to assess its potential for TCES. The results demonstrated that the release of oxygen increased steadily as the reduction temperature increased for all tested oxygen partial pressures, culminating at 0.02798 mol at 1473 K with P_{O_2} = 0.0005 atm. Conversely, the oxygen non-stoichiometry (δ) demonstrated a consistent upward trend, reaching a peak of 0.0559 at 1473 K and 0.0005 atm, suggesting a notable potential for reduction in low oxygen partial pressure settings. In the case of P_{O_2} = 0.0001 atm, the equilibrium oxygen concentration decreased concurrently from 2.992 at 1073 K to 2.896 at 1473 K.

ACKNOWLEDGEMENT

The author gratefully acknowledges the financial support from the National Science Foundation (NSF), Award CBET# 2501431.

REFERENCES

1. Bhosale RR, Alxneit I, Van Den Broeke LLP, Kumar A, Jilani M, Gharbia SS, et al. 2014. Sol-gel synthesis of nanocrystalline Ni-ferrite and Co-ferrite redox materials for thermochemical production of solar fuels. Materials Research Society Symposium Proceedings 1675:203–208.
2. Steinfeld A. 2013. Materials and Processes for Renewable Energy Technologies. Journal of Metals 65:1658–1659.
3. Dincer I and Aydin MI. 2023. New paradigms in sustainable energy systems with hydrogen. Energy Conversion and Management 283:116950.
4. Bhosale RR. 2019. Thermodynamic analysis of Ni-ferrite based solar thermochemical H_2O splitting cycle for H_2 production. International Journal of Hydrogen Energy 61:71.
5. Bhosale RR, Shende RV, and Gupta RB. 2021. Application of Zn-ferrite towards thermochemical utilization of carbon dioxide: A thermodynamic investigation. Energy Conversion and Management 245:114528.
6. Olabi AG and Abdelkareem MA. 2022. Renewable energy and climate change. Renewable and Sustainable Energy Reviews 158:112111.
7. Bhosale RR and Mahajani VV. 2013. Kinetics of thermal degradation of renewably prepared amines useful for flue gas treatment. Journal of Renewable and Sustainable Energy 5:063110.
8. Vaidya PD and Kenig EY. 2007. CO2-Alkanolamine Reaction Kinetics: A Review of Recent Studies. Chemical Engineering Technology 30:1467–74.
9. Takalkar GD, Bhosale RR, and AlMomani FA. 2019. Combustion synthesized A0.5Sr0.5MnO3-δ perovskites (where, A = La, Nd, Sm, Gd, Tb, Pr, Dy, and Y) as redox materials for thermochemical splitting of CO2. Applied Surface Science 489:80–91.
10. Logan BE and Elimelech M. 2012. Membrane-based processes for sustainable power generation using water. Nature 488:313–319.
11. Răboacă MS, Badea G, Enache A, Filote C, Răsoi G, Rata M, et al. 2019. Concentrating Solar Power Technologies. Energies (Basel) 12:1048.
12. Bhosale RR. 2019. Mn-ferrite based solar thermochemical water splitting cycle: A thermodynamic evaluation. Fuel 256:115847.

13. Chen X, Zhang Z, Qi C, Ling X, and Peng H. 2018. State of the art on the high-temperature thermochemical energy storage systems. Energy Conversion and Management 177:792–815.
14. Carrillo AJ, González-Aguilar J, Romero M, and Coronado JM. 2019. Solar Energy on Demand: A Review on High Temperature Thermochemical Heat Storage Systems and Materials. Chemical Reviews 119:4777–4816.
15. Abanades S. 2023. A Review of Oxygen Carrier Materials and Related Thermochemical Redox Processes for Concentrating Solar Thermal Applications. Materials 16:3582.
16. Bhosale RR, Kumar A, Ashok A, Sutar P, Takalkar G, Khraisheh M, et al. 2017. La-Based Perovskites as Oxygen-Exchange Redox Materials for Solar Syngas Production. MRS Advances 2:3365–3370.
17. Zhang D, De Santiago HA, Xu B, Liu C, Trindell JA, Li W, et al. 2023. Compositionally Complex Perovskite Oxides for Solar Thermochemical Water Splitting. Chemistry of Materials 35:1901–1915.
18. Takalkar GD, Bhosale RR, AlMomani FA, Rashid S, Qiblawey H, Saleh Saad MA, et al. 2021. Thermochemical splitting of CO2 using solution combustion synthesized lanthanum–strontium–manganese perovskites. Fuel 285:119154.
19. Scheffe JR, Weibel D, and Steinfeld A. 2013. Lanthanum–Strontium–Manganese Perovskites as Redox Materials for Solar Thermochemical Splitting of H2O and CO2. Energy & Fuels 27:4250–4257.

THERMOCHEMICAL ENERGY STORAGE USING CALCIUM FERRATE: THERMODYNAMIC AND DFT ANALYSIS

Rahul R. Bhosale[1]
[1] Department of Civil and Chemical Engineering, University of Tennessee at Chattanooga, 615 McCallie Ave, Chattanooga, TN 37403, USA
*Corresponding author e-mail: rahul-bhosale@utc.edu

Ref # EST-06

ABSTRACT

To assess the potential of calcium ferrate ($CaFeO_3$) for use in high-temperature solar thermochemical energy storage (TCES), its redox characteristics were systematically analyzed via density functional theory-based quantum chemical computations as well as computational thermodynamic analysis. Oxygen evolution and the associated oxygen non-stoichiometry (δ) were determined using equilibrium calculations performed over a range of oxygen partial pressures (0.05–0.0001 atm) and reduction temperatures (1073–1473 K). The analysis shows that oxygen release increases progressively with temperature, particularly under strongly reducing conditions. At 1473 K and an oxygen partial pressure of 0.0001 atm, the material exhibited δ values approaching 0.2175. These findings demonstrate that calcium ferrate possesses tunable redox behavior under varying thermodynamic conditions, suggesting its potential suitability as a redox material for high-temperature TCES systems.
Keywords: Calcium Ferrate, DFT, Thermodynamics, Energy Storage, Solar Energy

INTRODUCTION

The rapid growth in global energy demand [1,2], together with increasing concerns regarding climate change [3,4] and greenhouse gas emissions [5,6], has accelerated the development of renewable energy technologies [7,8] capable of providing sustainable power generation [9,10]. Among the various renewable energy systems, concentrated solar power (CSP) has emerged as a promising technology [11,12] that converts solar radiation into thermal energy using reflective mirrors that focus sunlight onto a central receiver. The captured heat is subsequently used to generate steam and drive turbines for electricity production. Despite its advantages, the continuous operation of CSP plants is hindered by the intermittent nature of solar irradiation, particularly during nighttime or periods of reduced sunlight caused by cloud cover. To address this challenge, the integration of efficient energy storage technologies is essentiall [13].

Thermochemical energy storage (TCES) systems enable CSP facilities to store excess solar heat during periods of high solar availability and release it when solar input is limited [14]. This capability supports consistent electricity generation, enhances the operational flexibility of CSP facilities, and improves their economic viability. Furthermore, TCES systems contribute to global sustainability objectives and facilitate the reliable integration of renewable energy into the power grid by allowing energy dispatch independent of real-time solar availability.

Among the numerous TCES concepts, systems based on metal oxide (MO) redox processes have received significant attention due to their ability to reversibly store and release thermal energy at high temperatures [15]. In these systems, the charging stage consists of an endothermic reduction reaction in which solar heat drives the release of oxygen from the metal oxide, reducing it. During discharge, oxygen reoxidizes the reduced oxide, triggering an exothermic reaction that releases the stored energy. This reversible redox cycle enables efficient storage and recovery of thermal energy in high-temperature solar systems.

Perovskite-type oxides (ABO_3) are emerging as attractive redox materials for high-temperature TCES systems, similar to solar thermochemical cycles for splitting H_2O and CO_2 [16–19]. These materials exhibit rapid oxygen diffusion kinetics and remarkable structural stability under repeated redox cycling. The following generic equation describes the reversible oxygen exchange processes associated with perovskite oxides:

$$ABO_{3-\delta_i} \leftrightarrows ABO_{3-\delta_f} + \frac{\delta_f - \delta_i}{2} O_2 \quad (1)$$

where δ_i represents the initial oxygen non-stoichiometry and δ_f corresponds to the oxygen deficiency after the endothermic reduction step. During the exothermic oxidation process, the oxygen non-stoichiometry returns from δ_f to δ_i, thereby completing the reversible TCES cycle.

The extent of oxygen exchange in the perovskite oxide systems is primarily governed by thermodynamic conditions such as the reduction temperature (T_{red}) and the oxygen partial pressure (P_{O_2}). Although numerous experimental studies have explored the redox performance of perovskite oxides for TCES applications, thermodynamic equilibrium analyses and efficiency evaluations remain relatively limited. On the other hand, density functional theory (DFT) calculations have emerged as a powerful tool for understanding and predicting the thermodynamic and defect properties of metal oxides used in TCES systems. In perovskite oxides, DFT can be employed to investigate oxygen vacancy formation energies, electronic structure, and redox behavior, thereby enabling the rational design and screening of materials with enhanced oxygen exchange capacity and redox stability. In this context, the present study investigates the thermochemical properties of calcium ferrate ($CaFeO_3$) as a potential redox material for high-temperature TCES applications via DFT and computational thermodynamic analysis as a function of variations in P_{O_2}

and T_{red}.

CALCIUM FERRATE: DFT ANALYSIS

To investigate the potential of calcium ferrate for TCES, DFT calculations were performed to analyze the thermodynamic properties governing oxygen vacancy formation and redox behavior. Key descriptors, including oxygen vacancy formation energy (OVFE), reaction enthalpy (ΔH), and Gibbs free energy change (ΔG), were evaluated to determine the feasibility of oxygen release and uptake during TCES cycles. The OVFE was calculated from the energy difference between the reduced and oxidized structures, along with the energy of the oxygen molecule. First-principles calculations were carried out within the spin-polarized DFT framework using the Quantum ESPRESSO simulation package, employing plane-wave basis sets and pseudopotentials to describe electron-ion interactions. The generalized gradient approximation (GGA) with the Perdew–Wang functional was used to account for exchange-correlation effects, and the DFT+U method was applied to better capture the strong electron correlation effects.

CALCIUM FERRATE: NON-STOICHIOMETRIC ANALYSIS

The following equation illustrates the reversible redox reaction connected to the TCES powered by calcium ferrate:

$$CaFeO_3 + \Delta H \leftrightarrow CaFeO_{3-\delta} + \frac{\delta}{2}O_2 \quad (2)$$

The amount of oxygen released as a function of P_{O_2} and T_{red} was measured in order to evaluate the TCES potential of calcium ferrate. Oxygen release rose monotonically with increasing T_{red} at all studied P_{O_2} levels, as Fig. 1 illustrates. The amount of oxygen released during the reduction (energy-storage) stage increased from 0.00088 mol at 1073 K to 0.01493 mol at 1473 K at P_{O_2} = 0.005 atm. The released oxygen increased from 0.00171 mol at 1073 K to 0.03129 mol at 1473 K with P_{O_2} = 0.001 atm, exhibiting a similar pattern. The highest reduction temperature of 1473 K consistently produced the most oxygen release under all investigated settings.

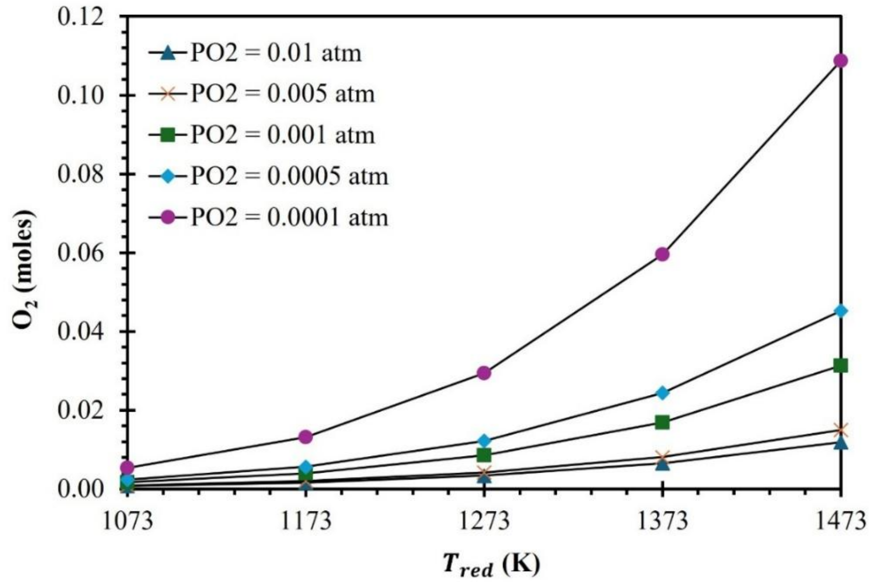

Fig. 1. Effect of P_{O_2} and T_{red} on oxygen release capacity of calcium ferrate.

The appropriate oxygen non-stoichiometry (δ) related to the heat reduction phase was calculated using the measured oxygen release from calcium ferrate. At all examined P_{O_2} levels, δ showed a progressive rise with increasing T_{red}, which is consistent with the reported increase in oxygen release. For instance, δ rose from 0.00176 at 1073 K to 0.02985 at 1473 K with P_{O_2} = 0.005 atm. Similarly, δ increased from 0.00341 at 1073 K to 0.06258 at 1473 K with P_{O_2} = 0.001 atm. The maximum reduction temperature of 1473 K consistently produced the highest δ values across all oxygen partial pressures.

The equilibrium oxygen content of calcium ferrate was calculated as a function of T_{red} using the estimated δ values. The results shown in Table 1 verify that at every P_{O_2} level, the equilibrium oxygen content of calcium ferrate falls as T_{red} rises. For example, when T_{red} increased from 1073 K to 1473 K, the equilibrium oxygen content of calcium ferrate decreased from 2.998 to 2.970 at P_{O_2} of 0.005 atm. Similarly, as T_{red} increased from 1073 K to 1473 K, the equilibrium oxygen content of calcium ferrate decreased from 2.997 to 2.937 at P_{O_2} = 0.001 atm. The equilibrium oxygen content of calcium ferrate decreased from 2.989 to 2.783 at P_{O_2} = 0.0001 atm and T_{red} = 1473 K.

Table 1. Effect of P_{O_2} and T_{red} on equilibrium oxygen content of calcium ferrate.

T_{red} (K)	P_{O2} = 0.01 atm	P_{O2} = 0.005 atm	P_{O2} = 0.001 atm	P_{O2} = 0.0005 atm	P_{O2} = 0.0001 atm
1073	2.999	2.998	2.997	2.995	2.989
1173	2.997	2.996	2.992	2.989	2.974
1273	2.993	2.992	2.983	2.976	2.941
1373	2.987	2.984	2.966	2.951	2.881
1473	2.976	2.970	2.937	2.909	2.783

CONCLUSIONS

To evaluate calcium ferrate's potential for solar thermochemical energy storage, this study examined its thermodynamic redox characteristics. The findings showed that, for all tested oxygen partial pressures, the release of oxygen increased continuously as the reduction temperature rose, peaking at 0.03129 mol at 1473 K with P_{O_2} = 0.001 atm. The oxygen non-stoichiometry (δ), on the other hand, showed a steady rising trend, peaking at 0.06258 at 1473 K and 0.0001 atm, indicating a significant capability for decrease under low oxygen partial pressure conditions. Concurrently, the equilibrium oxygen content dropped from 2.989 (almost stoichiometric values) at 1073 K to 2.783 at 1473 K in the case of P_{O_2} = 0.0001 atm.

ACKNOWLEDGEMENT

The author gratefully acknowledges the financial support from the National Science Foundation (NSF), Award CBET# 2501431.

REFERENCES

1. Dincer I and Aydin MI. 2023. New paradigms in sustainable energy systems with hydrogen. Energy Conversion and Management 283:116950.
2. Bhosale RR. 2019. Thermodynamic analysis of Ni-ferrite based solar thermochemical H_2O splitting cycle for H_2 production. International Journal of Hydrogen Energy 61:71.
3. Bhosale RR, Shende RV, and Gupta RB. 2021. Application of Zn-ferrite towards thermochemical utilization of carbon dioxide: A thermodynamic investigation. Energy Conversion and Management 245:114528.
4. Olabi AG and Abdelkareem MA. 2022. Renewable energy and climate change. Renewable and Sustainable Energy Reviews 158:112111.
5. Bhosale RR and Mahajani VV. 2013. Kinetics of thermal degradation of renewably prepared amines useful for flue gas treatment. Journal of Renewable and Sustainable Energy 5:063110.
6. Vaidya PD and Kenig EY. 2007. CO2-Alkanolamine Reaction Kinetics: A Review of Recent Studies. Chemical Engineering Technology 30:1467–74.
7. Bhosale RR, Alxneit I, Van Den Broeke LLP, Kumar A, Jilani M, Gharbia SS, et al. 2014. Sol-gel synthesis of nanocrystalline Ni-ferrite and Co-ferrite redox materials for thermochemical production of solar fuels. Materials Research Society Symposium Proceedings 1675:203–208.
8. Steinfeld A. 2013. Materials and Processes for Renewable Energy Technologies. Journal of Metals 65:1658–1659.
9. Takalkar GD, Bhosale RR, and AlMomani FA. 2019. Combustion synthesized A0.5Sr0.5MnO3-δ perovskites (where, A = La, Nd, Sm, Gd, Tb, Pr, Dy, and Y) as redox materials for thermochemical splitting of CO2. Applied Surface Science 489:80–91.
10. Logan BE and Elimelech M. 2012. Membrane-based processes for sustainable power generation using water. Nature 488:313–319.
11. Răboacă MS, Badea G, Enache A, Filote C, Răsoi G, Rata M, et al. 2019. Concentrating Solar Power Technologies. Energies (Basel) 12:1048.
12. Bhosale RR. 2019. Mn-ferrite based solar thermochemical water splitting cycle: A thermodynamic evaluation. Fuel 256:115847.
13. Chen X, Zhang Z, Qi C, Ling X, and Peng H. 2018. State of the art on the high-temperature thermochemical energy storage systems. Energy Conversion and Management 177:792–815.
14. Carrillo AJ, González-Aguilar J, Romero M, and Coronado JM. 2019. Solar Energy on Demand: A Review on High Temperature Thermochemical Heat Storage Systems and Materials. Chemical Reviews 119:4777–4816.
15. Abanades S. 2023. A Review of Oxygen Carrier Materials and Related Thermochemical Redox Processes for Concentrating Solar Thermal Applications. Materials 16:3582.
16. Bhosale RR, Kumar A, Ashok A, Sutar P, Takalkar G, Khraisheh M, et al. 2017. La-Based Perovskites as Oxygen-Exchange Redox Materials for Solar Syngas Production. MRS Advances 2:3365–3370.
17. Zhang D, De Santiago HA, Xu B, Liu C, Trindell JA, Li W, et al. 2023. Compositionally Complex Perovskite Oxides for Solar Thermochemical Water Splitting. Chemistry of Materials 35:1901–1915.
18. Takalkar GD, Bhosale RR, AlMomani FA, Rashid S, Qiblawey H, Saleh Saad MA, et al. 2021. Thermochemical splitting of CO2 using solution combustion synthesized lanthanum–strontium–manganese perovskites. Fuel 285:119154.
19. Scheffe JR, Weibel D, and Steinfeld A. 2013. Lanthanum–Strontium–Manganese Perovskites as Redox Materials for Solar Thermochemical Splitting of H2O and CO2. Energy & Fuels 27:4250–4257.

AN EXPERIMENTAL INVESTIGATION OF CHARGING TEMPERATURE EFFECTS ON THE ENERGY PERFORMANCE OF A PUMICE–$CACL_2$ COMPOSITE THERMOCHEMICAL MATERIAL

Asli Akyol Inada[1], Devrim Aydin[1,2], Yuehong Su[2], Saffa Riffat[2]*
[1] Department of Mechanical Engineering, Eastern Mediterranean University, G. Magosa, TRNC Mersin 10, Türkiye
[2] Department of Architecture and Built Environment, The University of Nottingham, University Park, Nottingham, NG7 2RD, UK
*Corresponding author e-mail: devrim.aydin1@nottingham.ac.uk

Ref # EST-07

ABSTRACT

In this study, the effect of charging temperature on the energy performance of the Pumice–$CaCl_2$ (P-$CaCl_2$) composite thermochemical material (TCM) was experimentally investigated. System performance is evaluated using both conventional efficiency and a newly defined effective energy efficiency. The conventional approach is based on the ratio of total heat output during discharging to total heat input during charging. In contrast, the effective energy efficiency accounts for both heat and mass transfer by relating the heat output per unit mass of moisture absorbed to the heat input per unit mass of moisture desorbed, thereby incorporating the desorption–absorption mass ratio in addition to heat flow effects for a more representative assessment. According to the testing results, the conventional and effective cyclic efficiencies dropped between 86.6-57.9% and 49.7-39%, respectively, with increasing charging temperatures of 71.2-84.2 °C. On the other hand, the moisture desorption rate increased from 56.6% to 75.2% with increasing charging temperature. The results showed that charging temperature plays a decisive role in cyclic efficiency, specific heat consumption and moisture desorption behaviour. Accordingly, the present study provides important insights into the selection and optimisation of charging temperatures in TCES systems.
Keywords: Thermochemical energy storage, Charging temperature, Sorption, Desorption, Energy efficiency

INTRODUCTION

With rising living standards and technological advancements, the need for energy is increasing sharply. The limited availability of fossil fuels such as coal, oil, and natural gas, which are frequently used today, and their negative environmental impacts have made the sustainability of energy systems questionable. Therefore, efforts to reduce dependence on electricity and oil-based energy sources have become crucial. In that regard, use of renewable energy sources such as solar and wind power in most effective manner is of great importance due to their environmentally friendly, and limitless availability [1]. Energy storage technologies play a significant role in efficiently storing these resources and making them available when needed. In particular, Thermochemical Energy Storage (TCES) systems offer long-term storage possibilities by storing heat at high densities for extended periods using reversible chemical reactions (endothermic-exothermic) [2-4]. The efficiency of TCES systems largely depends on the choice of materials used. These materials, generally salt hydrates, metal oxides, and certain chemical compounds, are used as storage materials and must exhibit long-term stability, be economical, and have a high storage capacity [5]. However, due to problems such as the low thermal conductivity of single-component materials, structural degradation, and slow reaction rates, the use and development of composite materials have increased significantly. Thermochemical composite materials (TCMs) are formed by incorporating salts such as $CaCl_2$, LiCl, $LiNO_3$, and $MgCl_2$ into porous matrices such as pumice, vermiculite, and similar materials, and they play an important role in improving the performance of TCES systems. Pumice (P) stone, as the main matrix, is frequently used as a carrier material in such applications due to its high porosity, light weight, thermal stability, and economic advantages [6]. In this study, the performance of P-$CaCl_2$ TCM at different charging temperatures was experimentally investigated under laboratory conditions.

MATERIALS AND METHODS

Synthesis of Composite Thermochemical Material

In present study, pumice with a diameter of 4–6 mm was selected as the main matrix material, and a P–$CaCl_2$ composite TCM was synthesised by impregnating $CaCl_2$ salt into the matrix to form the composite structure. The prepared P–$CaCl_2$ composite material was dried and then tested to determine its TCES performance. Within the study, the charging (dehydration) and discharging (hydration) behaviour of the material were examined. Specifically, the drying (desorption) behaviour of the material at different charging temperatures was evaluated, and the effect of charging temperature on the composite material's energy storage performance was analysed.

Experimental Setup and Application Procedure

Fig 1 shows the experimental setup of the TCES system. Here, Fig. 1a and Fig. 1b illustrate the discharging and charging process operations, respectively. The system consists of a fixed-bed TCES reactor integrated into a climate control unit. The climate control unit is equipped with a variable-speed radial fan and four electric heating elements for use during charging. Two of the four electric heating elements are 1 kW, and the other two are 0.5 kW. An ultrasonic humidifier is integrated at the inlet of the climate control unit to increase the relative humidity of the inlet air during discharging. The climate control unit and the TCES unit are designed to operate in an integrated manner, with the climate control unit adjusting the inlet air conditions to the desired level before the air enters the TCES reactor. The reactor has a rectangular shell measuring 370 × 330 × 460 mm and is surrounded by 40-mm-thick, foil-covered glass wool to reduce heat losses. Inside the reactor, a tray measuring 350 mm × 310 mm × 32 mm, with a wire-mesh floor, is positioned perpendicular to the airflow. This tray was used to place the composite TCM, ensuring the material is in direct contact with the airflow. The airflow velocity is controlled by a radial fan mounted at the inlet of the climate control unit.

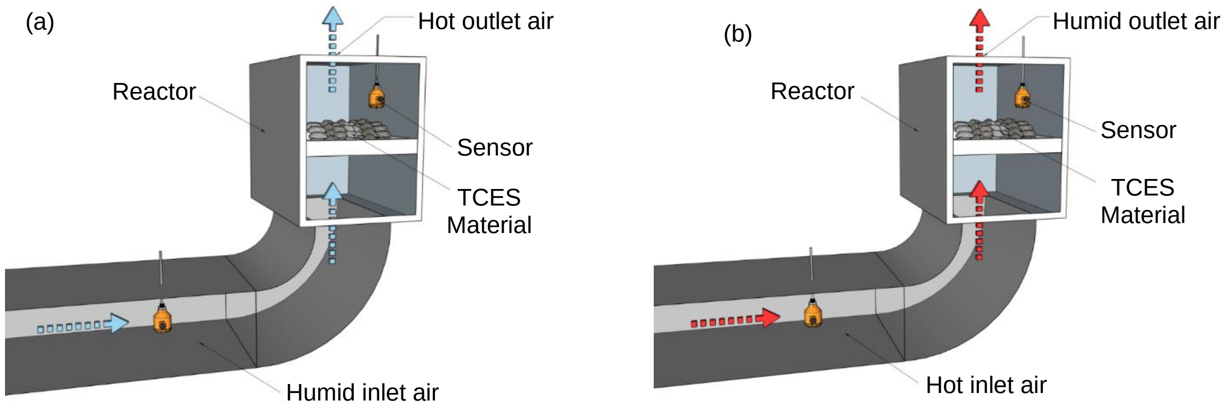

Fig. 1. Schematic representation of the experimental setup: (a) discharging process operation and (b) charging process operation.

Units and Equations

Equation (1) calculates the instantaneous heat output during the discharging ($\dot{Q}_{out}$) process, and Equation (2) calculates the instantaneous heat supply to the TCM during the charging process ($\dot{Q}_{in}$).

$$\dot{Q}_{out} = \dot{m}_d . c_p . (T_{out,d-} T_{in,d}) \quad (1)$$
$$\dot{Q}_{in} = \dot{m}_c . c_p . (T_{in,c-} T_{out,c}) \quad (2)$$

Where, T_i is the inlet temperature and T_o is the outlet temperature, $\dot{m}_d$ is the mass flow rate in the discharging process, c_p is the specific heat, $\dot{m}_c$ is the mass flow rate in the charging process.

The cumulative amount of energy released during the discharging process ($E_{d,cum}$) and cumulative amount of energy supplied to TCM during the charging process ($E_{c,cum}$) can be determined using the following equations:

$$E_{d,cum} = \dot{Q}_{out,ave} . t_d \quad (3)$$

$$E_{c,cum} = \dot{Q}_{in,ave} . t_c \quad (4)$$

Where, t_d and t_c denote discharging and charging durations, while $\dot{Q}_{out,ave}$ and $\dot{Q}_{in,ave}$ represent the average heat output and input rates during discharging and charging processes, respectively.

The heat storage energetic efficiency (First Law) is defined as the ratio of the $E_{d,cum}$ to $E_{c,cum}$:

$$\eta_I = \frac{E_{d,cum}}{E_{c,cum}} \quad (5)$$

The discharging specific heat output ($\boldsymbol{E_{d,spe}}$) (e.g. heat output per gram moisture sorption) is obtained by dividing the $\boldsymbol{E_{d,cum}}$ by mass change of TCM during the discharging (Δm_d);

$$\boldsymbol{E_{d,spe}} = \frac{\boldsymbol{E_{d,cum}}}{\boldsymbol{\Delta m_d}} \quad (6)$$

Similarly, the charging specific heat input ($\boldsymbol{E_{c,spe}}$) (e.g. heat input per gram moisture desorption) is obtained by dividing the $\boldsymbol{E_{c,cum}}$ by mass change of TCM during the charging (Δm_c);

$$\boldsymbol{E_{c,spe}} = \frac{\boldsymbol{E_{c,cum}}}{\boldsymbol{\Delta m_c}} \quad (7)$$

By obtaining the ratio of $E_{d,spe}$ to $E_{c,spe}$ the effective First Law (energy) Efficiency ($\eta_{I,eff}$) is determined;

$$\eta_{I,eff} = \frac{E_{d,spe}}{E_{c,spe}} \tag{8}$$

RESULTS AND DISCUSSION

Table 1 summarises the experimental results for three average inlet air temperatures during charging. Based on the experimental results presented in the table, the specific heat output ($E_{d,spe}$) during the three different discharging processes was found to be 3.28, 3.2, and 3 kJ/g, indicating a consistent heat output rate per gram of moisture sorbed. On the other hand, for the three charging cases at 71.2, 77.7, and 84.2 °C, the specific heat input ($E_{c,spe}$) was 6.66, 7.17, and 7.82 kJ/g, indicating an increasing rate of specific heat consumption at elevated charging temperatures.

Table 1: Summary of the experimental results at different charging inlet air average temperatures.

		Charging Temperature		
		71.2 °C	77.7 °C	84.2 °C
Discharging	$T_{in,d,ave}$ (°C)	24.5	22.5	22
	$T_{out,d,ave}$ (°C)	31.1	29.7	28.3
	$RH_{in,d,ave}$ (%)	66.6	73.1	86.2
	$RH_{out,d,ave}$ (%)	40.4	40.3	52
	$Q_{out,d,ave}$ (kW)	0.29	0.32	0.28
	m_{abs} (gr)	318	360	336
Charging	$T_{in,c,ave}$ (°C)	71.2	77.7	84.2
	$T_{out,c,ave}$ (°C)	66.2	70.4	76
	$RH_{in,c,ave}$ (%)	5.7	4.1	2.9
	$RH_{out,c,ave}$ (%)	9.9	9	7
	$Q_{in,c,ave}$ (kW)	0.22	0.33	0.36
	m_{des} (gr)	180	250	253

Fig. 2a presents a comparison of the η_I and η_{Ieff} values of the P–$CaCl_2$, while Fig. 2b shows the variation of the moisture absorption (m_{abs}) and desorption (m_{des}) amounts under three different conditions with average charging inlet temperatures of 71.2, 77.7, and 84.2 °C. The energy efficiency of TCES systems is generally defined by the ratio of the heat generated during discharging to the heat transferred to the system during charging. However, this approach does not account for the material's moisture uptake and release behaviour throughout the cycle. If the moisture absorbed during discharge is not completely released during charging, full cyclic efficiency cannot be achieved. Therefore, the concept of "effective energy efficiency" (η_{Ieff}), which also accounts for moisture change rates, is used to evaluate the system's actual cyclic performance. This approach clearly shows that even if heat transfer is equal, efficiency cannot reach 100% if moisture desorption remains low.

According to the data in Fig. 2a, when the average inlet charging temperature is 71.2 °C, η_I is 86.6%, and η_{Ieff} is 49.7%. When the inlet temperature is increased to 77.7 °C, η_I is 64.2%, and η_{Ieff} is 44.9%. At the highest charging temperature of 84.2 °C, η_I and η_{Ieff} drop to 57.9% and 39%, respectively. Fig. 2b shows the amount of moisture absorbed and desorbed by P–$CaCl_2$ composite TCM at different charging inlet temperatures. At an average charging inlet temperature of 71.2 °C, it absorbed 318 gr of moisture and released approximately 56.6% (180 gr). At an average charging inlet temperature of 77.7 °C, it absorbed 360 gr of moisture and desorbed approximately 69.4% (250 gr). At an average charging inlet temperature of 84.2 °C, it absorbed 336 gr of moisture and desorbed approximately 75.2% (253 gr). Results from Fig. 2a and Fig. 2b indicate that both η_I and η_{Ieff} decrease, while m_{des} improves with increasing charging temperature. This outcome indicates the critical importance of selecting the optimal charging temperature, which could be considered for future work.

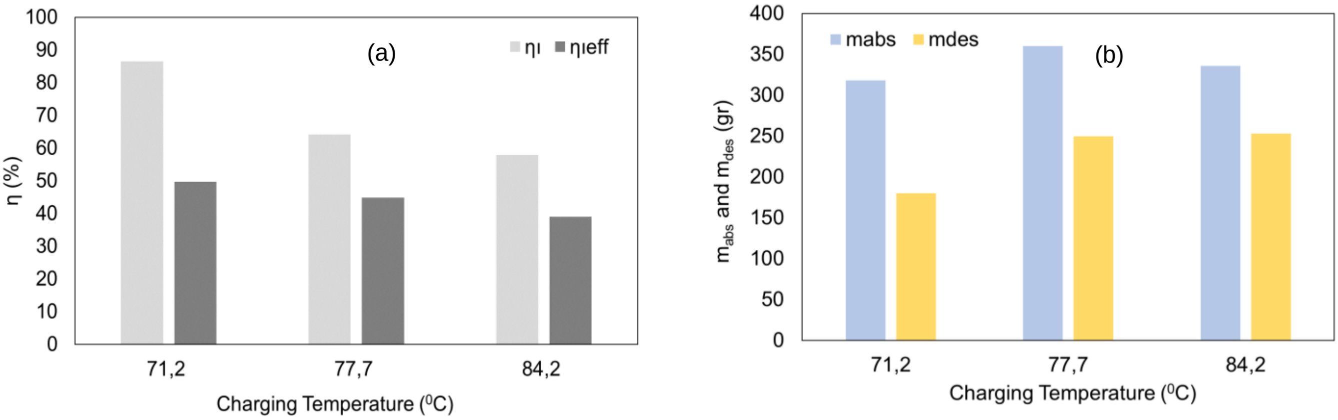

Fig. 2. Variation of (a) η_I and η_{Ieff} and (b) m_{abs} and m_{des} with charging temperature

CONCLUSIONS

In this study, the cyclic energy and moisture desorption performance of P–$CaCl_2$ composite TCM was investigated under different charging temperatures. Experimental results demonstrated that both charging temperature and air humidity have a key impact on the overall cyclic performance of the TCM. The main findings can be summarised as follows:

- Specific heat output during the discharging processes was found in the range of 3-3.28 kJ/g, while the specific heat input during charging processes increased in the range of 6.66-7.82 kJ/g with the rise in charging temperature.
- The amount of moisture desorption increased with increasing charging temperature. At average temperatures of 71.2, 77.7, and 84.2 °C, moisture desorption rates of 56.6%, 69.4%, and 75.2% were obtained, respectively.
- The highest η_I and η_{Ieff} were obtained as 86.6% and 49,7% at the lowest charging inlet temperature of 71.2 °C.
- Study results demonstrate that determining the optimum charging temperature in TCES applications is critical for both energy and humidity management.

ACKNOWLEDGEMENT

This work was supported by the Engineering and Physical Sciences Research Council (United Kingdom) through the Horizon Europe Guarantee via a Marie Skłodowska-Curie Fellowship [grant number: EP/Z002117/1].

REFERENCES

[1] Y. Wang *et al.*, “Development and system performance evaluation of new thermochemical energy storage composite materials for direct photothermal conversion at low temperature,” *Energy*, vol. 332, p. 137161, Sep. 2025, doi: 10.1016/J.ENERGY.2025.137161.

[2] H. Jarimi *et al.*, “Materials characterization of innovative composite materials for solar-driven thermochemical heat storage (THS) suitable for building application,” *Int. J. Low-Carbon Technol.*, vol. 14, no. 3, pp. 313–325, Sep. 2019, doi: 10.1093/IJLCT/CTX017.

[3] A. B. Çolak, D. Aydin, A. Al-Ghosini, and A. S. Dalkilic, “Discharging performance prediction of experimentally tested sorption heat storage materials with machine learning method,” *J. Energy Storage*, vol. 56, p. 106159, Dec. 2022, doi: 10.1016/J.EST.2022.106159.

[4] A. A. Inada and D. Aydin, “Performance Analysis of Salt-In-Pumice Composites Under Varying Air Velocities for Thermochemical Heat Storage,” *Futur. Cities Environ.*, vol. 11, Aug. 2025, doi: 10.70917/FCE-2025-032.

[5] A. A. Inada, M. Rezaei, and D. Aydin, “Recent developments on open thermochemical energy storage towards decarbonised building space heating and cooling,” *Int. J. Glob. Warm.*, vol. 35, no. 2–4, pp. 104–127, 2025, doi: 10.1504/IJGW.2025.145087;SUBPAGE:STRING:ACCESS.

[6] J. Aarts, H. Fischer, O. Adan, and H. Huinink, “Towards stable performance of salt hydrates in thermochemical energy storage: A review,” *J. Energy Storage*, vol. 114, p. 115726, Apr. 2025, doi: 10.1016/J.EST.2025.115726.

ELECTRIC VS FUEL: NIGERIA'S WELL TO WHEEL VEHICLE STUDY

Christopher Nwachinemelu[1], Meliz Hastunç[1]*
[1,2] Bahçeşehir Cyprus University, Faculty of Architecture and Engineering, Department of Electrical Electronics Engineering, Mustafa Kemal Avenue, Osmanlar Street 1, Alayköy, Nicosia, TRNC
nwachinemeluchidera@gmail.com
Ref # EVT-01

ABSTRACT

The transport sector of Nigeria is a major emissions source due to its reliance on imported fossil fuels. This study quantifies the environmental impact of existing vehicle segments, by applying a well to wheel analysis to European segment A to F petrol benchmark. By integrating upstream fuel logistics and direct combustion data, the analysis establishes a baseline carbon intensity ranging from 4.02 tonnes CO_2/yr for segment C to 6.86 tonnes CO_2/yr for segment F in internal combustion engine vehicles. In terms of battery electric vehicles, the well to wheel results ranges from 1.40 tonnes CO_2/yr for segment A to 1.87 tonnes CO_2/yr for segment F. The results show that the adoption of battery electric vehicles is one of the viable pathways to eliminate the high carbon floor and fulfil Nigeria's energy transition plans.

Keywords: Well to Wheel, Internal combustion engine, Greenhouse Gas Emission, Electric Mobility.

INTRODUCTION

Nigeria is the 14th largest country in Africa and the most populous country, with over 237 million people in 2025 [1]. Nigeria's transport sector is heavily dominated by Internal Combustion Engine Vehicles (ICEVs) [2]. This contributes significantly to national greenhouse gas emissions (0.3% of global emissions in 2023), high fuel consumption, and air pollution [3]. Previous studies on the transport system of Nigeria state that Nigeria is heavily dependent on imported fuel, which was approximately 63% between October 2024 and October 2025 [4].

The transport sector is characterized by a rapidly expanding vehicular fleet. Recent studies indicate that the national vehicle population grew to approximately 11.8 million units in 2018 and is increasing at a rate of 3.58% per year [5-6]. This also leads to severe traffic congestion, high fuel usage, and prolonged air quality challenges. Research shows that the transport sector contributes to 57% of the national CO_2 emissions [3]. To the author's knowledge, only a few studies have explored the potential environmental benefit of Battery Electric Vehicles (BEVs) compared to ICEVs in Nigeria [7-10]. Previously mentioned studies have addressed the decarbonisation of the transport sector and the infrastructural barriers to the adoption of BEVs [11-12]. In addition to this, most studies have relied on city specific research. However, there is currently a lack of research that utilizes Well to Wheel (WTW) framework to quantify the comparative environmental benefit of BEVs over ICEVs within Nigeria's context. WTW analysis compares the fuel pathway, which is appropriate for operational emission comparison. This paper provides a comprehensive, data-driven analysis of the entire fuel and vehicle cycle using Well to Wheel analysis, from extraction to vehicle operation in Nigeria.

The remaining of this article is organized as follows: Section two reviews related works and the current landscape of Nigeria, while Section three details the methodology and mathematical model used for the WTW analysis. Section four presents the baseline emission results for the selected vehicle model and concludes with recommendations for Nigeria's energy transition.

RELATED WORK

Several studies have been made on the environmental benefits of BEVs over ICEVs in Nigeria. However, the studies are limited and different in their approach, methods and scope. A notable study carried out a life cycle analysis (LCA), which involved a framework covering raw material extractions, manufacturing and end-of-life recycling. The study concluded that Electric Vehicles (EV) produce 28 – 41% lower greenhouse gas emissions than internal combustion ICEVs in Nigeria [8]. While LCA looks at the present, another study adopted a bottom-up framework to provide insight into future scenarios. Using a simulation-based approach to examine Nigeria's energy sector through 2050, this study established that the environmental benefits of BEVs are not static but scale with grid decarbonisation. It further showed that if Nigeria adopts a vehicle-to-grid (V2G) strategy, in which vehicles feed energy back into the grid, CO_2 emissions could be reduced by up to 72%. This highlights the potential of BEVs to support Nigeria's transition towards cleaner, renewable energy sources [9]. However, technical data alone does not account for structural barriers. To address this gap, a systematic review combined with mixed-methods analysis found that the environmental benefits of BEVs remain conditional, as grid inadequacies could constrain the green potential of EV adoption [13]. In conclusion, the existing body of work spanning lifecycle analysis, stakeholders' surveys, and simulation-based modelling consistently highlights the environmental benefit of battery electric vehicles BEVs in Nigeria.

Renewable energy potential in Nigeria

As of 2024, renewable energy was approximately 24.5% of Nigeria's total on-grid electricity generation. Nigeria's total renewable energy production represents approximately 0.03% to 0.05% of the world's total renewable electricity generation [3].

The solar irradiance benchmark of Nigeria is 19.8 MJ/m^2/day, which is approximately 5.5kWh/m^2/day, with values ranging from 3.5 MJ/m^2/day in the South to 7.0 MJ/m^2/day in the North. Solar energy currently accounts for roughly 5% to 7% of the total renewable capacity of Nigeria. On the other hand, hydropower accounted for 87.5% of Nigeria's total renewable energy market in 2024 [14-15].

METHODOLOGY

To accurately assess the decarbonisation potential of electric mobility in Nigeria, this study adopts a quantitative comparative research design based on WTW analysis, using European passenger car segments as benchmarks. The WTW method evaluates the environmental benefits of BEVs ICEVs by accounting for both upstream energy production WTT (Well to Tank) and downstream TTW (Tank to Wheel) within Nigeria. To determine the total annual emission impact, the WTW result was multiplied by the Total Kilometres Driven (TKD). Since, Nigeria lacks official vehicle-kilometre statistics, this analysis uses an annual mileage of 18,000 km per private passenger car. In the absence of country-specific data, this figure falls between 14,000 and 21,000 km/year as stated in Southern African vehicle-parc and transport-energy modelling studies, which are commonly used as regional benchmarks [16]. The calculation process for determining the total annual CO_2 impact for each vehicle are defined as follows:

1) WTT: For BEVs, this phase includes all upstream processes, which include fuel extraction, refining, transportation, distribution, power generation power distribution, up to the vehicle's batteries. While, ICEVs include the extraction, transportation, refining, and distribution.

2) TTW: for BEVs this phase starts from the power delivery system, motor up to the consumption by the vehicle. While for ICEVs it includes engine consumption, power delivery system, and up to the consumption by the vehicle.

ICEVs WTW Calculations

The total WTW emissions ($GHG_{WTW,\ ICEVs}$) in g.CO_2/yr are calculated by combining the well to tank WTT and tank to Wheel TTW values both measured in g.CO_2/L. Following this, the result is multiplied by the fuel consumption (F.E) of the vehicle in L/km. After obtaining the WTW value, the result is multiplied by the total Kilometres driven TKD to obtain the total annual impact per year. The equation of $GHG_{WTW,\ ICEVs}$ can be seen in Eq.(1), below [17].

$$GHG_{WTW,\ ICEVs} = [(GHG_{WTT} + GHG_{TTW}) \times F.E] \times (TKD) \quad (1)$$

BEVs WTW Calculations

In the case of BEVs, the tank to wheel TTW is zero. This is due to BEVs not producing direct tailpipe exhaust during operation. Therefore, the total environmental impact is mostly determined by the WTT phase [17].

$$GHG_{WTW,BEV} = \left[\left[\left(\left(\frac{WTTsolar}{\eta c} + TTW\right) \times P_s\right) + \left(\left(\frac{WTTng}{\eta c} + TTW\right) \times P_{NG}\right) + \left(\left(\frac{WTThydro}{\eta c} + TTW\right) \times P_h\right) + \right] \times V.E\right] \times (TKD) \quad (2)$$

As seen in Eq.(2), the total WTW emission ($GHG_{WTW,BEV}$) in gCO_2/yr is determined by the weighted well to tank WTT value of the electricity mix in Nigeria. This mix is defined by the weighting factor P_{NG}, P_h, and P_s , representing the percentage shares of natural gas (WTT_{Ng}), solar (WTT_{Solar}) and hydropower (WTT_{Hydro}), respectively. To reflect the real world, demand the Charging efficiency (ηc) is used to account for energy losses during transfer from the grid to the battery. By current calculations, P_{NG} accounts to 77.77%, P_h to 22.22%, and P_s to 0.06% [3]. These factors are multiplied by the vehicle's energy consumption to obtain the total $GHG_{WTW,BEV}$. Furthermore, the $GHG_{WTW,BEV}$ is multiplied by the total Kilometres driven TKD to acquire the total annual impact per year.

Vehicle Selection and Benchmarking

Table 1 shows the values used in the study for both battery electric vehicles BEVs and internal combustion engines ICEVs according to segments. The vehicle selection focuses on models that reflect the current Nigerian automotive market [18-19]. The models are compared with established fuel pathways to measure environmental impacts and assess the potential emissions reductions achievable through the adoption of electric vehicles.

Table1. Vehicle Efficiencies of vehicles

BEVs			ICEVs		
Segments	**Vehicles**	**Vehicle Efficiency (kWh/km)**	**Segments**	**Vehicles**	**Fuel Efficiency (L/km)**
A	Fiat 500e	0.144	A	Toyota-Aygo-X	0.049
B	Peugeot-e-208	0.1	B	Volkswagen Polo	0.05
C	Peugeot-e-308	0.169	C	peugeot-308	0.049
D	BMW i4	0.173	D	Volvo S60	0.071
E	Mercedes-Benz EQE	0.179	E	Mercedes-Benz E220d	0.051
F	BMW i7	0.194	F	Mercedes-Benz S350d	0.071

Result and Discussion

The WTW analysis shows a significant difference, and environmental advantage of BEVs over ICEVs across different vehicle segments. By utilizing Nigeria's energy mix, this study shows that BEVs drastically reduce greenhouse gas emissions compared to ICEVs [3].

The comparative Figure 1 shows that, BEVs carbon footprint is below 2.000 tonnes CO_2/yr across all analysed categories. The WTW result for segment A BEV shows 1.400 tonnes CO_2/yr while petrol-powered produces 4.022 tonnes CO_2/yr. The BEV luxury segment (F) achieves a WTW total of 1.872 tonnes CO_2/yr, which is substantially lower than that of its diesel counterpart, which produces 6.856 tonnes of CO_2, annually.

The visual evidence indicates that BEVs within the current energy framework reduces emissions by an average of 67.62% compared to petrol and 63.18% compared to diesel engines. Specifically, across the 6 analysed segments, BEVs achieved an average annual reduction of 3.505 tonnes CO_2/yr when compared to petrol and 2.981 tonnes CO_2/yr when compared with diesel. The results are driven by fundamental differences in energy conversion between the two technologies. BEVs are superior mainly because the TTW emission are zero; and BEVs eliminates the high intensity carbon phase entirely. While diesel powered vehicles demonstrates better volumetric fuel efficiency than petrol, this advantage is largely localized to the vehicle's operation. Interestingly, diesel often show a lower WTT impact during production and refining stage, but eventually outweighed by its high carbon output during use. However, the environmental impact of BEVs is largely due to WTT phase of Nigeria's grids, even with the current reliance on natural gas, the efficiency of centralized power generation ensures that the total WTW footprint remain significantly lower than that of any petrol or diesel vehicles.

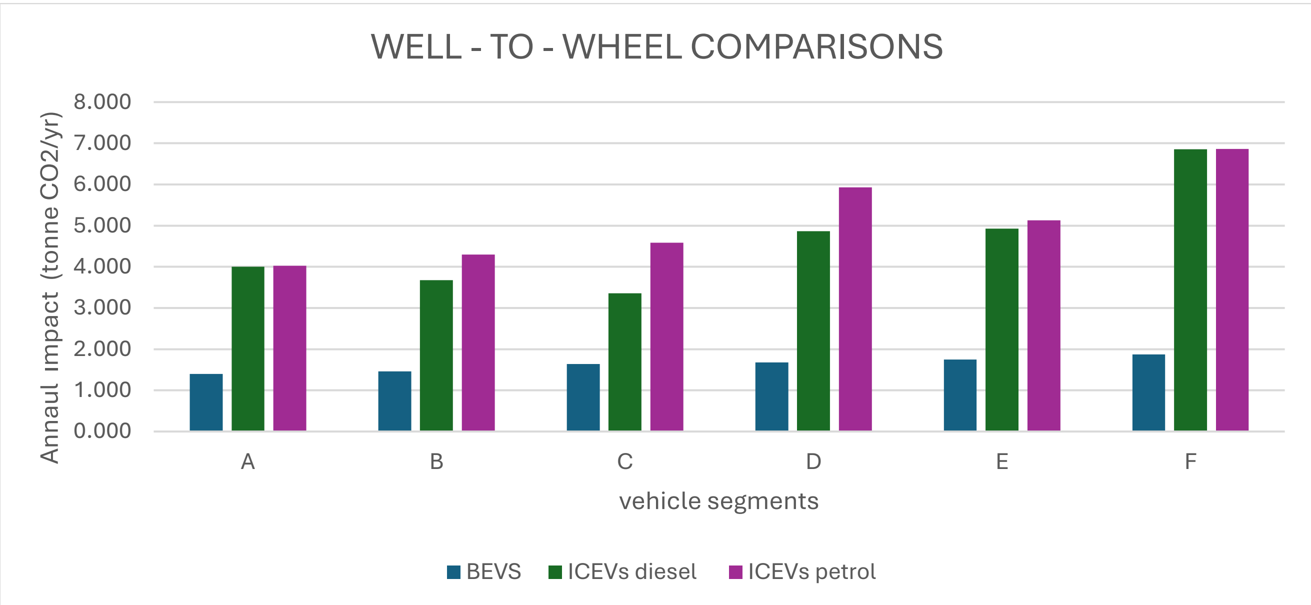

Figure 1 Comparison of WTW CO2 Emissions between BEV and ICEV models across Vehicle Segment in Nigeria

Conclusion

This research aimed to quantify the carbon footprint of Nigeria's automotive fleets and evaluate the potential transition to electric mobility by using WTW analysis. The study results showed that the adoption of BEVs in Nigeria offers a clear path to decarbonisation in Nigeria's transport sector. With the current reliance on solar, hydropower and natural gas, BEVs in segments A to F reduce annual CO_2 by approximately 67.62% in petrol vehicles. On the other hand, there is seen to be a reduction of 63.18% in diesel vehicles. To effectively maximise these benefits, Nigeria should continue expanding its capacity of renewable energy, especially solar, to further decrease the WTW carbon intensity of its expanding electric vehicle fleet. As Nigeria transitions from petrol to electric, this holistic accounting ensures that the emissions generated by the power grid to support growing demand do not outweigh the substantial environmental benefit of removing internal combustion engines from the road. Ultimately, this study serves as a baseline for future research, which will focus on the grid side implications of mass EV adoption, specifically analysing whether the national power infrastructure can maintain stability under increased load requirements.

REFERENCES

[1] https://worldpopulationreview.com/countries/nigeria Accessed on December 3, 2025
[2] https://theelectricityhub.com/mainstreaming-electric-vehicles-in-nigeria/ Accessed on December 3, 2025
[3] https://www.iea.org/countries/nigeria/emissions Accessed on January 2026
[4] https://www.nigeriainfo.fm/news/homepage/domestic-refineries-grow-role-but-imports-still-fuel-majority-of-nigerias-petrol-demand/ Accessed on December 4, 2025
[5] Amulah, N. C., Ekwe, E. B., Ishaq, M. I., & Oluwole, F. A. (2023). Grey model analysis of vehicle population, road transport energy consumption and vehicular emissions. Communications - scientific letters of the university of zilina, 25(1), A1-13.
[6] https://www.nigerianstat.gov.ng/elibrary/read/903 Accessed on January 16, 2026
[7] Adebayo, Adeyinka & Aluko-Olokun, Pelumi & jacob, adesola. (2025). Techno-economic and environmental comparative analysis of electric versus internal-combustion vehicles in nigeria. International journal of science architecture technology and environment. 02. 203-216. 10.63680/ijsate092549.021
[8] Dioha, M.O., Lei D. Tyler H. Rugglers, Sara B. Ken C. 2022 Exploring the role of electric vehicles in Africa's energy transition: A Nigerian case study iscience, 25(3)
[9] Poi, Elizabeth. (2025). The role of electric vehicles in enhancing sustainable transportation in Nigeria. 9. 126-137.
[10] Patrick B. Asu-Nandi, Okoli Thankgod Kenechukwu. 2024. Electric vehicle adoption as sustainable solution to economic growth and environmental challenges in Nigeria. Industrial Technology Education Researchers Journals. 7(2) 75–93
[11] Obele, J. D. (2025). Infrastructure readiness and the adoption of electric vehicles in Nigeria. BW Academic Journal, 2(1).
[12] Akujor, C. E., Uzowuru, E. E., Abubakar, S. S., & Amakom, C. M. (2022). Decarbonisation of the Transport sector in Nigeria. environmental health insights, 16, 11786302221125039.
[13] Safiya M.U., Hadiza A. A, Yahaya I. 2025. Climate change mitigation through sustainable transportation: a Comparative analysis of electric and hybrid vehicles in Nigeria. SEAHI Publication.
[14] Salu, Babatunde & Ogundari, Ibikunle & Akinbami, John-Felix & Akarakiri, Joshua. (2024). Determination of solar irradiance benchmarks for municipal off-grid photovoltaic power system development in Lagos state, Nigeria. Koozakar Festschrift. 64-75. 10.69798/k2365548.
[15] https://mordorintelligence.com Accessed on December 30, 2025
[16] Stone, A., Merven, B., Maseela, T., & Moonsamy, R. (2018). Providing a foundation for road transport energy demand analysis: The development of a vehicle parc model for South Africa. *Journal of Energy in Southern Africa*, *29*(2), 29-42. https://doi.org/10.17159/2413-3051/2018/v29i2a2774.
[17] Meliz Hastunc. 2024 Transition to electrical vehicles with an environmental and costs prospective in islands. A Thesis For The Degree of Doctor of Philosophy (PHD) In Energy System Engineering.
[18] https://mercedesblog.com/official-mercedes-eqe-with-a-range-up-to-660-km/?utm Accessed February 7, 2026
[19] https://www.ultimatespecs.com/car-specs/Fiat/9953/Fiat-500-by-Diesel-13-Multijet-16V-75HP.html?utm Accessed February 7, 2026

PREDICTIVE CO-OPTIMIZATION OF ENERGY AND THERMAL MANAGEMENT IN HEAVY-DUTY FUEL CELL VEHICLES

Dominik Köppel[1], Maximilian Bömerl[1], Stefan Jakubek[1], Christoph Hametner[1]*
[1] Institute of Mechanics and Mechatronics, TU Wien, Getreidemarkt 9, Vienna, 1060, Austria
*Corresponding author e-mail: christoph.hametner@tuwien.ac.at
Ref # EVT-02

ABSTRACT

The advancement of heavy-duty fuel cell electric vehicles (FCEVs) in hilly or mountainous terrain challenges fuel-economy and component-lifetime targets under packaging constraints. This paper proposes a predictive co-optimization that integrates energy management and battery thermal management on a unified decision level. Unlike hierarchical approaches, where fuel-optimal energy management is computed first and thermal management subsequently allocates cooling for a fixed power split, the proposed method allows limited energy-management adaptation to support thermal conditioning. Compared to the hierarchical baseline, the co-optimization substantially improves thermal conditions in demanding route topographies by mitigating critical temperature peaks while maintaining near-optimal fuel economy. By keeping charge and temperature within limits, the approach enhances vehicle operability and favors overall component lifetime. It can also inform system dimensioning by potentially enabling reduced component sizes without compromising performance.

Keywords: Fuel cell electric vehicles, Heavy-duty transportation, Predictive energy management, Predictive battery thermal management, Co-optimization

INTRODUCTION

Fuel cell electric vehicles (FCEVs) are a particularly viable solution for long-haul applications to decarbonize the heavy-duty transportation sector [1], while facing several challenges in meeting fuel economy, range and lifetime requirements [2], especially under high load and varying route topography. In heavy-duty vehicles, hybrid powertrain architectures combining the fuel cell system (FCS) with a supplementary battery are decisive for handling highly dynamic real-world driving conditions. Since FCS durability and fuel economy are favored by stationary and efficient FCS operation, the battery buffers transients caused by road gradients or acceleration phases and enables regenerative braking.

Energy management strategies (EMSs) determine the load distribution between the components and are therefore directly linked to fuel economy, component lifetime and vehicle operability [3]. In particular, for heavy-duty applications, the utilization of load forecasts within advanced predictive EMSs has been shown to allow mitigating the need for oversized batteries - undesired due to space and cost constraints - by enabling targeted SoC control. Predictive EMSs ensure operational feasibility even under demanding driving missions while yielding fuel economy benefits compared to non-predictive strategies [4].

Beyond conserving feasible power delivery, thermal management of both the battery and the FCS is crucial. Space and weight limitations similarly constrain cooling system design, necessitating either advanced temperature-aware adaptive EMSs to reduce battery stress once temperature limits are exceeded [5] or predictive thermal management strategies (TMSs) that proactively sustain safe operating limits. Hierarchical strategies, in which the EMS is optimized first, and the predicted heat generation is subsequently used in a separate thermal management optimization, have demonstrated advantages over non-predictive methods for battery thermal regulation [6] and FCS temperature regulation [7]. However, such hierarchical concepts have an intrinsic structural limitation: The EMS is optimized independently of thermal considerations, thus, the TMS can only react to predefined power trajectories. Consequently, even extended pre-cooling phases may fail to prevent single temperature peaks, although these are critical for vehicle functionality and component aging [8]. To overcome this limitation, previous studies developed integrated EMSs and TMSs by introducing thermal cost terms into MPC [9] or reinforcement learning frameworks [10], or by jointly considering SoC and battery temperature using PMP [11].

This work addresses this gap by proposing a novel predictive EMS and battery thermal management strategy (BTMS) co-optimization enabling simultaneous optimization of power split and battery thermal conditioning along the entire route. Unlike hierarchical approaches that rely on extensive pre-cooling, the proposed concept allows for strategically placed EMS adaptation during thermally critical mission segments. This approach enhances overall battery thermal conditions – highly relevant for vehicle functionality and component lifetime – while maintaining fuel economy benefits.

PREDICTIVE ENERGY AND THERMAL MANAGEMENT CO-OPTIMIZATION FRAMEWORK

The main contribution of this work is the integrated co-optimization that simultaneously determines optimal energy and battery thermal management along a known upcoming route. The proposed control concept, depicted in Fig. 1, follows a two-stage architecture. In the co-optimization stage, predictive route information is used to obtain optimal distance-based power-split and thermal-system references. During vehicle operation, real-time on-board controllers track these references and compensate for modeling errors and forecast uncertainties while fulfilling the system performance requirements.

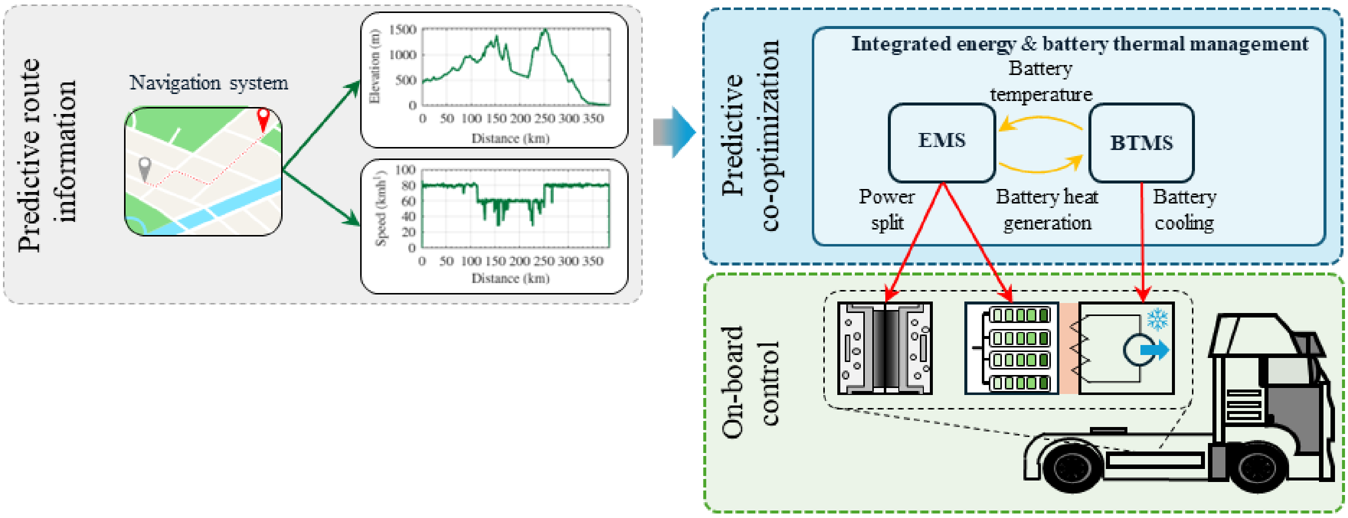

Fig. 1. Two-stage predictive energy and thermal management

Vehicle performance requirements

In the investigated scenario, a 38-t truck follows a demanding real-world mountainous route with steep gradients and 1500 m elevation difference. Meeting fuel economy, component lifetime, and load demand under the resulting highly dynamic load profile is challenging.

Conventional EMSs that focus solely on FCS-battery power split improve fuel economy through targeted SoC control. SoC limits are conserved to enable regenerative braking and maintain a sufficient charge buffer to guarantee vehicle drivability. While an efficiency-focused EMS already reduces waste heat, during highly dynamic or high-load phases, shifting loads towards the battery to maintain FCS efficiency can lead to critical battery heat generation, resulting in substantial battery temperature peaks that accelerate degradation and may reduce powertrain operability due to derating.

While hierarchical strategies address this issue by applying predictive pre-cooling to mitigate anticipated temperature peaks, even extended pre-cooling may fail under such driving conditions. Therefore, this paper proposes a joint EMS-BTMS co-optimization that allows slight EMS adaptations to ensure feasible battery temperatures.

Route-based EMS and BTMS co-optimization

To compute distance-based references computationally efficiently, the framework employs control-oriented models. First, predictive route information from the navigation system (see Fig. 1), including an elevation and speed forecast, is used in a longitudinal vehicle dynamics model – including aerodynamic drag, rolling resistance, gravitational force and traction force - to derive a distance-based load forecast.

Second, this load prediction is combined with simplified powertrain models, which preserve dominant system dynamics while minimizing computational effort:

- A map-based FCS model capturing power, efficiency and fuel consumption relations,
- An equivalent circuit battery model accounting for ohmic losses,
- A lumped-parameter battery thermal model.

The objective of the co-optimization is to minimize fuel consumption, considered by the stage cost $L_{\mathrm{EMS},k}$, while simultaneously keeping the battery temperature close to 25°C, represented by the stage cost $L_{\mathrm{BTMS},k}$, where distance is discretized in N sections, and k is the k-th segment. A brief formulation of the resulting optimization problem is

$$\min_{\substack{P_{\mathrm{fcs},1},\dots,P_{\mathrm{fcs},\mathrm{N}} \\ \dot{Q}_{\mathrm{chiller},1},\dots,\dot{Q}_{\mathrm{chiller},\mathrm{N}}}} \sum_{k=1}^{\mathrm{N}} \left[\alpha L_{\mathrm{EMS},k} + (1-\alpha) L_{\mathrm{BTMS},k}\right] \tag{1}$$

subject to

- Upper and lower SoC bounds and a terminal SoC at the end of the driving mission,
- Upper and lower battery temperature T_{bat} bounds and a terminal T_{bat} at the end of the driving mission,
- Upper and lower bounds for the FCS power P_{fcs},
- Upper and lower bounds for the battery power P_{bat},
- Upper and lower bounds for the chiller power $\dot{Q}_{\mathrm{chiller}}$.

The weighting factor α allows for shifting the optimization targets between fuel efficiency and battery thermal conditioning. The optimization problem Eq. (1) is efficiently solved using DP. The result of this optimization is distance-based references $P_{\text{fcs}}^{\text{ref}}$, $\dot{Q}_{\text{chiller}}^{\text{ref}}$, SoC^{ref} and $T_{\text{bat}}^{\text{ref}}$, which are used in real-time on-board control.

Real-time on-board control

For robust incorporation of the predictive control benefits into the vehicle, during the driving mission, simple two-degree-of-freedom control loops are used to track the co-optimized predictive references and to react to actual states (SoC and T_{bat}). The on-board power split setpoints are determined by

$$P_{\text{fcs}}^{\text{set}} = P_{\text{fcs}}^{\text{ref}} + r_{\text{EMS}}\left(\text{SoC}^{\text{ref}} - \text{SoC}\right) \tag{2a}$$

$$P_{\text{bat}}^{\text{set}} = P_{\text{el}} - P_{\text{fcs}}^{\text{set}}. \tag{2b}$$

The on-board chiller setpoint is defined as

$$\dot{Q}_{\text{chiller}}^{\text{set}} = \dot{Q}_{\text{chiller}}^{\text{ref}} + r_{\text{BTMS}}\left(T_{\text{bat}}^{\text{ref}} - T_{\text{bat}}\right). \tag{3}$$

These simple on-board controllers ensure real-time capability due to minimal computational complexity while compensating for any forecast uncertainties and modeling errors.

RESULTS AND DISCUSSION

To demonstrate the value of the proposed co-optimization, optimization results for a representative weighting factor $\alpha = 0.9$ are compared with those from a hierarchical approach. In the hierarchical approach, the EMS optimization with the sole stage cost $L_{\text{EMS},k}$ is optimized first using DP, yielding $P_{\text{fcs}}^{\text{ref}}$ and SoC^{ref}. Subsequently, battery ohmic losses are predicted and a second DP optimization solves the BTMS problem with stage cost $L_{\text{BTMS},k}$. The driving mission and the predictive references are shown in Fig. 2.

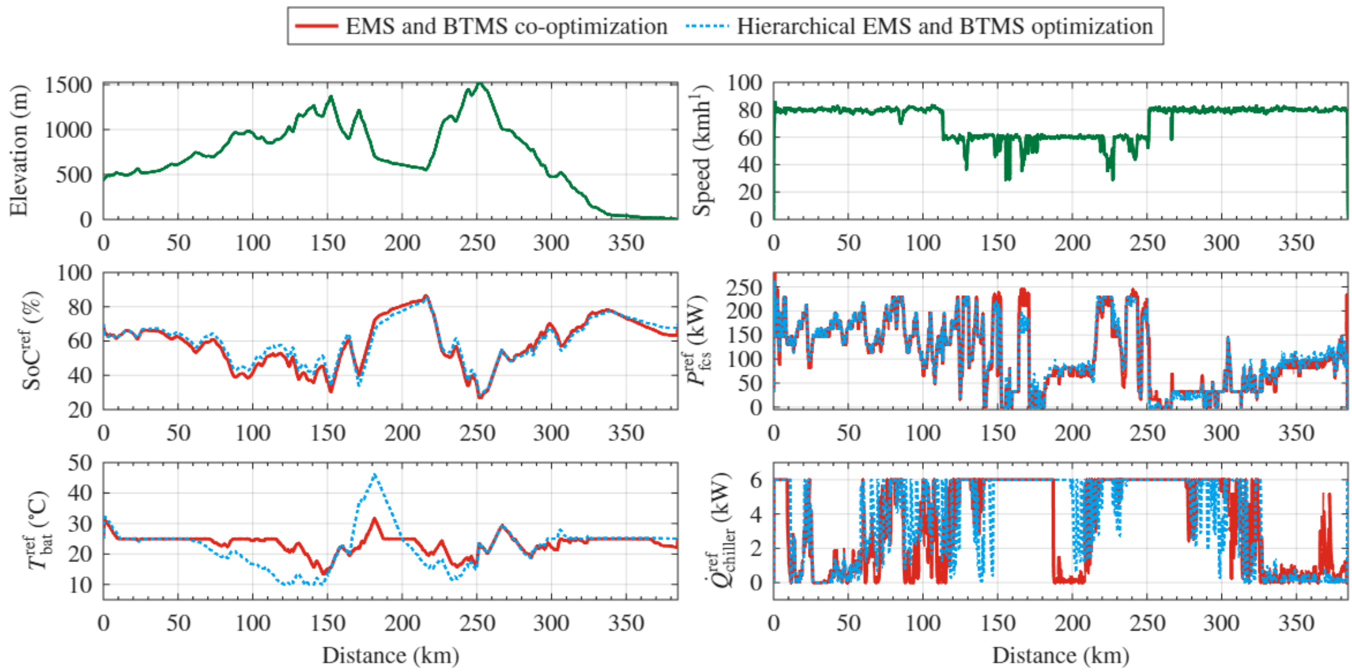

Fig. 2. Results for optimizing energy and battery thermal systems based on predictive route information: Proposed co-optimized references vs. references obtained from hierarchical optimization of the EMS and BTMS

The FCS power and SoC references are largely similar in both approaches. During downhill driving (from 170 to 215 km), the FCS operates in efficient regions to charge the battery. Conversely, during high-load phases before and after this section, the battery supports the FCS to avoid more inefficient high-load operating points. Through targeted SoC control, proactive charging before uphill sections (e.g., from 152 to 164 km) and discharging before downhill sections (e.g., from 215 to 252 km), both fuel efficiency and vehicle operability are achieved. However, the battery thermal conditions for both strategies significantly deviate. During the critical high-load phase (from 165 to 171 km), the hierarchical approach results in a temperature peak approximately 10°C higher than for the co-optimization,

despite earlier pre-cooling and increased cooling energy. This result underscores that temperature peaks during extreme driving missions cannot be mitigated solely by extended pre-cooling. Instead, minor adaptations of the EMS – which are not possible in the hierarchical strategy – are required to substantially support the cooling system. In the proposed EMS-BTMS-co-optimization, FCS usage is slightly increased during such critical driving conditions (from 165 to 171 km). By slightly increasing fuel cell power, the share of high battery C-rates is reduced, leading to lower ohmic losses and, eventually, lower temperature peaks. However, since the overall FCS power remains largely similar along the entire route, fuel economy is not compromised.
To investigate real-world applicability, the proposed co-optimization framework was additionally evaluated in on-board simulations using the controllers in Eq. (2) and (3). The results suggest that the previously observed trend persists even under uncertain forecasts (e.g., limited to speed limits and the elevation profile), indicating that similar behaviour can be expected when deployed in a real vehicle.

CONCLUSIONS

This study presents a novel predictive co-optimization strategy for energy and thermal management in heavy-duty fuel cell vehicles. In contrast to hierarchical methods, the joint optimization enables slight energy management adaptations during demanding driving missions to support the thermal system. Results demonstrate that these adaptations are essential for maintaining safe battery temperatures while preserving fuel economy. This initial investigation directly opens avenues for further analyses regarding the impact of the weighting factor α, the effect of the co-optimization targets on fuel cell and battery degradation stressors, an on-board performance comparison to non-predictive and hierarchical optimization and the impact of forecast uncertainties.
Moreover, the developed strategy can support system-level design decisions for fuel cell trucks by enhancing vehicle operability and performance with reduced component sizing requirements. Additionally, since both terms in the co-optimization objective function penalize either fuel cell or battery usage, the proposed approach also opens potential opportunities for balancing fuel cell and battery degradation.

ACKNOWLEDGEMENT

This work was funded by the Austrian Research Promotion Agency (FFG) in the scope of the project FC4HD (grant number 885044).

REFERENCES

1. Liu F, Zhao F and Hao H. 2018. The impact of fuel cell vehicle deployment on road transport greenhouse gas emissions: The china case. International Journal of Hydrogen Energy 43:22604–22621.
2. Kast J, Vijayagopal R, Gangloff JJ and Marcinkoski J. 2017. Clean commercial transportation: Medium and heavy duty fuel cell electric trucks. International Journal of Hydrogen Energy 42:4508–4517.
3. Ferrara A, Jakubek S and Hametner C. 2021. Energy management of heavy-duty fuel cell vehicles in real-world driving scenarios: Robust design of strategies to maximize the hydrogen economy and system lifetime. Energy Conversion and Management 232:113795.
4. Ferrara A, Jakubek S and Hametner C. 2023. Cost-optimal design and energy management of fuel cell electric trucks. International Journal of Hydrogen Energy 48:16420–16434.
5. Ferrara A, Hütter M and Hametner C. 2022. Adaptive energy management strategy to avoid battery temperature peaks in fuel cell electric trucks. IFAC-PapersOnLine 55:311–316.
6. Büyüker BC, Ferrara A and Hametner C. 2022. Predictive battery cooling in heavy-duty fuel cell electric vehicles. IFAC-PapersOnLine 55:304–310.
7. Anselma PG, Luciani S, and Tonoli A. 2023. Dynamic programming for thermal management of automotive fuel cell systems: Investigating hydrogen saving potential. IEEE Access 11:48080–48098.
8. Song Z, Pan Y, Chen H and Zhang T. 2021. Effects of temperature on the performance of fuel cell hybrid electric vehicles: A review. Applied Energy 302:117572.
9. Liu Y, Li M, Wang Y, Sun Z and Chen Z. 2024. Predictive energy management for fuel cell hybrid vehicles considering efficiency and safety. IEEE Transactions on Power Electronics 39:13842–13852.
10. Jia C, Liu W, He H and Chau K. 2025. Health-conscious energy management for fuel cell vehicles: An integrated thermal management strategy for cabin and energy source systems. Energy 333:137330.
11. Zheng C, Kim N, Park Y, Lim W, Cha S and Xu G. 2013. The effect of battery temperature on total fuel consumption of fuel cell hybrid vehicles. International Journal of Hydrogen Energy 38:5192–5200.

MULTIFUNCTIONAL CE-DOPED $LANIO_3$ PEROVSKITE FOR DIRECT AMMONIA-FUELED SOLID OXIDE FUEL CELLS

Ysa Francine N. Perez[1], Hoong-Yuei Wong[2], Wei-Cheng Huang[2], Chen-Yu Wu[3], Tai-Cheng Chen[4], Kristopher Ray S. Pamintuan[1], Horng-Yi Chang[2]*

[1] School of Chemical, Biological, and Materials Engineering and Sciences, Mapúa University, Intramuros, Manila, Philippines

[2] Department of Marine Engineering, National Taiwan Ocean University, Keelung 202301, Taiwan

[3] Metal Processing R&D Department, Metal Industries Research & Development Centre (MIRDC), Kaohsiung, 81160, Taiwan

[4] Department of Material Research, National Atomic Research Institute, Taoyuan, 32546, Taiwan

*Corresponding author e-mail: hychang@mail.ntou.edu.tw

Ref # FCT-01

ABSTRACT

Direct ammonia-fueled solid oxide fuel cells (AFSOFCs) are promising electrochemical energy conversion devices for carbon-free power generation. In this study, a series of Ce-doped $LaNiO_3$ (Ce-LNO) perovskite oxides with nominal compositions $Ce_xLa_{1-x}NiO_3$ (x = 0–0.30) were synthesized and evaluated as multifunctional anodes for AFSOFCs. XRD analyses indicates that the $LaNiO_3$ perovskite structure is retained at low Ce contents, while fluorite CeO_2 appears as a secondary phase with increasing dopant concentration. FESEM reveals that Ce incorporation effectively suppresses Ni grain growth, resulting in a porous microstructure favorable for gas diffusion and catalytic reactions. EDS mapping confirms a homogeneous distribution of La, Ni, Ce, and O, indicating intimate interfacial contact between the $LaNiO_3$-derived matrix and CeO_2. Half-cell electrochemical measurements demonstrate that Ce doping markedly enhances power density under both H_2 and NH_3 fuels, with a pronounced improvement under direct ammonia fuel operation. The optimal composition, 0.30Ce–LNO, delivers the highest peak power density, reflecting synergistic function among Ni segregation, increased oxygen vacancy concentration associated with Ce^{4+}/Ce^{3+} redox changes, and catalytically active Ni–CeO_2 interfacial sites for ammonia cracking. These results demonstrate that Ce-doped $LaNiO_3$ is a highly promising anode material for efficient and durable direct ammonia-fueled SOFCs.

Keywords: Direct ammonia-fuel, $LaNiO_3$ perovskite, Ce doping

INTRODUCTION

Ammonia has emerged as an attractive hydrogen carrier due to its high volumetric hydrogen density (108 kg $H_2 \cdot m^{-3}$), carbon-free composition, and well-established storage and transportation infrastructure. Ammonia-fueled solid oxide fuel cells (AFSOFCs) have attracted increasing attention as a promising power generation technology [1]. A critical challenge for AFSOFCs lies in the development of robust anode materials capable of simultaneously catalyzing ammonia decomposition and electrochemical hydrogen oxidation while maintaining structural and chemical stability, i.e., it needs to maintain highly active, stable, and cost-effective while operating at intermediate temperatures (400–700 °C) [2].

Conventional Ni-based cermet anodes exhibit high catalytic activity toward hydrogen oxidation but suffer from several drawbacks under ammonia atmospheres, including nitridation, particle agglomeration, redox instability, and severe performance degradation during thermal cycling [3].

Perovskite oxides (ABO_3) have been considered as a versatile candidate for SOFC anode owing to their compositional flexibility, redox stability, tunable electronic structure, and ability to segregate catalytically active metallic nanoparticles in situ via controlled reduction or exsolution processes [4,5]. Among them, $LaNiO_3$ has been extensively studied as it can transform into finely dispersed nickel nanoparticles anchored on a La-containing oxide matrix under reducing conditions [5,6]. This transformation enables $LaNiO_3$-based anodes to combine high catalytic activity for NH_3 fuel conversion with improved resistance to Ni particles sintering compared with conventional Ni–cermets [7]. However, the catalytic activity and durability of pristine $LaNiO_3$-derived anodes remain insufficient at intermediate temperatures, necessitating further compositional modification to optimize their performance in NH_3-fueled environments.

Cerium oxide can be introduced either through partial substitution of La^{3+} by Ce^{3+}/Ce^{4+} in $La_{1-x}Ce_xNiO_3$ or through the formation of $LaNiO_3$–CeO_2 composite anodes, leading to distinct structural and electrochemical characteristics under operating conditions [8]. Recent studies have demonstrated that Ce-modified $LaNiO_3$ systems exhibit significantly enhanced ammonia decomposition activity and improved stability, which are directly relevant to AFSOFC anode functionality. Podila et al. [9] reported that Ce substitution in $LaNiO_3$-based perovskites markedly enhances NH_3 cracking activity, achieving near-complete ammonia conversion at temperatures compatible with SOFC operation. Pinzón et al. [10] showed that Ce-containing $LaNiO_3$-derived catalysts exhibit superior low-temperature NH_3 decomposition compared with Ce-free counterparts, which was attributed to enhanced reducibility and improved

Ni dispersion. Those findings suggest that Ce modification not only promotes catalytic ammonia decomposition but also tailors the structural evolution of perovskite-derived anodes.

Extensive investigations of cerium- and rare-earth-based oxides have established that oxygen vacancies—arising from reversible redox behavior—play a decisive role in ammonia adsorption, N–H bond activation, and hydrogen formation kinetics [11]. However, the above material design strategies have remained largely disconnected, and their cooperative effects within a single perovskite catalyst architecture have not been systematically evaluated. At high Ce contents, the perovskite lattice may partially decompose into mixed oxide phases during synthesis or in situ reduction, leading to complex multiphase anode microstructures [8,10]. Clarifying the relationship between Ce distribution, phase evolution, and electrochemical performance is therefore essential for rational anode design.

The present study systematically investigates cerium-doped $LaNiO_3$ perovskite oxides as multifunctional anode materials for AFSOFCs. A compositional series of $La_{1-x}Ce_xNiO_3$ (x = 0.00–0.80) is synthesized and comprehensively characterized to elucidate the influence of Ce incorporation on phase stability, lattice distortion, and defect chemistry. Particular emphasis is placed on understanding how cerium doping modifies the structural and redox properties of the perovskite framework and NH_3 decomposition kinetics in thus anode.

MATERIALS AND METHODS

Ce-doped $LaNiO_3$ powders with nominal compositions $Ce_xLa_{1-x}NiO_{3-\delta}$ (x = 0.00 ~ 0.30) were synthesized via a modified Pechini polymeric precursor method. Stoichiometric amounts of $La(NO_3)_3{\cdot}6H_2O$, $Ce(NO_3)_3{\cdot}6H_2O$, and $Ni(NO_3)_2{\cdot}6H_2O$ were dissolved in deionized water, followed by the addition of citric acid and ethylene glycol under continuous stirring. The citric acid : metal and ethylene glycol : metal part of $LaNiO_3$ ratios were set to 1.5:1 and 3:1 respectively. Following the dissolution of nitrates in 50 mL of DI water then chelation with citric acid at 60 °C. Then, the addition of ethylene glycol at 80 °C to initiate polyesterification, subsequently dried at 120 °C overnight to yield foam gels. These foam gels were decomposed at 300°C, final calcination at 800 °C for 5 h.

The calcined powders were first sieved to improve homogeneity. The powder–PB-72 binder mixed aqueous solutions were subjected wet ball milling to enhance dispersion and reduce agglomerates. After milling, the slurry was dried at 80 °C to produce dry powders with a fine and homogeneous consistency. These powders were ground again with a mortar and pestle and re-sieved using 80-sized mesh to ensure uniform granulated size distribution, then, using a hydraulic press to form a disc. The pressed discs were sintered at 1050 °C to obtain porous pellets.

A horizontally fixed-bed reactor operating at atmospheric pressure was employed to carry out ammonia cracking tests for 1050 °C sintered porous discs, which exposed to pure NH_3 at a constant flow rate of 50 $mL{\cdot}min^{-1}$. The outgas stream was analyzed on-line by using a thermal conductivity detector (TCD) to calculate the H_2 content from NH_3 decomposition. The calcined Ce-LNO powders were prepared as paste and then printed on densified LSBC electrolyte by 1500 °C/6 h sintering. After 1050 °C/4 h cofiring, the Pt paste was printed the other surface of LSBC as a cathode to form Ce-LNO|LSBC|Pt half-cell. The Ag paste was printed on Ce-LNO anode side as the current collector.

The crystal structures of the calcined powders, sintered bodies were characterized by X-ray diffraction (XRD, Bruker D2 Phaser, CuKα radiation at a wavelength of λ = 1.5405 Å, scan speed of 4 $°min^{-1}$). Field-emission scanning electron microscopy (FESEM, Hitachi Field-Emission S4800 (EMAX)) equipped with energy-dispersive X-ray spectroscopy (EDS) was used to determine the microstructures, morphologies, and elemental composition. The Ce-LNO|LSBC|Pt half-cells were connected to Pt wires by clamping the wires to a spring-loaded sample holder, and tested under ammonia (anode side) and air (cathode side) atmospheres in the temperature range of 500–800 °C. Alternating current (AC) impedance analyses of the half-cells were performed using a Zahner Zennium instrument under open circuit conditions in the frequency range of 0.1 Hz–50x10^3 Hz. The voltage-current density (IV) and power density-current density (IP) of the fuel cells were measured using a Keithley 2400 source meter.

RESULTS AND DISCUSSION

XRD patterns, as shown in Figs. 1(a)-(f), indicate $Ce_xLa_{1-x}NiO_3$ powders calcined at 800 °C that confirm the formation of a rhombohedral $LaNiO_3$ perovskite structure for low Ce contents (x ≤ 0.10). With increasing Ce concentration, weak diffraction peaks corresponding to fluorite-type CeO_2 become discernible, which means partial solubility of Ce in the $LaNiO_3$ lattice and the coexistence of a secondary phase of NiO at higher doping levels. After sintering at 1050 °C, comparisons in Figs 1(g)-(j), the perovskite framework of LNO remains intact, demonstrating good thermal stability of the more Ce-modified structure.

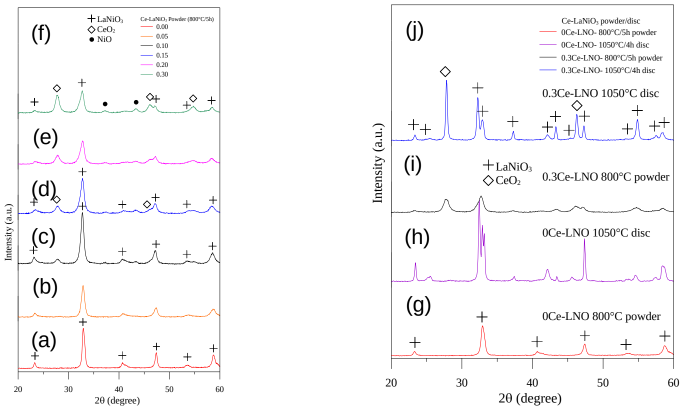

Fig. 1. X-ray diffraction (XRD) patterns of $Ce_xLa_{1-x}NiO_3$ (x = 0–0.30) (a)-(f) powders calcined at 800 °C, (g)-(j) comparisons of 800 °C and 1050 °C heat-treatment.

FESEM images of $La_{1-x}Ce_xNiO_3$ discs sintered at 1050 °C reveal that undoped $LaNiO_3$ consists of relatively homogeneous grains distribution with limited surface roughness (Fig. 1(a)). Upon Ce incorporation, the grain size of LNO decreases with CeO_2 grain growth and surface texture becomes more irregular, particularly for x = 0.15–0.30 shown in Figs. 1(d)-(f). At higher Ce content (x = 0.30), the microstructure exhibits a morphology with fine particles anchored on larger grains, which may be NiO segregation favorable for gas diffusion and catalytic reactions. Such a microstructural development is attributed to Ce-induced grain growth and more rough surface formation.

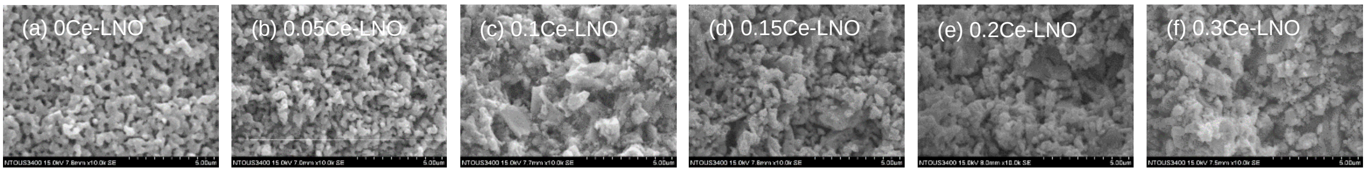

Fig. 2. FESEM images of $La_{1-x}Ce_xNiO_3$ discs sintered at 1050 °C, (a) x = 0, (b) x = 0.05, (c) x = 0.10, (d) x = 0.15, (e) x = 0.20, and (f) x = 0.30.

From EDS elemental mapping results, they demonstrate that Ce is evenly distributed throughout the $LaNiO_3$ matrix without evidence of localized Ce-rich agglomerates. For example, the 0.30Ce–LNO sample demonstrates uniform spatial distribution of La, Ni, Ce, and O throughout the calcined powder. Semi-quantitative EDS analysis reveals that the measured elemental ratios qualitatively follow the intended stoichiometry, although minor deviations from nominal compositions are observed. The inherent challenges associated with accurate oxygen quantification and matrix effects in complex oxide powders at this state. No obvious Ni elemental segregation is confirmed in Fig. 3 mapping, even the small particles distributed homogeneous in FESEM image of Fig. 3(a). However, further analyses are needed to suggest intimate contact between CeO_2, NiO and $LaNiO_3$ for establishing extended Ni–CeO_2 interfacial sites during reduction, which are known to enhance ammonia decomposition kinetics.

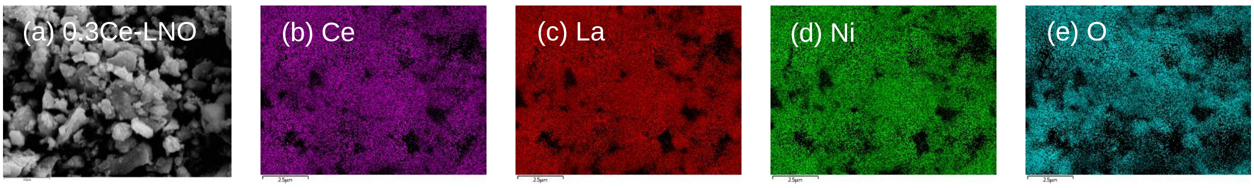

Fig. 3. FESEM image and corresponding EDS elemental mapping of the 0.30Ce–LNO sample showing the spatial distribution of (b) Ce, (c) La, (d) Ni, and (e) O.

The intrinsic ammonia decomposition activity of Ce-LNO porous discs was further evaluated by monitoring hydrogen generation as a function of temperature under pure NH_3 flow, as shown in Fig. 4(a). Overall, undoped LNO and Ce-LNO exhibit higher NH_3 decomposition ratio than only thermal cracking ammonia. Undoped LNO exhibits limited cracking activity below 500 °C, with hydrogen generation increasing gradually at higher temperatures. In contrast, all Ce-doped samples display significantly enhanced NH_3 cracking performance, particularly in the intermediate temperature range of 500–700 °C.

With increasing Ce content to 0.3, the onset temperature for rapid hydrogen generation shifts to lower value. The 0.30Ce–LNO achieves hydrogen generation exceeding other xCe-LNO at 450–700 °C. This pronounced enhancement can be attributed to the synergistic interaction between exsolved Ni nanoparticles and CeO_2 phase, where Ce^{4+}/Ce^{3+} redox couples facilitate hydrogen spillover and stabilize active Ni sites. In addition, the high oxygen storage capacity of CeO_2 promotes continuous removal of surface nitrogen species, alleviating catalyst poisoning during NH_3 decomposition.

The peak power density as a function of Ce dopant concentration shows a monotonic increase for both H_2 and NH_3 fuels, as shown in Fig. 4(b). While all half-cells exhibit higher power output under H_2 than NH_3. The enhancement induced by Ce doping is observed with pronounced under NH_3 operation. The 0.30Ce–LNO anode delivers the highest power density, reflecting optimized catalytic activity and charge transport properties.

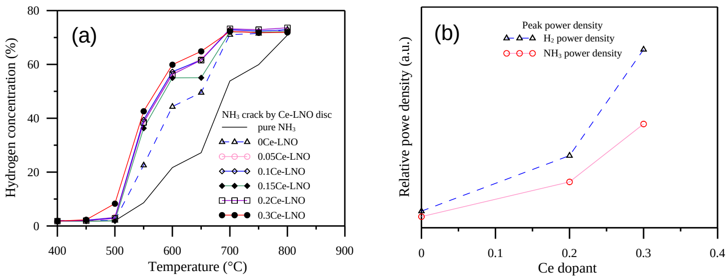

Fig. 4. (a) Temperature-dependent hydrogen generation obtained from ammonia cracking over xCe-LNO (x = 0–0.30) porous discs under pure NH_3 flow. (b) Peak power density of half-cells employing xCe-LNO anodes as a function of Ce dopant concentration under H_2 and NH_3 fuels.

CONCLUSIONS

Ce-doped $LaNiO_3$ perovskite oxides were investigated as anode materials for direct ammonia-fueled solid oxide fuel cells. Structural analysis confirms that Ce incorporation partially substitutes into the $LaNiO_3$ lattice at low dopant levels, while excess Ce forms a dispersed CeO_2 secondary phase at higher concentrations. Microstructural characterization reveals that CeO_2 grain growth effectively inhibits NiO grain growth and promotes the formation of a porous structure after 1050 °C sintering, which is beneficial for gas transport and electrochemical reactions. Elemental mapping demonstrates a uniform spatial distribution of La, Ni, Ce, and O, ensuring extensive Ni–CeO_2 interfacial contact upon reduction. Electrochemical testing shows that Ce doping significantly enhances SOFC performance under both H_2 and NH_3 fuels, with the most pronounced improvement observed during direct ammonia operation. The optimal 0.30Ce–LNO anode exhibits the highest peak power density, attributed to the synergistic effects of increased oxygen vacancy concentration, stabilized segregated Ni nanoparticles, and the catalytic activity of Ni–CeO_2 interfaces toward ammonia cracking.

ACKNOWLEDGEMENTS

The authors gratefully acknowledge the financial support from the National Science and Technology Council (NSTC), Taiwan, ROC (Grant Numbers NSTC 114-2221-E-019-060 and NSTC 114-2923-E-027-005). The authors also thank the Taiwan Experience Education Programs (TEEP) for additional support.

REFERENCES

[1] Portarapillo M, Bellucci SA, Russo D, di Benedetto A. 2025. Ammonia as a hydrogen carrier: energetic assessment of processes integrated with fuel cells for power generation. Energy Fuels 39:2843–2853.
[2] Lucentini I, Garcia X, Vendrell X and Llorca J. 2021. Review of the decomposition of ammonia to generate hydrogen. Industrial & Engineering Chemistry Research 60:18560−18611.
[3] Elmutasim O, Dhawale DS, Pinczes M, Giddey S, Paul G and Bhattacharya S. 2025. Mechanistic investigation of ammonia utilization pathways on a locally oxygen enriched Ni−YSZ anode for direct ammonia-fed solid oxide fuel cells: An Ab Initio study. ACS Sustainable Chemistry and Engineering 13:18242−18254.
[4] Humayun M, Li Z, Israr M, Khan A, Luo W, Wang C, Shao Z. 2025. Perovskite-type ABO_3 oxides in photocatalysis, electrocatalysis, and solid oxide fuel cells: State of the art and future prospects. Chemical Reviews 125:3165–3241.
[5] Jin Y, Fan K, Feng M, Wang Y, Chen H, Liu X. 2025. Highly synergistic Ni/CeO_2 interface with optimized NH_3 pretreatment for enhanced catalytic ammonia decomposition. Applied Surface Science 714:164434.
[6] Park JM, Kim JH, Lee SJ, Moon DJ. 2021. $LaNiO_3$-based perovskite-derived catalysts for ammonia decomposition. International Journal of Hydrogen Energy 46:16453–16464.
[7] Aydın Ö, Kazancıoğlu E, Kerscher F, Fendt S, Spliethoff H. 2025. Systematic investigation of Ni_3N formation in Ni–YSZ anodes of direct NH_3-utilizing SOFCs. 19th International Symposium on Solid Oxide Fuel Cells (SOFC XIX) A2025-03:59.
[8] He H, Chen X, Li J. 2023. Ni/CeO_2-based catalysts for ammonia decomposition. Catalysts 13:453.
[9] Podila S, Karakaya C, Kee RJ. 2022. Influence of Ce substitution in $LaMO_3$ (M = Ni, Co) perovskites for CO_x-free hydrogen production from ammonia decomposition. Arabian Journal of Chemistry 15:103808.
[10] Pinzón M, Romero-Sarria F, Centeno MA, Odriozola JA. 2022. Ni-based perovskite catalyst precursors for ammonia decomposition: Effect of Ce doping. Fuel 323:124384.
[11] Xu K, Liu JC, Wang WW, Zhou LL, Ma C, Guan X, Wang FR, Li J, Jia CJ, Yan CH. 2024. Catalytic properties of trivalent rare-earth oxides with intrinsic surface oxygen vacancy. Nature Communications 15:5751.

DEEP LEARNING–BASED WEATHER FORECASTING FOR PAKISTAN

Ebad Ul Haq[1], Muhammad Usama Haroon[2], Hafiz Muhammad Saqlain Nawaz[3], Murat Fahrioglu[4], Abdullah Ekinci[5], Cagri Yalkin[6]*

[1] Middle East Technical University (METU), Northern Cyprus Campus (NCC), Department of Electrical and Electronics Engineering, Guzelyurt, 99738, North Cyprus

[2] METU, NCC, Department of Sustainable Environment and Energy Systems, Guzelyurt, 99738, North Cyprus

[3] METU, NCC, Department of Sustainable Environment and Energy Systems, Guzelyurt, 99738, North Cyprus

[4] METU, NCC, Department of Electrical and Electronics Engineering, Guzelyurt, 99738, North Cyprus

[5] METU, NCC, Department of Civil Engineering, Guzelyurt, 99738, North Cyprus

[6] METU, NCC, Department of Business Administration, Guzelyurt, 99738, North Cyprus

*Corresponding author e-mail: ebad.ul@metu.edu.tr

Ref # FOR-01

ABSTRACT

Accurate weather forecasting is critical for energy planning, agriculture, and climate-resilient infrastructure in climate-vulnerable regions such as Pakistan. This study presents a data-driven short-term weather forecasting framework based on statistical and machine learning models applied to long-term historical meteorological data. Daily temperature, relative humidity, solar irradiance, and precipitation records are obtained from the NASA POWER dataset and complementary weather sources for multiple Pakistani cities. Linear Regression, Random Forest, Extreme Gradient Boosting (XGBoost), and Autoregressive Integrated Moving Average (ARIMA) models are developed and evaluated using a chronological train–validation–test strategy. Model performance is assessed using Mean Absolute Error (MAE), Mean Squared Error (MSE), and the coefficient of determination (R^2). Results show that XGBoost consistently achieves the highest accuracy for one-day-ahead temperature forecasting, with average MAE of approximately 1.4 °C and R^2 exceeding 0.94 across cities, while Random Forest and Linear Regression provide competitive performance. In contrast, the univariate ARIMA model exhibits limited predictive capability, particularly for highly variable precipitation. The findings highlight the effectiveness of ensemble machine learning models for short-term weather forecasting and their potential to support sustainable energy and environmental planning in Pakistan.

Keywords: Deep learning, Energy and Environment, Pakistan climate, Time-series modelling, Weather forecasting.

INTRODUCTION

Weather forecasting plays a critical role in energy management, agriculture, disaster preparedness, and environmental sustainability [1]. In Pakistan, increasing climate variability, heatwaves, and irregular precipitation patterns pose significant challenges to energy systems and socio-economic stability [2]. Climate change poses a major threat to humanity and ecosystems, intensifying global food insecurity as temperatures continue to rise. According to the IPCC, vulnerable crops such as wheat and cotton are at increasing risk, particularly in underdeveloped regions [3].

Numerical Weather Prediction (NWP) models are physics-based systems that simulate future atmospheric states, in contrast, modern machine learning and deep learning approaches provide data-driven alternatives capable of capturing nonlinear patterns and temporal dependencies in meteorological data [4]. Deep neural networks such as CNNs and LSTMs have shown strong performance in time-series forecasting tasks [5]. Machine learning models enhance NWP forecasts by learning nonlinear patterns that physics-based models may not capture [6].

Traditional weather forecasting began in the nineteenth century and involves analyzing large, complex atmospheric datasets with multiple dynamic parameters [7]. However, many recent studies rely on isolated methodologies, which can introduce bias and uncertainty in climate impact assessments. Moreover, limited historical data restrict the accuracy of empirical statistical models in predicting future yield–climate relationships [8]. Rainfall forecasting is vital for flood and drought management, yet numerical models and neural networks face limitations in accuracy and scalability [9].

Accurate forecasting of renewable energy generation is essential for maintaining grid stability, ensuring reliable power system operation, and reducing the operational costs associated with uncertainty [10]. This paper introduces novel deep learning algorithms designed to enhance day-ahead wind speed predictions, particularly by improving upon the Weather Research and Forecasting (WRF) model's accuracy [11].

This study evaluates machine learning and deep learning models for rainfall classification in Pakistan using historical climatic data, including temperature, humidity, pressure, and rainfall. Performance comparisons show that deep learning approaches outperform traditional models by effectively capturing nonlinear and temporal patterns, supporting their use in climate-related decision-making [12].

The study assesses deep learning models for real-time, short-term temperature prediction across multiple locations using historical meteorological data. Comparative results show that deep models better capture spatial and temporal patterns, improving nowcasting accuracy and supporting weather-dependent decision-making [13].

The study combines General Circulation Models with deep learning to project future temperature and precipitation trends for Lahore, Pakistan. By leveraging historical climate data, the integrated approach improves regional climate projections, capturing nonlinear patterns and providing more reliable insights for local adaptation planning [14].

The study uses four years of meteorological data to forecast solar Global Horizontal Irradiance in Islamabad using statistical models (SARIMAX, Prophet) and deep learning (ANN, CNN, LSTM), finding ANN, CNN, and LSTM excel in short-term forecasts while statistical methods perform well for longer horizons [15].

Precise weather forecasting is particularly critical for the integration of renewable energy systems into modern electric networks. Since solar and wind generation are inherently weather-dependent and variable, forecasting helps reduce uncertainty in power output, supports optimal scheduling and dispatch decisions, and enhances grid stability. Reliable predictions therefore enable higher renewable penetration while maintaining cost-effective power system operation.

DATASET AND PREPROCESSING

The primary data source used in this study is the NASA POWER (Prediction of Worldwide Energy Resources) dataset, which provides consistent and long-term meteorological observations. The dataset includes daily measurements of Air temperature, Relative humidity, Solar irradiance, and Precipitation (rainfall). The data are extracted for selected regions of Pakistan and undergo preprocessing steps including missing-value handling, normalization, and time-series windowing. Feature scaling is applied to improve training stability and model convergence.

METHODOLOGY

Figure 1 illustrates the overall workflow of the proposed machine learning–based weather forecasting framework. The process begins with the acquisition of long-term climatic data from the NASA POWER dataset and supplementary local weather sources. The collected data are then preprocessed to address missing values, remove inconsistencies, and apply appropriate normalization. Key meteorological variables, including temperature, relative humidity, solar irradiance, and precipitation, are selected and organized into supervised time-series datasets using a sliding window strategy and chronological train–validation–test splitting. These processed datasets are used to develop and evaluate multiple forecasting models, namely Linear Regression, Random Forest, Extreme Gradient Boosting (XGBoost), and Autoregressive Integrated Moving Average (ARIMA).

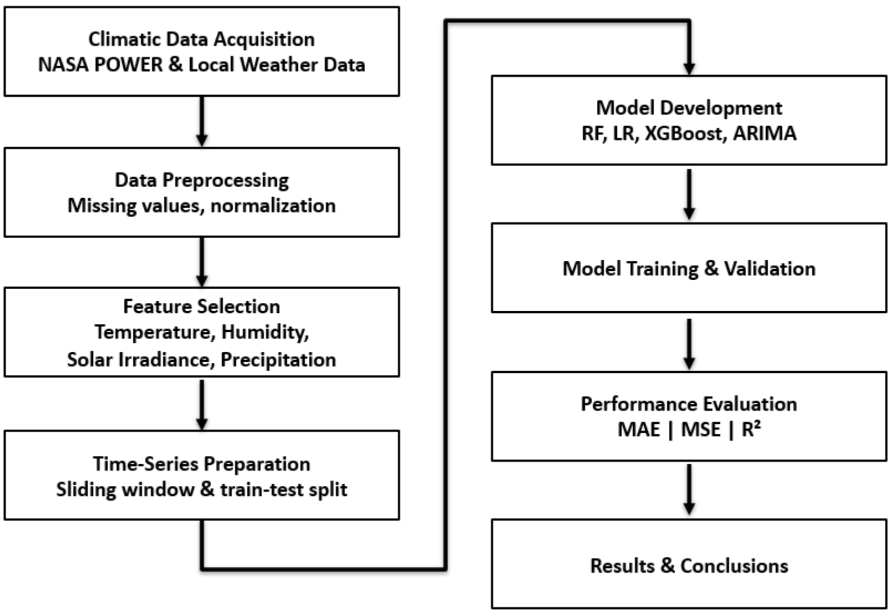

Figure 2 Flow of Data

The models are trained to predict key weather variables, including temperature, humidity, solar irradiance, and precipitation. Performance is evaluated using standard regression metrics:

- Mean Absolute Error (MAE)
- Mean Squared Error (MSE)
- Coefficient of Determination (R^2)

RESULTS AND DISCUSSION

Results

Model performance was evaluated for one-day-ahead forecasting across six Pakistani locations including Karachi, Lahore, Islamabad, Peshawar, Quetta, and Gilgit using MAE, MSE, and R^2 with coordinates defined for regional extraction. Given in the table 1, errors are reported in the same physical units as the target variables (T2M in °C, RH2M in %, PRECTOTCORR in mm/day), enabling direct interpretability [16].

Table 2 Target variables and their units

Target	MAE / MSE Units
T2M	Degrees Celsius (°C)
RH2M	Percentage (%)
PRECTOTCORR	Millimeters/day (mm/day)
R^2	Unitless (−∞ to 1)

Temperature (T2M)

Across all cities, XGBoost achieved the best overall temperature performance with average MAE ≈ 1.43 °C and R^2 ≈ 0.94 [17] in the given table 2, outperforming Random Forest and Linear Regression. City-level best test results for T2M were consistently obtained by XGBoost (e.g., Karachi MAE ≈ 0.72 °C; Islamabad MAE ≈ 1.42 °C; Gilgit MAE ≈ 1.68 °C). In contrast, the univariate ARIMA baseline showed large errors and negative R^2 (average MAE ≈ 12.88 °C; R^2 ≈ −2.83), indicating poor suitability for multivariate, nonlinear weather dynamics in this setting [18].

Table 3 Main targets of machine learning models with Temperature (T2M)

Model	MAE	R^2
XGBoost	1.43	0.94
Random Forest	1.54	0.94
Linear Regression	1.82	0.91
ARIMA	12.88	−2.83

Relative Humidity (RH2M)

From the given table 3, Humidity prediction showed moderate accuracy, with the best average results achieved by Linear Regression (average MAE ≈ 8.05%; R^2 ≈ 0.59). City-wise, Linear Regression was most frequently selected as the best RH2M model on the test split (e.g., Karachi MAE ≈ 6.51%, Lahore MAE ≈ 6.65%, Islamabad MAE ≈ 6.71%), while Quetta performed best with Random Forest (MAE ≈ 9.70%). ARIMA again underperformed substantially (average MAE ≈ 21.23%, R^2 ≈ −1.65) [19].

Table 4 Secondary targets of machine learning models with Relative Humidity (RH2M)

Model	MAE	R^2
Linear Regression	8.05	0.59
Random Forest	8.23	0.58
XGBoost	8.32	0.57
ARIMA	21.22	−1.65

Precipitation (PRECTOTCORR)

Precipitation remained the most difficult variable to predict. While ARIMA yielded the lowest average MAE (~1.99 mm/day), its R^2 stayed negative (≈ −0.11) as mentioned in table 4, suggesting limited explanatory power despite comparable absolute error [20]. ML models achieved small positive but low R^2 values (generally ≈ 0.06–0.09), consistent with precipitation's high stochasticity and intermittency. At the city level, ARIMA was often selected as the "best" by test MAE (e.g., Karachi, Lahore, Peshawar, Quetta, Islamabad), whereas Gilgit favored Linear Regression.

Table 5 Secondary targets with Precipitation (PRECTOTCORR)

Model	MAE	R^2
Linear Regression	2.34 mm	0.09
Random Forest	2.18 mm	0.08
XGBoost	2.26 mm	0.06
ARIMA	1.98 mm	−0.11

Discussion

The proposed models were evaluated for one-day-ahead forecasting using MAE, MSE, and R^2. For temperature prediction, XGBoost achieved the best performance with an average MAE of 1.43 °C and R^2 of 0.94 across all cities. Relative humidity forecasting showed moderate accuracy, with MAE around 8% and R^2 ≈ 0.6. Precipitation prediction remained challenging due to its stochastic nature, yielding lower R^2 values, which is consistent with prior studies. Overall, machine learning models significantly outperformed the statistical ARIMA baseline, highlighting the effectiveness of data-driven approaches for short-term weather forecasting.

CONCLUSIONS

This study developed a machine learning–based framework for short-term weather forecasting in Pakistan using long-term NASA POWER meteorological data. Results show that XGBoost achieved the best performance for one-day-ahead temperature prediction, with an average MAE of approximately 1.4 °C and R^2 above 0.94 across all cities. Relative humidity forecasting yielded moderate accuracy, with MAE around 8% and R^2 close to 0.6. Random Forest and Linear Regression provided competitive results, while the univariate ARIMA model showed limited predictive capability. The findings confirm the effectiveness of ensemble machine learning models for reliable short-term weather forecasting and climate-related planning.

REFERENCES

[1]. Shah, F.A., Meraj, A.B.E., Roman, M., Anwar, M., Zaib, A., Shams, S.S. and Hussain, F., 2026. Enhancing Weather Forecasting Accuracy: A Machine Learning Approach Using Genetic Algorithm and Random Forest. Global Research Journal of Natural Science and Technology.

[2]. Hassan, B., Qadir, A. and Ahmad, R.I., 2025. CLIMATE CHANGE AND WATER SCARCITY: ADAPTATION AND MITIGATION STRATEGIES IN PAKISTAN. International Journal of Social Sciences Bulletin, 3(10), pp.1-23.

[3]. Haider, S.T., Ge, W., Li, J., Rehman, S.U., Imran, A., Sharaf, M.A.F. and Haider, S.M., 2024. An ensemble machine learning framework for cotton crop yield prediction using weather parameters: a case study of Pakistan. IEEE Access, 12, pp.124045-124061.

[4]. Waqas, M., Humphries, U.W., Chueasa, B. and Wangwongchai, A., 2025. Artificial intelligence and numerical weather prediction models: A technical survey. Natural Hazards Research, 5(2), pp.306-320.

[5]. Mir, A.A., Khan, Z.A., Altmimi, A., Badar, M., Ullah, K., Imran, M. and Kazmi, S.A.A., 2021. Systematic development of short-term load forecasting models for the electric power utilities: The case of Pakistan. IEEE Access, 9, pp.140281-140297.

[6]. Markovics, D. and Mayer, M.J., 2022. Comparison of machine learning methods for photovoltaic power forecasting based on numerical weather prediction. Renewable and Sustainable Energy Reviews, 161, p.112364.

[7]. Fathi, M., Haghi Kashani, M., Jameii, S.M. and Mahdipour, E., 2022. Big data analytics in weather forecasting: A systematic review. Archives of Computational Methods in Engineering, 29(2), pp.1247-1275.

[8]. Shah, M.H., Shah, W., Syed, S., Ullah, I., Wang, Y. and Wang, Y., 2025. Impacts of Climate Change on Rice Production in Pakistan: A Perspective from a Deep Learning Approach. Atmosphere, 16(11), p.1305.

[9]. Fahad, S., Su, F., Khan, S.U., Naeem, M.R. and Wei, K., 2023. Implementing a novel deep learning technique for rainfall forecasting via climatic variables: An approach via hierarchical clustering analysis. Science of The Total Environment, 854, p.158760.

[10]. Abdul Baseer, M., Almunif, A., Alsaduni, I. and Tazeen, N., 2023. Electrical power generation forecasting from renewable energy systems using artificial intelligence techniques. Energies, 16(18), p.6414.

[11]. Christoforou, E., Emiris, I.Z., Florakis, A., Rizou, D. and Zaharia, S., 2023. Spatio-temporal deep learning for day-ahead wind speed forecasting relying on WRF predictions. Energy Systems, 14(2), pp.473-493.

[12]. Farman, H., Hussain, A., Baig, J., Hussain, S. and Farman, A., 2025. Performance Evaluation of Machine Learning and Deep Learning Models for Rainfall Classification Using Climatic Datasets of Pakistan. Journal of Computing & Biomedical Informatics, 9(02).

[13]. Zaka, F., Nafisah, I.A., Lin, J., Almazah, M.M., Hussain, I., Almazroui, M., Chakrabortty, R. and Louati, H., 2025. Real-time temperature nowcasting using deep learning models across multiple locations. Modeling Earth Systems and Environment, 11(3), p.165.

[14]. Nguyen, D.T., Ashraf, S., Le, M., Trung, L.Q. and Ali, M., 2023. Projection of climate variables by general circulation and deep learning model for Lahore, Pakistan. Ecological Informatics, 75, p.102077.

[15]. Haider, S.A., Sajid, M., Sajid, H., Uddin, E. and Ayaz, Y., 2022. Deep learning and statistical methods for short-and long-term solar irradiance forecasting for Islamabad. Renewable Energy, 198, pp.51-60.

[16]. Nasim, S.F. and Haider, N.G., 2024, September. Improving Pakistan Weather Forecasting Accuracy with Machine Learning: A Data-Driven Approach. In 2024 Global Conference on Wireless and Optical Technologies (GCWOT) (pp. 1-6). IEEE.

[17]. Ma, X., Fang, C. and Ji, J., 2020, January. Prediction of outdoor air temperature and humidity using XGBoost. In IOP conference series: earth and environmental science (Vol. 427, No. 1, p. 012013). IOP Publishing.

[18]. Mollick, T., Hashmi, G. and Sabuj, S.R., 2023. A perceptible stacking ensemble model for air temperature prediction in a tropical climate zone. Discover Environment, 1(1), p.15.

[19]. Segovia, J.A., Toaquiza, J.F., Llanos, J.R. and Rivas, D.R., 2023. Meteorological variables forecasting system using machine learning and open-source software. Electronics, 12(4), p.1007.

[20]. Islam, F.Z., Islam, R., Jamil, A. and Momen, S., 2022, May. Evaluation of Machine Learning Methods for Predicting Rainfall in Bangladesh. In 2022 IEEE 2nd Conference on Information Technology and Data Science (CITDS) (pp. 124-129). IEEE.

EXPLORING THE CHALLENGES OF DEVELOPING LOW-EMISSION HYDROGEN PRODUCTION TECHNOLOGIES IN TÜRKİYE: A PESTEL PERSPECTIVE

Melisa Öztekin Pala[1], *Ece Oyan*[2,3*]
[1] Yasar University, Faculty of Economics and Administrative Sciences, Department of Logistics Management, Universite Cad. No:37-39, Izmir, TR
[2] Competence Centre on Climate Change Mitigation in Energy-Intensive Industries (KEI), Karl-Liebknecht-Str. 33 03046 Cottbus, DE
[3] Bonn University, Faculty of Agricultural, Nutritional and Engineering Sciences, Institute for Food and Resource Economics, Nußallee 21, 53115 Bonn, DE
*Corresponding author e-mail: ece.oyan@z-u-g.org
Ref # HES-02

ABSTRACT

Low-emission hydrogen is critical for decarbonizing hard-to-abate sectors in emerging economies such as Türkiye. This study identifies and examines political, economic, social, technological, environmental, and legal challenges to developing low-emission hydrogen production technologies in Türkiye by combining a PESTEL framework with the fuzzy DEMATEL method. Fifteen challenges were defined from the literature and expert input, and their causal relationships were mapped. The results show that low technology readiness, regulatory uncertainties, and high investment costs are core drivers, while lack of subsidies and harmonised international standards act as important additional causes. Infrastructure gaps and lengthy patenting and licensing processes emerge mainly as downstream effects, highlighting priority areas for targeted policy intervention.

Keywords: Green production, low-emission hydrogen, Fuzzy DEMANTEL, Multi-criteria decision making

INTRODUCTION

The urgent need to decarbonize hard-to-abate sectors has brought low-emission hydrogen production technologies to the forefront of sustainable energy transition. In industrial applications, green hydrogen replaces fossil fuels in sectors like steel production, chemical manufacturing, and long-distance transportation (Sun et al., 2025). This transition reduces carbon emissions, enhances energy security, and allows industries to meet environmental regulations and achieve net-zero emissions without overhauling existing infrastructure.

Investing in the research and development (R&D) of low-emission hydrogen production technologies and the provision capacity of national financial support to ensure competitiveness in the market differ across countries (Bade et al., 2024). For example, the major global electrolyzer manufacturers are from global north countries like Germany, the United States (US), Japan, and Denmark (Wappler et al., 2022). Apart from the US, these countries are also pioneering in setting net-zero targets and announcing their future demand for green hydrogen. On the other hand, in the global south, domestic green hydrogen demand and attempts to develop production technologies are still less widespread (Zainal et al., 2024). These countries generally face problems such as energy insecurity, environmental degradation, and increasing energy demand. However, they are also the ones with enormous renewable energy potential.

Moreover, due to mechanisms like the Carbon Border Adjustment Mechanism (CBAM) of the European Union (EU), decarbonizing major manufacturing industries has become an urgent task for the trading partners of the EU, including Türkiye. Therefore, the potential and importance of green hydrogen deployments are increasingly recognized (Agyekum et al., 2024). Especially emerging economies like Türkiye are interested in developing low-emission hydrogen technologies to increase energy supply security and ensure environmental sustainability (Arslan & Yılmaz, 2024).

This study identifies the challenges in Türkiye's green hydrogen production technologies field and provides strategic planning and information to policymakers and other stakeholders. To do so, it analyzes the interactions of political, economic, social, technological, environmental, and legal (PESTEL) challenges in developing green hydrogen production technologies in Türkiye, with a holistic approach. Therefore, the research questions of this study are as follows:

- **Research Question 1:** What are the main challenges in developing low-emission hydrogen production technologies in Türkiye?
- **Research Question 2:** How do the political, economic, social, technological, environmental, and legal challenges that Türkiye faces in developing low-emission hydrogen production technologies affect each other?

MATERIALS AND METHODS

PESTEL Analysis

PESTEL analysis is a comprehensive analysis method that examines the environmental factors of an organization or a project/strategy (Teixeira et al., 2024). By analyzing an issue through six distinct lenses, PESTEL provides a systems-thinking framework that helps public policymakers grasp the interconnected nature of the systems they seek to change. It is especially preferred in barrier, challenge, and driver studies where categorization is required (Nazir & Sharifi, 2024; Kokkinos et al., 2023; Teixeira et al., 2024).

In this study, the challenges of developing low-emission hydrogen production technologies in Türkiye are classified and defined based on the pillars of the PESTEL analysis, considering the literature review.

Table 1. Challenges of Developing Green Hydrogen Production Technologies in Türkiye

Pillars of PESTEL	**Challenges**	**Author(s)**	**Explanation(s)**
Political	(1) Uncertainties in Regulatory Frameworks	Hassan et al. (2024)	Regulatory uncertainties in low-emission hydrogen production technologies, such as the non-standardization of approval processes and incompatibility of technical standards, may restrict the sector's development.
	(2) Lack of subsidy and incentive mechanisms	Kokkinos et al. (2023); Yetiskin et al. (2023)	The lack of policies and regulations for low-emission hydrogen production and the deployment of Carbon Capture, Storage, and Utilization (CCSU) technologies cannot steer industry players in a particular direction. Government incentives and policies influence the adoption of hydrogen technologies.
	(3) Lack of a carbon pricing mechanism	Esmaeili (2018); Gür (2022)	Having an emissions trading market is critical for the successful implementation of the carbon-capturing technology in Türkiye
Economical	(4) High Investment Cost	Zainal et al. (2024); de Anrade (2024); Aysun & Kabukcuoglu (2019); Shirmohammad et al. (2020)	Low-emission hydrogen production and CCSU technologies are generally costly. Economic factors can affect hydrogen's competitive advantage and economic sustainability.
	(5) Uncertainty on system cost of electrolysis in the future	Fazeli et al. (2022)	The system cost of an electrolyzer represents all expenses related to establishing and operating an electrolysis facility to produce hydrogen (CAPEX, costs of auxiliary components, installation, operation, and maintenance).
	(6) Incomplete options to hedge against risks	Côté & Salm (2022)	Due to limited risk management options, companies operating in the sector may be less resilient to financial uncertainties, which may negatively affect investments and growth in the sector.
	(7) Lack of skilled labor	Beasy et al. (2023)	Developing a workforce to support a hydrogen economy depends upon education and training availability. Industry stakeholders and their engagement in the hydrogen sector are enablers that can (and should) be utilized to advance fit-for-purpose and responsive education and training.
Social	(8) Lack of Public Acceptance due to conflicting interests over resources	Agyekum et al. (2022); Kokkinos et al. (2023); Rasul et al. (2022)	The public's lack of knowledge about the advantages and disadvantages of hydrogen as clean energy limits the technology's acceptance, and society's reaction to this technology impacts the industry.
	(9) Lack of trust in the rule of law	Ashari et al. (2024)	Protection of intellectual property rights and fear of favoritism
Technological	(10) Lack of Infrastructure	Ishaq, Dincer & Crawford (2022)	The need for appropriate infrastructure for storing, transporting, and distributing hydrogen limits the growth of the hydrogen economy. This infrastructure needs to be developed and expanded.
	(11) Supply chain uncertainties	Olabi et al. (2024)	Uncertainties in the supply chain concerning the accessibility, dependability, and efficiency of these technologies can have a substantial impact on the scalability, cost-efficiency, and viability of low-emission hydrogen initiatives. For instance, setbacks or interruptions in providing essential components or materials required for producing electrolyzers could impede the implementation of low-emission hydrogen infrastructure.
	(12) Low technology readiness level	Chelvam et al. (2024)	Since the technologies used in low-emission hydrogen production and CCSU have not yet been proven and fully accepted, the areas of preference for these technologies are limited.

Environmental	(13) Water scarcity	Mehmeti et al., (2018); Zainal et al. (2024)	In low-emission hydrogen production technologies, some production methods can increase water consumption, put pressure on water resources, and contribute to local water scarcity problems. This highlights the need to develop and adopt water-efficient and sustainable production methods, which could otherwise negatively impact the sustainability of water resources and the water needs of communities.
Legal	(14) Uncertain and lengthy patenting and licensing processes	Li & Zheng (2024); Agyekum et al. (2024)	Long waiting times experienced by developers in the licensing process, dealing with complex regulations, and uncertainties in obtaining permits are among the main challenges that prevent the progress of hydrogen projects.
	(15) Lack of harmonized international standards and cross-border environmental regulations	Agyekum et al. (2022)	The absence of common standards and regulations hinders the diffusion of hydrogen, which restrains its potential. Formulating a common international framework is critical to preventing unfair competition and free-riding

Fuzzy DEMATEL Method

The fuzzy DEMATEL (Decision Making Trial and Evaluation Laboratory) method is an analysis method used in complex decision-making processes (Büyüközkan et al., 2024) and can be applied especially in complex and uncertain systems (Ghasemian Sahebi et al., 2024). This method adopts the basic principles of DEMATEL, but uses fuzzy logic to handle uncertainties, where clear boundaries are blurred or unclear (Singh et al., 2024).

Table 2 summarizes each methodological step for the combined analysis of PESTEL with fuzzy DEMANTEL. After determining challenges in the context of pillars of PESTEL analysis (Step 1), these challenges are reviewed for accuracy by a group of academics and industry experts (Step 2). Experts anticipate weighing these challenges with pairwise comparisons amid information collection. After that, fuzzy DEMATEL is applied to determine the causal relationship between these challenges (Step 3-7).

Table 2. Summary of methodological steps

Steps	Explanation
1	Criteria set is determined
2	Expert opinions are collected on a linguistic scale
3	The Fuzzy Direct Relationship Matrix is defined.
4	The Normalised Fuzzy Direct Relationship Matrix (X)
5	Fuzzy Total Relationship Matrix (T)
6	Defuzzification with CFCS
7	The relation (D-R) and prominence value (D+R)

RESULTS AND DISCUSSION

The casual diagram down below shows casual relationship between challenges determined previously. The challenges (see Table 1) (C1, C2, C4, C6, C8, C12, C13 and C15) above the y-axis are in the cause group. The factors below the y-axis (C3, C5, C7, C10, C11, C14) are in the effect group, meaning they are affected by other factors. The location of each factor on the horizontal and vertical axes allows us to determine how much it affects and is affected in the system.

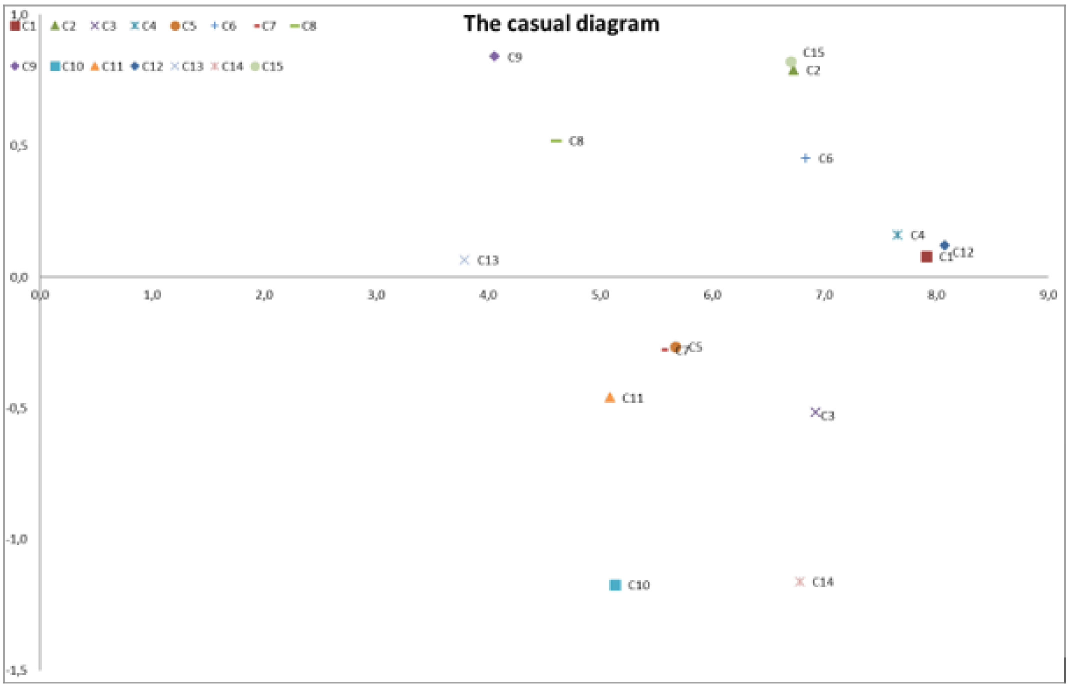

Figure 1. The casual diagram

The fuzzy DEMATEL analysis identified Low Technology Readiness Level (C12), Uncertainties in Regulatory Frameworks (C1), and High Investment Cost (C4) as key dual-role factors that both influence and are influenced by other elements in the system. These are the main drivers triggering system-wide changes and thus require priority attention in policy and investment decisions. Lack of subsidy and incentive mechanisms (C2) and Lack of harmonised international standards (C15) emerged as strong cause factors influencing other variables, though to a lesser extent than C1, C4, and C12. Incomplete options to hedge risks (C6) and Lack of public acceptance (C8) showed moderate influence and dependency, indicating a more limited systemic role. Lack of trust in rule of law (C9) and Water scarcity (C13) were weakly connected, suggesting minimal systemic impact.

In the effect group, Lack of infrastructure (C10) and Uncertain and lengthy patenting and licensing processes (C14) were strongly affected by other factors, representing major result variables. Meanwhile, Lack of a carbon pricing mechanism (C3), Lack of skilled labour (C7), Uncertainty about future electrolysis costs (C5), and Supply chain uncertainties (C11) occupied intermediate positions, acting as balancing factors within the system.

The results highlight that improving technological readiness, reducing regulatory uncertainties, and addressing high investment costs are critical levers for advancing low-emission hydrogen production. Targeted policy instruments such as consistent regulations, financial incentives, and international standards could amplify positive systemic change. Additionally, strengthening infrastructure and patenting frameworks should be viewed as downstream outcomes of progress in these core areas.

CONCLUSION

This study demonstrates that the development of low-emission hydrogen production technologies in Türkiye is constrained by a tightly coupled set of challenges, with technological readiness, regulatory certainty, and investment costs at the center of the causal structure. Strengthening these core areas through stable and transparent regulation, targeted subsidy and incentive schemes, and clearer carbon pricing signals would not only reduce perceived risks but also unlock progress on downstream outcomes such as infrastructure build-out and more efficient patenting and licensing processes. The prominence of international standards and cross-border regulations underscores that Türkiye's hydrogen strategy must be aligned with evolving global rules, including mechanisms such as CBAM, to safeguard competitiveness in export-oriented industries. Policymakers should therefore prioritize an integrated policy package that simultaneously advances technology maturity, de-risks investment, and harmonizes legal frameworks, thereby enabling the country to leverage its renewable potential and play a stronger role in the global green hydrogen value chain.

REFERENCES

Due to lack of available space, the reference list will be provided upon request.

EXPERIMENTAL ASSESSMENT OF TITANIA AND FERRIC OXIDE-BASED CATALYSTS FOR PHOTOCATALYTIC HYDROGEN PRODUCTION

Mohamad Ayoub[1], Ibrahim Dincer[1]*
[1]Clean Energy Research Laboratory (CERL), Faculty of Engineering and Applied Science, Ontario Tech. University, 2000 Simcoe Street North, Oshawa, Ontario L1G 0C5, Canada
*Corresponding author e-mail: mohamad.ayoub@ontariotechu.net
Ref # HES-03

ABSTRACT
In this work, transition metal oxide-based photocatalysts are utilized for photocatalytic hydrogen production assessment, namely Titania, Ferric Oxide, and a mixture between Titania and Ferric Oxide. For the mixed photocatalyst case, the mass ratio of Titania to Ferric Oxide is maintained at 1:1. The results indicate that ferric oxide achieves a hydrogen concentration of 9 ppm, while titania reaches 14 ppm, corresponding to a 55% enhancement. The mixture of Titania and Ferric Oxide demonstrates a higher performance with a hydrogen concentration of 16 ppm, representing a 14% enhancement over sole Titania and 77% over Ferric Oxide. The highest energy efficiency achieved is 0.169%, which is attributed to the mixture of Titania and Ferric Oxide.

Keywords: Hydrogen; Hydrogen production; Photocatalyst; Solar Energy

INTRODUCTION
Photocatalytic hydrogen production relies on the utilization of photoactive materials that can initiate water splitting reactions upon contact with an electrolyte. A fundamental requirement for these materials is that their conduction band level must be higher than the standard hydrogen potential. In other words, not all photoactive materials are able to perform photocatalytic hydrogen production or water splitting reactions [1]. After electrons are excited to the conduction band, they participate in the water splitting reactions. Conventionally, sacrificial agents (SA), or hole scavengers, are employed to prevent electron-hole recombination events by donating electrons to replace excited ones.

The use of precious metal catalysts significantly increases system cost and hinders commercialization [2], which places transition metal oxide–based catalysts in a favourable spot. Transition metal oxides are abundant, have lower costs, and bear tunable bandgaps. vIn this work, transition metal oxide-based photocatalysts are utilized for photocatalytic hydrogen production assessment, namely Titania, Ferric Oxide, and a mixture between Titania and Ferric Oxide. The performance of these photocatalysts is assessed through their hydrogen production concentration in a batch process.

MATERIALS AND METHODS
For this work various materials are used for the photocatalytic hydrogen production assessment. Potassium Hydroxide (KOH) (ACS reagent ≥ 85 % pellets, Sigma Aldrich) is used to make up the electrolyte. Triethanolamine (TEOA) (Reagent grade 98 %, Sigma Aldrich) is used as a Sacrificial Agent (SA), Titanium (IV) oxide (TiO_2) (21 nm primary particle size, ≥ 99.5 % trace metal basis, Sigma-Aldrich) and Iron (III) Oxide (Ferric Oxide) (powder $<5\mu m, \geq 99\%$, Sigma-Aldrich) are used as photocatalysts. The experimental setup used in this work is shown in Fig. 1. OAI TriSOL solar simulator is used as a light source with an intensity of 700 W/m^2, DFRobot hydrogen sensor is used to measure the hydrogen concentration throughout the batch process assessment, and the solutions used for the photocatalytic hydrogen assessment are made up of 0.1 M of KOH, 1 M of TEOA, and 15 mg/100 ml of photocatalyst. For the case of the Titania-Ferric Oxide photocatalyst, the mass ratio is set as 1:1.

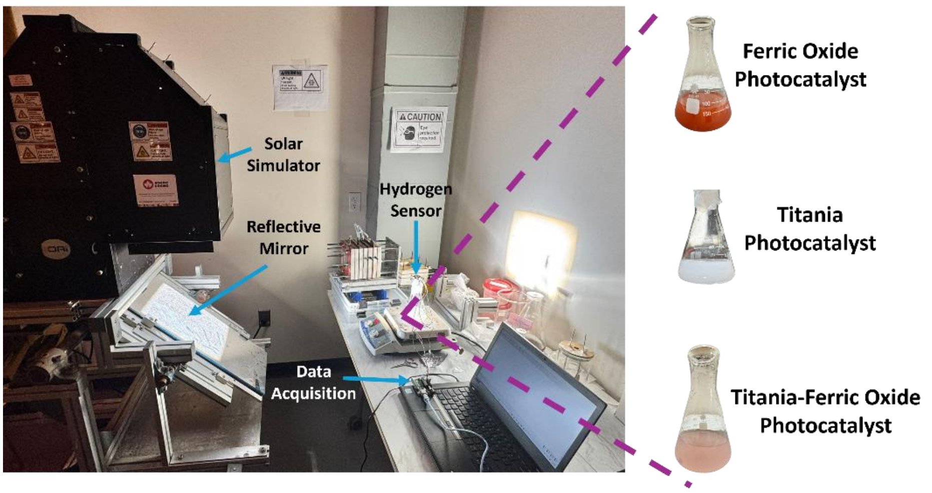

Fig. 1. The experimental setup used for the photocatalytic hydrogen production assessment

RESULTS AND DISCUSSION
The results of this work are represented by the hydrogen concentration (in ppm) throughout the batch process, which is set at 30 minutes, as well as the energy efficiency of the photocatalytic hydrogen generation, and are shown in

Fig. 2. The hydrogen concentration results are shown in Fig. 2. (a) where the Ferric Oxide photocatalyst achieves a hydrogen gas concentration of 9 ppm within the headspace of the reaction flask. The titania catalyst on the other hand shows a superior performance with respect to that of Ferric Oxide at 14 ppm, which is a 55% enhancement. Titania has a much higher bandgap than Ferric Oxide, meaning that it absorbs photons that bear higher energy, which leads to a noticeable difference in the hydrogen production, although sacrificing excitation events that would happen due to the lower-energy photons within the incident spectrum. The third permutation being a mixture of Titania and Ferric Oxide with a mass ratio of 1:1, the hydrogen concentration achieved within the same period of time is set at 16 ppm, which is a 14% enhancement over the sole Titania and 77% over Ferric Oxide. This mixture allows both catalysts to operate in a complimentary manner, where the Ferric Oxide absorbs the lower-energy photons, and the Titania absorbs the higher-energy photons, benefiting from both extremities of the incident spectrum. The highest energy efficiency achieved is attributed to the mixture of Titania and Ferric Oxide at 0.169%, which is shown in Fig. 2. (b).

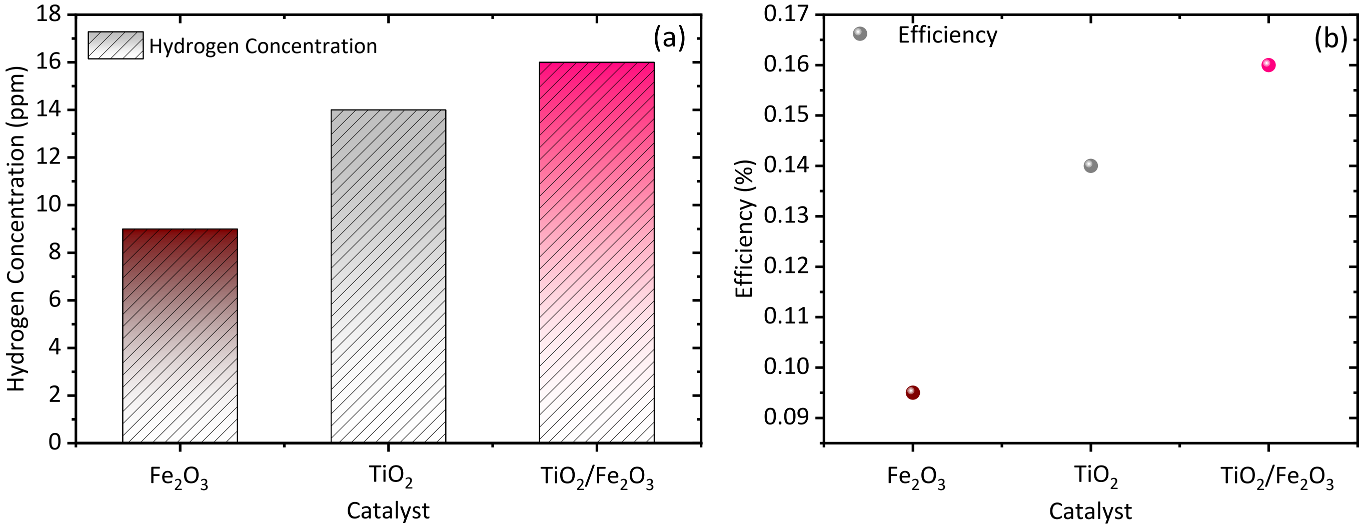

Fig. 2. The photocatalytic hydrogen production results for the different photocatalysts (a) concentration in ppm and (b) energy efficiency

CONCLUSIONS

Three transition metal oxide-based photocatalysts are used for photocatalytic hydrogen production assessment. The photocatalysts consist of Titania, Ferric Oxide, or a mixture of both. The hydrogen production assessment is conducted through a batch process which uses TEOA as a sacrificial agent along with the aforementioned photocatalysts.

- The mixture of Titania and Ferric Oxide achieved the highest hydrogen concentration at 16 ppm within 30 minutes.
- Titania showed a 55% enhancement in hydrogen concentration compared to Ferric Oxide.
- The highest energy efficiency of 0.169% is obtained using the Titania–Ferric Oxide mixture.

REFERENCES

[1] M. Ayoub and I. Dincer, “Experimental evaluation of photocatalytic and photoelectrochemical hydrogen fuel production with metal-based catalysts, electrodes and coatings in a novel manner,” Fuel, vol. 406, p. 136722, Feb. 2026, doi: 10.1016/j.fuel.2025.136722.

[2] A. M. M. I. Qureshy and I. Dincer, “Development of a new solar photoelectrochemical reactor design for more efficient hydrogen production,” Energy Convers. Manag., vol. 228, p. 113714, Jan. 2021, doi: 10.1016/j.enconman.2020.113714.

GREEN BIOELECTROLYTE DERIVED FROM TEA WASTE FOR HYDROGEN PRODUCTION USING ACIDIC WATER ELECTROLYSIS

A.Yagmur Goren[1,2], Ibrahim Dincer[2]*
[1] Clean Energy Technologies Institute, Yıldız Technical University, İstanbul, Turkiye
[2] Clean Energy Research Laboratory, Faculty of Engineering and Applied Science, OntarioTech University, Ontario, Canada
*Corresponding author e-mail: ayagmur.goren@yildiz.edu.tr; Aysegul.Kara@ontariotechu.ca

Ref # HES-04

ABSTRACT
Investigations for efficient and clean energy sources have accelerated as a result of the shift to sustainable energy systems, and hydrogen (H_2) is considered a promising energy carrier due to its high energy density and zero carbon emissions. Water electrolysis is one of the most reliable manufacturing methods for producing high-purity H_2, especially when combined with renewable energy sources. However, purified water and synthetic electrolytes are usually needed for electrolysis operations, which raises operating costs and restricts the sustainability of large-scale applications. As a result, designing substitute electrolyte systems using inexpensive, renewable resources has emerged as a key area of research. In this regard, an acid-assisted extraction method was used for producing a bioelectrolyte obtained from tea waste, and its potential to produce H_2 by electrolysis was evaluated in this study. The 1 M bioelectrolyte achieved a current density of about 280 mA/cm^2 at 0.75 V using carbon-based electrodes, and this is much higher than the 60 mA/cm^2 obtained with 1 M KOH. Overall, these findings show that bioelectrolyte formed from tea waste can both increase electrochemical activity and facilitate waste valorization. Consequently, the suggested strategy offers an appealing path for economical and sustainable H_2 production in electrolysis processes.

Keywords: Bioelectrolyte, Tea waste, Hydrogen production, Waste management, Sustainability

INTRODUCTION
The investigations for alternative energy sources that can replace fossil fuels while reducing their negative effects on the environment have accelerated due to the growing demand for clean, sustainable energy on a worldwide scale. Because of its high energy density and ability to produce only water as a by-product during consumption, hydrogen (H_2) has attracted substantial interest among the many alternatives [1]. Consequently, H_2 is thought to be a suitable energy source for emerging low-carbon energy systems. For instance, steam reforming, thermochemical conversion, biological processes, and electrochemical water splitting are some of the methods that can be used to produce H_2. Since it can produce high-purity H_2 and be combined with renewable energy sources, water electrolysis is regarded as the most attractive technology. However, the large-scale application of conventional electrolysis systems may be limited by their reliance on high-purity water and carefully regulated electrolyte solutions, particularly in areas where water is scarce [2].
Moreover, researchers are now investigating other electrolyte sources, such as wastewater and industrial effluents, due to the growing demand for freshwater resources. Recent research has shown that many kinds of low-grade water, including treated wastewater, can be used directly in electrolysis systems to produce H_2 while also supporting water reuse processes [3]. Nevertheless, enormous amounts of acidic wastewater, including strong acids like sulfuric acid (H_2SO_4) are produced by numerous industrial operations, including metal processing, chemical manufacture, and mineral processing. Before being discharged, these acidic effluents are usually neutralized with alkaline chemicals, a procedure that produces a lot of sludge and enhances treatment expenses. As a result, managing acidic industrial effluent is still difficult from a sustainability point of view.

Namely, recent studies have started to examine the potential of these wastewater streams as useful resources within circular economy frameworks, rather than only regarding them as contaminants. Specifically, conductive media appropriate for electrochemical operations can be obtained from acidic waste streams, which may lessen the demand for artificial electrolytes [4]. Simultaneously, the use of materials produced from biomass in electrochemical systems received greater interest because of their affordability, sustainability, and availability. Biomass can be converted into electrolyte components or functional electrochemical compounds that can improve electrolysis efficiency [5]. For instance, lignocellulosic materials are processed in acidic solutions to promote H_2 production during electrochemical conversion in biomass-assisted electrolysis systems that have been studied.
However, there are still several significant gaps in the existing literature despite these significant advancements. The direct use of biomass-derived electrolytes produced from actual waste materials is still relatively unexplored, with the majority of current research concentrating on the use of purified electrolytes or model organic molecules. Furthermore, rather than using biomass as a source of soluble electroactive species within the electrolyte, most investigations on biomass-assisted electrolysis focus on using biomass as a solid feedstock or electrode precursor. In order to address waste management issues and reduce dependency on traditional synthetic electrolytes, more research is required to determine whether it is feasible to produce conductive and electrochemically active bioelectrolytes through the interaction of acidic media with abundant organic wastes.
Therefore, tea waste was used in this work as a biomass resource to produce a biomass-derived bioelectrolyte. In particular, a hydrolysate rich in soluble organic and ionic species was produced by digesting tea waste in H_2SO_4 solution, and this filtrate was then used as the electrolyte solution in the electrolysis system. The electrocatalytic

performance of the produced bioelectrolyte was thoroughly examined under various electrolyte molarities to assess the electrochemical potential of this strategy. Additionally, the impact of electrode material on hydrogen evolution reaction (HER) performance was investigated using two widely used conductive substrates: graphite paper and carbon Toray paper electrodes. The obtained results showed that the hydrolysate formed from biomass can be used as an alternative acidic electrolyte medium and has promising potential for producing H_2 sustainably while contributing to the value of organic waste streams.

MATERIALS AND METHODS

In this section, the synthesis procedure of the tea waste-derived bioelectrolyte is reported in more detail. Moreover, the analysis of the electrocatalytic performance of the bioelectrolytes is discussed. In this study, tea waste samples were utilized as feedstock, and the biochar suspensions were produced using a 3.7 M H_2SO_4 solution as the solvent (Fig.1). The acid solution was gradually supplemented with the crushed waste materials until a final concentration of 37 g/L was reached. To promote the oxidation and decomposition of the tea waste biomass, the resultant mixture was kept at 60 °C for 2 h. To guarantee sufficient mixing, the suspension was continuously stirring during this period. The color of the mixture progressively became darker as the reaction proceeded on, eventually becoming a uniform black sludge. Then, the solid fraction was separated from the suspension by filtering it through coarse filter after the process. Following that, the bioelectrolyte product was collected and kept for subsequent use in a glass container.

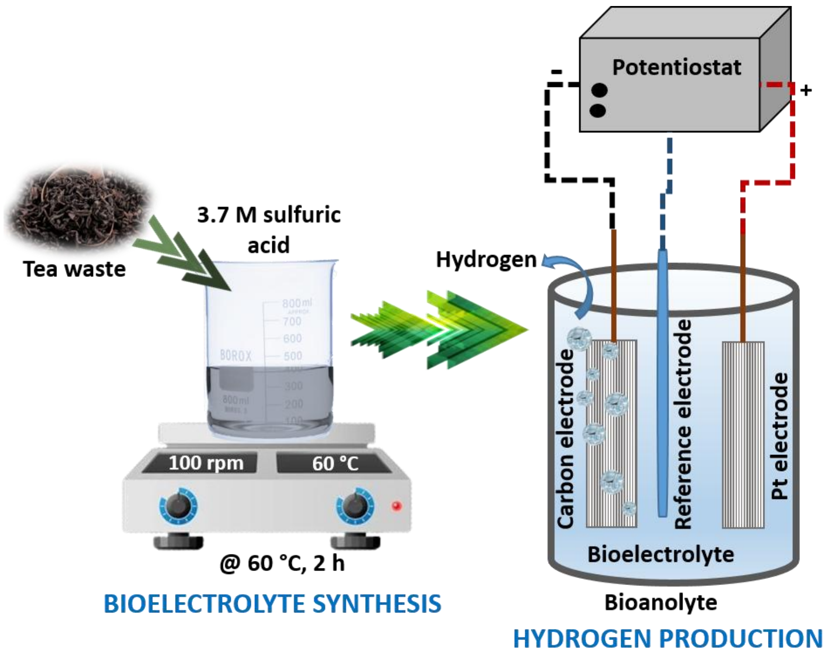

Fig. 1. Schematic illustration of the bioelectrolyte production and electrochemical analysis set-up.

A Gamry-3000 potentiostat/galvanostat in a three-electrode cell is used to assess the electrocatalytic performance of the produced bioelectrolyte. The reference electrode in this cell was an Ag/AgCl electrode, the working electrode was the carbon Toray paper and graphite paper electrodes, and the counter electrode was a platinum mesh in various bioelectrolytes (0.5 and 1 M) and 1 M KOH electrolyte solutions. The oxygen evolution reaction (OER) and HER performance of the proposed electrolyte solutions were evaluated using linear sweep voltammetry (LSV) at a scan rate of 10 mV/s in the potential value range of 0-1.4V and -1.2 to -0.6, respectively. Moreover, cyclic voltammetry (CV) is also carried out at different scan rates (10 to 100 mV/s) in the potential window of -0.2 to 0.8 to assess the cyclic stability of the electrolytes and better comprehend the behavior of electrochemistry. The Nernst equation, ERHE = ESCE + 0.059×pH (where ESCE = +0.241 V and pH 14), was then used to convert the observed potentials to the reversible hydrogen electrode (RHE) scale [6].

RESULTS AND DISCUSSION

The electrochemical performance of the carbon paper electrode was evaluated in different electrolyte environments, including KOH and tea waste-derived bioelectrolytes at concentrations of 0.5 M and 1 M. As presented in the polarization curves (Fig. 2a and 2b), the current density increased significantly with increasing electrolyte concentration for both electrodes. The highest current density was obtained in the 1 M tea waste-based bioelectrolyte, reaching almost 270–280 mA/cm^2 at 0.75 V. In comparison, the 1 M KOH electrolyte exhibited a considerably lower current density of 60 mA/cm^2 at the same potential. Moreover, at lower concentration, the 0.5 M bioelectrolyte produced almost 25 mA/cm^2, whereas 0.5 M KOH generated only 15 mA/cm^2 of current density.

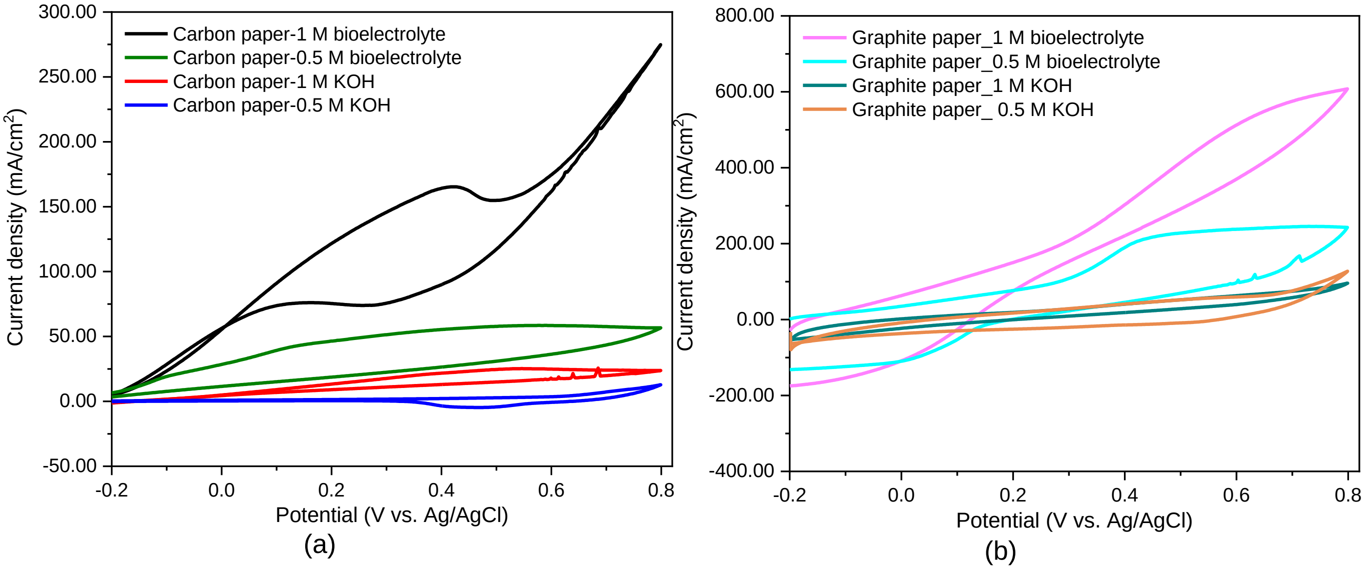

Fig. 2. The CV results of the bioelectrolytes using (a) a carbon paper electrode and (b) a graphite paper electrode.

CONCLUSIONS

In this study, an acid-assisted extraction method was effectively used to produce a tea waste-derived bioelectrolyte, which was then assessed for electrochemical H_2 production. According to the electrochemical measurement, the bioelectrolyte greatly increased the current density when compared to the traditional KOH electrolyte. The 1 M bioelectrolyte produced approximately 270-280 mA/cm^2 at 0.75 V, whereas 1 M KOH only produced roughly 60 mA/cm^2 under similar conditions. The presence of electroactive organic compounds made from tea waste and the high proton availability in the acidic medium play a role in the enhanced performance. The results of this study suggest that bioelectrolytes produced from biomass can efficiently increase electrochemical activity while also facilitating waste valorization. Overall, the suggested method is a viable and sustainable approach to producing substitute electrolytes for environmentally friendly H_2 production systems.

REFERENCES

1) Dincer I. 2023. Hydrogen 1.0: A new age. International Journal of Hydrogen Energy 48:16143-16147.
2) Jiao S, Fu X, Wang S, Zhao Y. 2021. Perfecting electrocatalysts via imperfections: towards the large-scale deployment of water electrolysis technology. Energy Environmental Science 14:1722-1770.
3) Devda V, Chaudhary K, Varjani S, Pathak B, Patel AK, Singhania RR, Taherzadeh MJ, Ngo HH, Wong JWC, Guo W. 2021. Recovery of resources from industrial wastewater employing electrochemical technologies: status, advancements and perspectives. Bioengineered 12:4697-4718.
4) Jin W, and Zhang Y. 2020. Sustainable electrochemical extraction of metal resources from waste streams: from removal to recovery. ACS Sustainable Chemical Engineering 8:4693-4707.
5) Xu G, Chen X, Xu W, Shi Q, Lu Y, Liu W. 2026. Lignocellulosic biomass in electrochemical energy conversion and value-added chemicals production. Green Chemistry DOI: 10.1039/D5GC06399J.
6) Bhabal R, Bhide A, Gupta S, Fernandes R, Patel N. 2024. Maximizing bifunctionality for overall water splitting by integrating H2 spillover and oxygen vacancies in CoPBO/Co_3O_4 composite catalyst. Small Science 4:2400343.

AN INTEGRATED HYDROGEN PRODUCTION AND ENERGY RECOVERY SYSTEM FOR WASTEWATER TREATMENT PLANTS

Ahmet Faruk Kilicaslan[1*], Ibrahim Dincer[1]
[1] CERL, FEAS, Ontario Tech. University, 2000 Simcoe Street North, Oshawa, Ontario L1G 0C5, Canada
*Corresponding author: ahmet.kilicaslan@ontariotechu.net

REF # HES-05

ABSTRACT
This study proposes a novel integrated energy system for wastewater treatment plants to simultaneously produce electricity, hydrogen, and useful heat. The proposed configuration integrates dark fermentation, sludge incineration, a Brayton cycle gas turbine, an integrated bioelectrochemical reactor composed of microbial fuel cells, microbial electrolysis cells, and photoelectrochemical units, together with an alkaline electrolyzer. In this paper, parametric analysis is performed to investigate the effects of effluent biochemical oxygen demand and dissolved oxygen concentration on the oxygen transfer requirement of the aeration process under different wastewater strength conditions. The results show that increasing effluent biochemical oxygen demand from 15 to 30 mg/L reduces the oxygen transfer rate from about 30.73 to 26.49 kg/h. In contrast, increasing the dissolved oxygen concentration from 2 to 4 mg/L increases the oxygen transfer requirement from 29.36 to 39.90 kg/h.

Keywords: Wastewater treatment, Hydrogen, Energy, Exergy, Efficiency

INTRODUCTION
Wastewater treatment plants (WWTPs) play a critical role in protecting water resources and public health. However, conventional WWTPs are highly energy intensive facilities due to the substantial electricity demand associated with biological treatment and aeration processes. Improving the energy performance of these systems and recovering useful resources from wastewater streams therefore becomes an important research focus [1]. Wastewater contains significant amounts of organic matter that can be utilized as a potential energy source. Various technologies, including anaerobic digestion, thermochemical conversion, and bioelectrochemical systems, are widely investigated to recover energy from wastewater treatment processes [2]. Among these approaches, hydrogen (H_2) production from wastewater attracts increasing attention due to its potential as a clean and sustainable energy carrier.

Several studies investigate H_2 production using microbial electrolysis cells (MEC), microbial fuel cells (MFC), and dark fermentation (DF) systems. These technologies enable the conversion of organic matter present in wastewater and sludge into H_2 and electricity through biological and electrochemical pathways. However, most existing studies focus on individual technologies, while integrated systems that combine multiple H_2 production pathways within wastewater treatment facilities remain limited [3]. Therefore, this study proposes an integrated energy system for wastewater treatment plants that enables simultaneous wastewater treatment, H_2 production, and energy recovery.

In this study, a parametric analysis investigates the effects of effluent biochemical oxygen demand (BOD) and dissolved oxygen (DO) concentration on the standard oxygen transfer rate (SOTR) of the aeration process. These parameters directly influence the oxygen transfer requirement and significantly affect the energy demand of biological treatment units. The present study therefore focuses on aeration-related operational parameters, while future work evaluates the integrated configuration through a comprehensive thermodynamic assessment, including detailed energy and exergy analyses to evaluate the overall system inputs, outputs, and energy recovery potential.

SYSTEM DESCRIPTION
This study proposes a novel integrated energy system for WWTPs to simultaneously produce electricity, H_2 and useful heat while improving the overall energy performance of the facility. The main objective is to enhance energy recovery from wastewater streams and reduce the dependency of WWTPs on external electricity supply. In addition, the proposed configuration aims to transform conventional wastewater treatment plants into H_2 producing facilities.

Figure 1 illustrates the schematic diagram of the proposed integrated system. The configuration integrates DF, sludge incineration, a Brayton cycle gas turbine, an integrated bioelectrochemical reactor, and an alkaline electrolyzer for simultaneous electricity and H_2 production. Through the integration of thermochemical and bioelectrochemical pathways, the system enables efficient utilization of wastewater derived resources and allows simultaneous energy recovery, H_2 production, and wastewater treatment within a single platform.

A conventional wastewater treatment plant includes primary, secondary, and tertiary treatment stages to remove solids, organic matter, and pathogens. In the proposed system, raw sludge collected from the primary clarification unit is directed to the DF reactor. Due to its high organic content, raw sludge serves as a suitable substrate for biological H_2 production under anaerobic conditions.

The H_2 rich gas produced in the DF unit is then sent to a gas separation unit for purification. Meanwhile, waste activated sludge from the secondary clarification unit is supplied to the integrated bioelectrochemical reactor.

The integrated reactor consists of MFC, MEC, and PEC units operating in an integrated configuration. The MFC unit generates electricity through the oxidation of organic matter present in wastewater. The electricity generated in the MFC is supplied to the MEC unit to support H_2 production, while the remaining electrical demand of the MEC system is provided by the gas turbine power cycle. The PEC unit utilizes solar irradiation to further enhance hydrogen generation.

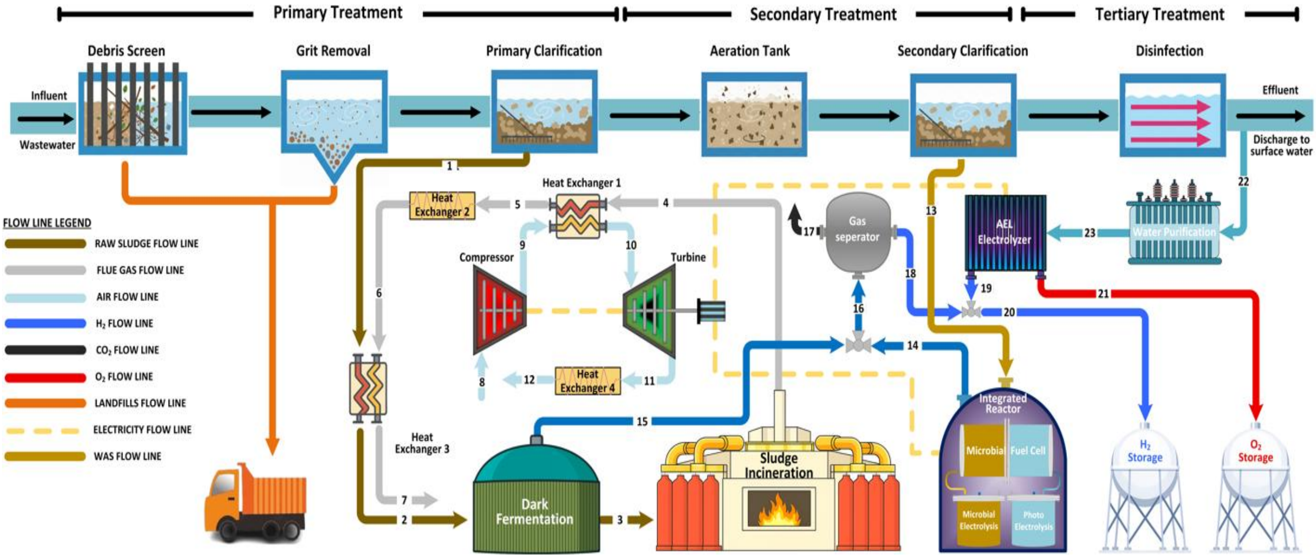

Figure 1. Schematic representation of the proposed integrated energy system.

In addition to the bioelectrochemical pathway, sludge incineration is used to recover thermal energy from sludge residues. The flue gases generated during sludge incineration drive a Brayton cycle gas turbine system to produce electricity. The generated power is partially used to support the electrochemical processes within the system. An alkaline electrolyzer is also incorporated in the proposed configuration to produce additional H_2 and oxygen (O_2). The generated O_2 by the electrolyzer can be utilized within the wastewater treatment process to partially satisfy the aeration demand.

MODELING AND ANALYSIS

The O_2 demand of the activated sludge process is evaluated based on organic matter removal and biomass production. The modelling framework used in this study for estimating biomass production, O_2 transfer requirement, and standard oxygen transfer rate is based on the approach reported in [4].

The biomass production during biological treatment is calculated as follows,

$$VSS_5 = Q \cdot Y_{obs} \cdot (BOD_{in} - S) \tag{1}$$

The O_2 transfer requirement associated with organic removal and biomass growth is expressed as follows,

$$OTR_f = \frac{Q(S_0 - S)}{BOD_5/BOD_L} - 1.42VSS_5 \tag{2}$$

where OTR_f represents the oxygen transfer requirement, S_0 and S denote influent and effluent soluble BOD concentrations, and BOD_5/BOD_L is the ratio of five-day BOD to ultimate BOD.

Finally, the SOTR is calculated using aeration system parameters:

$$SOTR = \frac{OTR_f}{\alpha F\left[\frac{C^*_{\infty 20}}{\beta}\left(\frac{C_{st}}{C^*_{s20}}\right)\left(\frac{P_b}{P_s}\right) - C\right](1.024)^{(20-T)}} \tag{3}$$

where α, β, and F are aeration correction factors, C is the DO concentration in the aeration basin, and T is the operating temperature.

RESULTS AND DISCUSSION

Figure 2 presents the variation of SOTR with respect to effluent BOD and DO concentrations under different influent wastewater strengths. In this study, influent wastewater strengths of 110, 190, and 350 mg/l are considered to represent low, medium, and high loading conditions typically observed in municipal wastewater treatment plants. Moreover, the effluent BOD range of 15-30 mg/l is selected to show common discharge limits and operational conditions in biological treatment systems. Similarly, the DO range of 2-4 mg/l is investigated since it corresponds to the typical operating range used in aeration basins to maintain stable biological activity.

Figure 2a shows that SOTR slightly decreases as the effluent BOD increases from 15 to 30 mg/L for all wastewater strengths. Over this range, SOTR decreases from 30.73 to 26.49 kg/h for the low strength, from 53.32 to 49.08 kg/h for the medium strength, and from 98.51 to 94.27 kg/h for the high strength. This behavior occurs because higher effluent BOD indicates lower organic removal during treatment, which reduces the O_2 demand of the biological process.

Figure 2(b) illustrates the effect of DO concentration on SOTR. As the DO level increases from 2 to 4 mg/L, the required SOTR increases for all wastewater strengths. Specifically, SOTR rises from 29.36 to 39.90 kg/h for the low strength, from 51.98 to 70.65 kg/h for the medium strength, and from 97.23 to 132.15 kg/h for the high strength.

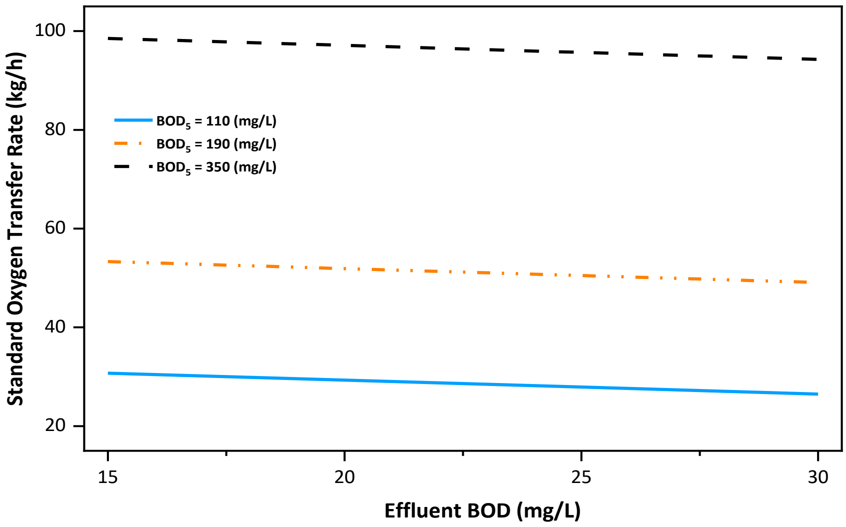

(a)

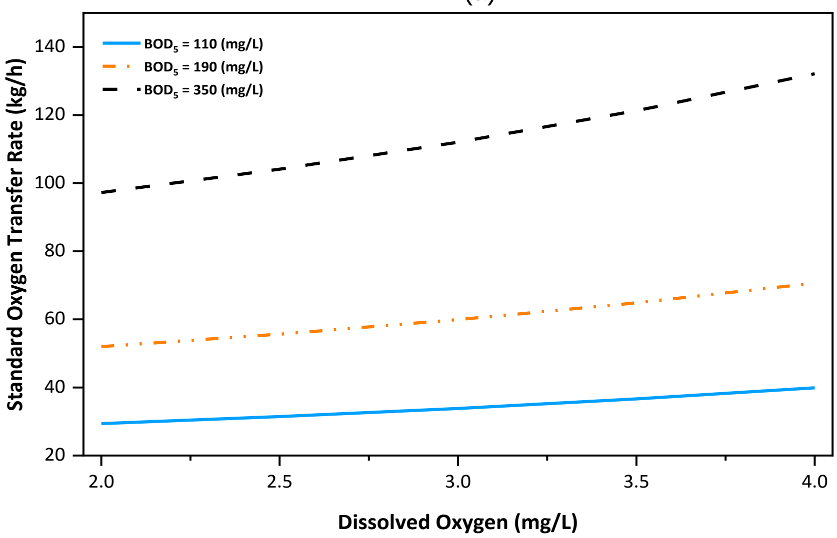

(b)

Figure 2. Variation of SOTR with (a) BOD_e and (b) dissolved oxygen under different influent BOD_5 conditions.

CONCLUSIONS

This study evaluates the influence of effluent BOD and DO levels on the SOTR under low, medium, and high wastewater strength conditions. The results show that increasing effluent BOD from 15 to 30 mg/L reduces SOTR from 30.73 to 26.49 kg/h, 53.32 to 49.08 kg/h, and 98.51 to 94.27 kg/h for low, medium, and high strength wastewater, respectively. In contrast, increasing the DO level from 2 to 4 mg/L increases SOTR from 29.36 to 39.90 kg/h, 51.98 to 70.65 kg/h, and 97.23 to 132.15 kg/h for the same conditions.

Future work will focus on a comprehensive energy and exergy analysis of the proposed integrated system. The overall system inputs and outputs will be evaluated to determine the energy recovery potential and overall system performance.

REFERENCES

1. Qambar AS and Al Khalidy MM. 2022. Optimizing dissolved oxygen requirement and energy consumption in wastewater treatment plant aeration tanks using machine learning. Journal of Water Process Engineering 50:103237.
2. Walczak J, Karolinczak B and Zubrowska-Sudol M. 2023. Effect of co-digestion and hydrodynamic disintegration on the methane potential of sewage sludge and organic fraction of municipal solid waste with consideration of the carbon footprint. Energy 282:128949.
3. Ebrahimi A and Houshfar E. 2022. Thermodynamic analysis and optimization of the integrated system of pyrolysis and anaerobic digestion. Process Safety and Environmental Protection 164:582-594.
4. Metcalf W and Eddy C. 2003. Wastewater Engineering: Treatment and Resource Recovery. New York, McGraw-Hill.

INVESTIGATION OF HYDROGEN PRODUCTION AND SODIUM HYPOCHLORITE FORMATION IN A GRANULAR ACTIVATED CARBON-BASED NaCl ELECTROLYSIS SYSTEM

Sevde Elmali[1], Ibrahim Dincer[1]*
[1]*Clean Energy Research Laboratory (CERL), Faculty of Engineering and Applied Science, Ontario Tech. University, 2000 Simcoe St. North, Oshawa, Ontario L1G 0C5, Canada*
[*]Corresponding author e-mail: sevde.elmali@ontariotechu.net

Ref # HES-06

ABSTRACT
In this study, the effect of applied voltage on hydrogen production and NaOCl formation during the electrolysis of a 0.5 M NaCl solution was experimentally investigated. A two-chambered closed electrolysis cell with granular activated carbon electrodes was used in the experiments. Hydrogen production results showed that the system performed fastest at 3.5 V, achieving higher hydrogen production in a shorter time. NaOCl analysis revealed that the highest formation was obtained at 2.2 V, and the amount of NaOCl decreased significantly as the voltage increased. The findings showed that the applied voltage directly affects product distribution; high voltages support hydrogen production, while low voltages are more favorable for NaOCl formation. In conclusion, it was determined that the operating voltage in activated carbon-based NaCl electrolysis systems should be selected depending on the target product.

Keywords: Hydrogen production, NaCl electrolysis, sodium hypochlorite, activated carbon electrode; Renewable energy; Energy

INTRODUCTION
Rising energy demand, the environmental impact of fossil fuels, and the need to transition to sustainable energy systems have increased the importance of hydrogen as a clean energy carrier. Due to its high specific energy content and the fact that it primarily returns to water upon use, hydrogen is seen as a significant alternative in future energy systems. Therefore, it is emphasized that water-splitting-based electrolytic processes hold an important place among sustainable hydrogen production methods and have strong potential, especially when integrated with renewable energy [1].

Yossan et al. [2] compared the effects of different catholytes on hydrogen production in microbial electrolysis cells and also investigated NaCl solution as an alternative catholyte. They highlighted that NaCl solution offers a lower-cost option compared to buffer solutions. However, they noted that the hydrogen production rate decreased with increasing pH when the catholyte was reused. In conclusion, the study revealed that NaCl-based media are viable for low-cost hydrogen production, but operating conditions must be carefully controlled.

Erden et al. [3] experimentally investigated the hydrogen production performance using the NaCl-based chlor-alkali method in this study. The aim of the study was to determine the effect of cell voltage, temperature, and electrolyte flow rate on hydrogen production in a NaCl solution. Experiments were conducted using a 1 M NaCl solution at voltages of 3, 4, and 5 V, as well as under different temperature and flow rate conditions. The results showed that hydrogen production increased with increasing voltage and temperature, but chlorine-based fouling and electrode corrosion also occurred on the anode side. The researchers stated that hydrogen production could be successfully achieved in systems containing NaCl, but side reactions and anode fouling were significant limitations.

In this study, the hydrogen production behavior of a 0.5 M NaCl solution under electrolysis at voltages of 2.2 V, 3.0 V, and 3.5 V was experimentally investigated, and the times taken to reach a specific hydrogen level were compared. A closed electrolysis cell consisting of two chambers was used in the experiments; both chambers were filled with granular activated carbon to form the electrode structure. Furthermore, experiments were conducted for one hour at the same voltage values, and the amount of NaOCl formed was evaluated using the iodometric titration method. Thus, the aim of this study was to experimentally determine the effect of the applied voltage on both hydrogen production and NaOCl byproduct formation in an activated carbon-based electrolysis system.

MATERIALS AND METHODS
In this study, electrolysis experiments were performed using a 0.5 M NaCl solution to investigate the formation of hydrogen and sodium hypochlorite (NaOCl). The closed electrolysis cell can be seen in Figure 1, used in the experiments consisted of two separate chambers. Both chambers were filled with granular activated carbon to form the electrode structure. The electric current supplied from a direct current (DC) power supply was first transmitted to copper wires placed inside the cell, and then transferred through these wires to the granular activated carbon bed. Thus, the activated carbons acted as electrode material. In addition, the entire surface of the chambers was designed to be in contact with the electrolyte, thus aiming to increase the electrochemical interaction surface area. The experiments were conducted at three different voltage values: 2.2 V, 3.0 V, and 3.5 V. The gas produced during electrolysis was connected via a tube to a gas collection unit containing a hydrogen sensor. This allowed for monitoring hydrogen formation over time and a comparison of the time to reach a specific hydrogen level for each voltage. To determine NaOCl formation, 1-hour electrolysis experiments were also performed at the same voltage values. Liquid samples obtained at the end of the experiment were analyzed using the iodometric titration method. In this analysis, 5 mL of 10% KI and 5 mL of 2 M HCl were added to the sample, and then the released iodine was titrated with a suitable titrant. NaOCl formation was evaluated based on the volume of titrant consumed.

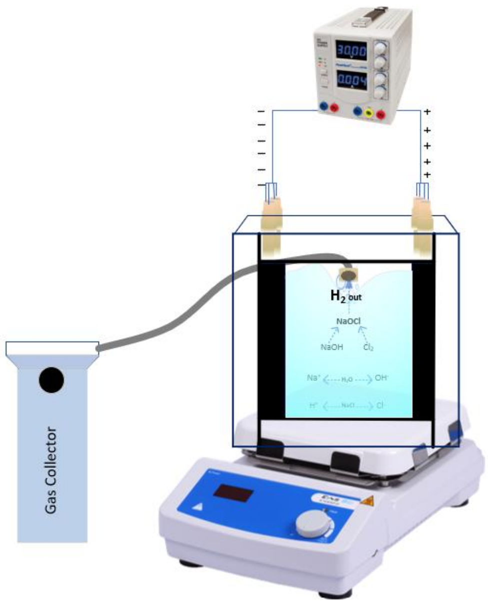

Fig.1. Schematic representation of the experimental electrolysis setup system in 0.5 M sodium chloride (NaCl) solution.

RESULTS AND DISCUSSION

When the hydrogen production curves are examined in Figure 2, it is seen that the applied voltage has a significant effect on the production behavior. When 3.5 V is applied, hydrogen formation starts earlier and higher production values are reached in a shorter time compared to other voltages. This can be attributed to the increase in the electrochemical reaction rate and the acceleration of hydrogen formation with increasing voltage. In particular, the fact that the 3.5 V curve shows a steeper increase after approximately 2.5 minutes indicates that the system provides faster gas production under this voltage.

In contrast, hydrogen production started later and increased more slowly below 2.2 V and 3.0 V. Interestingly, the graph shows that the 2.2 V curve slightly exceeds the 3.0 V curve at the end. While it is normally expected that the hydrogen production rate will increase with increasing voltage, this result suggests that factors other than voltage, such as the state of the active regions on the electrode surface, ion transport, local temperature variations, bubble accumulation, and internal resistance, may also be influential in the system. In particular, the bubbles that formed under the 3.0 V condition, partially covering the electrode surface, or irregularities in the current distribution may have limited the theoretically expected performance increase.

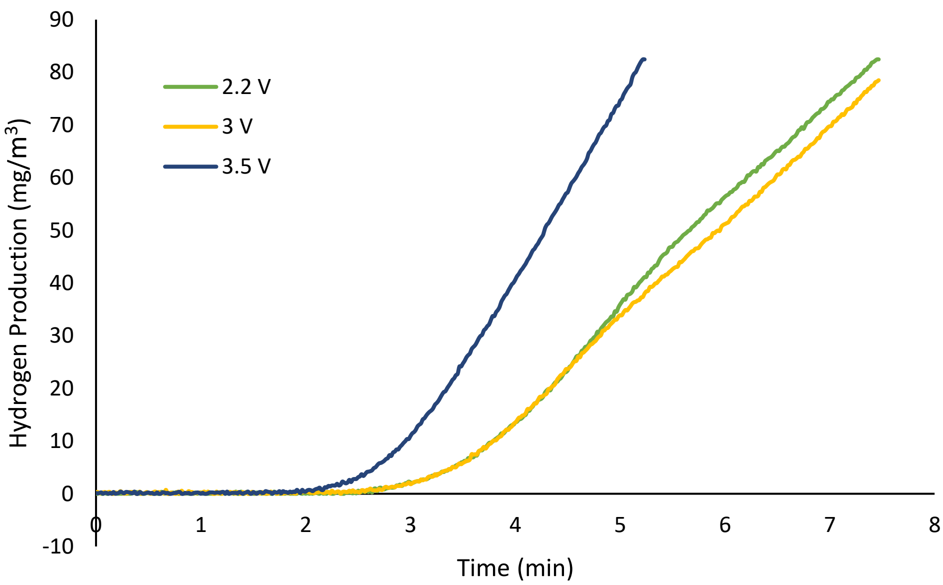

Fig.2. Change in hydrogen production over time at 2.2 V, 3.0 V, and 3.5 V.

The results of NaOCl formation showed that the applied voltage had a significant effect on the product distribution. According to the iodometric titration results, the NaOCl content obtained was approximately 298 mg/L below 2.2 V and approximately 74.5 mg/L below 3.0 V. At 3.5 V, NaOCl formation was almost not observed. The results show that NaOCl formation is higher under low voltage conditions and that this byproduct decreases as the voltage increases. This situation may be related to the increase in temperature at high voltages, the dominance of side reactions, or the decomposition of the active chlorine species formed.

CONCLUSIONS

The results of this study showed that the voltage applied during the electrolysis of a 0.5 M NaCl solution had a decisive effect on both hydrogen production and NaOCl byproduct formation. According to the hydrogen production curves, 3.5 V resulted in the fastest hydrogen formation, while production was slower at 2.2 V and 3.0 V. In contrast, iodometric titration results revealed that NaOCl formation was higher at lower voltages. The highest NaOCl content was calculated as approximately 298 mg/L at 2.2 V and 74.5 mg/L at 3.0 V, while formation was negligible below 3.5 V.

These results indicate that increasing the voltage in the system accelerates hydrogen production while reducing NaOCl formation. Therefore, the study shows that the applied voltage significantly affects not only the hydrogen yield but also the product distribution. Overall, higher voltages appear more advantageous for hydrogen production, while lower voltages are more favorable for NaOCl formation. Therefore, the system needs to be optimized under different operating conditions depending on which product is prioritized. Further studies investigating the effects of temperature control, reaction time, and electrode structure will contribute to improving both hydrogen production performance and byproduct selectivity.

REFERENCES

4) Dincer, I., & Zamfirescu, C. (2012). Sustainable hydrogen production options and the role of IAHE. International Journal of Hydrogen Energy, 37(21), 16266–16286. https://doi.org/10.1016/j.ijhydene.2012.02.133

5) Yossan, S., Xiao, L., Prasertsan, P., & He, Z. (2013). Hydrogen production in microbial electrolysis cells: Choice of catholyte. International Journal of Hydrogen Energy, 38(23), 9619–9624.https://doi.org/10.1016/j.ijhydene.2013.05.094

6) Erden, M., & Karakilcik, M. (2023). Experimental investigation of hydrogen production performance of various salts with a chlor-alkali method. *International Journal of Hydrogen Energy*, *52*, 546–560. https://doi.org/10.1016/j.ijhydene.2023.08.049

NANOFLUIDS AND HYBRID NANOFLUID CONVECTION HEAT TRANSFER IN A TUBE

*Amirreza Radmanesh[1], Nihad Dukhan[1]**
[1] Mechanical Engineering, University of Detroit Mercy, Detroit, MI, 48334, USA
*Corresponding author e-mail: dukhanni@udmercy.edu
Ref # MSC-02

ABSTRACT

A hybrid nanofluid (HNF) is a fluid that contains two or more kinds of chemically-distinct nanoparticles dispersed in a base liquid. HNFs are the new generation of ordinary nanofluids (NFs). HNFs are supposed to be more effective heat transfer fluids than NFs, as they present higher thermal conductivity, low viscosity and synergistic effects among nanoparticles. These effects are caused by different-size nanoparticles forming ordered arrangements around liquid molecules and acting as bridges among little aggregations of smaller nanoparticles. In this paper, simulations of heat transfer of HNFs and NFs in an open pipe are compared. The NFs and HNFs are made from aluminum oxide Al2O3 and TiO2 nanoparticles suspended in deionized water. The comparison is made at the same solid particle volume concentration and hydraulic and thermal conditions. The simulation domain is a circular pipe having an internal diameter 5.25 cm and a length 16.51 cm. The pipe is subjected to constant heat flux of 15518 W/m2. At the inlet, the fluid's temperature was constant at 298 K, and a Reynolds number of 1798 (entrance velocity 0.029 m/s). The mesh-independent results show that the heat transfer performance of HNFs is superior to that of NFs.

Keywords: Nanofluids, Hybrid nanofluids, Convection, Simulations

INTRODUCTION

Nanofluids are typically liquids with solid nanoparticles (< 100 nm) of metals (e.g. copper, silver, and gold) or metal oxides (e.g. alumina, titania, and iron oxide) suspended in them. Base fluids are usually coolants such as water, ethylene glycol and refrigerants. Graphene nanosheets and carbon nanotubes have been used due to their higher thermal conductivity. Nanofluids were proposed as coolants in Argonne National Laboratory (USA) in 1995 [1]. Scientific research of nanofluids has been dramatically increasing ever sense.

The common base fluids have poor thermal conductivities, and adding nanoparticles increases their conductivity. Nanoparticles also enhance the convective heat transfer coefficient [2]. The enhanced heat transfer comes with a penalty: increased viscosity and density, which leads to higher pressure drop. Nonetheless, nanofluids are viewed as the next generation coolants. Some guidelines for choosing nanofluids for enhanced heat transfer in applications have been published, e.g. [3].

A hybrid nanofluid is an advanced nanofluid that contains two or more kinds of chemically-distinct nanoparticles dispersed in a single base liquid. HNFs are a relatively recent evolution of nanotechnology. While ordinary nanofluids have been around since 1995, HNFs have started receiving increased attention around 2015. HNFs are more effective heat transfer fluids than ordinary nanofluids (mono-nanoparticle fluids), as they present higher thermal conductivity, low viscosity and synergistic effects. These effects are caused by some nanoparticles forming ordered arrangements around base liquid molecules and acting as bridges among little aggregations of smaller nanoparticles. These peculiar HNFs' phenomena lead to effective heat transfer networks. Also, by hybridizing the appropriate combination of nanoparticles, one can get the desired heat transfer effect even at low particle concentrations [4].

Currently there is a lack of understanding of transport phenomena of HNFs. The research on HNFs began to emerge about 10 years ago, and is still limited both experimentally and numerically [5]. The vast majority of recent papers is focused on thermophysical properties of HNFs, e.g., [6-8]. Other investigations are specifically focused on the thermal conductivity of HNFs due to its vital role in heat transfer enhancement, and on viscosity due to its role in pressure drop, e.g., [9-13].

Recently, Skouras et al. [14] investigated thermal conduction in hybrid nanofluids; and Khan et al. [15] provided a study on the thermophysical features of hybrid nanomaterials for of solar thermal applications of heat exchangers. Investigations of HNFs properties and applications in various applications continue to appear in the literature. For example, Singh [16] investigated hybrid nanofluids for low-carbon chemical processes, and Zia et al. assessed the improvement in heat transfer and thermal stability of hybrid nanofluids

The literature on convection heat transfer characteristics of HNFs is relatively small, especially for heat transfer in the common geometry of clear pipes. Nonetheless, studies clearly indicate that HNFs yield high rates of heat transfer [17,18].

SIMULATIONS

The single-phase model (SPM) of nanofluids treats nanoparticles and base fluid as a single phase, and assumes that local thermal equilibrium holds between the two constituents. These assumptions are justified due to small size of nanoparticles. Governing equations that are used for conventional fluids can be used for single-phase nanofluids. Thermophysical properties of nanofluids need to be determined and inserted in these governing equations. Many researchers [19,20] reported that heat transfer in nanofluids can be modelled using the SPM.

The volume fraction of nanofluids is the solid nanoparticles volume divided by the mixture volume prior to mixing:

$$\varphi = \varphi_s / \varphi_{tot} \qquad (1)$$

In the current study, the nanofluids were made from aluminum oxide Al2O3 and TiO2 suspensions in deionized (DI) water. The hybrid nanofluid was made by suspending Al2O3 and TiO2 in DI water with 50:50 of the two kinds of nanoparticles. In all cases, the volume fraction was 1.5%. The thermal conductivity of HNFs can be calculated from [21, 22] as:

$$\frac{k_{hnf}}{k_{bf}} = \left[\frac{k_{TiO2} + 2k_{bf} - 2\varphi_{TiO2}(k_{bf} - k_{TiO2})}{k_{TiO2} + 2k_{bf} + \varphi_{TiO2}(k_{bf} - k_{TiO2})}\right]$$

The density and the specific heat can be obtained from [21, 23]] as:

$$\rho_{hnf} = (1-\varphi)\rho_{bf} + (0.5-\varphi)\rho_{Al2O3} + (0.5-\varphi)\rho_{TiO2}$$

$$C_{hnf} = \frac{(1-\varphi)\rho_{bf}C_{bf} + (0.5\times\varphi)\rho_{Al2O3}C_{Al2O3} + (0.5\times\varphi)\rho_{TiO2}C_{TiO2}}{\rho_{hnf}}$$

and the viscosity from [21-23]

$$\frac{\mu_{hnf}}{\mu_{bf}} = \frac{1}{(1-\varphi_{TiO2})^{2.5}(1-\varphi_{Al2O3})^{2.5}}$$

Nanofluids and HNF flew through a heated pipe shown schematically in Fig. 1. At the inlet, the fluid temperature Ti was 298 K, and the entrance velocity ui was 0.029 m/s, which is in the laminar flow regime. On the external surface of the pipe a constant uniform heat flux q″ = 15518 W/m2 is applied. The k-ε model is the most common model utilized to simulate flow characteristics. The primary reasons for choosing this model are as follows: Robustness and reasonable accuracy for a wide range of flows and heat transfer simulations [24, 25].

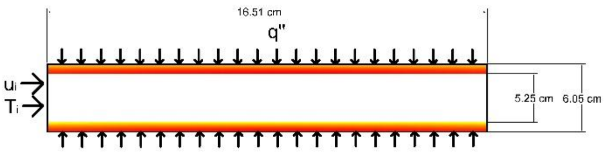

Fig. 1. Schematic of the simulated heat transfer system

All simulations were conducted utilizing ANSYS Fluent 2021 R1 on a local station AMD Ryzen 7 1st Gen - RYZEN 7 1700X Summit Ridge (Zen) 8-Core 3.4 GHz (3.8 GHz Turbo) with dual processors, 64 cores, and 32.0 GB RAM. Mesh-independent was achieved. The final mesh consisted of uniform square-shaped elements with near-wall higher density to capture any small temperature variations. The run took approximately 25 minutes to converge.

RESULTS

Figure 2 shows the variation in surface temperature as a function of distance from the entrance for the two nanofluids and the hybrid nanofluid- all the same volume fraction of 1.5%. The case for clear water is also included for reference. The two nanofluids are seen to produce approximately the same wall temperature along the pipe, which indicates similar heat-transfer performance. For the two nanofluids, the wall temperature is significantly lower than that for water. The hybrid nanofluid is seen to produce a much lower wall temperature, which indicates a superior performance of this advanced fluid compared to mono nanofluids. The gaps between the surface temperature for all fluids is seen to increase along the pipe.

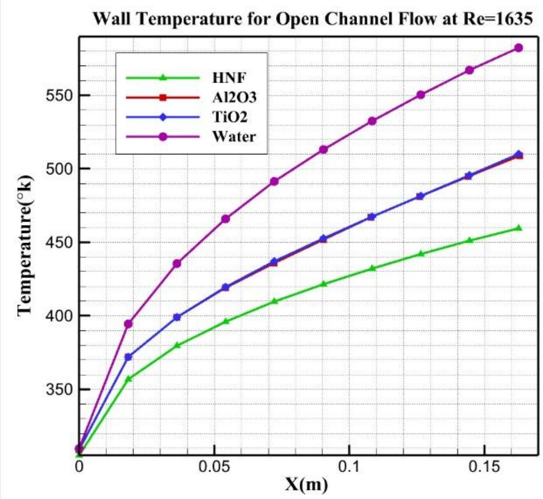

Fig. 2. Surface temperature along the pipe for all fluids

Clearly, there is thermal development in all cases: the temperature starts to increase gradually with a changing slope. Thermal development will be assessed by looking at the local Nusselt number as shown below.

Another way of looking at the convection heat transfer of these fluids is to plot the local Nusselt number Nu_x as shown in Fig. 3. The number is obtained from

$$Nu_x = q''D / k(T_{wx} - T_{bx}) \qquad (2)$$

where q'' is the surface heat flux, D is the pipe's internal diameter, k is the conductivity of the fluid, and T_{wx} and T_{bx} are the local wall and bulk temperatures, respectively. It should be noted that the local bulk temperature can be obtained from ANSYS.

As expected, the Nusselt number starts high at the entrance and decreases along the flow direction. It seems to be approaching a constant value (independent of distance) starting at about 15.2 cm, which indicates full thermal development. After this point, the increased in Nusselt number of HNF over the nanofluids is about 23.5%, indicating better heat transfer for the former. This is a considerable amount that has serious implications for heat transfer equipment, and can be employed in various applications where a cooling fluid is needed.

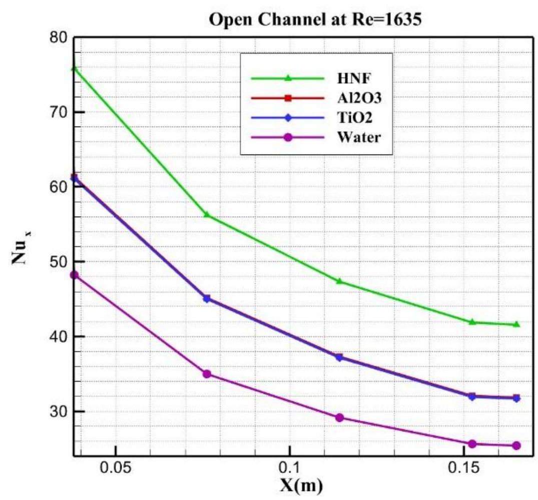

Fig. 3. Local Nusselt number along the pipe for all fluids

CONCLUSION

Convective heat transfer simulations for two nanofluids and one hybrid nanofluid made from the same nanoparticles at the same volume concentration of 1.5% were conducted. The common case of a heated circular pipes having a constant surface heat flux was analysed. The single-phase model was adopted for the nanofluids, and their properties were obtained from correlations in the literature. The wall temperature for the hybrid nanofluid was seen to be significantly lower than that obtained with each of the two nanofluids; and the local Nusselt number for the hybrid nanofluids was much higher than those for the ordinary nanofluids. These two items indicate better heat transfer performance of the hybrid nanofluid. The results are encouraging but other cases need to be investigated to further establish the superiority of hybrid nanofluids as coolants. The effect of flow Reynolds number and the volume concentration on heat transfer needs to be pursued.

REFERENCES

[1] Choi, S.U.S. and Eastman, J.A., Enhancing thermal conductivity of fluids with nanoparticles, in Conference: 1995 Inte. mech.l eng. cong. exh., San Francisco, CA, 12-17 Nov 1995

[2] Buongiorno, J., Convective Transport in Nanofluids. J. Heat Transfer, 2005. 128(3): p. 240-250.

[3] Asadi, A., A guideline towards easing the decision-making process in selecting an effective nanofluid as a heat transfer fluid. En. Conv. Manag., 2018. 175: p. 1-10.

[4] Baby, T. and R. Sundara, Experimental investigation of the thermal transport properties of a carbon nanohybrid dispersed nanofluid. Nanoscale, 2011. 3: p. 2208-14.

[5] Zhang, S., et al., Turbulent heat transfer and flow analysis of hybrid Al2O3-CuO/water nanofluid: An experiment and CFD simulation study. Applied Thermal Engineering, 2021. 188: p. 116589.

[6] Kumar, V., et al., Efficacy evaluation of oxide-MWCNT water hybrid nanofluids: An experimental and artificial neural network approach. Colloids and Surfaces A: Physicochemical and Engineering Aspects, 2021. 620: p. 126562.

[7] Alarifi, I.M., et al., Feasibility of ANFIS-PSO and ANFIS-GA Models in Predicting Thermophysical Properties of Al2O3-MWCNT/Oil Hybrid Nanofluid. Materials, 2019. 12(21).

[8] Zawawi, N.N.M., et al., Experimental investigation on stability and thermo-physical properties of Al2O3–SiO2/PAG nanolubricants with different nanoparticle ratios. Journal of Thermal Analysis and Calorimetry, 2019. 135(2): p. 1243-1255.

[9] Wanatasanapan, V.V., M.Z. Abdullah, and P. Gunnasegaran, Effect of TiO2-Al2O3 nanoparticle mixing ratio on the thermal conductivity, rheological properties, and dynamic viscosity of water-based hybrid nanofluid. Journal of Materials Research and Technology, 2020. 9(6): p. 13781-13792.

[10] Zadkhast, M., D. Toghraie,A. Karimipour, Developing a new correlation to estimate the thermal conductivity of MWCNT-CuO/water hybrid nanofluid via an experimental investigation. Journal of Thermal Analysis and Calorimetry, 2017. 129(2): p. 859-867.

[11] Afrand, M., Experimental study on thermal conductivity of ethylene glycol containing hybrid nano-additives and development of a new correlation. Applied Thermal Engineering, 2017. 110: p. 1111-1119.

[12] Asadi, A., et al., An experimental and theoretical investigation on heat transfer capability of Mg (OH)2/MWCNT-engine oil hybrid nano-lubricant adopted as a coolant and lubricant fluid. Applied Thermal Engineering, 2018. 129: p. 577-586.

[13] Hamid, K.A., et al., Experimental investigation of thermal conductivity and dynamic viscosity on nanoparticle mixture ratios of TiO2-SiO2 nanofluids. International Journal of Heat and Mass Transfer, 2018. 116: p. 1143-1152.

[14] Skouras, E.D., N.P. Karagiannakis, and V.N. Burganos, Thermal Conduction in Hybrid Nanofluids and Aggregates. Nanomaterials, 2024. 14(3): p. 282.

[15] Khan, M.N., et al., Overview of solar thermal applications of heat exchangers with thermophysical features of hybrid nanomaterials. Nanoscale Advances, 2024. 6(1): p. 136-145.

[16] Singh, J. (2026). Hybrid Nanofluids for Low-Carbon Chemical Processes. J Eng. and Applied Science Technology, 8(1), 1–6.

[17] Bhattad, A., J. Sarkar, and P. Ghosh, Heat transfer characteristics of plate heat exchanger using hybrid nanofluids: effect of nanoparticle mixture ratio. Heat and Mass Transfer, 2020. 56(8): p. 2457-2472.

[18] Maddah, H., et al., Factorial experimental design for the thermal performance of a double pipe heat exchanger using Al2O3-TiO2 hybrid nanofluid. International Communications in Heat and Mass Transfer, 2018. 97: p. 92-102.

[19] Kim, S., et al., Comparison of CFD simulations to experiment for heat transfer characteristics with aqueous Al2O3 nanofluid in heat exchanger tube. International Communications in Heat and Mass Transfer, 2018

[20] Ebrahimnia-Bajestan, E., et al., Experimental and numerical investigation of nanofluids heat transfer characteristics for application in solar heat exchangers. International Journal of Heat and Mass Transfer, 2016. 92: p. 1041-1052.

[21] Khashi'ie, N.S., et al., Flow and heat transfer of hybrid nanofluid over a permeable shrinking cylinder with Joule heating: A comparative analysis. Alexandria Engineering Journal, 2020. 59(3): p. 1787-1798.

[22] Rajesh, V., M.A. Sheremet, and H.F. Öztop, Impact of hybrid nanofluids on MHD flow and heat transfer near a vertical plate with ramped wall temperature. Case Studies in Thermal Engineering, 2021. 28: p. 101557.

[23 Bezaatpour, M. and M. Goharkhah, Three dimensional simulation of hydrodynamic and heat transfer behavior of magnetite nanofluid flow in circular and rectangular channel heat sinks filled with porous media. Powder Technology, 2019. 344: p. 68-78.

[24] Ansys, I., ANSYS Fluent User's Guide 2021 R1. Theory Guide, 2021.

[25] Launder, B.E. and D.B. Spalding, Lectures in mathematical models of turbulence. 1972, London: Academic Press.

ELECTROLYSIS-BASED HYDROGEN AND AMMONIA AS ELEMENTS OF SUSTAINABLE AGRICULTURAL INTENSIFICATION IN SUB-SAHARAN AFRICA

Andreas Stamm[1*], Christine Bosch[2]
[1] German Institute of Development and Sustainability (IDOS), Transformation of Economic and Social Systems, Tulpenfeld 6, 53113 Bonn, Germany
[2] Hohenheim University, Department of Social and Institutional Change in Agricultural Development, Wollgrasweg 43, 70599 Stuttgart, Germany
*Corresponding author e-mail: andreas.stamm@idos-research.de

Ref # MSC-03

ABSTRACT

Nitrogen fertilizer as a core element of plant nutrition is crucial for improved food security. This is especially important for Sub-Sahara Africa, with extremely low rates of fertilizer application per hectare of arable land, an already high proportion of people with insufficient food intake and a significant population growth in the next decades. Nitrogen fertilizer is today produced in large ammonia synthesis plants applying technologies with very high emissions of greenhouse gases. Technological innovation, specifically small-scale electrolysis-based hydrogen and ammonia production offer a pathway for a paradigm shift in N-fertilizer production. The main difference between traditional and electric Haber-Bosch plants is that the economic logic of the former depends on a continuous supply of natural gas, which leads to a concentration on only a few locations internationally. However, if the process is based on electrolytic hydrogen, it can basically be carried out anywhere where there is a large potential for renewable energies and clean water. This allows ammonia and N fertilisers to be produced closer to the farm gate and with much lower greenhouse gas emissions.

Keywords: Low Emission Hydrogen, Nitrogen fertilizers, Food security, Sub-Sahara Africa

INTRODUCTION

Since around 2020, the European Union and many countries (e.g. Germany) approved ambitious strategies to develop a Low-Emission Hydrogen (LEH_2) economy. The vision was based on the idea, that a new international energy geography might significantly alter trade patterns of energy carriers [1, 2]. Industrialized countries would import significant quantities of clean LEH_2 and derivatives (ammonia, methanol, Sustainable Aviation Fuels (SAF)) to decarbonize activities that are not suitable for direct electrification, such as iron and steel production or aviation. On the other hand, production patterns could emerge that are more diverse than those for fossil fuels. While their locations are necessarily tied to natural deposits of oil, gas, or coal, green hydrogen (GH_2) can basically be produced anywhere where there is sufficient potential for renewable energies. Developing countries rich in solar and wind energy could establish new global value chains and create urgently needed jobs.

Around five years after the adoption of hydrogen strategies in Europe, however, it is clear that some assumptions were too optimistic, particularly with regard to the speed at which a new energy geography could emerge [3]. Neither the supply of GH_2 nor its demand have so far significantly been scaled up. Large-scale projects along the supply chain have been cancelled or significantly postponed, e.g. a planned H_2-pipeline between Norway and Germany, which would have enabled a secure supply of LEH_2 to industrial customers in Central Europe. However, we assume that the development of a LEH_2 economy will remain on the agenda as long as there is an international commitment to limit greenhouse gas (GHG) emissions and global warming. In this context, it is important to identify courses of action that will yield benefits in the short term while also serving as a bridge until technological maturity and cost reductions allow the emergence of a global hydrogen economy [4].

Committed to the goals of broad economic growth within planetary boundaries, we propose to place one focus in the coming years on the production and application of low-emission fertilizers especially in sub-Sahara Africa. This can contribute to several development goals, as will be explained below.

SUB-SAHARA AFRICA: AN UNDER-FERTILIZED WORLD REGION

For food production, plant nutrition is core. In addition to securing or restoring decent levels of soil health, the application of external nutrients is seen as indispensable by most researchers. The core macronutrients for plants are nitrogen (N), phosphorus (P), and potassium (K), in addition other relevant elements should be mentioned, such as iron, sulphur, and calcium. Following FAO and International Fertilizer Association (IFA) data [5], the quantitative relation of applying fertilizers globally are N: 56%, P: 24% and K: 20%. Levels of fertilizer consumption per hectare of arable land increased continuously over the past decades, globally from around 55 kg/ha in 1972 to 134 kg/ha in 2022. The differences among the world regions are very significant. In 2022 (last available data) agricultural enterprises of all sizes in East Asia/Pacific applied 321 kg/ha, in South Asia 201 kg/ha, in Latin America and the Caribbean 187 kg /ha and in the EU 124 kg/ha. Sub-Saharan Africa stands out as a world region with extremely low fertilizer application rates, reaching only 18 kg in 2022, up from 10 kg in 1972 [6].

The under-fertilization of arable land in Sub-Saharan Africa and its evident connection to malnutrition has repeatedly raised the attention of researchers and policy makers. In 2006, African Union adopted the "Abuja Declaration on Fertilizer for the African Green Revolution", stating that "*No region of the world has been able to expand agricultural growth rates and tackle hunger without increasing fertilizer use*." [7]. At that time, fertilizer application rates in Africa were only 8 kg/ha, or 10% of the world average. The Abuja Declaration set the goal of raising application rates to 50 kg/ha by the year 2015. However, in 2025, the application rates in Africa had only increased to 18 kg/ha. Thus, in 2024, a new AU Declaration was approved at the "Africa Fertilizer and Soil Health Summit" in Nairobi / Kenya [8]. The Declaration took a more comprehensive approach, embedding the fertilizer applications in concepts of an improved soil health and committed to "reverse land degradation and restore soil health on at least 30% of degraded soils by 2034. However, the urgent need to increase the application of fertilizers on arable land was reiterated, committing to triple domestic production and distribution of organic and inorganic fertilizers by 2034.

Regional overviews (e.g. by FAO and IDRC) clearly show that Africa is the continent with by far the lowest levels of food security and the only world region, where insufficient food availability and hunger tend to worsen over time. This situation cannot be attributed to one single but to a bundle of factors, e.g. conflicts, natural disasters, climate change, the COVID 19 pandemic and its aftermath. But also, low levels of fertilizer application add to long-term food insecurity. For instance, reduced plant growth due to deficient plant nutrition does not only affect crop yields but also nutritional content and the amounts of biomass which remains on the arable land or can be used to feed livestock or obtain usable biomass for soil health improvements, e.g. through composting [9]. In addition, decreasing soil fertility may incentivize farmers to expand the area of land under cultivation, which may lead to increased deforestation [10].

AFRICA IN A DEFICIENT SYSTEM OF INTERNATIONAL NITROGEN FERTILIZER VALUE CHAINS

In the following, we will focus primarily on nitrogen fertilizers, the quantitatively most important group of fertilizers. Phosphorus and potassium fertilizers are also traded internationally to a large extent, but their supply chains are primarily rooted in natural deposits, e.g., potassium in Canada and phosphorus in Morocco. Nitrogen fertilizers and their precursor, ammonia, are today also traded in highly concentrated supply chains. However, the location pattern of primary production has a lot to do with the technology used and can be fundamentally altered by a switch in technology, here: from fossil fuels based to LEH_2-based processes.

The core of the production of N-Fertilizers is the synthesis of ammonia (NH_3). Ammonia synthesis was developed by Fritz Haber and Carl Bosch in the first decades of the 20th century, based on the research done by Justus Liebig in the 19th century. The Haber-Bosch process (HBP) is seen as fundamental for increasing food production and assuring nutrition for a rapidly growing world population. The amounts of synthetized NH_3 grew steadily since the invention of the HBP, from less than half a million tons annually in the 1920s to 180 million tons in 2020. The number of facilities which synthesize ammonia is rather small for an industry of global reach, reaching around 500 plants in 2020 [11]. In Sub-Saharan Africa only six facilities currently produce ammonia / nitrogen fertilizer [12]. This implies that a huge proportion of N-fertilizers has to be imported. In 2024, the most important suppliers of Africa were the Russian Federation (28%) and China (14%) [13].

The reasons for this concentrated location pattern are basically two: 1) the traditional and today clearly dominant technology for HBP is Steam Methane Reforming (SMR). SMR is a chemical process where natural gas (mostly methane, CH_4) reacts with steam (H_2O) at high temperature to produce hydrogen as the main product. Subsequently, H2 is introduced to the Haber-Bosch reactor, where H_2 and N_2 are processed to form NH_3. SMR is capital-intensive. Economies of scale tend to give large plants a competitive advantage over smaller units. 2) Unit costs fall especially sharply when both SMR and the HBP operate for long or continuous periods. Long or permanent run times require the permanent availability of natural gas as the main feedstock. Most HBP facilities are, thus, located close to natural-gas pipelines or major gas fields. Techno-economic reasons impede a decentralization. This may be a very crucial reason for substituting SMR based HBP by electric HBP (see the next chapter).

ELECTROLYTIC HYDROGEN IN HABER-BOSCH: THE POTENTIAL FOR A PARADIGM SHIFT THROUGH GREEN AMMONIA

The HBP is, in general, agnostic to the "colours" of hydrogen. With some adaptations, existing reactors may continue to be used, utilizing LEH_2 instead of grey hydrogen for NH_3 synthesis. However, considering the huge amount of hydrogen one would require, it is more likely that existing NH_3 plants fed with natural gas may be retrofitted and combined with a Carbon Capture and Storage (CCS) facility, producing so-called blue ammonia. The main reasons for going to this option would be that one may lower the process-related GHG emissions which reach the atmosphere while continuing to use existing facilities and avoiding stranded assets. What it would not imply, however, would be mitigating the problems related to a centralized location pattern [14]. Long international supply chains imply that the farmers, who are the final clients of N-fertilizers, are exposed to a series of risks: Erratic price fluctuations in the early 2000s led to more than triple the prices for N-fertilizers in some moments, which made the product unaffordable for many farmers not only in Africa. In many countries in Africa, governments subsidize the market prizes of fertilizers, which absorbs significant parts of the budgets available for the support of farmers. Being exposed to the fluctuations in international prizes make the programming of public spending even more challenging. Finally, in times of increasing international conflicts, risks for a more radical interruption of international fertilizer supply chains exist. Thus, decentralized location patterns for fertilizer production facilities can be seen as part of a comprehensive risk avoidance and an increased food security and sovereignty in Africa [15, 16].

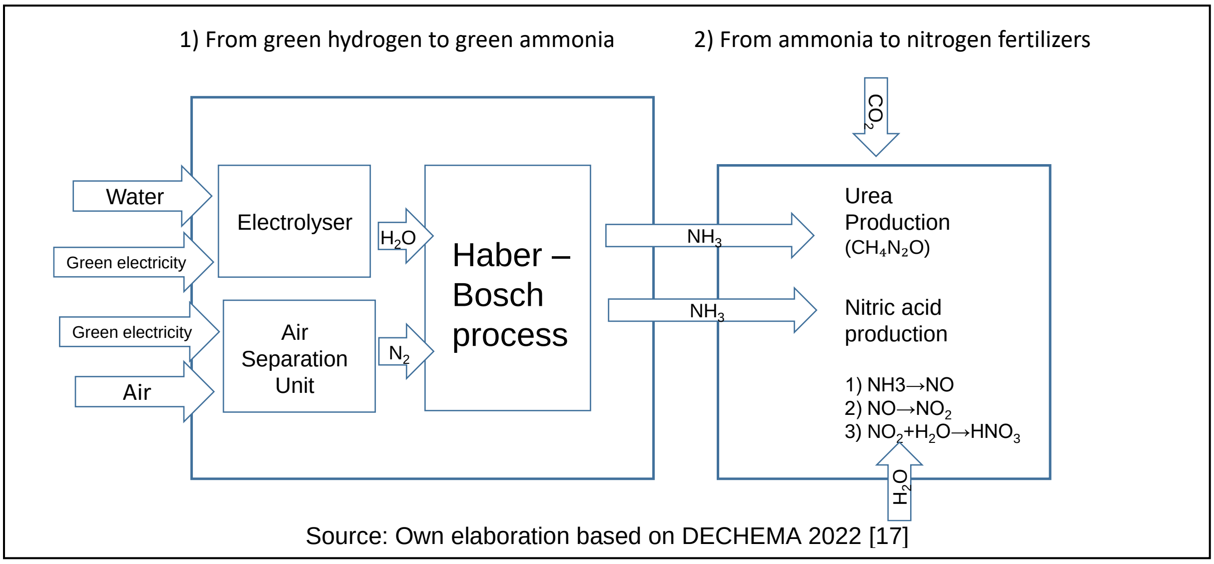

Figure 1: Production chain of green ammonia and important nitrogen fertilizers

HBP based on LEH_2 allow for much smaller ammonia plants compared to traditional natural gas or coal-fed facilities. However, techno-economic factors constitute a minimum threshold which may be difficult to fall below. The main difference between traditional and electric HBP is that the first option depends on a secured supply of methane to produce H_2 from SMR, while the latter can be based on GH_2 which can be produced at any place with good renewable energy resources and a good supply of high-quality water. With currently mature technologies, the HBP as such is not very different in the electric version compared to the traditional method. This means that sufficient energy has to be available to generate the high temperature and pressure needed for the Haber-Bosch loop. This implies that NH_3 and nitrogen fertilizer production will not be economically feasible on the level of individual smallholder farms.

The Kenya Nut Farm Company can serve as an example of what makes sense from a techno-economic perspective. The company farms around 3.200 hectares and produces different lines of nuts, coffee and dried fruits. In 2023, the company entered into a partnership with US-based TalugAG to start the first commercial green ammonia plant in Africa. The system is powered by a 2.1 MW solar farm and produces approximately one tonne of green ammonia per day. The project started operation in late 2023 and until today, no major technical hurdles were publicly reported [18]. The system which Talus installed is meant to be containerized and modular, implying it could also be installed in other parts of the Global South with comparable conditions of renewable energy and water potentials and farms that need to be supplied with N-fertilizer. In addition to large commercial farms, this could become a cost-competitive solution for the decentralized production of nitrogen on the level of mid-sized cooperatives and larger villages [19].

CONCLUSIONS: THE WAY AHEAD

A series of papers have recently been published which show that several alternatives to traditional centralized HBP-based ammonia production are under development and promising, with varying levels of technology readiness and with specific advantages and disadvantages each. Three avenues seem to be most promising to contribute to social inclusion and environmental sustainability in Africa:

- Decentralized and electrified HBP which is the topic of this paper;
- Electrochemical conversion of nitrogen to ammonia, which still has low levels of technology readiness [20] and
- Ammonia recuperation from wastewater, which could be an option to generate NH3 for fertilizers, while reducing the growing problem of eutrophication of water bodies, especially in fast growing urban and peri-urban areas [21].

We assume that for a variety of reasons blue and green ammonia will be further developed in parallel and may compete for the attention of policy makers, technology developers and investors. When it comes to the decentralized and electrified HBP, we assume it has reached a relatively high level of technology readiness. We sketched the first on-site green ammonia facility operating in Kenya and may assume that there will be further installations of this kind in the future. We see two interlinked avenues for further research:

- An extended study on the techno-economic feasibility of electric HBP, determining the production costs per kg under various structural conditions. For instance, while the plant in Kenya is powered by solar energy only, combining wind and solar energy or using hydropower or geothermal energy could increase the full-load hours of the electrolyser employed, which might reduce the unit cost. The production costs would then have to be compared to the farm-gate price of conventional N-fertilizer. This could determine the possible price gaps, which might have to be covered by national funds or international climate- and/or development finance.

- The discussion of possible institutional settings for decentralized N-fertilizer production with the potential of benefitting not only commercial export-oriented farms as in the Kenya case, but also producers of staple crops for the domestic markets. Cooperatives and producers´ organizations, sometimes have a long history in the Global South and could be critically analysed as possible role models.

REFERENCES

[1] H2-Diplo / GIZ (2023): The Structure of the Emerging International Hydrogen Trade and their Geopolitical Considerations. Berlin

[2] Badgett A, Ruth MF, Smith C, Keller M, Terrapon-Pfaff J, Viebahn P, Pregger T and Monnerie N (2025) Considerations of a possible global hydrogen energy trade. Front. Energy Res. 13:1632179. doi: 10.3389/fenrg.2025.1632179

[3] International Energy Agency (IEA) (2025): Global Hydrogen Review 2025. Paris: IEA

[4] Stamm, A (2025): The vision of a global hydrogen economy. Hydrogen's trend and its meaning for low- and middle-income countries. The Current Column 01-09-2025. IDOS: Bonn

[5] https://www.fertilizer.org/market-intelligence/ifastat/, last accessed 25/02/2026

[6] https://data.worldbank.org/indicator/AG.CON.FERT.ZS

[7] International Fertilizer Development Centre (IFDC) / African Fertilizer and Agribusiness Partnership (AFAP) (2023): Implementation of the Abuja Declaration on Fertilizer for an African Green Revolution.

[8] Africa Fertilizer and Soil Health Summit, May 2024, Draft Nairobi Declaration. https://au.int/sites/default/files/documents/44056-doc-AFSHS_Decl_4_II_Rev_2_E.pdf

[9] Dimkpa C, Adzawla W, Pandey R, Atakora WK, Kouame AK, Jemo M and Bindraban PS (2023) Fertilizers for food and nutrition security in sub-Saharan Africa: An overview of soil health implications. Front. Soil Sci. 3:112393

[10] Pierre, JF, Goodwin, A. (2025): Underuse of Fertilizer in Africa is an Environmental Catastrophe. International Fertilizer Development Centre, https://ifdc.org/2025/12/05/underuse-of-fertilizer-in-africa-is-an-environmental-catastrophe/

[11] International Energy Agency (IEA) (2021): Ammonia Technology Roadmap, Towards more sustainable nitrogen fertiliser production. Paris: IEA

[12] AfricaFertilizer, International Fertilizer Development Centre (IFDC): 2024 Register of Fertilizer Manufacturing and Processing Facilities in Sub-Saharan Africa, https://hub.ifdc.org/items/45a49d49-0012-4c28-a090-95e3199e1513

[13] Own calculation based -on: https://www.trademap.org/Index.aspx

[14] World Bank (2025): Decarbonizing Ammonia and Nitrogen Fertilizers with Clean Hydrogen. Livewire 2025/140. Washington: World Bank

[15] Fernández, CA, Chapman, O., Brown, MA, Alvarez-Pugliese, CE, Hatzell, MA (2024): Achieving Decentralized, Electrified, and Decarbonized Ammonia Production, Environ. Sci. Technol. 58, 6964−6977

[16] Tonelli, D., Rosa, L., Gabrielli, P. , Patente, A., Contino, F. (2024): Cost-competitive decentralized ammonia fertilizer production can increase food security, Nature Food 5: 469–479

[17] DECHEMA e.V. (2022): Perspective Europe 2030 - Technology options for CO2- emission reduction of hydrogen feedstock in ammonia production. Frankfurt am Main

[18] https://farmersreviewafrica.com/kenya-nut-company-installs-first-commercial-on-site-green-ammonia-system-for-carbon-free-fertilizer-production/#google_vignette

[19] Tonelli, D. et al. (2024): Small-scale decentralized ammonia production could become cost-competitive by 2030, Nature Food 5: 467–468

[20] Ahmadi, M., Nazemi, M. (2025): Sustainable, electrified, and decentralized ammonia synthesis from diverse nitrogen feedstocks, Cell Reports, Physical Science 6: 10249

[21] Yang, H., Lim, S.Y., Lee, G. et al. (2026): Hydrogen production from wastewater via ammonia gas recovery. npj Clean Water, unedited version: www.nature.com/articles/s41545-026-00558-7

INTEGRATING ENERGY, EXERGY, AND ENTROPY INTO NATIONAL POLICY AND PROCESS OPTIMIZATION: A THERMODYNAMIC PERSPECTIVE ON SUSTAINABLE DEVELOPMENT

Nurdan Güven[1], Zafer Utlu[2]*
[1]İstanbul Atlas University Faculty of Humanities and Social Sciences Department of Business Administration, İstanbul, Türkiye
[2]İstanbul Atlas University Faculty of Engineering and Natural Sciences Department of Industrial Engineering İstanbul, Türkiye
* Corresponding author email; zafer.utlu@atlas.edu.tr

Ref # MSC-05

ABSTRACT

Sustainable development challenges require integrated approaches linking thermodynamics with policy and engineering. Current frameworks rely mainly on energy-based metrics, often neglecting exergy and entropy, limiting system performance evaluation. This study proposes a framework integrating energy, exergy, and entropy into policy design and process optimization. The approach assesses energy systems in terms of quantity, quality, and irreversibility, identifying sources of exergy destruction and entropy generation. Results show that energy-only metrics lead to inefficiencies, while thermodynamic indicators improve system performance and policy coherence. The study highlights the importance of aligning policy with thermodynamic principles to achieve more efficient and sustainable energy systems.

Keywords; Political Systems; Governance Efficiency; Open Systems; Institutional Dynamics; Sustainability; Energy; Entropy; National Policy Analysis

INTRODUCTION

The transition toward sustainable development has become a central objective of contemporary energy systems, driven by growing concerns over climate change, resource scarcity, and environmental degradation. In response, national governments have increasingly adopted policies aimed at improving energy efficiency, reducing greenhouse gas emissions, and promoting low-carbon technologies [1]. However, these policy frameworks are predominantly based on aggregate energy metrics and carbon accounting approaches, which often fail to capture the fundamental physical constraints governing energy systems. Conventional energy analysis focuses on the quantity of energy flows without adequately addressing energy quality or the irreversibilities inherent in energy conversion processes. In contrast, thermodynamic concepts such as exergy and entropy provide a more comprehensive framework for evaluating system performance. Exergy analysis enables the assessment of the maximum useful work potential of a system, while entropy generation serves as a direct measure of irreversibility and the degradation of energy quality [2]. Together, these concepts allow for a more physically grounded understanding of efficiency that goes beyond conventional energy metrics.

Despite their theoretical importance, entropy and exergy considerations remain largely absent from national policy frameworks and are insufficiently integrated into process engineering and optimization practices. In particular, entropy generation representing unavoidable losses due to thermodynamic irreversibility is rarely considered in policy evaluation, even though it directly reflects the physical limits of energy systems. This omission can lead to policies that inadvertently promote energy pathways associated with high entropy production and significant exergy destruction.

The lack of alignment between thermodynamic principles and policy design can result in inefficient resource allocation and suboptimal system configurations. Policies that prioritize energy efficiency in purely quantitative terms may overlook the cumulative effects of entropy generation across energy conversion chains. As highlighted in the literature, ignoring energy quality and thermodynamic limits can distort both economic and policy assessments of energy systems [3,4].

This study addresses this gap by proposing an integrated framework that incorporates energy, exergy, and entropy analysis into national policy development and process optimization. By linking thermodynamic rigor with engineering design and policy strategy, the research aims to support more coherent, efficient, and sustainable energy systems.

LITERATURE REVIEW

Thermodynamic Analysis: Energy, Exergy, and Entropy

Thermodynamic analysis provides the foundation for understanding energy systems. While first-law analysis ensures energy conservation, it fails to capture the degradation of energy quality during conversion processes. Exergy analysis overcomes this limitation by quantifying the maximum useful work obtainable from a system relative to its environment [5]. Entropy represents the degree of disorder and irreversibility, with its generation directly indicating the loss of useful energy potential and thermodynamic inefficiency [2]. The combined use of exergy and entropy enables a more comprehensive evaluation of system performance by identifying both the location and magnitude of inefficiencies.

Entropy Generation and Process Optimization

In process engineering, minimizing entropy generation is a key principle for improving efficiency. Bejan [2] demonstrated that reducing irreversibility enhances system performance. Similarly, exergy-based optimization methods identify critical inefficiencies in industrial processes and energy systems [6], allowing simultaneous consideration of energy quantity, quality, and irreversibility. However, the integration of entropy analysis into higher-level decision-making, such as policy design, remains limited.

Energy Policy and Thermodynamic Constraints

Energy policy research traditionally focuses on economic and environmental aspects, often neglecting thermodynamic constraints. Ignoring entropy generation and exergy destruction can lead to inefficient system configurations [3]. Recent studies emphasize incorporating physical principles into policy analysis to better evaluate system limits and opportunities [7,8]. Nevertheless, most national frameworks still rely on simplified energy metrics without considering energy quality and irreversibility.

Policy Misalignment and Research Gap

Policy misalignment occurs when objectives fail to reflect thermodynamic realities, promoting inefficient pathways with high irreversibility. This can undermine sustainability goals by increasing resource consumption [9]. Despite extensive research in engineering and policy, integration between these domains remains limited. This study addresses this gap by proposing a multidisciplinary framework that incorporates energy, exergy, and entropy into policy and process optimization for more sustainable energy systems.

METHODOLOGY

This study adopts an integrated analytical framework that combines energy, exergy, and entropy analysis to evaluate energy systems from both engineering and policy perspectives. The approach is designed to bridge micro-level process performance with macro-level policy outcomes, enabling a more comprehensive assessment of system efficiency and sustainability [5].

At the most basic level, system performance is first evaluated using conventional energy analysis based on the first law of thermodynamics. Energy efficiency is expressed as:

$$\eta_{energy} = \frac{E_{out}}{E_{in}} \qquad (1)$$

where E_{in} represents the total energy input and E_{out} denotes the useful energy output. Although widely used in both engineering and policy contexts, this metric does not account for differences in energy quality or the irreversibilities inherent in real processes [5].

To address this limitation, exergy analysis is introduced to evaluate the maximum useful work potential of energy flows. Exergy efficiency is defined as:

$$\eta_{exergy} = \frac{Ex_{useful}}{Ex_{input}} \qquad (2)$$

Exergy destruction within the system, which represents thermodynamic inefficiencies, is determined by:

$$Ex_{destroyed} = Ex_{input} - Ex_{output} - Ex_{loss} \qquad (3)$$

This formulation allows for the identification of performance losses that are not visible in energy-based analysis [5,6].

In addition to exergy analysis, entropy generation is used to quantify irreversibility. The total entropy generation within a system can be expressed as:

$$S_{gen} = \sum \frac{Q}{T} + S_{internal} \qquad (4)$$

where Q represents heat transfer at temperature T, and $S_{internal}$ accounts for internally generated entropy. The relationship between entropy generation and exergy destruction is given by the Gouy–Stodola theorem:

$$Ex_{destroyed} = T_0 \cdot S_{gen} \qquad (5)$$

where T_0 is the ambient temperature. This equation establishes a direct link between thermodynamic inefficiency and entropy production [2,5]. The analysis is conducted across multiple stages of energy systems, including energy conversion, distribution, and end-use processes. By applying these thermodynamic indicators, the study identifies critical points where exergy destruction and entropy generation are concentrated. To further enhance system performance, thermodynamic optimization principles are applied. Specifically, the methodology aims to minimize entropy generation while maximizing exergy efficiency. These criteria are widely recognized as fundamental principles in thermodynamic system optimization [2,6]. Finally, to connect thermodynamic analysis with policy evaluation, a comparative framework is developed. Existing policy-driven system configurations are assessed alongside thermodynamically optimized alternatives. This enables the identification of discrepancies between policy objectives and physical system performance, forming the basis for policy-relevant insights.

POLICY IMPLICATIONS

The findings of this study reveal significant limitations in current national energy policies, particularly in their reliance on energy-based performance indicators. While energy efficiency, defined as $\eta_{energy} = E_{out}/E_{in}$, is commonly used in policy frameworks, it fails to capture the qualitative aspects of energy use and the irreversibilities associated with real processes [3,8].
In contrast, exergy efficiency η_{exergy} and entropy generation S_{gen} provide a more accurate representation of system performance. High levels of entropy generation, as expressed through the relationship $Ex_{destroyed} = T_0 \cdot S_{gen}$, indicate substantial thermodynamic inefficiencies that are often overlooked in policy evaluation [2,5]. This leads to a structural misalignment between policy objectives and physical system realities.
This misalignment has important economic implications. Exergy destruction represents the loss of useful work potential, which can be interpreted as a hidden economic cost. Similarly, entropy generation reflects irreversible losses that reduce overall system efficiency. Previous studies have emphasized that neglecting energy quality in economic and policy analysis can distort resource allocation and long-term system performance [3,8].
From a policy perspective, these findings highlight the need to move beyond purely energy-based indicators toward a more comprehensive framework that includes exergy and entropy. Incorporating these thermodynamic metrics into policy design would allow for a more accurate evaluation of energy systems and support better alignment between policy goals and physical constraints [7].
Furthermore, thermodynamically informed policies can improve resource allocation by prioritizing systems with higher exergy efficiency and lower entropy generation. This approach would help avoid unnecessary energy conversions and reduce avoidable system losses, contributing to more effective and sustainable energy strategies [9].
More broadly, the integration of thermodynamic principles into policy frameworks contributes to a more rational and physically grounded approach to sustainable development. By aligning policy decisions with thermodynamic limits, it becomes possible to enhance both the efficiency and sustainability of national energy systems.

RESULTS AND DISCUSSION

The integrated analysis of energy, exergy, and entropy provides important insights into the performance of energy systems beyond conventional energy-based assessments. The results clearly indicate that while energy efficiency values may appear relatively high, exergy efficiency is significantly lower due to irreversible losses occurring throughout energy conversion and utilization processes. This discrepancy highlights the limitations of relying solely on first-law efficiency metrics in both engineering and policy contexts [5]. Across the analyzed system stages, substantial exergy destruction is observed, particularly in energy conversion processes where high-quality energy is degraded into lower-quality forms. This degradation is directly reflected in increased entropy generation, confirming the presence of significant thermodynamic irreversibilities. The relationship between exergy destruction and entropy generation, as described by the Gouy–Stodola theorem, reinforces the importance of considering entropy as a key indicator of system inefficiency [2].The results further demonstrate that process optimization based on thermodynamic criteria can significantly reduce inefficiencies. Systems designed to minimize entropy generation and maximize exergy efficiency exhibit improved performance compared to conventional configurations. These findings underline the importance of incorporating thermodynamic optimization principles into process engineering practices [6].
From a system-level perspective, the analysis reveals that policy-driven energy configurations often diverge from thermodynamically optimal solutions. In many cases, energy pathways promoted by policy frameworks involve multiple conversion stages, leading to cumulative exergy losses and increased entropy production. Although such pathways may align with emission reduction targets or energy supply strategies, they may be inefficient when evaluated from a thermodynamic standpoint.
This divergence reflects a broader issue of policy–thermodynamics misalignment. Policies typically prioritize indicators such as energy consumption and emissions, without adequately accounting for energy quality and irreversibility. As a result, systems that are thermodynamically suboptimal may still be considered favorable within existing policy frameworks. This misalignment becomes particularly evident when comparing energy-based efficiency η_{energy} with exergy-based efficiency η_{exergy}, where significant gaps indicate hidden inefficiencies. The implications of these findings extend beyond technical performance. Exergy destruction represents a loss of useful work potential, which can be interpreted as an economic loss, while entropy generation reflects irreversible system degradation. Therefore, thermodynamic inefficiencies translate into broader economic and sustainability challenges, reinforcing the need for more comprehensive evaluation criteria [3,8]. Furthermore, the results highlight the importance of system-level thinking in sustainable energy development. Isolated improvements in individual processes may not lead to overall system efficiency if they are embedded within inefficient energy pathways. A holistic approach that considers the entire energy chain is essential for minimizing cumulative losses and improving overall system performance.In summary, the results demonstrate that integrating energy, exergy, and entropy analysis provides a more accurate and physically grounded assessment of energy systems. The discussion emphasizes that current policy frameworks may inadvertently support inefficient configurations, and that incorporating thermodynamic principles into decision-making processes is essential for achieving truly sustainable and efficient energy systems.

CONCLUSIONS

This study has demonstrated that conventional energy-based approaches are insufficient for capturing the true performance and sustainability of energy systems. By integrating energy, exergy, and entropy analysis into a unified framework, the research highlights the critical role of thermodynamic principles in both process optimization and national policy development. The findings reveal a fundamental misalignment between current policy frameworks and thermodynamic realities. Policies that rely primarily on energy efficiency and emission-based indicators fail to account for energy quality and irreversibility, leading to significant exergy destruction and elevated entropy generation across energy systems. This misalignment not only reduces overall system efficiency but also introduces hidden economic costs through the loss of useful work potential and inefficient resource allocation.

By incorporating exergy and entropy into system evaluation, the study provides a more physically grounded understanding of energy efficiency. The results demonstrate that thermodynamic optimization through minimizing entropy generation and maximizing exergy efficiency—can significantly improve both process-level performance and system-wide sustainability outcomes. Moreover, the integration of these principles into policy design offers a pathway toward more coherent and effective energy strategies. From a policy perspective, the study underscores the necessity of moving beyond purely quantitative energy metrics toward a more comprehensive framework that reflects thermodynamic constraints. Embedding exergy and entropy indicators into national energy policies can enhance decision-making processes, align policy objectives with physical system limits, and support more efficient allocation of resources. More broadly, this research contributes to bridging the gap between engineering and policy disciplines. Sustainable development cannot be achieved solely through technological advancements or policy interventions in isolation; rather, it requires an integrated approach that is consistent with the fundamental laws of thermodynamics. By introducing a thermodynamically informed perspective into policy and strategy development, this study provides a foundation for more rational, efficient, and sustainable energy systems. Future research should further explore the operationalization of exergy and entropy-based indicators within policy frameworks, as well as their application across different national contexts and energy systems. Such efforts will be essential for advancing sustainable energy transitions that are not only environmentally sound but also physically and economically efficient.

References

[1] International Energy Agency (IEA), *World Energy Outlook*, 2023.
[2] A. Bejan, *Advanced Engineering Thermodynamics*, Wiley, 2016.
[3] R. U. Ayres and B. Warr, *The Economic Growth Engine*, Edward Elgar, 2009.
[4] J.-M. Jancovici, “Energy and Economic Growth,” 2012.
[5] I. Dincer and M. A. Rosen, *Exergy: Energy, Environment and Sustainable Development*, Elsevier, 2013.
[6] T. J. Kotas, *The Exergy Method of Thermal Plant Analysis*, Butterworth-Heinemann, 2013.
[7] J. M. Cullen and J. M. Allwood, “Theoretical efficiency limits for energy conversion devices,” *Energy Policy*, 2010.
[8] P. E. Brockway et al., “Energy rebound effects and economic growth,” *Ecological Economics*, 2019.
[9] F. W. Geels, “The multi-level perspective on sustainability transitions,” *Research Policy*, 2014.

PASSIVE COOLING OF PHOTOVOLTAIC CELLS USING CARBON NANO FIBER ENHANCED PHASE CHANGE MATERIAL

Hussain Shawish[1], Murat Özdenefe[1]*
[1] Eastern Mediterranean University, Department of Mechanical Engineering Famagusta, North Cyprus via Mersin 10, Turkey.
*Corresponding author e-mail: hussain.shawish@emu.deu.tr
Ref # PVT-01

ABSTRACT

This study investigates the use of carbon nanofiber-enhanced phase change material (NPCM) as a passive cooling system for photovoltaic (PV) panels under indoor conditions. RT25HC PCM was enhanced with 1% carbon nanofibers (CNF) to improve its thermal conductivity and filled into a finned aluminum container attached to the back of the PV panel. Indoor experiments were conducted using a 500 W halogen lamp to simulate solar radiation of approximately 700 W/m². The performance of three cases: reference PV (ref-PV), PV with pure PCM (PCM-PV), and PV with nano-enhanced PCM (NPCM-PV) was evaluated in terms of average panel temperature and electrical efficiency. The results showed that both PCM-based cooling systems reduced PV temperature and improved efficiency compared to the reference case. Faster charging rate is encountered in the NPCM compared to the pure PCM, resulting in lower PV temperature during melting process. The average panel temperature decreased by 9.97% with PCM and 8.27% with NPCM across the complete test period. Correspondingly, the average efficiency increased from 12.9% for the reference PV to 13.2% and 13.1% for the PCM-PV and NPCM-PV, respectively.

Keywords: Photovoltaics, Passive cooling, NPCM.

INTRODUCTION

Photovoltaic (PV) technology is widely used to harness solar energy by converting incoming solar radiation into electricity. During this conversion process, only a portion of the solar energy is transformed into electrical power, while a large part is converted into heat. The rise in PV cell temperature negatively affects their efficiency. It has been reported that the conversion efficiency decreases by about 0.4–0.65% for every 1°C increase in PV temperature [1].

To mitigate this temperature rise, many studies have investigated passive cooling systems using Phase Change Materials (PCM) attached to the back of PV panels. PCM can absorb excess heat during the day and release it later at night, helping to regulate panel temperature. However, the charging and discharging rates of PCM are often limited due to their low thermal conductivity. To overcome this limitation, researchers have explored the use of nanomaterials mixed with PCM to enhance thermal conductivity, forming nano-enhanced PCM (NPCM).

Rao et al. [2] prepared an NPCM by adding 1% graphene nanoplatelets and 1% carbon nano powder to OM34 PCM. The mixture was filled into an internally finned aluminum container attached to the back of the PV panel. Outdoor experiments showed a 28.5% improvement in PV efficiency with NPCM, compared to 22.5% with pure PCM. Similarly, Tuncer et al. [3] studied an NPCM prepared by mixing 1% iron nanoparticles with RT42 PCM and placing it in a finned aluminum box behind the PV panel. Their results showed a 17.93% reduction in average PV temperature with NPCM, compared to 14.48% with pure PCM. This temperature reduction led to a 15.51% increase in average PV efficiency using NPCM, compared to 11.12% with pure PCM. Kameswara Rao et al. [4] investigated another NPCM made by adding 0.9% graphene nanoflakes to HS36 PCM. Outdoor experiments showed a 25.25% increase in average PV efficiency with NPCM, compared to 20.1% with pure PCM. Phukaokaew et al. [5] examined PCM mixed with metal oxide nanoparticles, including aluminum oxide (Al_2O_3), copper oxide (CuO), and magnesium oxide (MgO), at 6% by weight. Indoor experiments under halogen lamps showed that MgO-based NPCM achieved the highest temperature reduction of 5.2°C, resulting in a 14.11% increase in electrical efficiency compared to the reference PV panel. Jamil et al. [6] compared two NPCMs: one prepared with 0.5% silica and the other with 0.5% carbon black mixed with PT58 PCM. Outdoor results showed greater temperature reduction by the carbon black-based NPCM.

The present study investigates the use of carbon nanofiber-enhanced PCM (NPCM) in a passive PV cooling system, which, to the best of the authors' knowledge, has not been previously examined. Hence, this work aims to contribute to the existing literature by evaluating the cooling performance of the CNF-NPCM.

METHODOLOGY

The PCM used in the current study is RT25HC with melting point of 25°C, thermal conductivity of 0.2 W/m.K and heat storage capacity of 230 kJ/kg. Carbon nano fibers (CNF) is utilized to enhance the thermal conductivity of the PCM. First the PCM is melted then around 1% concentration of CNF is added to the PCM. After that, nano material homogenizer is used to mix the CNF with the PCM. The prepared NPCM is then poured into an aluminum container equipped with internal fins. This container is attached to the back of the PV. In total around 2.7kg PCM is mixed with around 27g of CNF. Indoor experiments were performed to investigate average panel temperature and efficiency considering three cases: sole PV (ref-PV), PV with PCM-passive cooling system (PCM-PV) and PV with NPCM-passive system (NPCM-PV). 500W halogen lamp was used to simulate solar radiation generating around 700W/m² average radiation on the PV surface. 55W polycrystalline PV was utilized during the tests. Three k type thermocouples were attached at different point of the front surface of the PV to record the average surface temperature during the test which is used to assess the performance of the cooling systems. The experimental setup is shown in Fig. 1. In addition, the recorded average panel temperature is used to calculate the PV efficiency using Eq. (1) [7]:

$$\eta = \eta_{ref}\left[1 - \beta_{ref}\left(T_{PV} - T_{ref}\right)\right] \quad (1)$$

Where, η_{ref} is the PV module efficiency at reference conditions (equals to 14.50%), β_{ref} is the temperature coefficient (equal to 0.004 K^{-1} for crystalline silicon modules), T_{PV} is the recorded panels' temperature and T_{ref} is the temperature at reference conditions (equals to 25°C).

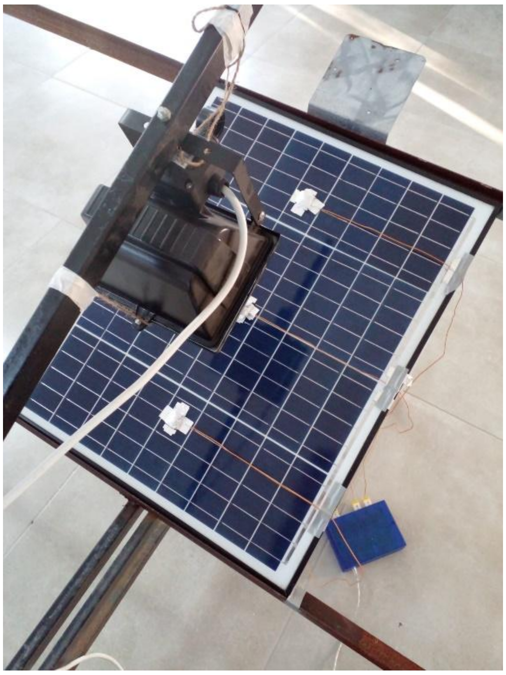

Fig. 1. Experimental setup.

RESULTS AND DISCUSSION

The recorded average PV temperature and calculated efficiency of the three considered cases, i.e. ref-PV, PCM-PV and NPCM-PV are presented in this section. These results are obtained from indoor tests that spanned 4 hours in a space with ambient temperature of around 20°C.

The average PV temperature of the three considered cases is presented in Fig. 2. As shown by the figure, lower temperatures are encountared in the PVs equipped with passive cooling systems. It took the ref-PV about 40 minutes to reach steady state temperature of around 54°C. by attaching passive cooling systems to the PV, this increase in temperature was delayed to about 240 minutes in the PCM-PV, and to about 200 minutes in the NPCM-PV. Moreover, the time average panel temperature for the entire test was around 52.62°C, 47.37°C (9.97% reduction), and 48.27°C (8.27% reduction) for the ref-PV, PCM-PV and NPCM-PV respectively. Despite the higher average PV temperature in NPCM-PV case compared to the PCM-PV, it can be seen from the figure that at early stage of the test the temperature of the PV with NPCM was lower compared to that with pure PCM. This indicates that heat was absorbed at a higher rate by the NPCM, which also resulted in a faster melting rate. Melting started in the NPCM at after around 30 minutes and stopped at around the 100th minute. This increase in melting rate is cause by the addition of CNF which forms heat transfer pathways inside the PCM matrix improving its thermal conductivity. On the other hand, although melting in the pure PCM started around the same time it stopped at around the 180th minute. The reason average temperature of the NPCM-PV was higher than PCM-PV is that despite the lower temperatures at the early stage, as the melting process is completed sooner in the NPCM this means it cannot absorb as much heat from the PV, so the PV temperature start to rise earlier as the radiation is continuously falling on the PV surface. The temperature in PCM-PV case was higher at early stage compared to the NPCM-PV, but this temperature was maintained for longer time as the melting process is slower in the pure PCM, and so the PV temperature started to rise at later time when the milting ended. Another reason that could have attributed to the encountered temperature trend is the reported slight drop in the latent heat of the PCM by the addition of nanomaterials [4][8]. It also worth noting that in the indoor conditions the radiation is kept constant at high value, but considering outdoor conditions the radiation will hit peak values around noon before dropping, so it could be the case that melting of the NPCM will complete at later time of the day when the radiation is dropping, and accordingly the PV temperature will not rise as much. The PV efficiency of the three considered cases is shown in Fig. 3. Following the PV temperature results, higher efficiency values are achieved in the PVs equipped with passive cooling systems. The average efficiency for the ref-PV, PCM-PV and NPCM-PV was around 12.9%, 13.2% and 13.1% respectively.

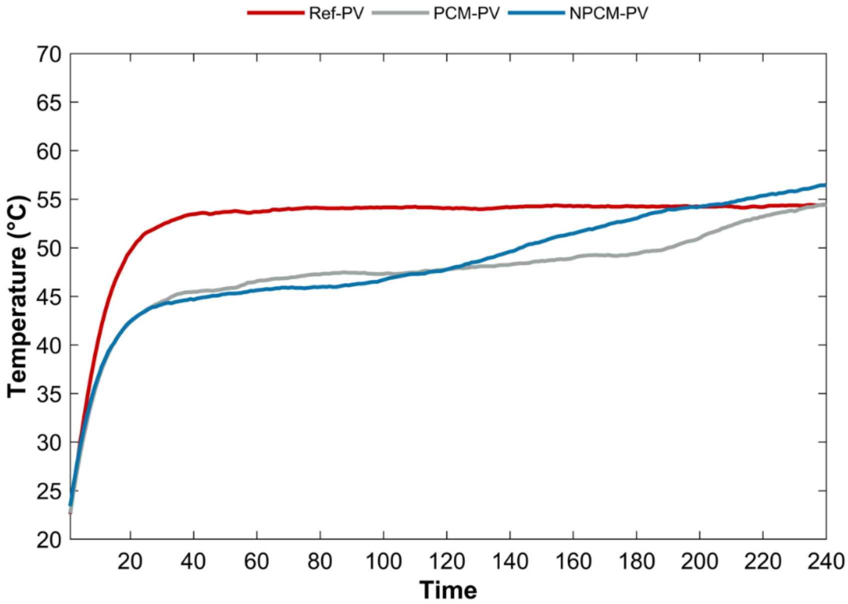

Fig. 2. Average PV temperature for the considered cases.

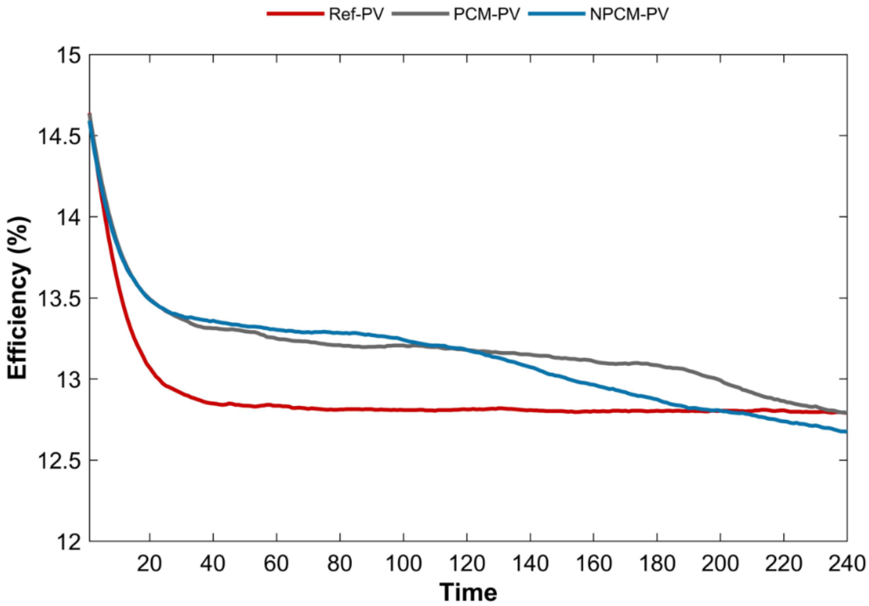

Fig. 3. PV efficiency for the considered cases.

CONCLUSIONS

In this study, the performance of a nano-enhanced PCM passive cooling system for PV panels was experimentally evaluated under indoor conditions and compared with pure PCM cooling and a reference PV panel without cooling. RT25HC PCM was enhanced with 1% carbon nanofibers and placed in a finned aluminum container attached to the back of the PV panel. A halogen lamp was used to simulate solar radiation, and the thermal and electrical performance of the systems was analyzed. The main findings are summarized as follows:

- Both PCM and NPCM passive cooling systems reduced the average PV panel temperature compared to the reference case.
- The PCM-PV case achieved the highest temperature reduction (9.97%), followed by the NPCM-PV case (8.27%).
- The rise in panel temperature was significantly delayed in both cooling cases compared to the reference PV.

- Higher electrical efficiencies were achieved with passive cooling, with average efficiencies of 13.2% for PCM-PV and 13.1% for NPCM-PV, compared to 12.9% for the reference PV.
- Although lower temperatures are encountered in the NPCM-PV case early in the test, the PV temperature of the PV starts to rise sooner as the melting process completes faster. This suggests the need for the optimization of the PCM amount to benefit from the lower PV temperature associated with faster charging rate.

REFERENCES

[1] T. Ma, H. Yang, Y. Zhang, L. Lu, and X. Wang. 2015. Using phase change materials in photovoltaic systems for thermal regulation and electrical efficiency improvement: A review and outlook. *Renew. Sustain. Energy Rev.*, vol. 43, pp. 1273–1284.

[2] D. K. Rao, P. Sundaram, K. Selvakumar, D. V. Krishna, A. Sathishkumar, and S. C. Kim. 2025. Performance assessment of nano-enhanced organic PCM embedded in heat sinks for PV panel thermal management under outdoor conditions. *Appl. Therm. Eng.*, vol. 280, no. P1, p. 128140.

[3] A. D. Tuncer, E. Y. Gürbüz, İ. Şahinkesen, A. Georgiev, and A. Keçebaş. 2024. Passive cooling of photovoltaic panels with latent heat storage unit: Analyzing the effects of using fins and iron nanoparticles on the performance, economy and environmental impact. *Energy*, vol. 288.

[4] D. Kameswara Rao, K. Sudhakar Reddy, and V. V. Subba Rao. 2024. Influence on solar PV performance integrated with heat sinks and nano-enhanced phase change material. *Proc. Inst. Mech. Eng. Part E J. Process Mech. Eng.*

[5] W. Phukaokaew, A. Suksri, K. Punyawudho, and T. Wongwuttanasatian. 2024. Thermal management of photovoltaic module using affordable organic phase change material combined with nano metal oxide particles enhancer. *Heliyon*, vol. 10, no. 24, p. e41054.

[6] F. Jamil, M. Khiadani, H. M. Ali, M. A. Nasir, and S. Shoeibi. 2023. Thermal regulation of photovoltaics using various nano-enhanced phase change materials: An experimental study. *J. Clean. Prod.*, vol. 414, no. May, p. 137663.

[7] K. Kant, A. Shukla, A. Sharma, and P. H. Biwole. 2016. Thermal response of poly-crystalline silicon photovoltaic panels: Numerical simulation and experimental study. *Sol. Energy*, vol. 134, pp. 147–155.

[8] Z. Said *et al.* 2024. Nano-enhanced phase change materials: Fundamentals and applications. *Prog. Energy Combust. Sci.*, vol. 104, no. May, p. 101162.

THERMAL MANAGEMENT OF PV PANELS USING MACHINE LEARNING FOR OPTIMAL PCM TYPE AND THICKNESS SELECTION

Wisam K. Hussam[1], Mohammed. Abdul-Niby[2], Abeer A. Al Anazi[1], Omar A. Yousef[1], Gregory J. Sheard[3]*
[1] Australian University, College of Engineering, Mechanical Engineering Department, West Mishref, Safat 13015, Kuwait
[2] Australian University, College of Engineering, Electrical and Electronic Engineering Department, West Mishref, Safat 13015, Kuwait
[3] Monash University, Department of Mechanical and Aerospace Engineering, Melbourne, Clayton 3800, Australia
*Corresponding author e-mail: w.alsaadi@au.edu.kw
Ref # PVT-02

ABSTRACT

Elevated operating temperatures significantly reduce the performance of photovoltaic (PV) panels, motivating the use of phase change materials (PCMs) for passive thermal management. This study investigates the optimal selection of PCM type and thickness using a machine-learning-based framework under both hot and cold climatic conditions. Four PCMs (RT28, OM37, OM42, and RT54) with thicknesses ranging from 20 to 50 mm are evaluated. A dynamic PV–PCM thermal model is used to generate training data, and several machine-learning algorithms are assessed for PV temperature prediction. Among them, Gaussian Process Regression (GPR) with a Matern 5/2 kernel demonstrates superior accuracy, achieving coefficients of determination exceeding 0.99. The trained GPR model is then applied to identify optimal PCM configurations by minimizing peak PV temperature during critical daytime hours. The results reveal a strong seasonal dependence of PCM performance. During hot months, OM37 achieves the lowest PV temperature at a moderate thickness of 30 mm, whereas higher-melting PCMs (OM42 and RT54) require a thickness of 50 mm for effective cooling. In contrast, during cold months, RT28 performs best with a 20 mm thin layer, with limited benefit from increasing thickness. These findings confirm that climate-specific PCM design is essential for effective PV thermal management.

Keywords: Thermal management, PCM, Machine learning, Energy efficiency, optimization

INTRODUCTION

Photovoltaic (PV) modules are susceptible to operating temperature, and excessive heat accumulation reduces electrical efficiency, accelerates material degradation, and shortens service life. This issue is particularly critical in regions characterized by high solar irradiance and elevated ambient temperatures, where PV modules often operate well above their optimal temperature range [1]. Consequently, effective thermal management has become an essential aspect of PV system design.

Passive thermal management using phase change materials (PCMs) has attracted considerable attention due to its simplicity and its ability to absorb excess thermal energy without requiring external power. Several studies demonstrated that integrating PCMs with PV modules can significantly limit temperature rise and enhance electrical performance by maintaining the module temperature closer to optimal operating conditions [2,3].

The effectiveness of PCM-based cooling depends strongly on thermophysical properties such as melting temperature, latent heat, and thermal conductivity, as well as PCM layer thickness [4]. Improper PCM selection may lead to premature melting or insufficient heat absorption under varying climatic conditions.

In addition, recent studies have explored enhancing PCM thermal performance through the development of composite materials and the incorporation of high thermal conductivity additives. Nevertheless, determining optimal PCM configurations across different materials, thickness, and climatic conditions using simulation approaches can be computationally intensive [5].

Machine learning offers an efficient alternative by capturing complex relationships between environmental conditions, PCM properties, and PV thermal behaviour. Therefore, this study proposes a machine-learning-based framework to determine the optimal PCM type and thickness for PV thermal management under both hot and cold climatic conditions.

MATERIALS AND METHODS

Figure 1 illustrates the PV–PCM configuration analysed in this study, comprising a glass cover, PV cells, a PCM layer, and rear insulation. Heat exchange occurs via convection and radiation at both the top and back surfaces, while conduction transfers heat from the PV module to the PCM layer.

The electrical efficiency of the PV module, expressed as a function of temperature, is given by [6] as

$$\eta_{pv} = \eta_{ref}\left[1 - \gamma_{ref}\left(T_{pv} - T_{ref}\right)\right],$$

where η_{ref} is the reference efficiency under standard test conditions (STC), γ_{ref} is the temperature coefficient, and T_{PV} is the PV temperature.

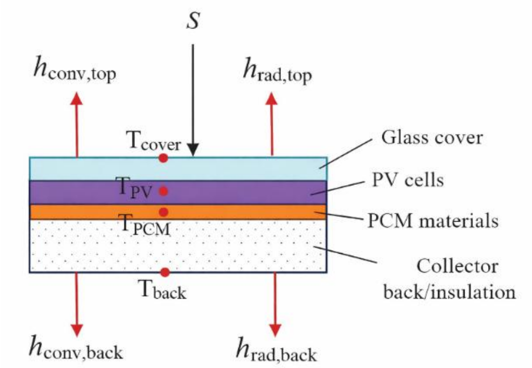

Fig. 1. Schematic of the PV–PCM module showing incident solar irradiance S, heat transfer at the top and back surfaces, and temperature nodes for the glass cover, PV cells, PCM layer, and back insulation.

Four PCMs (RT28. OM37, OM42, and RT54) with different melting temperatures were evaluated with thicknesses ranging from 20-50 mm. The thermophysical properties of the PCM were obtained from previous experimental studies [6,7]. Simulation data generated from the PV-PCM thermal model were used to train several machine-learning algorithms, including bagged trees, boosted trees, and Gaussian Process Regression (GPR). Model performance was evaluated using RMSE, MAE, and R^2.

RESULTS AND DISCUSSION

Seasonal Variation of Solar Irradiance and Ambient Temperature

Figure 2 illustrates the seasonal variation of global horizontal irradiance and ambient temperature. During summer months, high irradiance combined with elevated ambient temperatures increases PV operating temperature significantly. In contrast, winter months exhibit lower temperatures, reducing thermal losses and improving PV efficiency.

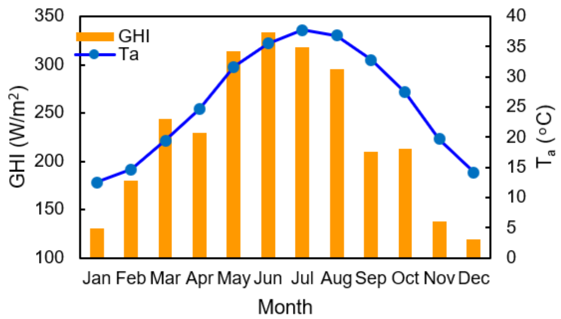

Fig. 2. Monthly average solar Irradiance and ambient temperature profiles highlighting seasonal climatic variations.

Effect of PCM Type and Thickness on PV Temperature Profile

Figure 3 compares PV temperature profiles for bare and PCM-integrated configurations under peak summer conditions. The bare PV module exhibits the highest operating temperature with a pronounced peak around solar noon. Integrating PCMs reduces PV temperature significantly, and the cooling effect increases with PCM thickness. Thin PCM layers (20–30 mm) provide partial temperature reduction but become less effective during peak hours due to early melting. Thicker PCM layers (40–50 mm) provide sustained cooling by increasing latent heat storage capacity. PCMs with melting temperatures closer to typical PV operating temperatures, particularly OM37 and OM42, achieve greater peak temperature reduction.

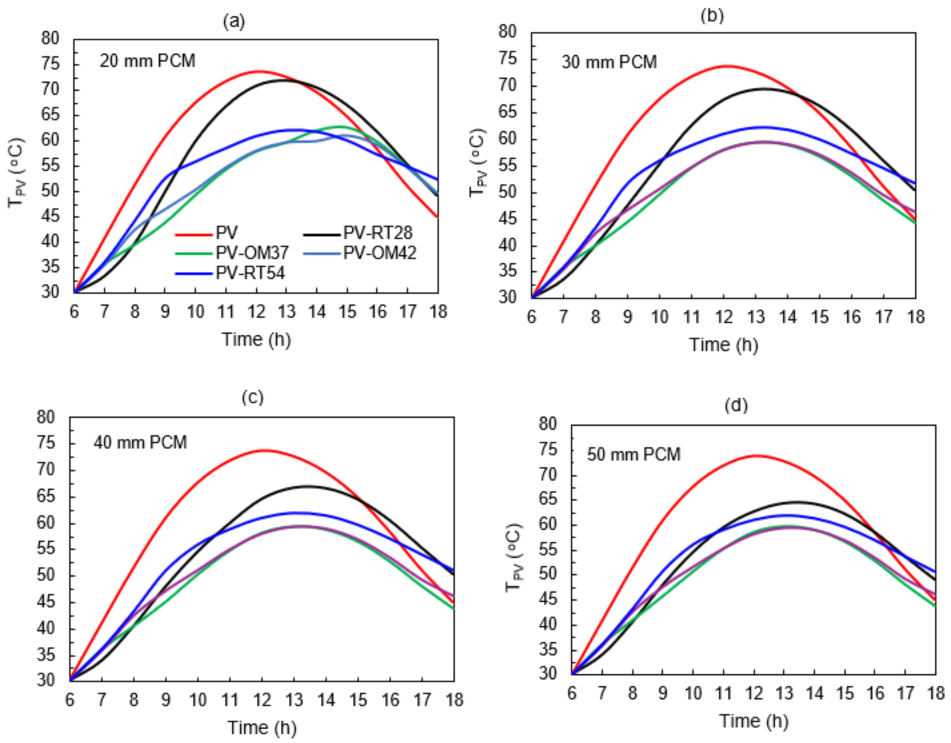

Fig. 3. PV temperature profiles for a bare module and PCM-integrated configurations with different PCM types and thicknesses under peak summer conditions: (a) 20 mm, (b) 30 mm, (c) 40 mm, and (d) 50 mm.

Machine Learning Prediction Performance

Several machine-learning models were evaluated to predict PV temperature. Among them, Gaussian Process Regression with a Matern 5/2 kernel demonstrated the highest accuracy, achieving RMSE values below 0.52 °C for hot months and 0.32 °C for cold months. As shown in Fig. 4, the predicted temperatures exhibit strong agreement with the simulation results, confirming the reliability of the GPR model for predicting PV temperature under varying climatic conditions.

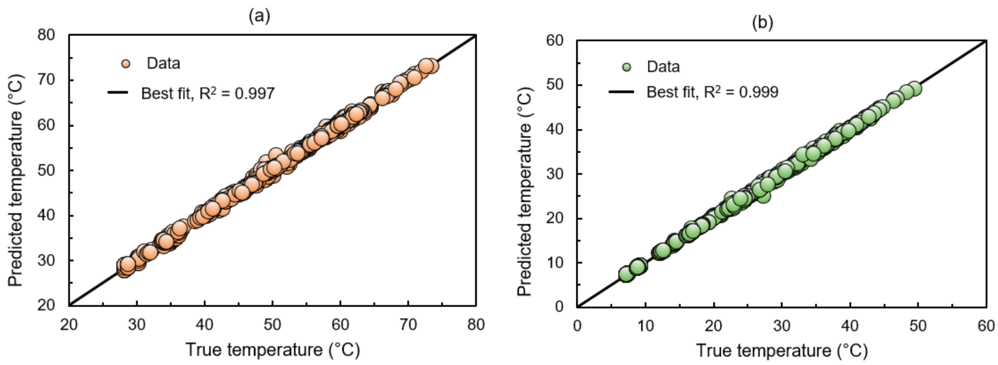

Fig. 4. Scatter plot of the Matern 5/2 Gaussian Process Regression (GPR) machine-learning model–predicted PV temperature versus numerical simulation data for (a) hot and (b) cold months.

Optimal PCM Type and thickness selection using Machine Learning

The trained GPR model was used to determine optimal PCM configurations by minimizing peak PV temperature between 10:00 and 16:00. During hot months, OM37 with a thickness of 30 mm achieved the lowest peak PV temperature (60 °C). Higher melting-temperature PCMs such as OM42 and RT54 required thicker layers (50 mm) to provide sufficient thermal storage. During colder months, RT28 performed best with a thinner 20 mm layer, achieving the lowest PV temperature due to its lower melting temperature. These results demonstrate that PCM performance is strongly climate dependent and that no single PCM configuration is optimal throughout the year.

Table 1: Optimal PCM thickness and maximum PV temperature predicted using the Matern 5/2 GPR model for hot and cold months.

PCM	Hot months		Cold months	
	Thickness (mm)	TPV (°C)	Thickness (mm)	TPV (°C)
RT28	50	64.53	20	35.94
OM37	30	59.97	50	41.25
OM42	50	60.24	50	41.50
RT54	50	62.82	50	43.57

CONCLUSIONS

This study proposed a machine-learning-based framework for optimizing phase change material (PCM) type and thickness to improve the thermal management of photovoltaic (PV) panels under varying climatic conditions Gaussian Process Regression with a Matern 5/2 kernel demonstrated excellent prediction accuracy for PV temperature. Results indicate that optimal PCM configuration is strongly season dependent. OM37 with a thickness of 30 mm provides the most effective cooling during hot months, while RT28 with a 20 mm layer performs best during colder conditions. The proposed approach enables rapid identification of climate-specific PCM designs while significantly reducing computational effort compared with conventional numerical optimization.

Future work will focus on experimental validation of the proposed machine-learning framework using measured PV temperature data under real operating conditions.

ACKNOWLEDGEMENT

The authors gratefully acknowledge the support provided by the Mechanical Engineering Department at the Australian University of Kuwait.

REFERENCES

[1] Huang MJ, Eames PC and Norton B. 2004. Phase change materials for limiting temperature rise in building integrated photovoltaics. Solar Energy 80:1121–1130.

[2] Hasan A, McCormack SJ, Huang MJ and Norton B. 2010. Evaluation of phase change materials for thermal regulation enhancement of building integrated photovoltaics. Solar Energy 84:1601–1612.

[3] Hasan A, Sarwar J, Alnoman H and Abdelbaqi ES. 2017. Yearly energy performance of a photovoltaic–phase change material (PV–PCM) system in hot climate. Solar Energy 146:417–429.

[4] Skoplaki E and Palyvos JA. 2009. On the temperature dependence of photovoltaic module electrical performance. Solar Energy 83:614–624.

[5] Sharifzadeh E, Rahimi M, Azimi N and Abolhasani M. 2024. Thermal management of photovoltaic panels using phase change materials and hierarchical ZnO/expanded graphite nanofillers. Energy 306:132324.

[6] Ranawade V and Nalwa KS. 2023. Multilayered PCMs-based cooling solution for photovoltaic modules: Modelling and experimental study. Renewable Energy 216:119136.

[7] Amalu EH and Fabunmi OA. 2022. Thermal control of crystalline silicon photovoltaic (c-Si PV) module using docosane phase change material (PCM) for improved performance. Solar Energy 234:203–221.

ENERGY AND EXERGY ASSESSMENT OF A SOLAR PTC-DRIVEN POLYGENERATION SYSTEM FOR POWER, COOLING, FRESHWATER AND HYDROGEN PRODUCTION

Berke Eyyamoglu[1]; Keyvan Bahlouli[1], Idowu Ibukun[1], David Ogbemudia[1], Victor Adebayo[2]*
[1]Energy System Engineering Program, Mechanical Engineering Department, Faculty of Engineering, Cyprus International University, Nicosia, N. Cyprus via Mersin 10, Türkiye
[2] Mechanical engineering department, Middle East Technical University, Northern Cyprus Campus.
*Corresponding author e-mail: beyyamoglu@ciu.edu.tr
Ref # REP-01

ABSTRACT

This study proposes a novel solar-integrated multigeneration system and addresses the thermodynamic analysis of the system. The proposed system utilizes existing solar energy via parabolic collectors to integrate an organic Rankine cycle for electricity generation, a single-effect absorption refrigeration system for cooling production, a humidification-dehumidification desalination unit for fresh water production, and a proton exchange membrane unit for hydrogen production. One of the main objectives of the study is to examine the effects of the ORC pressure ratio and different working fluids on the useful outputs of the system. Accordingly, five different organic working fluids (r245fa, toluene, R123, n-octane and n-butane) are considered to examine their effects on the system. The results show that increasing the ORC pressure ratio increases the net power output and hydrogen production. However, with the increase in ORC power output, there is a decrease in freshwater and cooling capacity due to the transfer of energy to the ARS and the availability of waste heat energy in the ORC condenser. While fluids with high critical temperatures, such as N-octane and toluene, provide relatively higher power output, fluids with lower critical temperatures, such as R245fa and n-butane, offer advantages in cooling capacity and fresh water production.

Keywords: Sustainable Energy, Solar, Hydrogen, Freshwater, Clean Energy

INTRODUCTION

Energy demand, one of the most critical issues in today's world, is increasing day by day due to growth in population, urbanization, and industrialization. Furthermore, considering sustainability issues and the depletion of non-renewable resources, it is essential to obtain sufficient amounts of eco-friendly, clean, and affordable energy [1,2]. Among renewable energy sources, solar energy, which has the highest potential to meet the world's energy demand, plays a vital role in achieving sustainable energy by reducing the consumption of primary energy sources [3]. Utilizing the potential of solar energy and integrating it into polygeneration systems that produce multiple useful outputs can yield sustainable, economical, and highly efficient results [3–5]. Among all concentrating solar thermal technologies, parabolic trough collectors (PTCs) are considered one of the most practical and feasible options for meeting medium-temperature applications at temperatures between 150°C and 400°C [4]. ORC systems, which are at the forefront of medium-range applications due to their high reliability, low maintenance costs, and superior efficiency, are widely discussed in the literature in their combinations with PTCs [6–9]. The low-grade heat discarded from ORC condensers can be effectively used to operate an absorption refrigeration system (ARS) for cooling production or in humidification-dehumidification (HDH) desalination systems for freshwater production. Furthermore, excess electrical energy produced can be converted into hydrogen via proton exchange membrane (PEM) electrolysis, thus enabling energy storage in chemical form. There are several studies that examine polygeneration systems driven by solar energy, with various configurations and different useful outputs, from a thermodynamic and thermoeconomic assessment [1,5]. Khalid and Kumar [8] proposed a new PTC-based polygeneration system to meet the electricity, cooling, hydrogen, and fresh water needs of a residential area and evaluated it from a thermodynamic perspective. The proposed system drives the ORC unit via parabolic collectors, and the generated electrical energy is directed to a vapor compression cycle (VCC) for cooling and an electrolyzer for hydrogen production. Fresh water is obtained by freezing and desalination using cooling produced by the VCC. The researchers reported the energy and exergy efficiencies of the system as 17.5% and 10.9%, respectively, based on their thermodynamic analysis. In another similar study, Almohammadi et al. [7] proposed a trigeneration system powered by solar energy, aiming to achieve useful outputs of cooling power and fresh water. In this proposed system, which uses an ORC unit for power generation, the waste heat from the ORC condenser feeds both the desiccant cooling system and the HDH system, thus providing both cooling and fresh water. In their parametric analysis, the authors considered six different organic working fluids, as well as parameters such as ORC evaporation pressure and ORC turbine inlet temperature, to examine their effects on the system's performance. According to the study results, the highest useful outputs were obtained with cyclohexane fluid, and it was reported that the system outputs increased with increasing turbine inlet temperature and evaporation pressure. Although previous studies have addressed performance evaluations by proposing multigeneration systems in various configurations, a comprehensive thermodynamic evaluation of multigeneration systems that simultaneously produce cooling, electricity, fresh water, and hydrogen is still needed.In particular, investigating the effects of different working fluids on system performance and calculating the exergy destruction rates of each system component to identify irreversible processes in the system are vital for performance and economic improvement. Therefore, this study proposes a solar-powered multigeneration system integrating

ORC, absorption cooling, HDH desalination, and PEM electrolysis, and addresses a comprehensive energy and exergy analysis of this system.

SYSTEM DESCRIPTION

Figure 1 shows a schematic diagram of the proposed solar-driven polygeneration system. The proposed system consists of parallel-connected PTCs, a stratified thermal storage tank to reduce temperature fluctuations, an ORC unit for power generation, a single effect ARS unit for cooling effect, an HDH desalination system for fresh water production, and a PEM electrolyzer for hydrogen production. The heat transfer fluid used in the collector loop is Syltherm 800. The heat transfer fluid (HTF) exiting from the bottom of the tank enters the collector circuit, absorbs solar radiation, increases its temperature, and is then directed to the TES tank where the thermal energy is stored as sensible heat. The hot HTF exiting the top of the storage tank is directed to the ORC's heat recovery system (HRS). The hot HTF provides the necessary thermal energy for the ORC's working fluid, causing the fluid to vaporize and expand in the turbine, thus enabling the system to generate electricity. The organic vapor, exiting the turbine at low pressure, enters the recuperator, transferring its heat to the high-pressure fluid exiting the pump and preheating the fluid before it enters the HRS. The HTF at the HRS outlet then enters the generator of the single-effect ARS system using a LiBr-H2O fluid pair, providing the cooling production of the cycle. Then the HTF returns to the bottom of the storage tank, closing the PTC-ORC-ARS cycle. The waste heat from the ORC condenser runs the HDH desalination system. In the dehumidifier, cold saline entering the condenser via a heat exchanger increases its temperature and is sprayed onto the packing material in the humidifier. This packing material then comes into contact with the relatively cool air from the dehumidifier, causing the water to evaporate and humidifying the air. The humid and warm air then enters the dehumidification unit, where it cools by transferring its heat to surfaces at lower temperatures and is partially condensed to produce fresh water. Finally, while a fraction of the net electrical energy produced by the ORC goes to households, another portion goes to the PEM electrolyzer where water is separated into oxygen and hydrogen with the help of electricity. This hydrogen energy is considered a useful output and contributes to the overall energy and exergy efficiency of the system.

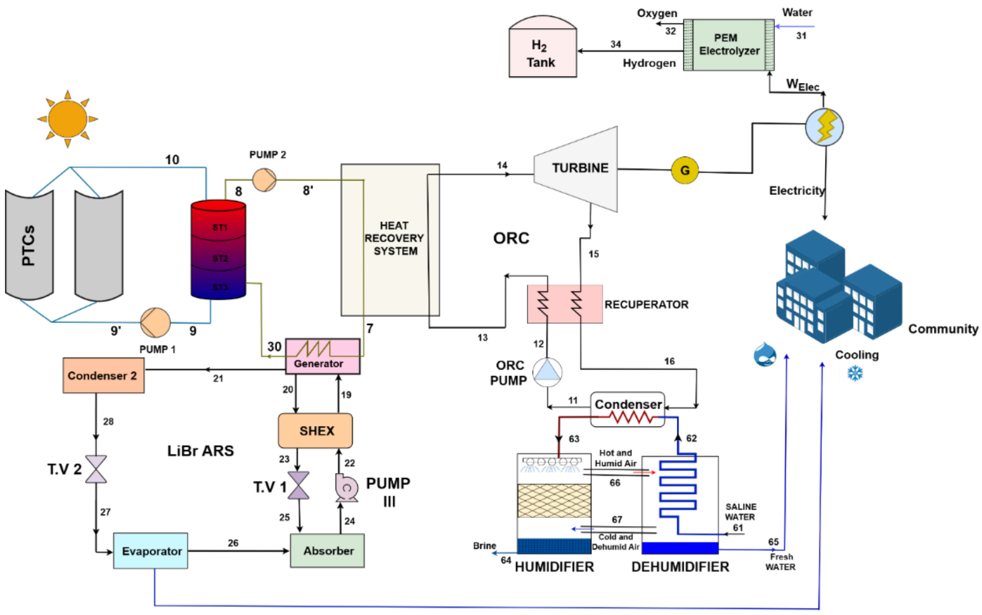

Fig.3. Schematic diagram of the proposed solar-driven polygeneration system

THERMODYNAMIC MODELING AND ANALYSIS

In this study, the Engineering Equation Solver (EES) software is used to assess the thermodynamic performance of the solar-integrated polygeneration system. The thermodynamic properties of the ORC working fluids, seawater, and moist air were obtained from EES's built-in libraries. Additionally, five different organic working fluids (r245fa, toluene, R123, n-octane and n-butane) were evaluated within the ORC subsystem to investigate their effects on system performance. The selection of working fluids is based on their thermodynamic suitability for medium-temperature solar energy applications. Table 1 presents several of the input parameters required for modeling.

The system is analyzed using a steady-state control volume formulation. The overall system energy and exergetic efficiency is defined as follows [1,3]:

$$\eta_{en} = \frac{\dot{Q}_{cool}+\dot{W}_{net}+\dot{m}_{H_2}LHV_{H2}}{\dot{Q}_{sol}} \quad (1)$$

$$\eta_{ex} = \frac{\dot{E}_{cool}+\dot{W}_{net}+m_{H_2}\bar{e}_{ch,H2}+\dot{m}_{fw}e_{fw}}{\dot{E}_{sol}} \quad (2)$$

Where $\dot{m}_{H_2}$ and $\dot{m}_{fw}$ denote produced hydrogen and freshwater mass flow rate, respectively, while $\bar{e}_{ch,H2}$ and e_{fw} represent specific chemical exergy of hydrogen (kJ/kg) and freshwater specific exergy (kJ/kg), respectively. The performance criterion of the HDH unit is determined by the Gain Output Ratio (GOR), which is the ratio of latent heat to the thermal energy supplied to the HDH unit [1].

$$GOR = \frac{\dot{m}_{fw}h_{fg}}{\dot{Q}_{con}} \quad (3)$$

Table 6: Several input parameters for system modelling [1,3,4,6]

Description	**Parameter**	**Value**	**Description**	**Parameter**	**Value**
Reference temperature	(T_0)	25 °C	HDH effectiveness	ε_{HDH}	0.85
Reference pressure	(P_0)	101.3 kPa	PEM operating temperature	T_{PEM}	353 K
Solar irradiation	(G_b)	800 W/m²	Active cell area	A_{act}	0.05 m²
No of collector rows	N_{col}	20	Number of cells	N_{cell}	100
ORC pressure ratio	PR	0.8	Anode pre-exponential factor	j_a^{ref}	1.7x10⁵
ORC condenser temperature	T_{con}	90 °C	Cathode pre-exponential factor	j_c^{ref}	4.6x10³
Seawater salinity	-	35 g/kg	Fraction of net electricity uses for PEM	f_{pem}	0.2
HTF mass flow rate at single module	$\dot{m}_{HTF}$	0.8 kg/s	Lower Heating Value	LHV	120 MJ/kg

RESULTS AND DISCUSSION

In the reference case, the key performance outputs of the system using Toluene as the working fluid are presented in Table 2. It provides approximately 143 kW of net power output and has an exergy efficiency of 19.89% and an energy efficiency of 65%. In this study, to examine the effects of the proposed system on useful outputs, the pressure ratio, representing the ratio of high pressure in the ORC to the critical pressure of the working fluid, is investigated in the range of 0.7-0.9, together with five different organic working fluids. Figure 2 illustrates the effects of these parameters on the system's net power, cooling, hydrogen, and freshwater production outputs. Figure 2a shows that the net power output tends to increase with increasing pressure ratio in all fluid cases examined. Due to their relatively high critical temperatures to the heat source, fluids such as n-octane and toluene yield higher power outputs, while fluids with relatively lower critical temperatures, such as R245fa and n-butane, have lower power generation outputs. Toluene and n-octane achieve a net electrical output of approximately 143 kW, while R245fa and n-butane remain below 50 kW. However, the increased pressure ratio leads to a decrease in cooling capacity for fluids such as n-octane and toluene, as more heat is transferred to the ORC (see Figure 2b). Figure 2c shows that the pressure ratio is directly proportional to hydrogen production. This is directly related to the higher net power availability for electrolysis. Conversely, freshwater production decreases as the net power output of the ORC increases due to the availability of waste heat in the condenser (see Figure 2d).

Table 7: Key performance outputs of the proposed system

Performance of the System (Reference case)	**Value**	**Performance of the System (Reference case)**	**Value**
Cooling output (kW)	560	Hydrogen Production (kg/h)	0.64
Net power output (kW)	143.3	GOR	1.69
Energy efficiency (%)	65.5	Exergy efficiency (%)	19.89
Freshwater Production (kg/s)	0.38	Total exergy destruction rate (kW)	1265

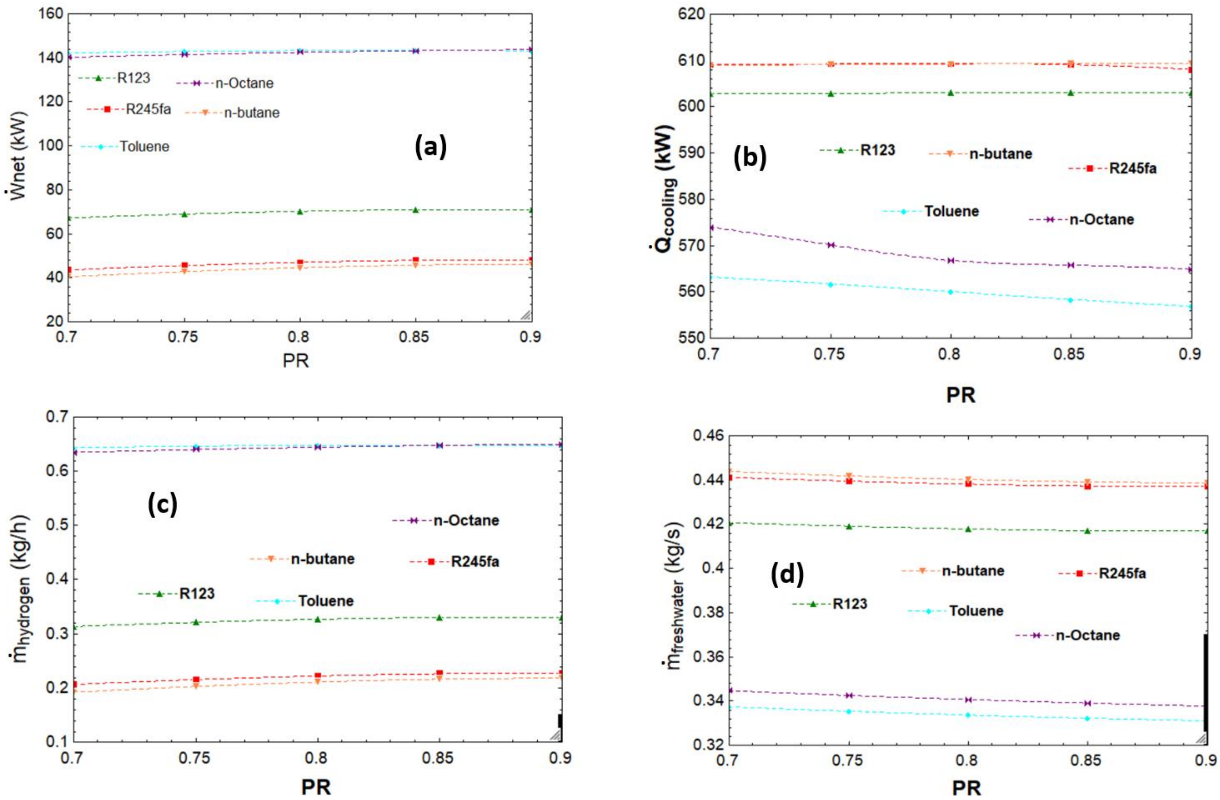

Fig. 4. Effects of ORC pressure ratio and organic fluids to the system's a) Net power b) Cooling Capacity c) hydrogen production d) Fresh water production

CONCLUSIONS

This study proposes a novel solar-integrated polygeneration system and addresses its comprehensive thermodynamic analysis. The proposed system aims to provide simultaneous electricity, cooling, hydrogen, and fresh water production for a community by integrating an ORC unit, ARS, PEM electrolyzer, and HDH desalination system. This study investigated the effect of ORC pressure ratio on a polygeneration system for different working fluids. R245fa and n-butane offer more balanced cooling and desalination performance, while fluids which has higher critical temperatures, like n-octane and toluene, have advantages in the production of higher electricity and hydrogen as well as in performance criteria like exergy efficiency. Accordingly, the working fluid selection should be made according to the intended operational purpose of the system.

REFERENCES

[1] Elghamry, R., and Hassan, H., 2022, "Two-Objective Optimization of a Hybrid Solar-Geothermal System with Thermal Energy Storage for Power, Hydrogen and Freshwater Production Based on Transcritical CO2 Cycle," Renew. Energy, 183, pp. 51–66.

[2] Sharifishourabi, M., Dincer, I., and Mohany, A., 2024, "Performance and Environmental Impact Evaluations of a Novel Multigeneration System with Sonic Hydrogen Production and Energy Storage Options," J. Energy Storage, 78(1), p. 109987.

[3] Eyyamoglu, B., and Bahlouli, K., 2025, "Performance and Economic Analysis of a Nanofluid-Based Solar-Driven Trigeneration System for a Residential Building in Cyprus," Appl. Therm. Eng., 277, p. 127001.

[4] Nwajei, D. M., and Bahlouli, K., 2026, "Dynamic Simulation of a Solar Based Organic Rankine Cycle for Working Fluid Selection in a Hybrid Microgrid: A Location-Based Performance Assessment," Energy Convers. Manag., 352, p. 121061.

[5] Karapekmez, A., and Dincer, I., 2021, "Development of a Multigenerational Energy System for Clean Hydrogen Generation," J. Clean. Prod., 299(11), p. 126909.

[6] Gogoi, T. K., and Saikia, S., 2019, "Performance Analysis of a Solar Heat Driven Organic Rankine Cycle and Absorption Cooling System," Thermal Science and Engineering Progress.

[7] Almohammadi, B. A., Al-Zahrani, A., Refaey, H. A., Attia, E. A., and Fouda, A., 2023, "Energy Analysis of a Novel Solar Tri-Generation System Using Different ORC Working Fluids," Case Studies in Thermal Engineering, 45, p. 102918.

[8] Khalid, F., and Kumar, R., 2023, "Thermodynamic Assessment of a New PTC Operated Polygeneration System for Fresh Water, Cooling, Electricity and Hydrogen Production for a Residential Community," Int. J. Hydrogen Energy, 48(99), pp. 38991–39001.

[9] Khalid, F., and Akbulut, U., 2025, "Exergoeconomic Evaluation and Optimization of a Solar-Powered Polygeneration System Producing Freshwater, Electricity, Hydrogen, and Cooling," Int. J. Hydrogen Energy, 140, pp. 931–940.

DESIGN OF A RENEWABLE ENERGY AND WASTE MANAGEMENT SYSTEM FOR HYDROGEN, FRESH WATER AND OXYGEN PRODUCTION

[1]Ayse Sinem Meke, [1]Ibrahim Dincer and [2]Ali Khalvati*
[1] Clean Energy Research Laboratory (CERL), Faculty of Engineering and Applied Science, Ontario Tech. University, 2000 Simcoe Street North, Oshawa, Ontario L1G 0C5, Canada
[2] Viona Consulting INC., Agro-Environmental Innovation and Technology, Research and Development Company, Thornhill, Ontario L3T 0C6, Canada
*Corresponding author e-mail: ayse.meke@ontariotechu.net

Ref # REP-03

ABSTRACT
This study introduces a novel waste-integrated multigeneration system that simultaneously produces electricity, green hydrogen, freshwater, high-purity oxygen, and district heating by utilizing municipal wastewater sludge, wind energy, and recovered thermal energy. The system is modeled using detailed mass, energy, and exergy balance equations, achieving 42% energy and 52% exergy efficiencies under steady-state conditions. It annually produces 463.18 kt of hydrogen, 9.21 kt of freshwater, and 3674.28 kt of oxygen, which supports a coupled fish-farming unit for sustainable aquaculture. Overall, the system demonstrates strong alignment with circular economy and sustainability principles by integrating waste management, energy production, water recovery, and food generation within a single efficient platform.

Keywords: Wastewater, Hydrogen, Energy, Exergy

INTRODUCTION
Global warming and environmental degradation demand a shift from fossil fuels to sustainable energy sources [1]. Wind and hydrogen have emerged as key carbon-free options [2]. Meanwhile, municipal wastewater offers an untapped resource rich in organics and nutrients that can be converted into energy and valuable by-products [3].

This study presents a novel waste-to-resource multigeneration system that co-produces hydrogen, oxygen, freshwater, and district heating using real municipal sludge and wastewater. Integrating microbial electrolysis, alkaline electrolysis, and MED, it uniquely combines biological and electrochemical processes for enhanced energy and exergy recovery.

SYSTEM DESCRIPTION
Figure 1 presents the schematic layout of the integrated multigeneration system developed for the Harmony Creek Wastewater Treatment Plant. The configuration consists of six main subsystems. These units are interconnected through heat, mass, and power flows to enable efficient and continuous operation. The biogas fuels the CB-ORC subsystem, where the Brayton cycle drives the gas turbine for electricity generation. The exhaust gases heat the Organic Rankine Cycle, which uses R245fa as the working fluid to generate additional power. The MEC subsystem converts wastewater organics into hydrogen, carbon dioxide, and treated effluent. The alkaline electrolyzer produces hydrogen and oxygen using electricity from renewable sources and freshwater from the MED unit. The MED subsystem employs low-grade heat from the ORC condenser to produce freshwater. This integrated design enables efficient recovery of energy and resources from wastewater and renewable inputs.

THERMODYNAMIC ANALYSIS
Mass, energy, and exergy balance equations were developed for each subsystem to evaluate overall thermodynamic performance. The governing equations for the overall system energy efficiency and exergy efficiency are presented below to assess the integrated performance based on total input and output flows:

$$\eta = \frac{\dot{m}_{H_2}\, x\, LHV_{H_2} + \dot{m}_{fw}\, x\, LHV_{fw} + \dot{m}_{O_2}\, x\, h_{O_2} + \dot{Q}_{net}}{\dot{W}_{in,WT}} \quad (1)$$

$$\psi = \frac{\dot{m}_{H_2}\, x\, ex_{H_2} + \dot{m}_{fw}\, x\, ex_{fw} + \dot{m}_{O_2}\, x\, ex_{O_2} + \dot{Q}_{net}}{\dot{W}_{in,WT}} \quad (2)$$

RESULTS AND DISCUSSION
The thermodynamic and resource recovery performance of the proposed waste-integrated multigeneration system was evaluated through energy and exergy analyses. Figure 2 compares the energy and exergy efficiencies of the subsystems and the overall configuration. The Brayton cycle achieves the highest exergy efficiency (87%), while the Organic Rankine Cycle maintains balanced performance (63% energy, 65% exergy). Electrochemical subsystems show moderate efficiencies, with the alkaline electrolyzer (54% energy, 56% exergy) outperforming the MEC (13% energy, 23% exergy). The overall system attains 42% energy and 52% exergy efficiency, demonstrating the benefit of waste heat recovery and renewable integration.

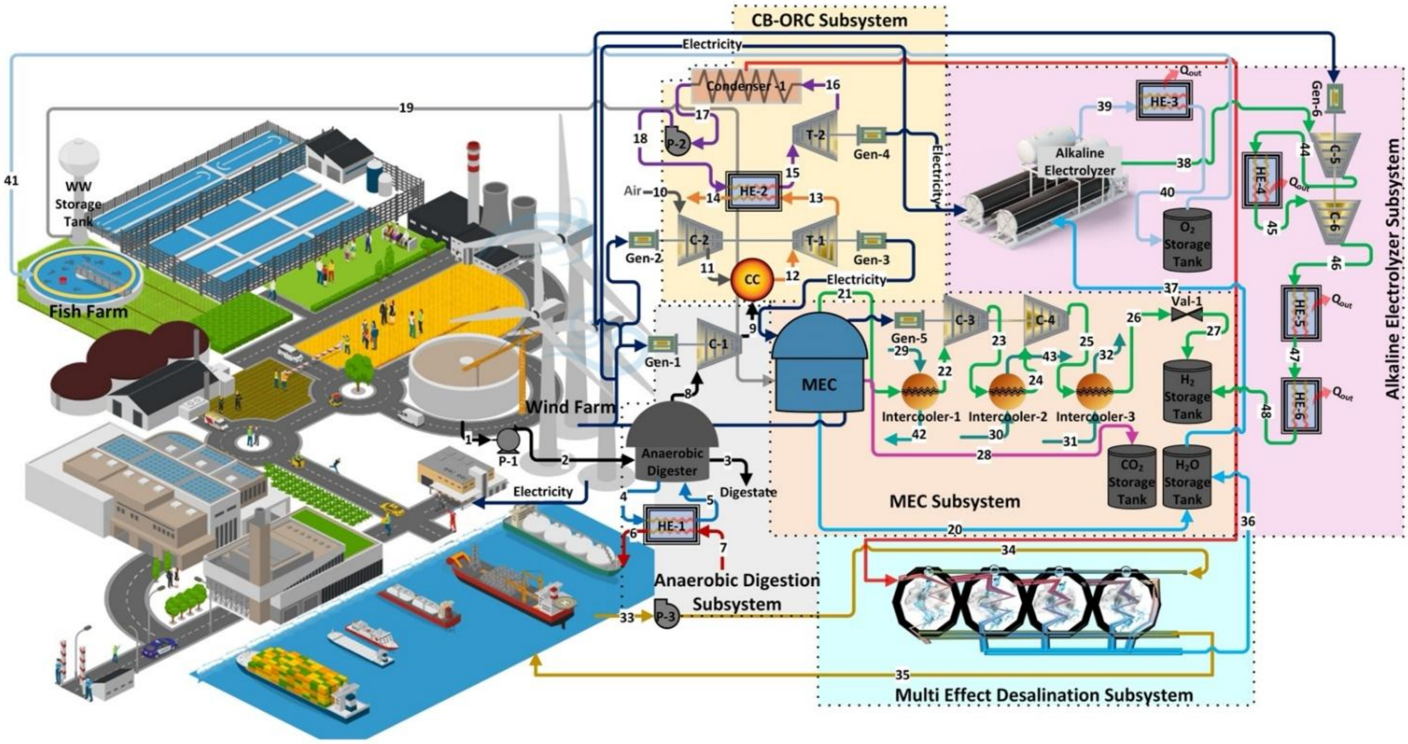

Figure 5: Schematic representation of designed system.

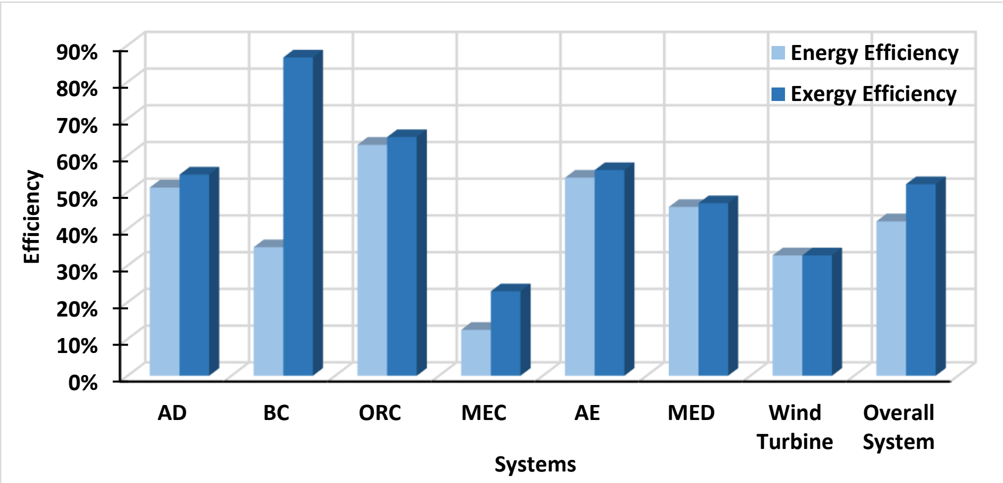

Figure 2: Comparison of energy and exergy efficiencies for each subsystem and the overall system.

CONCLUSIONS

This study developed a waste-integrated multigeneration system that co-produces electricity, hydrogen, oxygen, freshwater, and district heating using municipal sludge, wind energy, and recovered heat. The system achieved 42% energy and 52% exergy efficiency, showing strong thermodynamic and environmental performance. Annually, it produces 472 kilo tonnes of hydrogen, 9.4 kilo tonnes of freshwater, and 3,776 kilo tonnes of oxygen while providing 97.22 MW of district heating and demonstrates a scalable pathway for sustainable energy-water-waste integration.

REFERENCES

1) Alyamani, R., Solangi, Y. A., & Magazzino, C. (2025). Evaluating the driving factors and performance of OPEC member countries in transitioning to renewable energy towards climate change mitigation. Journal of Cleaner Production, 487, 144640.
2) Li, H., Mu, W., Huang, W., Torvanger, A., & Chen, T. (2025). Bioenergy utilization and greenhouse gas emission reduction: A global impact assessment. Renewable Energy, 250, 123115.
3) Dik, A., Sun, H., Calautit, J. K., Kutlu, C., Boukhanouf, R., & Omer, S. (2025). Sustainable urban energy dynamics: Integrating renewable energy and electric vehicles in a European context. Energy Conversion and Management, 340, 119972.

WAVE ENERGY CHALLENGES IN THE MEDITERRANEAN SEA

Salih E. Uzun[1], Uğur Atikol[2]*
[1] Mechanical Engineering, Eastern Mediterranean University, Gazimağusa, North Cyprus
[2] Energy Research Center, Eastern Mediterranean University, Gazimağusa, North Cyprus
*Corresponding author e-mail: 21601001@emu.edu.tr
Ref # RES-02

ABSTRACT

The Mediterranean Sea presents a unique challenge in the application and development of wave energy. The regional wave energy resources are between low and moderate with variations such as coastal and islands energy transition to consider in its application. This study provides a literature survey of wave energy potential and application of Wave energy converters (WECs) in the Mediterranean Basin. Peer- reviewed resources are considered and the results indicate that Western Mediterranean basin shows comparatively higher mean wave power while eastern regions display a lower mean with higher seasonable variability. Literature further shows that the main applications of wave energy in Mediterranean divided into nearshore, offshore and breakwater-integrated devices with contextual suitability, access to already existing infrastructure and maintenance accessibility. While application of wave energy converters still faces challenges such as economic viability, long term survivability under harsh weather events and long-term operational application with reliable data. The Key barriers to commercially viable wave energy converter can be circumvented with the technology-resource matching and integrated techno-economic evaluation. This is even more apparent for the Mediterranean region.

Keywords: Wave Energy, Mediterranean Sea, Wave Energy converter, Resource assessment, Levelized cost of electricity

INTRODUCTION

Marine renewable energy is one of the up-and-coming complementary components of Sustainable energy. Within this new field, wave energy offers better predictivity and higher energy density relative to the other intermittent renewable sources. Main focus of wave energy applications has been historically taken place in Atlantic Ocean, while never research has been popping up for semi-enclosed and moderate energy seas such as Mediterranean [1]. Compared to the Open ocean characteristics, Mediterranean basic exhibits distinct oceanographic properties. With short wave periods and generally lower wave height because of the fetch-limited geometry of the basin. Even with these characteristics, there are various research demonstrates exploitable wave power in certain regions, especially around the western region of the Mediterranean.[2] Moreover, Mediterranean basin includes numerous islands communities and coastal urban centres that rely on expensive imported fuel, therefore increasing the need for localized marine energy systems. [3,4]. Various studies have evaluated basin scale evaluates wave energy potential of the Mediterranean via long term hindcast models and numerical wave simulations. These assessments states special variability across sub-basin and highlight seasonal changes such as improvements in winter seasons. These characteristics can be deployed alongside solar energy for a stable energy production in regions where solar energy efficiency drops [2,5]. More recent studies utilize reanalysis data sets from Copernicus Marine Environment monitoring service to provide improved spatial resolution and multi-decadal consistent simulations. [6–8]. While assessing the available resources are important, another aspect of it is to investigate the wave energy converter (WEC) concepts utilized. Unlike wind and solar, wave energy converters is not a mature enough field for an industry standard to be establish. There are thousands of wave energy converter designs with varying degrees of success. In this Literature survey, only WEC deployed in Mediterranean are considered.[9,10]. WEC concepts such as, near shore and offshore applications are discussed under Sustainability section below [9,11–14]. From the available research, testing and evaluating the resources characteristics in the region to the sustainable wave energy technologies deployed remains limited. Therefore, this Literature survey aims to compare the resources availability, discuss promising wave energy technologies, and suggest further action for the Mediterranean.

CHALLENGES AND LIMITATIONS

Division of Wave Energy potential in the Basin: Basin scale analysis done in the Mediterranean shows that the western basin, particularly areas that are influenced by the Atlantic inflow have shown to have longer fetch conditions and have presents comparatively higher mean wave power.[15,16]. The central Mediterranean exhibits moderate potential while eastern basin generally displays lower overage wave potential with higher seasonal variability, due to limited fetch and calmer prevailing conditions. [5,15]. While Mediterranean has a moderate wave potential compared to the Atlantic, localised hotspots have been identified as seen from Figure 1. Alboran sea, Gulf of Lion, western Sardinia and certain regions of Aegean Sea show higher localized wave potential. These places indicate that when choosing the application of wave energy converters, it is just as important to consider resource characteristics as the WEC technologies.[5]. Moderate resource levels indicate that large scale offshore applications and arrays may face economic challenges whereas distributed systems, nearshore applications and scaled down WEC could provide more viable path forwards.

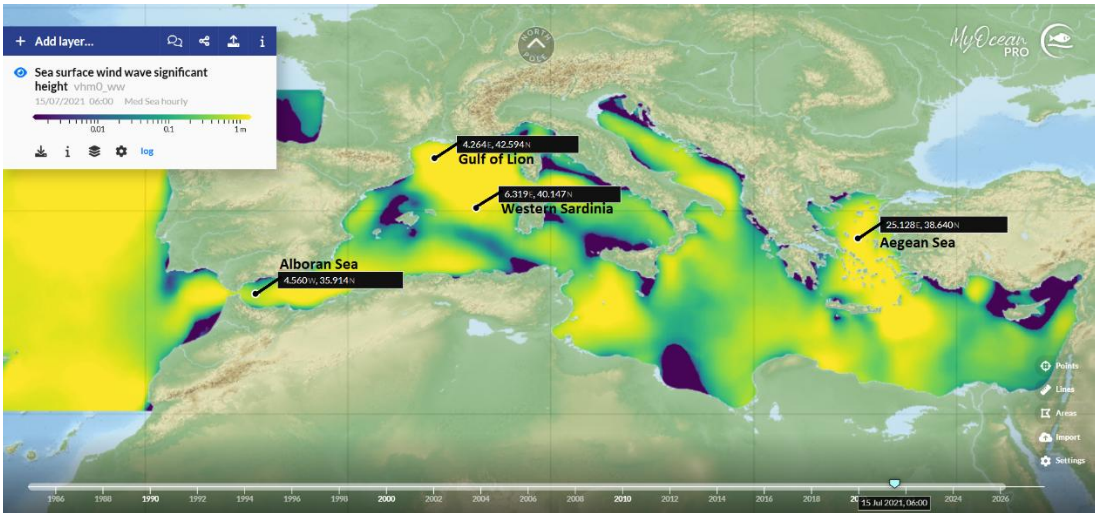

Figure 6 Open access Copernicus Wave Sea surface significant wave height data viewer showcasing Basin potential [17]. "This study has been conducted using E.U. Copernicus Marine Service Information; https://doi.org/10.48670/mds-00376"

Seasonal variability and Design Implications: One of the defining characteristics of Wave energy in the Mediterranean is the Seasonality. Most studies hindcast studies report significant concentration of energy during winter months compared to the tamer summer conditions as seen from Table 1 [2,5]. This variability effects the capacity factor, grid integration strategies and storage requirements in the WEC deployment. While extreme weather conditions are known to be less frequent and the wave height and frequency lower compared to the conditions faced by the Atlantic, they should still be considered. Survivability plays a big role in capital cost due to reinforcement in infrastructure and mooring techniques required. On the contrary, milder weather conditions may aid maintenance accessibility and reduce downtime required. [18] Available research states that when robust techno economic modelling is deployed with probabilistic evaluation of energy yield, it positively effects the long-term financial analysis and decision making [19].

Table 1 Mean Seasonal Wave Energy from MEDSEA_MULTIYEAR_WAV_006_012 dataset for 2025 [17,20]

Seasons	Average Wave Energy Flux (kW/m)	Seasons	Average Wave Energy Flux (kW/m)
Autumn	7.754	Spring	8.046
Winter	9.38	Summer	3.212

Sustainability and readiness of Wave Energy technologies: One of the main challenges WEC in Mediterranean faces are the limited capacity factor and the expensive levelized cost of electricity (LCoE). Deployment and maintenance of wave energy converters are expensive and in most cases is not industrialized due to lack of design convergence. Most wave energy converters tested in Mediterranean as seen from Table 2, have only been deployed for short period and yet to be properly integrated into existing infrastructure. While wind turbines and solar farms have established standards and competitive development to drive the costs of down.

Table 2 and Figure 2 sows that, while Tidal application for the Marine Energy is considered to be the most technologically mature and predictable form of ocean energy. Due to the need for coastal reshaping (Resource limitations and higher economic barriers of entry) and Legal, Operational feasibility concerns (Installation windows, maintenance costs, planning and licensing), it has yet to be used widespread around Europe [21]. Renewable energy in the European region has the advantage of interconnectivity of the power grid as well as an existing political and economic infrastructure for developing greener energy sources like Capital granting schemes (Innovation Fund) and Europe's Zero emission goal by 2050, making the goal to reach blue energy not a dream but an eventuality. [1,22]. On the other hand, few types of near shore and offshore technologies have been mentioned in the Table 2 showcasing their use cases and limitations. The LCoE and Technology readiness levels (TRL) allows the reader a better idea of the state for techno-economic feasibility.

Breakwater integrated WEC Systems: have been deployed in the Mediterranean as a particularly sustainable option. The prototype WEC OBREC have been installed in Naples and REWEC3 Oscillating water column have been implemented in Italy to demonstrate the feasibility of overtopping type devices especially when they are used alongside existing harbour infrastructure[23]. Shared civil infrastructure benefits from lower costs, reduce mooring requirements, simplifies grid connections and maintenance.[11].

Floating and Offshore Systems: A good representation of Offshore deployment strategies are floating systems such as ISWEC, tested around the Pantelleria Island. These devices use gyroscopic inertia principles and are suited for deep water applications. With these types of WEC, a mooring system are generally required to connect the WEC to the seabed and transport the produced electricity. One of the challenges faced by these systems are the increased complexity and installation costs therefore while offshore systems can achieve higher exposure to more energetic waves, it is required to consider cost benefit trade-offs for Mediterranean conditions. [9]

Table 2. Summary of Wave energy technologies used in Mediterranean.

Type	Configuration	TRL	LCoE	Capacity	Advantages	Challenges	Source
Tidal	**Horizontal Axis Turbine (HAT)**	8–9	~81 £/MWh	100 kW–2 MW	Predictable resource, high energy density, near-continuous output	Marine fatigue, cavitation, installation limits, grid access	[24]
	Tidal Kite	6–8	~99 €/MWh	0.1–0.5 MW	Operates in low current sites	PTO reliability, tether drag, subsea O&M	[21]
	Barrage	9	Site-specific	240–254 MW	Proven technology, high output	Environmental impact, high CAPEX	[24]
	SR2000	~8	-	~2 MW	Easier maintenance	Mooring loads, grid connection	[25]
WEC	**Point Absorber**	5–8	100–1000 €/MWh	1 kW–600 kW	Modular, omnidirectional capture	Survivability, O&M complexity, load variability	[26]
	Attenuator	~7	~190£/MWh	375–750 kW	High yield, wave-aligned	Structural mass, control complexity	[27]
	Oscillating Water Column	7–9	-	400 kW–2.8 MW	Mature, sheltered turbine	Air turbine efficiency (~60%), noise	[28]
	Terminator / Overtopping	~7	~77 €/MWh	2.5–7 MW	High single-device capacity	Large structure, extreme loading	[26]
	OWSC	-	~50 €/MWh	0.2–2 MW	Effective in shallow waters	Sediment impact, nearshore loads	[29]
	OPWEC	Early stage	~3 £/kWh	~50 kW	Multi-float configuration	Low efficiency, sealing issues	[29]

Key Barriers: Despite technological breakthroughs, several barriers persist. These are, moderate average wave power density, limited long-term operational datasets, high capital costs relative to energy yield and regulatory and permitting challenges. Sector reports indicate that the need for demonstration projects, improved reliability data and integrated techno-economic framework to achieve commercial viability [1,3,30].

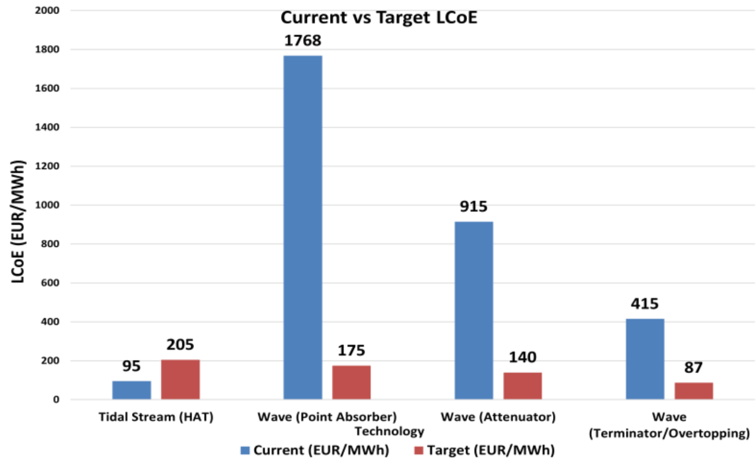

Figure 7 LCoE of WEC current vs target values

Figure 2 states, wave energy still has a long way to reach the target requirements set by the UK and Europe. While the technology is developing, a collaborated effort and case by case basis needs to be applied for the application of WEC converters. Feasibility of wave energy is a complex a multi-faceted endeavour that needs to be delved deeper.

CONCLUSIONS

The Mediterranean Sea exhibits moderate but regionally variable wave energy potential. Western sub-basins demonstrate higher resource availability, while eastern regions show lower energy flux but higher seasonal concentration levels. Literature indicates that in nearshore applications, breakwater WEC systems align well with resource characteristics and infrastructure in coastal regions. Offshore WEC systems are technically feasible but face economic and structural challenges under moderate conditions. Future research should prioritize long term performance monitoring, probabilistic energy yield assessment, comprehensive techno-economic analysis with feasibility and LCoE, alongside simulations based on wave equations. A recent simulation tool, Wave Energy Converter Simulator (WEC-SIM) developed by (NLR) and (Sandia), enabling stakeholders to reduce experimental requirements, improve design control, and lower deployment costs. Technology-resource matching and infrastructure integration appear central to advancing wave energy deployment within the Mediterranean basin.

REFERENCES

1. OES | OES Annual Report 2024 [Internet]. [cited 2026 Feb 23]. Available from: https://www.ocean-energy-systems.org/publications/oes-annual-reports/document/oes-annual-report-2024/
2. Dialyna E, Tsoutsos T. Wave Energy in the Mediterranean Sea: Resource Assessment, Deployed WECs and Prospects. Energies 2021, Vol 14,. 2021 Aug 5;14(16). doi:10.3390/en14164764
3. Ocean Energy Technologies Patents Deployment Status and Outlook [Internet]. [cited 2026 Feb 23]. Available from: https://www.irena.org/Publications/2014/Aug/Ocean-Energy-Technologies-Patents-Deployment-Status-and-Outlook
4. Magagna D, Uihlein A. Ocean energy development in Europe: Current status and future perspectives. International Journal of Marine Energy. 2015 Sep 1;11:84–104. doi:10.1016/j.ijome.2015.05.001
5. Besio G, Mentaschi L, Mazzino A. Wave energy resource assessment in the Mediterranean Sea on the basis of a 35-year hindcast. Energy. 2016 Jan 1;94:50–63. doi:10.1016/j.energy.2015.10.044
6. Orejarena-Rondón AF, Panfilova M, de León SP, Restano M, Sabia R, Benveniste J. High-resolution mapping of wave energy resources in the Mediterranean Sea using satellite altimetry. Energy Reports. 2026 Jun;15:109133. doi:10.1016/j.egyr.2026.109133
7. Mediterranean Sea Waves Reanalysis | Copernicus Marine Service [Internet]. [cited 2026 Feb 23]. Available from: https://data.marine.copernicus.eu/product/MEDSEA_MULTIYEAR_WAV_006_012/description
8. Galanis G, Hayes D, Zodiatis G, Chu PC, Kuo YH, Kallos G. Wave height characteristics in the Mediterranean Sea by means of numerical modeling, satellite data, statistical and geometrical techniques. Marine Geophysical Research. 2012 Mar;33(1):1–15. doi:10.1007/s11001-011-9142-0
9. Mattiazzo G. State of the Art and Perspectives of Wave Energy in the Mediterranean Sea: Backstage of ISWEC. Frontiers in Energy Research. Frontiers Media S.A.; 2019. doi:10.3389/fenrg.2019.00114
10. Pelagos. Promoting innovative nEtworks and cLusters for mArine renewable energy synerGies in mediterranean cOasts and iSlands Diagnostic study of the Mediterranean marine energy resources potential. 2014. Report.
11. VIDEO: REWEC3 wave energy converter - Offshore Energy [Internet]. [cited 2026 Feb 25]. Available from: https://www.offshore-energy.biz/video-rewec3-wave-energy-converter/
12. ISWEC - MOREnergy Lab [Internet]. [cited 2026 Feb 25]. Available from: https://morenergylab.polito.it/iswec/
13. Calheiros-Cabral T, Rosa-Santos P, Taveira-Pinto F, Lara JL. Harnessing wave energy through breakwater integration: A review of technologies, deployment strategies and an open-access database. Renewable and Sustainable Energy Reviews. 2025 Nov 1;223(2):115975. doi:10.1016/j.rser.2025.115975
14. Cagninei A, Raffero M, Bracco G, Giorcelli E, Mattiazzo G, Poggi D. Productivity analysis of the full scale inertial sea wave energy converter prototype: A test case in Pantelleria Island. Journal of Renewable and Sustainable Energy. 2015 Nov 1;7(6). doi:10.1063/1.4936343
15. Dialyna E, Tsoutsos T. Wave energy in the mediterranean sea: Resource assessment, deployed wecs and prospects. Energies (Basel). 2021 Aug 2;14(16). doi:10.3390/en14164764
16. Sierra JP, Mösso C, González-Marco D. Wave energy resource assessment in Menorca (Spain). Renew Energy. 2014 Nov 1;71:51–60. doi:10.1016/J.RENENE.2014.05.017
17. Korres G, Ravdas M, Zacharioudaki A, Denaxa D, Sotiropoulou M, Oikonomou C. Copernicus Marine MyOcean Viewer. Mediterranean Sea Waves Reanalysis- MEDSEA_MULTIYEAR_WAV_006_012 [Internet]. E.U. Copernicus Marine Service Information (CMEMS). Marine Data Store (MDS); 2026 [cited 2026 Mar 10]. Available from: https://data.marine.copernicus.eu/-/mgyvby5irz doi:https://doi.org/10.48670/mds-00376
18. Rusu E. Evaluation of the wave energy conversion efficiency in various coastal environments. Energies (Basel). 2014;7(6):4002–18. doi:10.3390/en7064002
19. Soukissian TH, Denaxa D, Karathanasi F, Prospathopoulos A, Sarantakos K, Iona A, Georgantas K, Mavrakos S. Marine renewable energy in the Mediterranean Sea: Status and perspectives. Energies. MDPI AG; 2017. doi:10.3390/en10101512
20. Mediterranean Sea Waves Reanalysis | Copernicus Marine Service [Internet]. [cited 2026 Mar 12]. Available from: https://data.marine.copernicus.eu/product/MEDSEA_MULTIYEAR_WAV_006_012/description
21. Magagna D. Ocean energy : technology development report. Publications Office of the European Union; 2020.
22. IRENA. ABOUT IRENA [Internet]. 2014. Report. Available from: www.irena.org
23. Rombado G, Cooke N, Kan W, Pasquale Contestabile, Vincenzo Ferrante. Prototype Overtopping Breakwater for Wave Energy Conversion at Port of Naples. Conference: International Ocean and Polar Engineering Conference [Internet]. 2016 Jul [cited 2026 Feb 25]. Available from: www.isope.org
24. E E S D. Wave energy Utilization in Europe Current Status and Perspectives European Thematic Network on Wave Energy. Report.
25. Dr. Ir. Matthijs SOEDE. Study on Lessons for Ocean Energy Development 2 EUROPEAN COMMISSION. EUROPEAN COMMISSION. 2017. doi:10.2777/389418
26. Guo C, Sheng W, De Silva DG, Aggidis G. A Review of the Levelized Cost of Wave Energy Based on a Techno-Economic Model. Energies 2023, Vol 16, Page 2144. 2023 Feb 22;16(5):2144. doi:10.3390/EN16052144
27. Drew B, Plummer AR, Sahinkaya MN. A review of wave energy converter technology. Proceedings of the Institution of Mechanical Engineers, Part A: Journal of Power and Energy. 2009. p. 887–902. doi:10.1243/09576509JPE782
28. Magagna D, Shortall R, Telsnig T, Uihlein A, Vázquez Hernández C. Supply chain of renewable energy technologies in Europe An analysis for wind, geothermal and ocean energy [Internet]. 2017. doi:10.2760/271949
29. Bozzi S, Besio G, Passoni G. Wave power technologies for the Mediterranean offshore: Scaling and performance analysis. Coastal Engineering. 2018 Jun 1;136:130–46. doi:10.1016/j.coastaleng.2018.03.001
30. Dalton G, Allan G, Beaumont N, Georgakaki A, Hacking N, Hooper T, Kerr S, O'Hagan AM, Reilly K, Ricci P, Sheng W, Stallard T. Economic and socio-economic assessment methods for ocean renewable energy: Public and private perspectives. Renewable and Sustainable Energy Reviews. 2015;45:850–78. doi:10.1016/J.RSER.2015.01.068

SUSTAINABLE ENERGY DEVELOPMENT AND POLICY CHALLENGES: THE CASE OF KANO STATE

Abubakar Yahuza Ado[1], Meliz Hastunç[1]
[1] Bahçeşehir Cyprus University, Faculty of Architecture and Engineering, Department of Electrical Electronics Engineering, Mustafa Kemal Avenue, Osmanlar Street 1, Alayköy, Nicosia, TRNC
*Corresponding author e-mail: abubakaryahuza4999@gmail.com
Ref # RES-03

ABSTRACT

Kano State faces growing sustainability challenges driven by rapid urbanization, population growth, and infrastructural deficits. Unreliable electricity supply, environmental degradation, and limited renewable energy deployment continue to hinder sustainable development. This study examines sustainable energy development in Kano State, Nigeria, focusing on electricity access constraints, policy implementation effectiveness, and renewable energy potential. A qualitative literature review was conducted using peer-reviewed studies and official policy documents published between 2020 and 2025. The findings show that persistent electricity shortages increase reliance on fossil fuel–based self-generation, raising economic costs and carbon emissions. Rapid urbanization further intensifies infrastructure pressure, water stress, environmental degradation, and inefficient waste management. Although Kano has strong solar energy potential, deployment remains limited due to financial constraints, regulatory inefficiencies, and weak institutional coordination, highlighting a gap between policy ambition and implementation. The literature further implies that strengthening renewable energy financing mechanisms, improving policy coordination, and promoting energy efficient urban infrastructure could escalate sustainable energy development and reduce environmental impacts in Kano state.

Keywords: Sustainable energy, Renewable energy, Electricity access, Policy implementation, Kano State

INTRODUCTION

Sustainability refers to the ability to meet the needs of the present without compromising the ability of the future generation to reach their needs integrating environmental protection, economic growth, and social equity [1]. It incorporates the three core aspects of sustainability: social justice, environmental preservation, and economic viability. While Sustainable energy development is defined as the long-term transformation of energy systems to establish affordable, reliable, and environmentally friendly energy supply while reinforcing economic growth social wellbeing. it involves improving energy efficiency, expanding renewable energy technologies, imposing strong policy implementation mechanisms that promotes low carbon and resilient energy systems and strengthening energy infrastructure [3].

In developing regions, sustainability is critical particularly because of the huge population growth and tight infrastructure intensifying pressures on energy systems and natural resources. Clean reliable access of energy plays a key role in achieving sustainable development, particularly in sub-Saharan Africa, where lack of stable energy constrains industrialization, sustainable economic growth, and climate resilience. Worldwide, there are over 675 million people without energy access of which Sub-Saharan Africa accounts for around 540-550 million people which constitute 80% of its global population [4]. Despite being amongst the largest African economy and having enormous clean energy resources, Nigeria has been plagued with aggravated energy access shortage. Inadequate energy generation, poor transmission, inadequate infrastructure, limited investment, and affordability constraints continue to limit energy access, suppressing economy growth, and progress toward achieving sustainable development [5].

Kano state, one of the most populous and economically notable states in the Northern region, is characterised by growing industrial action, urban expansion and increasing demand of electricity. Kano also characterised by a high potential of solar irradiation, positions itself as a strategic case for renewable energy deployment [6]. Kano State faces multiple interconnected sustainability challenges driven by rapid urbanization, population growth, and infrastructural deficits. As one of the fastest-growing urban centers in northern Nigeria, the state experiences increasing pressure on water supply, sanitation, and waste management systems. Inadequate solid waste disposal and weak wastewater management contribute to public health risks and environmental pollution in Nigerian cities [7,8]. Air pollution is further intensified by the widespread use of petrol and diesel generators due to unreliable electricity supply, increasing emissions and environmental degradation [9]. Rapid population growth and urban expansion have also raised electricity demand, while supply remains unstable and insufficient for residential, commercial, and industrial needs [10]. This persistent energy deficit increases reliance on self-generated fossil-fuel energy, leading to higher costs and carbon emissions [11].
Additionally, Kano's location in the Sudano-Sahelian zone increases its vulnerability to climate variability, rising temperatures, desertification, and water stress [12]. These interconnected environmental, climate, and energy challenges highlight the urgent need for a transition to sustainable and renewable energy systems. Existing studies underlines many sustainable energy development pathways for improving energy access in developing regions. These include the expansion of decentralized renewable energy systems such as rooftop photovoltaic systems and solar mini-grids, enhancement of energy efficiency, investing in modern grid infrastructure, and strong and supportive

policy frameworks that encourage private sector participation and renewable energy financing. research also emphasize the importance of integrating renewable energy into urban planning, promoting clean energy technologies, and strengthening institutional quality to assure effective implementation of energy policies [13,14]. Against this background, this paper objective is to critically examine sustainable energy challenges in Kano state, and evaluate the potential of renewable energy integration as a viable pathway toward improving energy security, improving economic development, and striving toward achieving sustainable development goals (SDG) specifically SDG7 (Affordable and clean energy) and SDG13 (climate action). This study attempts to offer insights that might guide policy formulation and sustainable energy planning in the area by evaluating the current energy landscape and the prospects for renewable energy deployment.

Literature review

Existing studies examine Nigeria's sustainability and energy challenges from environmental, technical, infrastructural, and policy perspectives. Research highlights deficiencies in urban waste management, wastewater treatment, and air quality control, with heavy reliance on diesel and petrol generators contributing to pollution, environmental degradation, and public health risks [15,16]. Studies also indicate that Nigeria possesses significant yet underutilized renewable energy resources [17]. High solar irradiation in northern regions supports photovoltaic deployment, while hydropower potential is estimated at about 13,000 MW for large-scale and 3,500 MW for small-scale projects; wind and biomass also remain largely untapped [18,19]. Despite this potential, renewable energy contributes only marginally to the national grid due to financial, infrastructural, and institutional constraints [20].

Rapid urbanization and population growth have further widened the electricity demand–supply gap in Nigeria's power sector [21]. Consequently, industries, businesses, and households have become increasingly dependent on fossil-fuel–based self-generated power, which raises production and operational costs [22]. Policy studies similarly identify regulatory inefficiencies, fragmented financing, and weak governance as key barriers to sustainable energy development [23]. Several research also propose sustainable energy development strategies to address these challenges. Such as expanding decentralized renewable energy systems such as and rooftop photovoltaic installations, solar mini-grids, enhancing energy efficiency in urban, industrial and sectors, and improving national grid infrastructure [24]. Contrary to that, researchers also emphasize the importance of supportive regulatory frameworks, renewable energy financing mechanisms, and promotes private sector participation to accelerate renewable energy deployment in Nigeria and other developing economies [25]. However, despite growing scholarly attention to Nigeria national renewable energy policies and energy improvement strategies mostly emphasize federal level, while only limited research addresses sub-national implementation, particularly in northern states, despite recent decentralization reforms under the Electricity Act 2023 [26,27].

Although existing studies examine Nigeria's energy crisis, environmental management, renewable energy potential, and policy reforms, most address these issues separately and largely at the national level [28,29]. This fragmented focus limits understanding of how sustainability policies interact and are implemented at the sub-national scale. Despite Kano State's strategic importance, marked by rapid urbanization, persistent electricity deficits, and high solar potential, research on state-level sustainability policy implementation, infrastructure readiness, and institutional coordination remains limited [30]. In particular, there are few empirical studies examining how recent decentralization reforms lead to practical improvements in Kano's energy sector. Therefore, this study critically reviews sustainability policies and existing literature related to Kano State to identify key institutional, structural, and environmental factors influencing sustainable energy transition and to support evidence-based strategies for improving energy and environmental sustainability in northern Nigeria.

DISCUSSION

The reviewed findings show that sustainability challenges in Nigeria are closely associated with inadequate environmental management, insufficient energy infrastructure, and weak policy implementation. Research [15,16] focuses on environmental sustainability and highlights the negative impacts of the widespread use of diesel and petrol generators, including environmental degradation, air pollution, and public health risks. In contrast, studies [17,18] underline Nigeria's significant renewable energy potential, noting that high solar irradiation in the northern region and substantial hydropower resources could support large-scale renewable energy deployment. While these studies agree that Nigeria possesses abundant renewable energy resources, they differ in their explanations for the slow deployment of renewable energy. Research [19] emphasizes that this gap is primarily due to infrastructural and financial limitations, whereas [20] highlights institutional weaknesses such as weak governance structures and regulatory inefficiencies. This divergence suggests that sustainable energy challenges in Nigeria are multidimensional, involving both institutional capacity and resource management.

Similarly, research [21] identifies population growth and rapid urbanization as key drivers of the widening electricity demand–supply gap in Nigeria's energy sector. Meanwhile, [22] indicates that electricity shortages have increased dependence on fossil-fuel-based self-generation, particularly diesel and petrol generators, which significantly raises operational costs for industries, businesses, and households. Moreover, most of these analyses evaluate the issue primarily at the national level. The findings of the present study suggest that these challenges are particularly evident in Kano State, where rapid urban expansion and high population density place additional pressure on already strained infrastructure systems. Consequently, unreliable electricity supply not only increases reliance on fossil-fuel generators but also indirectly exacerbates socioeconomic and environmental challenges, including wastewater management inefficiencies, urban pollution, and water supply constraints. However, [23] also highlights governance and policy barriers as major constraints to sustainable energy development in Nigeria.

Previous studies point to fragmented financing structures, limited institutional coordination, and weak regulatory enforcement as key obstacles to the effective implementation of renewable energy policies. Although federal policies have increasingly promoted renewable energy development and energy sector reforms, particularly through the Electricity Act 2023, relatively few studies [24,25] have examined how these reforms translate into practical outcomes at the state or local levels.

From a broader perspective, the comparison of existing studies suggests that Nigeria's sustainable energy challenges are often framed separately as governance, environmental, or economic issues. However, the findings of this study indicate that these dimensions are closely interconnected in Kano State. Although renewable energy resources (particularly solar energy) are technically viable in the region due to favorable climatic conditions, infrastructural and institutional barriers limit large-scale deployment. Therefore, improving renewable energy adoption will depend not only on expanding renewable energy technologies but also on strengthening investment frameworks, improving institutional coordination, and enhancing policy implementation at the state level.

Based on the findings of this study and insights from existing literature, several strategies could support sustainable energy development in Kano State. From a policy perspective, accelerating sustainable energy development requires stronger policy implementation mechanisms and targeted institutional reforms. Improving institutional coordination between federal and state energy authorities is necessary to ensure the effective implementation of energy policies and regulatory frameworks. Integrating renewable energy planning into urban development and infrastructure planning will support better balancing of energy supply and demand and help establish realistic and achievable policy goals. In addition, policies that prioritize renewable energy adoption in industrial, household, and commercial sectors should be promoted. Raising public awareness about the environmental and economic implications of using diesel and petrol generators is also essential. Finally, significant investment from both government and private sectors will be required to achieve sustainable energy development.

CONCLUSIONS

This study examines sustainable energy development in Kano State through qualitative review of policy documents and academic literature. The research indicates that sustainability constraints in Kano State are not primarily due to a lack of resources but rather to structural and institutional weaknesses that hinder effective implementation. Unreliable electricity supply remains a major constraint to sustainable development, increasing reliance on fossil fuel based self-generation and raising both environmental and economic costs. Rapid urbanization further intensifies infrastructure stress, environmental degradation, water pressure, and inefficient waste management. Deployment of these resources, such as solar power, remains limited due to funding constraints, regulatory inefficiencies, weak monitoring systems, and limited federal and state institutional coordination. This study reveals a persistent gap between policy ambition and implementation. While recent electricity sector decentralization reforms create new opportunities for state-level governance, achieving meaningful sustainability outcomes will depend on strengthening institutional capacity, ensuring investment security, improving regulatory frameworks, and integrating energy planning with broader urban sustainability strategies. Overall, the transition toward a sustainable energy system requires institutional reform and stronger policy implementation mechanisms, in addition to technical expansion.

REFERENCES

[1] World Commission on Environment and Development, *Our Common Future*. Oxford, U.K.: Oxford University Press, 1987. Retrieved on 06.02.26
[2] S. Angorani, "Assessing the triple bottom line: A cross-sectional analysis of economic, social, and environmental sustainability in contemporary development projects," Indonesian Journal of Economics, Business, Accounting, and Management (IJEBAM), vol. 3, no. 4, pp. 20–38, 2025. [Online]. Available: https://journal.seb.co.id/ijebam/article/view/65
[3] I. Khan and M. Sahabuddin, "Chapter 1 - Sustainability—Concept and its application in the energy sector," in *Renewable Energy and Sustainability*, I. Khan, Ed. Elsevier, 2022, pp. 1–22. ISBN: 9780323886680. [Online]. Available: https://doi.org/10.1016/B978-0-323-88668-0.00005-X
[4] International Energy Agency (IEA), International Renewable Energy Agency (IRENA), United Nations Statistics Division (UNSD), World Bank, and World Health Organization (WHO), *Tracking SDG 7: The Energy Progress Report 2023*. Washington, DC, USA: World Bank, 2023. [Online]. Available: https://trackingsdg7.esmap.org/. Retrieved on 06.02.26
[5] M. Mukhtar, S. Obiora, N. Yimen, Z. Quixin, O. Bamisile, P. Jidele, and Y. I. Irivboje, "Effect of inadequate electrification on Nigeria's economic development and environmental sustainability," *Sustainability*, vol. 13, no. 4, Art. no. 2229, 2021. doi: 10.3390/su13042229.

[6] A. A. Bashir, A. Ahmed, A. Ibrahim, and S. A. Aliyu, “Assessment of solar radiation potential in Kano, northwestern Nigeria using the Angström–Prescott empirical model for renewable energy planning,” *International Journal of Applied and Advanced Engineering Research*, 2025. doi: 10.70382/mejaaer.v9i5.029. [Online]. Available: https://doi.org/10.70382/mejaaer.v9i5.029
[7] R. M. Musa, “An Assessment of Environmental Solid Waste Management in Kano Metropolis,” Jalingo Journal of Social and Management Sciences, vol. 4, no. 4, Aug. 2023.
[8] H. Abdullahi, M. Z. Asmawi, and A. R. Abd Aziz, “Relationship between Urban Growth and Water Pollution: Experience of Kano Metropolis, Nigeria,” *Journal of Hunan University (Natural Sciences)*, vol. 50, no. 8, 2023.
[9] K. Owebor, C. Okereke, O. E. Diemuodeke *et al.*, “A systematic review of literature on the decarbonization of the Nigerian power sector,” *Energy, Sustainability and Society*, vol. 15, p. 34, 2025. doi: 10.1186/s13705-025-00527-x. [Online]. Available: https://doi.org/10.1186/s13705-025-00527-x
[10] N. A. Muhammad, M. G. Mustapha, A. S. Yahaya, N. Tijjani, A. L. Musa, A. S. Yunusa, and G. S. Shehu, “Assessment of wind power potential at Kano State Nigeria for efficient energy utilization,” Sarcouncil Journal of Engineering and Computer Sciences, vol. 1, no. 7, pp. 1–11, 2022.
[11] M. A. Jimoh and B. Raji, “Electric grid reliability: An assessment of the Nigerian power system failures, causes and mitigations,”CovenantJournal of Engineering Technology, 2023. [Online]. Available: https://journals.covenantuniversity.edu.ng/index.php/cjet/article/view/330
[12] I. Azare, M. Abdullahi, A. Adebayo, I. Dantata, and T. Duala, “Deforestation, desert encroachment, climate change and agricultural production in the Sudano-Sahelian Region of Nigeria,” Journalof Applied Sciences and Environmental Management, vol. 24, no. 1, pp. 127–132, 2020, doi: 10.4314/jasem.v24i1.18.
[13] A. Korkovelos, H. Zerriffi, M. Howells, M. Bazilian, H.-H. Rogner, and F. F. Nerini, “A retrospective analysis of energy access with a focus on the role of mini-grids,” *Sustainability*, vol. 12, no. 5, p. 1793, 2020, doi:10.3390/su12051793.
[14] P. M. Falcone, “Sustainable energy policies in developing countries: A review of challenges and opportunities,” *Energies*, vol. 16, no. 18, p. 6682, 2023, doi:10.3390/en16186682.
[15] C. N. Igwe, U. N. Ngwoke, O. T. Okugbo, O. Ikpowonsa-Eweka, C. V. Ego, E. A. Omoyajowo, and I. C. Maduako, “Air quality and public health in metropolitan cities in Nigeria: Implications. A review,” *International Journal of Research and Scientific Innovation*, vol. XII, no. II, pp. 50–60, Feb. 2025, doi: 10.51244/ijrsi.2025.12020006.
[16] “Appraising raw exhaust pollutant gases emissions from industrial generators using statistics and machine learning approaches,” *Journal of the Nigerian Society of Physical Sciences*, vol. 7, no. 4, p. 2725, Aug. 2025, doi: 10.46481/jnsps.2025.272.
[17] U. A. Dodo and E. C. Ashigwuike, “In-depth physico-chemical characterisation and estimation of the grid power potential of municipal solid wastes in Abuja city,” *Energy Nexus*, vol. 10, p. 100192, 2023, doi: 10.1016/j.nexus.2023.100192.
[18] A. A. Bisu, T. G. Ahmed, U. S. Ahmad, and A. D. Maiwada, “A SWOT analysis approach for the development of photovoltaic (PV) energy in Northern Nigeria,” *Cleaner Energy Systems*, vol. 9, p. 100128, 2024, doi: 10.1016/j.cles.2024.100128.
[19] A. H. Abdullahi, A. Ahmed, J. H. Umar, Z. Yusuf, S. I. Ajobunu, and D. Abashiya, “Spatial analysis of site suitability for solar photovoltaic plants in Kaduna Metropolis, Kaduna State, Nigeria,” *International Journal of Sustainable Green Systems*, vol. 10, no. 4, pp. 68–78, Dec. 2024.
[20] Y. Shao, Z. Yang, Y. Yan, Y. Yan, F. Israilova, N. Khan, and L. Chang, “Navigating Nigeria's path to sustainable energy: Challenges, opportunities, and global insight,” *Energy Strategy Reviews*, vol. 59, p. 101707, 2025. doi: 10.1016/j.esr.2025.101707. [Online]. Available: https://www.sciencedirect.com/science/article/pii/S2211467X25000707
[21] N. O. Bashiru, M. A. Isiaka, and S. A. Lawal, “Determinants of electricity demand in Nigeria: A non-linear autoregressive distributed lag (NARDL) analysis,” *International Journal of Research and Scientific Innovation*, May 2024. doi:10.51244/ijrsi.2024.1104056. [Online]. Available: https://doi.org/10.51244/ijrsi.2024.1104056
[22] K. A. Adeyeye and C. Mbohwa, “Decentralized energy transition in urban Nigeria: Institutional barriers and policy pathways for hybrid renewable energy systems,” *Oxford Open Energy*, vol. 4, p. oiaf010, 2025. doi: 10.1093/ooenergy/oiaf010. [Online]. Available: https://doi.org/10.1093/ooenergy/oiaf010
[23] A. T. Ajia, “Policy challenges and opportunities for renewable energy development in Nigeria: A systematic review,” *African Journal of Environmental Sciences and Renewable Energy*, vol. 18, no. 1, pp. 115–137, 2025. doi: 10.62154/ajesre.2025.018.010660. [Online]. Available: https://doi.org/10.62154/ajesre.2025.018.010660
[24] A. T. Ajia, “Policy challenges and opportunities for renewable energy development in Nigeria: A systematic review,” African Journal of Environmental Sciences and Renewable Energy, vol. 18, no. 1, pp. 115–137, 2025, doi:10.62154/ajesre.2025.018.010660.
[25] T. A. Ajia, “Renewable Energy Policy and Sustainable Development in Nigeria: A Systematic Scoping Review,” *J. Energy Res. Rev.*, vol. 17, no. 6, pp. 1–16, 2025, doi: 10.9734/jenrr/2025/v17i6416.
[26] O. A. Somoye, “Energy crisis and renewable energy potentials in Nigeria: A review,” *Renew. Sustain. Energy Rev.*, vol. 188, p. 113794, 2023, doi: 10.1016/j.rser.2023.113794.
[27] A. Hadiza, U. Shuaibu, S. Akuson, and A. E. Menson, “Renewable energy adoption and environmental pollution in Nigeria: An empirical evidence,” *J. Econ. Allied Res.*, vol. 10, no. 2, pp. 54–69, 2025.
[28] C. Okereke, S. Okoh, T. Ogenyi, and G. Olorunfemi, “Assessment of climate awareness, policy development, and action across Nigerian states,” *Frontiers in Climate*, vol. 7, 2025, doi: 10.3389/fclim.2025.1650172.

DESIGN OF A HOLISTIC ENERGY SYSTEM FOR INUIT OFF-GRID COMMUNITIES

Yasmin Hafez[1*], *Ibrahim Dincer*[1]
[1] Clean Energy Research Lab (CERL), Faculty of Engineering and Applied Science, Ontario Tech University, 2000 Simcoe Street North, Oshawa, Ontario L1G 0C5, Canada
*Corresponding author e-mail: yasmin.hafez@ontariotechu.net

Ref # RES-04

ABSTRACT

Remote Inuit communities on the shores of Newfoundland and Labrador remain highly dependent on diesel fuel, causing severe energy costs and greenhouse gas emissions (GHG). This study proposes and thermodynamically evaluates a multigeneration integrated renewable energy system designed specifically for these communities. The system combined two locally abundant renewable resources in the area which are tidal energy and wood-waste biomass gasification. The system is used to simultaneously produce electricity, space heating using ground source heat pump and biodiesel for inter-island ferry transport through a microalgae-to-biofuel pathway. Power generation is achieved through combined Brayton and Steam Rankine cycle, along with tidal turbine. The CO_2 from gasification is biologically sequestered through a cyanobacteria photobioreactor. The system is projected to supply approximately 30,000 MWh/yr of electricity, 132,000 MWh/yr of thermal energy, and 30,000 MWh/yr of ferry fuel, reducing community GHG emissions by approximately 92% relative to the diesel-only baseline.

Keywords: Biomass Gasification, Tidal Energy, Hydrogen Storage, Off-grid Communities, Multigeneration Energy Systems

INTRODUCTION

Indigenous and Inuit communities across Newfoundland and Labrador (NL) face persistent energy security challenges. Cut off from the provincial grid, they depend entirely on diesel fuel for electricity, oil-fired heating, and marine ferries. This leads to Canada's highest fuel costs and frequent disruptions during extreme cold weather. Yet these islands have rich untapped resources: strong tidal currents and abundant wood-waste biomass from forestry activities.

Multigeneration energy systems offer a promising solution. Research shows they achieve far higher energy and exergy efficiencies than single-output systems. Prior studies have explored biomass-based Brayton-Rankine cycles, hydrogen production, and ground source heat pumps, but none have focused on remote Indigenous islands combining tidal and biomass inputs with marine biodiesel needs.

This study proposes and assesses a multigeneration system integrating tidal energy, biomass gasification, hydrogen compression, ground-source heating, and microalgae biodiesel production for NL Inuit communities of about 1200 households. It quantifies GHG reductions versus diesel baseline. Unlike existing projects using solar, wind, and hydro renewables, our design addresses these communities' unique tidal-biomass resources and ferry diesel dependence. Such solutions will help achieve sustainable development.

SYSTEM DESCRIPTION

The proposed System, shown in Fig. 1, combines five closely linked subsystems that share fluid streams, electrical connections, and waste heat recovery loops. The system is designed for a reference coastal island community of approximately 1200 households and operates under steady-state conditions, with negligible kinetic or potential energy effects. The ambient (dead-state) conditions are taken as 10 °C and 101.3 kPa, typical of coastal Newfoundland.

Locally sourced wood waste is crushed, dried, and gasified in a two-stage reactor to produce syngas, which is cleaned and shifted to maximize hydrogen yield. A pressure swing adsorption unit separates high-purity hydrogen while producing biochar as a useful by-product. The purified syngas drives a combined Brayton–Rankine power cycle, with a gas turbine producing electricity and its exhaust heat recovered by a steam bottoming cycle to increase overall efficiency.

Hydrogen extracted from the gasification process is compressed in three intercooled stages and stored at 700 bar in high-pressure tanks, powered by electricity from tidal turbines. This stored hydrogen serves as a renewable energy reserve, replacing conventional diesel storage. A ground-source heat pump supplies district space heating for community use. Finally, carbon dioxide from the biomass combustion stream feeds a microalgae photobioreactor, where it supports algae growth for biodiesel production. The resulting biofuel can power inter-island ferries, closing the carbon loop while providing a local, renewable fuel source.

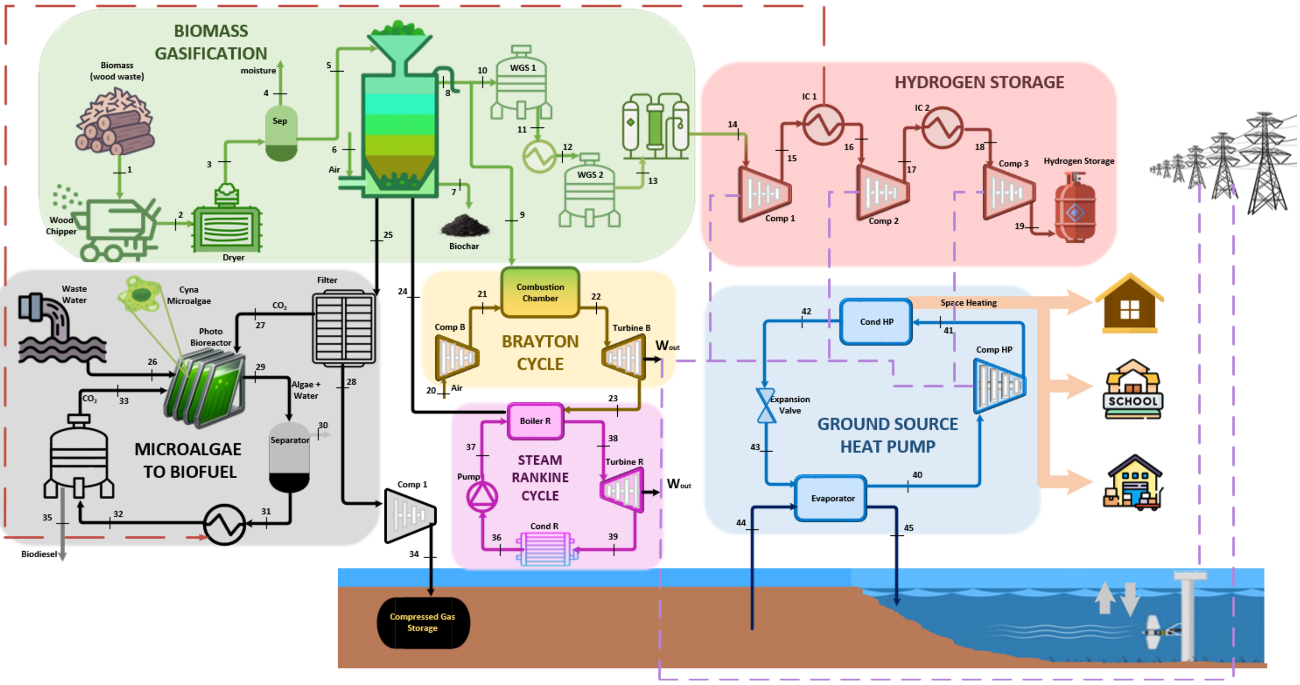

Fig. 1. Schematic drawing of the proposed system for Inuit off-grid island communities in Newfoundland

RESULTS AND DISCUSSION

Fig. 2 compares preliminary estimates of community energy demand with the supply from the proposed integrated biomass system across electricity, space heating, and ferry fuel categories. Electricity demand is about 24,000 MWh per year and is based on Newfoundland annual reports [1], while space heating demand is about 120,000 MWh per year and reflects sub-arctic design loads typical for Newfoundland and Labrador. Ferry fuel demand is about 30,000 MWh per year and is estimated from a small coastal fleet. The results indicate that the system meets or exceeds electricity and space heating needs, while displacing about 20% of current diesel ferry fuel, with further improvement possible through scale-up and algae optimization.

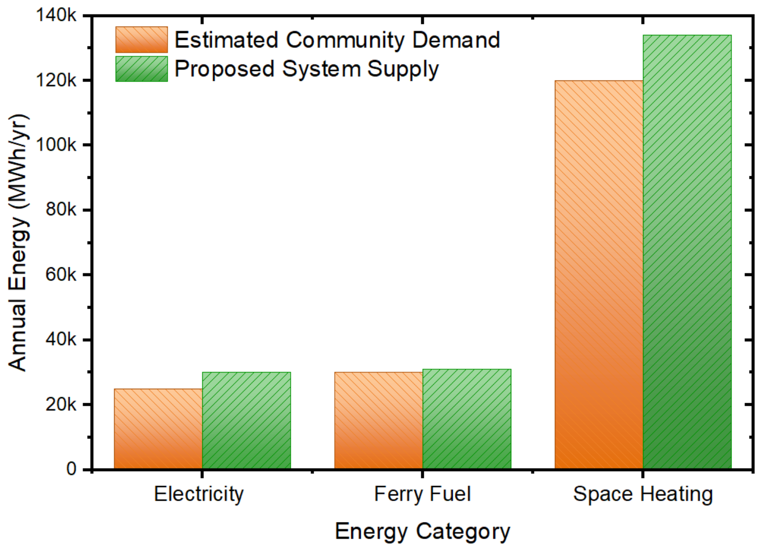

Fig. 2. Preliminary comparison of estimated community energy demand versus the proposed system supply for the communities

Fig. 3 illustrates greenhouse gas emissions. The diesel-only baseline emits around 1,946 tonnes of CO_2 equivalent annually across end-uses, based on Environment and Climate Change Canada's diesel emission factor [2]. The proposed system slashes this to 152 tonnes CO_2 equivalent per year, which represents a 92% reduction. Residual emissions arise from the displaced 20% ferry diesel, minor infrastructure manufacturing/installation impacts, and net biogenic carbon from biomass not fully re-absorbed by the microalgae photobioreactor. These outcomes align with GHG reductions in comparable biomass multigeneration studies. Highest exergy destruction is anticipated in the combustion chamber, as seen across referenced systems, to be modeled precisely in future Aspen Plus simulations.

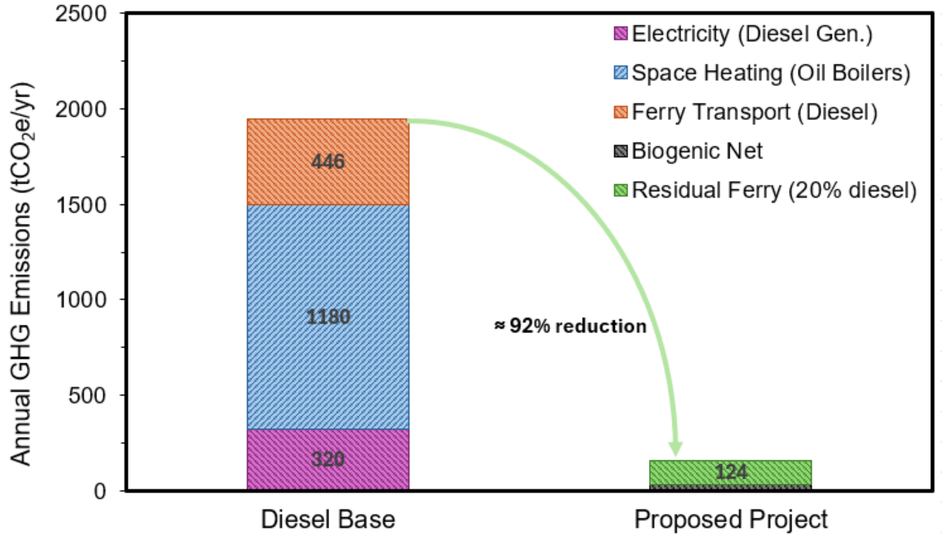

Fig. 3. GHG emission comparison between diesel-only baseline and the proposed system scenario for the reference community, data from [4]

CONCLUSIONS

This study shows a new design for a renewable energy system for Inuit off-grid island communities in Newfoundland and Labrador. It uses tidal energy, solar panels, and wood waste gasification to make electricity, hydrogen, heating, and biodiesel all together. For 1200 homes, it gives about 30,000 MWh electricity, 132,000 MWh heating, 150 tonnes hydrogen, and 180,000 litres biodiesel yearly. Algae uses 70% of gasification CO_2 to make biodiesel, replacing 20% of ferry diesel. It cuts CO_2 emissions by 92%, from 1,946 to 152 tonnes per year.

REFERENCES

1. https://www.gov.nl.ca/em/files/NLHydroAnnualReport2024.pdf, Accessed on April 12, 2026
2. https://publications.gc.ca/collections/collection_2024/eccc/En84-294-2024-eng.pdf, Accessed on April 13. 2026

AN EMPIRICAL ANALYSIS OF POWER INTERRUPTIONS AND DEMAND STRESS IN AN ISOLATED ISLAND POWER SYSTEM: EVIDENCE FROM NORTH CYPRUS

Quadri Yinka Quadri[1], Victor Ayodeji Oluwasusi[2]*
[1] Cyprus International University, Faculty of Engineering, Energy Systems Engineering Department, Haspolat, Nicosia, North Cyprus
[2] Near East University, Faculty of Artificial Intelligence and Informatives, Computer Information Systems Department, Near East Boulevard, Nicosia, North Cyprus
*Corresponding author e-mail: qquadri@ciu.edu.tr
Ref # UTL-01

ABSTRACT

Power system reliability in isolated power systems is heavily influenced by the variability of demands and other operational constraints. However, there is limited empirical evidence based on modern power system operation data. This article presents an investigation of the relationship between daily demand stress and power interruption days in Northern Cyprus using official KIB-TEK utility data for the 2024 calendar year. Daily peak demands, minimum demands, and interruption days are used to create power system reliability indicators and interruption metrics. Comparison of days with and without power outages, and days with low and high demand stress, indicates that days with power outages have slightly higher average peak demands. Moreover, days with high demands alone are not sufficient to explain power interruption days. Most days have no power outages or have only single interruption days. On the other hand, there are few days with multiple interruption days. This indicates that power system reliability is not solely influenced by demands but also by other factors such as power system operations.

Keywords: Demand stress, Electricity reliability, Island power systems, Northern Cyprus, Operational data analysis, Power interruptions.

INTRODUCTION

In this short paper, a structurally tighter reliability envelope is observed in small, isolated power systems. Studies have shown that a lack of generation diversity, reserve constraints, and poor interconnection options increase the impact of any imbalances in supply and demand, especially in periods of high demand [1],[2]. This problem is further complicated in the context of electrification and energy transitions, as these increase the variability in net demand [3]. Recent studies also suggest that reliability problems in power systems tend to cluster around peak demand conditions, with outages depending on a combination of adequacy and network constraints [4], [5] .

In this paper, a case study is presented for Northern Cyprus, where a predominantly islanded electricity system is observed. The system is dominated by thermal sources, with operational outages frequently reported in utility records, especially around peak demand conditions [6]. The 2024 production and statistics summary reports generation across key thermal units (e.g., Teknecik steam units, Kalecik DG, Teknecik diesel), alongside photovoltaic (PV) capacity reporting [7], [8]. This highlights a system that remains heavily dependent on dispatchable thermal generation, even as PV capacity continues to expand [2].

The 2024 outage statistics report provides detailed outage data, including outage start and restoration times, outage location, and outage causes, including ‘Üretim Yetersizliği,’ ‘Havai Hat Arızası,’ and so forth. Such detailed outage data provides a structured approach to reliability analysis, especially at a daily granularity.

From a theoretical perspective, two practical needs for constrained grids are emphasized in this study, especially in constrained systems. Firstly, a focus is observed in the literature on operational diagnostics, especially in systems where detailed Supervisory Control and Data Acquisition (SCADA) data is not readily available [9], [10]. For this study, a stress-aware reliability characterization approach is also observed, where reliability is characterized in two conditions: low stress and high stress.

Aim and contribution

This short paper proposes a method for operational data analysis, with a focus on quantifying outage incidence and burden as a function of differing daily demand conditions for Kıbrıs Türk Elektrik Kurumu (KIB-TE) 2024. By leveraging daily demand summaries, or P_max_MW, P_min_MW, in combination with outage event logs, a daily dataset is constructed, and outages are evaluated with respect to (a) outage vs. non-outage days, and (b) high stress vs. low stress demand conditions. The paper is intentionally pragmatic in that a reproducible operational data analysis is proposed that leverages publicly available or utility-reported data, potentially suitable for annual updates without requiring access to any utility-specific SCADA data. In contrast to prior work that relies on modeled scenarios or high-resolution SCADA data, this paper demonstrates that publicly reported utility data is sufficient to produce relevant reliability results for isolated power systems.

METHODOLOGY

The research data used in this study comes from the officially published operational data of KIB-TEK for the 2024 calendar year. The data comes from three sources, which have been combined accordingly: the Electricity Consumption

(Tuketim) Report, which contains daily system demand indicators such as daily peak demand, daily minimum demand, and peak hour data; the Interruption (Kesinti) Reports, which contain outage data including start times, restoration times, areas, and cause of interruption; and the Production & Statistics Summary (2024), which contains monthly electricity production data by type and overall system data to provide context to the operation of the system and the generation mix. All data analysis in this study was performed on a daily system level, resulting in 366 daily data points for the 2024 calendar year. Sub-daily resolution was only used to examine outage timing and duration.

For each day d, P_max_MW and P_min_MW, representing the daily peak demand and daily minimum demand, are defined based on the reports of consumption. Eq. (1) represents the range of daily demand. In order to normalize the daily peak demand with respect to typical operating conditions, a stress index is defined as in Eq. (2).

$$\Delta P_d = P\_max\_MW_d - P\_\mathrm{min}\_\mathrm{MW}_d \tag{1}$$

$$S_d = \frac{P\_max\_MW_d}{\overline{P\_max\_MW}} \tag{2}$$

The denominator of Eq. (2). is the yearly average of the daily peak demand values of the year 2024. In order to demarcate the intervals with high stress, the threshold based on the percentile is used. A high-stress day is defined by Eq. (3).

$$P\_max\_MW_d > P\_max\ \_MW_{75\%} \tag{3}$$

where $P\_max\_MW_{75\%}$ is the 75th percentile of daily peak demand values across the full year. The days for which the duration is less than or equal to the above-mentioned threshold are classified as low-stress days. This method does not involve the application of any arbitrary fixed thresholds and allows the classification of stress levels based on the observed system behavior. Each outage event reported in the interruption reports has a start time and a restoration time associated with it. For each outage event i, the interruption duration is calculated using Eq. (4).

$$t_i = End_i - Start_i \tag{4}$$

This short analysis is structured around four methodological steps: Demand characterization: indicators of daily demand are aggregated to describe the overall system load profile and variability during 2024. Outage vs. non-outage: demand characteristics are compared on days with recorded outages and days with no recorded outages. Stress-condition: outage frequency and outage duration are assessed under high stress and low stress demand conditions. Temporal analysis of outages: the distribution of outage start times is examined and compared with peak demand times.

RESULTS AND DISCUSSION

Table 1 compares the characteristics of daily demand patterns of outage and non-outage days. It is noticed that while the average peak demand of outage days is comparable to non-outage days, the median peak demand and the average daily demand range of non-outage days are considerably high. This indicates that high levels of demand are not related to outage days. This suggests that outage occurrences are not primarily driven by absolute demand magnitude, but may instead be associated with operational, maintenance-related, or network-level factors.

Table 1. Comparison of Daily Demand Characteristics on Outage and Non-Outage Days in Northern Cyprus (2024)

Day Type	**Mean peak demand (MW)**	**Median peak demand (MW)**	**Mean daily demand range Delta_P (MW)**	**Mean stress index**	**Number of days**
Outage days	236.8496241	234.63	3.096541353	1.01568815	133
Non-outage days	231.1030472	239.29	18.84763948	0.991044961	233

As depicted in Table 2, the number of days with recorded interruption is more during high-stress demand conditions compared to low-stress days. Also, the mean outage time on outage days is more during high-stress conditions, suggesting an increased level of stress as the demand is approaching its upper limit. This may imply that while high levels of demand may not be the direct cause of power outages, high-stress conditions may exacerbate the level of power interruptions. As the level of demand approaches the limits of the power systems, reduced flexibility may lead to increased restoration periods.

Table 2. Outage Occurrence and Duration Under High- and Low-Demand Stress Conditions (2024)

Stress category	**Number of days**	**Days with outages (%)**	**Mean outage duration on outage days (min)**
High-stress days	92	42.4	1751.2

Low-stress days	274	34.3	1286.3

Fig. 1 shows the daily peak demands for the year 2024, where outage days are marked. This indicates that outage days are not limited to peak demands but cover the whole spectrum. Figure 2 also shows the trend for monthly outage frequency to follow the seasonality of the average peak demands for the year. This indicates that outages are also influenced by broader seasonal operating conditions and not solely isolated extreme demand events which supports [11], [12].

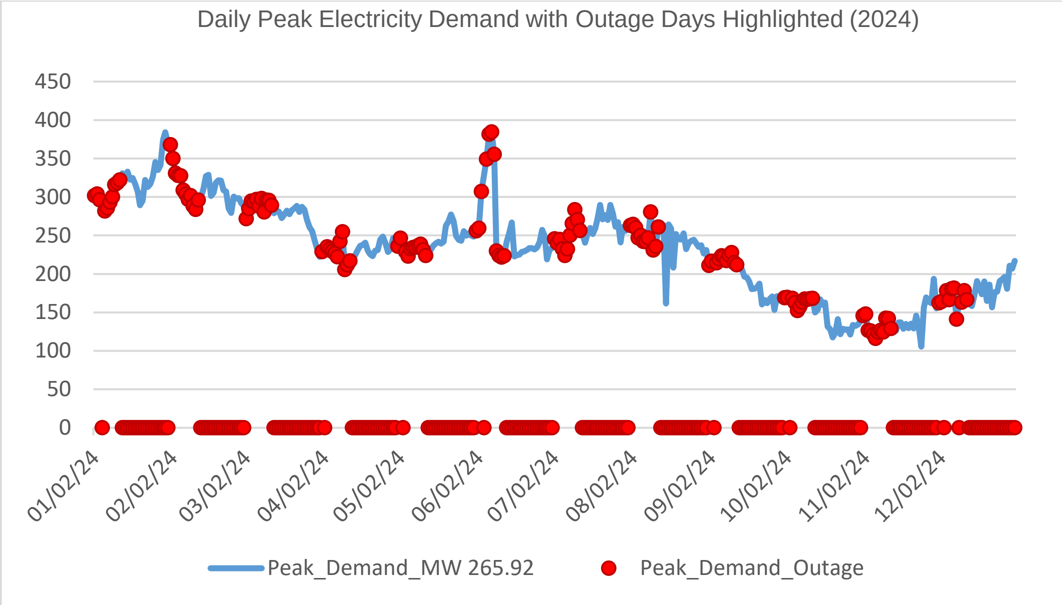

Fig. 1. Daily Peak Electricity Demand with Outage Days Highlighted

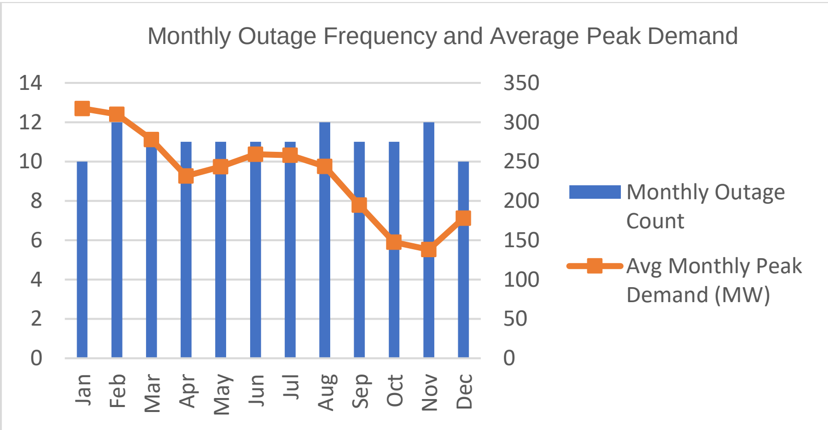

Fig. 2. Monthly Outage Frequency and Average Peak Demand

Fig. 3 depicts a comparison of the average peak demands on outage days versus non-outage days in the year 2024. It is observed that the average peak demands on outage days are slightly higher than those on non-outage days, but the overlapping range indicates that peak demands do not necessarily cause the occurrence of outage days. Although it is observed that outage days have higher peak demands on average, it is also observed that outage days can have similar peak demands as non-outage days, which indicates that not all days with high peak demands are outage days. Fig. 4 presents a distribution of outage days over the entire time period of the study. It is observed that most days have no or one outage, while days with multiple outages are not commonly observed in the distribution of outage days. However, a small fraction of days has a high concentration of outage days, which indicates the presence of an episodic stress event rather than a high outage frequency over the entire year.

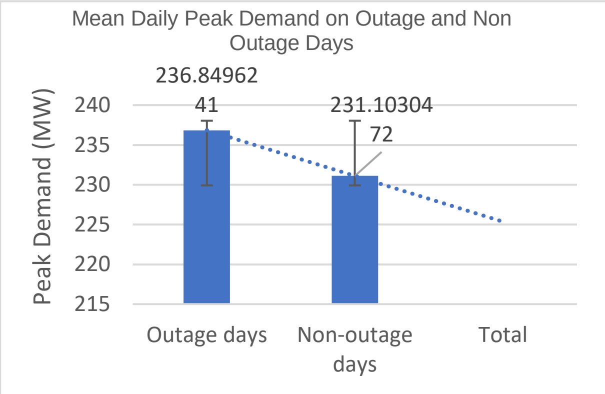

Fig. 3. Mean Daily Peak Demands

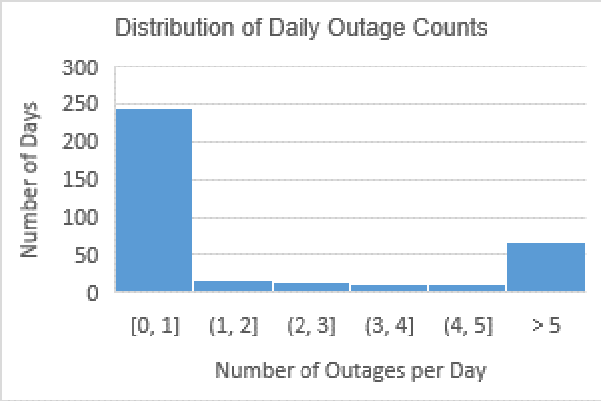

Fig. 4. Distribution of Daily Outage Counts

Discussion

The results show that, in fact, demand stress not only increases the occurrence probability and the severity of power interruptions, but elevated demand itself does not entirely explain the occurrence of interruptions in the Northern Cyprus power system. The occurrence of non-outage days with high peak demand and large demand variability suggests that operational factors such as generation availability, maintenance scheduling, and network conditions play a significant role in determining reliability outcomes of the power system. This is in line with recent studies highlighting the multi-facets of power interruptions in constrained and islanded systems.

Limitations

The basis of the analysis is publicly available reports on the operational details of the grid rather than high-resolution SCADA or network details. Therefore, the results of the analysis should be understood to be based on associations at the level of the overall grid, without details of feeder-level constraints, unit commitment strategies, reserve margins, or transmission-related issues. Also, outage causes are aggregated in a binary fashion, which may involve multiple causes not necessarily explicitly identifiable in the available details of the grid or the outages themselves.

REFERENCES

[1] M. Kjær, H. Wang, and F. Blaabjerg, "Adequacy evaluation of an islanded microgrid," *Electron.*, vol. 10, no. 19, 2021, doi: 10.3390/electronics10192344.

[2] E. Karapidakis, S. Yfanti, and C. Kouknakos, "Sustainable Energy Transition in Island Systems with substantial RES and Electricity Storage," *WSEAS Trans. Environ. Dev.*, vol. 19, pp. 1434–1447, 2023, doi: 10.37394/232015.2023.19.130.

[3] A. Ahmad and I. Dobson, "Extracting resilience events from utility outage data based on overlapping times and locations," no. November, pp. 2–4, 2025, [Online]. Available: http://arxiv.org/abs/2511.12685

[4] S. Zhou, Y. Li, C. Jiang, Z. Xiong, J. Zhang, and L. Wang, "Enhancing the resilience of the power system to accommodate the construction of the new power system: key technologies and challenges," *Front. Energy Res.*, vol. 11, no. September, pp. 1–12, 2023, doi: 10.3389/fenrg.2023.1256850.

[5] N. K. Carrington, I. Dobson, and Z. Wang, "Extracting Resilience Metrics from Distribution Utility Data Using Outage and Restore Process Statistics," *IEEE Trans. Power Syst.*, vol. 36, no. 6, pp. 5814–5823, 2021, doi: 10.1109/TPWRS.2021.3074898.

[6] K. Zamani, "KIB-TEK Sistem Kontrol Merkezi OCAK 2024 Günlük Kesinti Raporları," 2024.

[7] E. N. Düşük, T. Saatİ, E. N. Yüksek, and T. Mw, "KIBRIS TÜRK Sistem Kontrol Merkezi 2024 Tüketim Verileri Sistem Kontrol Merkezi 2024 Tüketim Verileri," 2024.

[8] KIB-TEK, "KIBRIS TÜRK ELEKTRİK KURUMU 2024 YILI Üretim ve Tüketim Değerleri," p. 2024, 2024.

[9] D. Wang, Y. Yuan, R. Cheng, and Z. Wang, "Data-Driven Outage Restoration Time Prediction via Transfer Learning with Cluster Ensembles," *IEEE Trans. Power Syst.*, vol. 39, no. 1, pp. 83–96, 2024, doi: 10.1109/TPWRS.2023.3236513.

[10] M. B. Shafik, Z. M. S. Elbarbary, B. Siqi, A. M. Azmy, and M. G. Hussien, "Distribution networks reliability assessment considering distributed automation system with penetration of DG units and SOP devices," *Energy Reports*, vol. 9, pp. 6199–6210, 2023, doi: 10.1016/j.egyr.2023.05.224.

[11] M. Abdelmalak, J. Cox, S. Ericson, E. Hotchkiss, and M. Benidris, "Quantitative Resilience-Based Assessment Framework Using EAGLE-1 Power Outage Data," *IEEE Access*, vol. 11, no. December 2022, pp. 7682–7697, 2023, doi: 10.1109/ACCESS.2023.3235615.

[12] I. Dobson, "Analyzing Cascading Failures and Blackouts Using Utility Outage Data," pp. 29–47, 2024, doi: 10.1007/978-3-031-48000-3_2.

The conference is organized by

Energy Research Center (ERC) of
Eastern Mediterranean University

With partners

Ontario Tech University

National Hydrogen Association Türkiye

AEE Cyprus Chapter — Association of Energy Engineers

Gold sponsor

ACS

Silver sponsors

Korineum Golf & Beach Resort

Lefkoşa Türk Belediyesi

TÜFEKÇİ GROUP

AEE — Association of Energy Engineers